Computational modeling of metabolic reprogramming in rheumatoid arthritis synovial fibroblasts and cancer-associated fibroblasts

Sahar Aghakhani

université
PARIS-SACLAY

Computational modeling of metabolic reprogramming in rheumatoid arthritis synovial fibroblasts and cancer-associated fibroblasts

Modélisation computationnelle de la reprogrammation métabolique des fibroblastes synoviaux de polyarthrite rhumatoïde et fibroblastes associés au cancer

Thèse de doctorat de l'université Paris-Saclay

École doctorale n°577 : Structure et Dynamique des Systèmes Vivants (SDSV)
Spécialité de doctorat : Biologie computationnelle
Graduate School : Sciences de la Vie et de la Santé

Thèse préparée dans les unités de recherche *GenHotel – Laboratoire Européen de Recherche pour la polyarthrite rhumatoïde* (Univ. Paris-Saclay, Univ. Evry) et *EPI Lifeware* (Inria Saclay) sous la direction d'**Anna NIARAKIS**, maîtresse de conférences et **Sylvain SOLIMAN**, chargé de recherche hors classe

Thèse soutenue à Paris-Saclay, le 22 septembre 2023, par

Sahar AGHAKHANI

Composition du Jury

Membres du jury avec voix délibérative

Natacha BESSIS Professeure, Université Sorbonne Paris Nord	Présidente
Laurence CALZONE Ingénieure de recherche, Institut Curie	Rapportrice
Vera PANCALDI Chargée de recherche, Centre de Recherche en Cancérologie de Toulouse	Rapportrice
Sabine PERES Professeure, Université Lyon 1	Examinatrice
Denis THIEFFRY Professeur, École Normale Supérieure	Examinateur

THESE DE DOCTORAT

NNT : 2023UPASL083

université PARIS-SACLAY

ÉCOLE DOCTORALE
Structure et dynamique des systèmes vivants (SDSV)

Titre : Modélisation computationnelle de la reprogrammation métabolique des fibroblastes synoviaux de polyarthrite rhumatoïde et fibroblastes associés au cancer

Mots clés : Modélisation computationnelle, reprogrammation métabolique, immunométabolisme, fibroblastes synoviaux de polyarthrite rhumatoïde, fibroblastes associés au cancer.

Résumé : Les fibroblastes sont les cellules les plus abondantes du tissu conjonctif et sont des régulateurs essentiels de divers processus physiologiques. Cependant, sous l'influence de stimuli spécifiques, ils peuvent présenter des comportements agressifs et contribuer à la physiopathologie de certaines maladies. En particulier, la destruction du cartilage et des os constatée dans la polyarthrite rhumatoïde est largement initiée et soutenue par les fibroblastes synoviaux (RASFs). De même, les fibroblastes associés au cancer du sein (CAFs) jouent un rôle important dans l'initiation et la progression du cancer ainsi que dans la résistance aux traitements. À ce jour, il n'existe pas de traitement curatif pour ces maladies, mais plutôt des traitements symptomatiques visant à réduire les dommages ultérieurs et à améliorer la qualité de vie des patients. Compte tenu de l'implication des fibroblastes dans leur pathogenèse, une nouvelle piste pourrait résider dans le développement de thérapies ciblant ces derniers. À cet égard, nous cherchons à décrypter les rôles clés des RASFs et des CAFs, en nous concentrant sur la caractéristique commune qui semble être à l'origine de leur activation et de leur contribution aux symptômes de la maladie associée, leur reprogrammation métabolique. Pour élucider les mécanismes pathogènes globaux et accélérer l'identification de cibles thérapeutiques innovantes, nous avons développé un cadre de modélisation hybride innovant couvrant les multiples couches biologiques de la signalisation, régulation génique et métabolisme. Nous avons ensuite intégré ce pipeline dans un outil python du nom de MetaLo. En commençant par construire des bases de connaissances statiques sous la forme de cartes d'interactions moléculaires standardisées nous inférons par la suite des modèles de régulation Booléens cellule et maladie-spécifique pour les RASFs et les CAFs. Une fois leur cohérence biologique évaluée et validée, ces modèles sont couplés à un réseau générique du métabolisme central humain. En couvrant plusieurs strates biologiques, notre framework permet d'évaluer l'impact des systèmes de régulation des fibroblastes sur la distribution de leurs flux métaboliques dans des conditions maladies-spécifiques. En plus de reproduire la reprogrammation métabolique des RASFs et des CAFs observée expérimentalement, nos simulations *in-silico* soutiennent l'hypothèse originale selon laquelle, à l'instar des CAFs, les RASFs subissent un effet Warburg inversé. En reprogrammant leurs voies métaboliques centrales par le biais de ce dernier processus, les RASFs et les CAFs s'adaptent à leur nouvel environnement, maintiennent leurs phénotypes agressifs et participent activement à l'amplification de la pathogenèse de la maladie associée. HIF1 a été identifié comme le principal acteur moléculaire de ce mécanisme dans les deux maladies. Compte tenu des altérations métaboliques et des facteurs de régulation similaires, nous suggérons l'existence d'un mécanisme commun régissant la transformation phénotypique des fibroblastes par le biais d'un effet Warburg inversé induit par HIF1 dans la polyarthrite rhumatoïde et le cancer. Par conséquent, nous proposons de cibler HIF1 comme une voie prometteuse dans le traitement de la polyarthrite rhumatoïde et du cancer en ciblant la reprogrammation métabolique des RASFs et des CAFs.

université PARIS-SACLAY
ÉCOLE DOCTORALE
Structure et dynamique des systèmes vivants (SDSV)

Title : Computational modeling of metabolic reprogramming in rheumatoid arthritis synovial fibroblasts and cancer-associated fibroblasts

Keywords : Computational modeling, metabolic reprogramming, immunometabolism, rheumatoid arthritis synovial fibroblasts, cancer-associated fibroblasts

Abstract : Fibroblasts are the most abundant cells in connective tissue and are essential regulators of various physiological processes. However, under the influence of specific stimuli, they can exhibit aggressive behaviors and contribute to disease physiopathology. In particular, the cartilage and bone destruction occurring in rheumatoid arthritis is largely initiated and sustained by synovial fibroblasts (RASFs). Similarly, breast cancer-associated fibroblasts (CAFs) are greatly involved in cancer initiation, progression, and resistance to therapy. To date, there is no cure for these diseases but rather symptomatic treatments aimed at reducing further damage and improving the patients quality of life. Yet, considering the involvement of fibroblasts in their pathogenesis, a new lead may lie in the development of fibroblast-directed therapies. In this regard, we seek to decipher RASFs and breast CAFs critical roles, focusing on the common feature that seemingly drives their activation and contribution to the associated diseases debilitating symptoms, namely their metabolic reprogramming. To unravel the comprehensive pathogenic mechanisms and accelerate the identification of innovative therapeutic targets, we developed a novel hybrid modeling framework covering the multiple biological layers of signaling, gene regulation, and metabolism. We further packaged said pipeline in a python tool of the name MetaLo. Starting by constructing static knowledge bases in the form of standardized molecular interaction maps, we inferred cell- and disease-specific Boolean regulatory models for RASFs and breast CAFs. Once their biological coherence is thoroughly evaluated and validated, they are coupled with a generic reconstruction of human central metabolism in a context-specific manner. By spanning across multiple biological strata, our framework allows the assessment of fibroblasts regulatory impact upon their metabolic flux distribution under disease-specific conditions. Besides confirming the experimentally-observed metabolic reprogramming of RASFs and breast CAFs, simulations supported the original hypothesis that, similarly to CAFs, RASFs undergo a reverse Warburg effect. By reprogramming their central carbon metabolic pathways through the latter process, both RASFs and breast CAFs adapt to their new environment, sustain their aggressive phenotypes, and actively participate in the amplification of the associated disease pathogenesis. HIF1 was identified as the primary molecular driver of this mechanism in both situations. Given the shared metabolic alterations and regulatory driver, we further suggested the existence of a common mechanism directing the phenotypic transformation of fibroblasts through a HIF1-driven reverse Warburg effect in rheumatoid arthritis and breast cancer. Therefore, we propose the targeting of HIF1 as a promising path in the treatment of rheumatoid arthritis and cancer by addressing RASFs and breast CAFs metabolic reprogramming.

ACKNOWLEDGEMENTS

First, I would like to thank Dr. Laurence Calzone and Dr. Vera Pancaldi for kindly accepting to be reviewers of this PhD manuscript and for their constructive feedback and encouragements. Let me also take this opportunity to thank the other members of the jury, Pr. Sabine Peres, Pr. Natacha Bessis, and Pr. Denis Thieffry for agreeing to be examiners of this PhD thesis.

I would like to thank the members of my PhD committee, Dr. Inna Kuperstein, Dr. Andreas Draëger, and Pr. Sabine Peres (*again*) for their valuable remarks and constructive scientific discussions over the years.

I would like to thank my amazing PhD co-directors, Pr. Anna Niarakis and Dr. Sylvain Soliman, for their invaluable guidance, support and continuous encouragement over the last three years. Our sup' meetings were always insightful and I gained considerable knowledge from our discussions, which will definitely guide me through the rest of my career. I am also deeply greateful that you never gave into your impulses to tear each other apart (in front of me?) and for your commitment to always find a free buffet or catering service which warmed my heart.

I would like to thank Dr. Elisabeth Petit-Teixeira for welcoming me at the GenHotel, always providing all necessities to pursue my work in good conditions, and for her open-mindedness which fueled lively discussions. I would also like to thank Dr. Valérie Chaudru for her warm welcome and always high spirits, and all other members of the GenHotel for making the last three years as joyful and pleasant as possible: Dr. Quentin Miagoux, my first office roommate, for his cheerfulness and various (and often very unexpected) topics of conversation which made the best coffee/tea breaks I ever had; Dr. Vidisha Singh, for being one of the nicest and most caring

people I have ever met despite her many attempts to poison me with spices too hot to handle; (soon-to-be Dr.) Nawel Zerrouk, for being my thesis sidekick, going through each steps with me, and for being the fastest and best code debugger in the history of bioinformatics; (a-little-bit-longer-but-pretty-soon-to-be-anyway Dr. and PharmD) Sacha E. Silva Saffar, for being the easiest intern to co-supervise, most supporting office roommate ever, and for having taken over from Quentin as the only man in the lab' with flying colors; and Pilar Rodriguez for her help, infectious good humor, and unfailing optimism.

I would also like to thank Dr. François Fages for his warm welcome within the Lifeware team, and for never letting me starve to death with the priceless gift of lunch tickets, along with all current or past members of the group: Dr. Eléa Thibault Greugny, (soon-to-be Dr.) Marine Collery, Dr. Mathieu Hemery, Dr. Julien Martinelli, Dr. Jérémy Grignard, and all others for never letting me forget the preciousness of living in the great city of Evry, all the insightfull talks and good times spent over a cup of coffee/tea, and for giving me some of my best cinematic sessions ever through the heated debates between Sylvain and François.

I would like to thank all members of the Direction of Research and Valorization (DiReV) of University Paris-Saclay, and particularly Dr. Jessica Pericaud, Dr. Bruno Bost, Dr. Tania Di Gioia, Pierrick Grimaud, and Eline Goutereau for welcoming me during the three years of my complementary mission. It was a real pleasure working with you and developing new skills. Thank you for all the bò bún parties and fun!

To make sure I am not forgotting anyone, I would like to thank all the people I have worked with over the past three years, both in the administrative departments and on scientific tasks. I would like to thank Genopole and SFBI for the scholarships and financial aid I have received, Florence Hervy for her

administrative help, Dr. Marek Ostaszewski, Dr. Piotr Gawron, Dr. Tomas Helikar, for their technical help, Dr. Fatima Mechta-Grigoriou and Dr. Yann Kieffer for access to private data, *to name just a few*…

I would also like to express my deepest gratitude to my parents, Shohreh Daneshpour and Nozar Aghakhani, who have always supported each and every one of my decisions, both professional and personal, and who always made it a priority to offer their children a supportive environment in which to grow. I am fully conscious of all the sacrifices they made to be able to offer us this lifestyle, and will forever be grateful to them. A word for my little brother, Ali Aghakhani, whose sense of humor and casualness towards this thesis always motivated me to do better. I am enjoying seeing the man you are becoming. Finally, I would like to thank all remaining members of my family, uncles, aunts, cousins, and grandparents for their constant support over the years.

I would like to thank my best friend ever, (soon-to-be PharmD) Céline Sabra, for believing in me more than I would have ever believed in myself and for being the rock she was in every way and at every moment. I am grateful to have ever found such a good friend and hope to reciprocate. I would also like to thank two of my greatest friends, Benjamin Marteau and Ludovic Prudent, who stood by me every step of the way, in failures and successes. A word for new, but no less important friends, (soon-to-be Dr.) Aïda Tavakoli and Kian Habibian, and all other great friends whom challenging circumstances have brought into my life. I am grateful to be fighting such battles alongside you.

Finally, I would like to thank my partner, Zihan Mahmud, for his unconditional love and support, each step of the way and in every aspect of my life. To many new adventures by your side…

RESUME EN FRANÇAIS

Défini en 2011 comme « l'interface entre les disciplines historiquement distinctes de l'immunologie et du métabolisme » **[1]**, le domaine de l'immunométabolisme s'est imposé comme un champ de recherche majeur en biologie cellulaire. Cette discipline présente de multiples facettes et applications, notamment en apportant un regard unique sur les mécanismes pathologiques complexes afin d'identifier de nouvelles cibles thérapeutiques.

Un sujet bien connu de l'immunométabolisme est la reprogrammation métabolique que subissent certains acteurs cellulaires, acquérant un phénotype agressif associé à des caractéristiques pathogènes dans des maladies liées à l'immunité. Le décryptage de ces mécanismes complexes et multiniveaux, à l'interface entre processus métaboliques et processus immunitaires, pourrait élargir le paysage thérapeutique de maladies actuellement incurables.

En effet, pour survivre au sein de leur environnement, les organismes présentent deux caractéristiques fondamentales : l'ensemble des réactions nécessaires au maintien de la vie, appelé métabolisme, et la capacité de résister à un agent ou à un processus nocif ou pathogène, appelée immunité. Leur implication conjointe dans les processus pathologiques n'est donc pas surprenante. Pourtant, et jusque très récemment, les sous-systèmes immunologiques et métaboliques étaient considérés comme totalement indépendants et leurs interactions étaient largement négligées dans le développement thérapeutique. Dans ce contexte, l'immunométabolisme soutient que la capacité à résister à un agent ou à un processus nocif est liée à une distribution efficace des nutriments au sein-même des cellules et que les processus métaboliques sont étroitement régis par des cascades de régulation immunitaire.

La fonction centrale du métabolisme consiste en la production d'énergie sous forme d'adénosine triphosphate (ATP) pour construire des molécules complexes et générer de la biomasse. Dans les cellules normales des tissus sains, la manière la plus courante d'y parvenir est l'oxydation du pyruvate glycolytique à travers le cycle de l'acide tricarboxylique (TCA) mitochondrial, alimentant la phosphorylation oxydative (OXPHOS). Globalement, 36 molécules d'ATP y sont produites par molécule de glucose à travers le transfert d'électrons en présence d'oxygène. Cependant, en 1927, Otto Warburg, lauréat du prix Nobel, a identifié pour la première fois une altération des voies métaboliques pour la production d'énergie dans les cellules cancéreuses **[23]**, aujourd'hui reconnue sous le nom d' « effet Warburg ». La glycolyse aérobie génère alors quatre molécules d'ATP par molécule de glucose convertie en pyruvate et en lactate, contournant de manière significative les voies mitochondriales. Au-delà de la propriété fondatrice de l'effet Warburg, à savoir une forte absorption de glucose alimentant la glycolyse et entraînant une forte sécrétion de lactate, et ce même en présence d'oxygène **[26]**, cette reprogrammation métabolique s'est ensuite révélée couvrir d'autres changements bioénergétiques. Enfin, nous réalisons aujourd'hui que cette reprogrammation métabolique ne se limite pas qu'aux cellules cancéreuses. Elle peut affecter les cellules stromales du microenvironnement tumoral qui peuvent subir leur propre effet Warburg, généralement pour soutenir les cellules cancéreuses adjacentes. Cette relation réciproque est connue sous le nom d'effet Warburg inversé **[27]**. Il a également été démontré récemment que diverses cellules non cancéreuses peuvent subir une reprogrammation métabolique afin de s'adapter et survivre, c'est le cas des macrophages, cellules T ou cellules dendritiques dans diverses conditions pathologiques non cancéreuses **[28]**.

La reprogrammation métabolique de ces acteurs en cellules présentant un phénotype agressif permettrait non seulement de leur fournir l'énergie

nécessaire, mais également l'absorption et l'incorporation de nombreux nutriments dans leur biomasse afin de soutenir une biosynthèse à grande échelle, prolifération rapide, survie, invasion et autres attributs associés à leur phénotype agressif **[32]**. Ces cellules reprogrammées sur le plan métabolique et dotées de phénotypes agressifs contribuant fréquemment aux processus pathogènes, l'élucidation de leurs altérations métabolique pourrait permettre d'améliorer la prise en charge thérapeutique des maladies associées.

Deux cas de reprogrammation métabolique d'un acteur cellulaire dans une maladie complexe ont été abordés dans cette thèse de doctorat : les fibroblastes associés au cancer du sein (CAFs) ainsi que les fibroblastes synoviaux de polyarthrite rhumatoïde (RASFs).

En effet, les altérations métaboliques des fibroblastes semblent exercer un rôle déterminant dans l'acquisition d'un phénotype agressif et dans leur activité pathogène au sein de ces deux maladies. La transformation de fibroblastes sains en RASFs, caractérisés par une prolifération accrue et une résistance à l'apoptose, contribue à la chronicité de la polyarthrite rhumatoïde (PR) et à l'inflammation des articulations. Il en va de même pour les CAFs et leurs interactions avec les cellules cancéreuses qui contribuent à la croissance et à l'invasion des tumeurs ainsi qu'à la résistance au traitement. Le ciblage immunométabolique suggère que la repolarisation de cellules liées à l'immunité, telles que les RASFs et les CAFs, vers des phénotypes sains et non agressifs par la manipulation de leur métabolisme pourrait représenter une approche prometteuse pour diminuer leur activité pathogéniques. Or, pour répondre aux besoins métaboliques des RASFs et des CAFs, il est nécessaire de démêler leurs processus complexes et d'identifier leur(s) moteur(s) ou régulateur(s) principal(aux). Les méthodes computationnelles semblent adaptées à l'acquisition de nouvelles connaissances biologiques sur des maladies complexes et encore incurables, en intégrant diverses couches

d'informations biologiques et en exploitant leurs caractéristiques statiques et dynamiques. Un formalisme de modélisation hybride, couvrant les diverses caractéristiques biologiques de la régulation génique, de la signalisation intracellulaire et du métabolisme pathologique, pourrait rendre compte de la dynamique des interconnexions immuno-métaboliques des RASFs et des CAFs. Dans cette thèse, nous avons donc proposé l'utilisation d'approches computationnelles pour déchiffrer les mécanismes sous-tendant la transformation des RASFs et des CAFs, acteurs clés de la pathogénèse de la maladie associée, par leur reprogrammation métabolique afin de proposer des cibles thérapeutiques innovantes.

Cela a notamment été obenu à travers les différents sous-objectif suivants :

(1) L'exploitation d'approches computationnelles statiques et dynamiques dans les contextes cellulaires et pathologiques des RASFs et des CAFs, couvrant signalisation cellulaire, régulation génique et métabolisme, afin de décrypter le comportement émergent des fibroblastes en intégrant de multiples mécanismes biologiques.

Bien que les RASFs et les CAFs partagent de nombreuses similitudes, nous avons été contraints de prendre en compte les différentes caractéristiques pathologiques et les micro-environnements distincts de la PR et du cancer du sein qui conduisent à leur reprogrammation métabolique. De plus, puisque les fibroblastes sont des systèmes complexes avec une variété de processus biologiques impliqués, une attention supplémentaire a été accordée à l'intégration de multiples couches d'informations qui permettraient les interconnexions entre les stimuli extracellulaires : les cascades de signalisation intracellulaires, l'activité des facteurs de transcription, la régulation de l'expression génique et, enfin et surtout, les processus métaboliques.

Plus précisément, nous avons commencé par construire des cartes d'interactions moléculaires de pointe pour la PR et les CAFs génériques, en améliorant les travaux publiés précédemment, à savoir la RA-map **[200]** et la CAF-map de l'« *Altas of Cancer Signaling Network* » (ACSN) **[204]**. L'objectif premier étant de cartographier avec précision et de manière mécanistique les voies impliquées dans la pathogenèse des deux maladies. Nos nouvelles cartes, la RA-map V2 et la CAF-map V2, sont donc des représentations graphiques standardisées, qui s'engagent pleinement à respecter les principes FAIR **[226]** de la communauté pour la facilité de recherche, l'accessibilité, l'interopérabilité et la reproductibilité. En effet, les deux cartes d'interactions moléculaires ont été rendues librement accessibles via la plateforme de navigateur web MINERVA **[234]**. Leur contenu est conforme aux normes SBGN PD **[189]**, **[227]** pour la représentation, SBML **[229]** pour le format, MIRIAM pour les annotations **[233]**, PMIDs pour les références et CALM pour la biocuration **[231]**. Toutes les entités sont annotées à l'aide des symboles HGNC **[205]** pour les composants de signalisation et de régulation génique et BiGG **[232]** pour les composants métaboliques. L'utilisation d'identifiants standard pour les entités présentes dans nos cartes a permis d'assurer leur compatibilité avec d'autres outils et de faciliter l'intégration de données omiques. Enfin, les annotations détaillées et l'accès facilité au contenu permettent une réutilisation transparente et facilitée des ressources. En outre, la construction manuelle de nos cartes permet d'avoir une plus grande confiance dans les informations représentées par rapport aux reconstructions automatiques, de fournir des informations mécanistiques détaillées et de pallier au manque de données omiques nécessaires à l'inférence automatique de réseaux dans certains contextes biologiques comme ceux-ci.

La RA-map V2 et la CAF-map V2 représentent les premières tentatives de visualiser et de simplifier les informations complexes concernant les

interconnexions métaboliques et régulatoires détaillées dans la PR et les CAFs génériques. Il s'agit de bases de connaissances statiques permettant de résumer les connaissances actuelles sur les voies biologiques moléculaires et les entités impliquées significativement dans la pathogenèse des maladies associées. Ces cartes permettent en outre de visualiser des données expérimentales, de mettre en évidence certains aspects des processus biologique affecté et d'identifier les différences entre diverses conditions. Leur analyse topologique nous a également permis d'étudier la distribution du réseau et d'identifier les nœuds structurels ayant potentiellement un fort pouvoir de régulation.

L'étude de cartes d'interaction moléculaires statiques nous limitant dans l'analyse de la dynamique des RASFs et des CAFs, nous en avons inferré automatiquement des modèles Booléens dynamiques et exécutables. Ces derniers représentent de formidables ressources pour décrypter, de manière qualitative, les processus biologiques complexes sous-tendus par des propriétés dynamiques. Ils sont très adaptés à l'étude des processus de signalisation cellulaire et de régulation génique véhiculant des flux de signaux. Les deux modèles de régulation ont par la suite été contextualisés pour reproduire les conditions biologiques des RASFs et des CAFs. Cela a été obtenu en combinant des approches de curation manuelle et basées sur des données omiques afin de garantir une spécificité cellulaire élevée et la confiance dans les interactions décrites et les conditions initiales utilisées. Les modèles des RASFs et des CAFs sont conformes aux normes de biologie systémique du format SBML-*qual* **[244]**, sont entièrement annotés et sont librement accessibles dans deux référentiels de modèles biologiques, à savoir Cell Collective **[245]** et BioModels **[246]**, **[247]**. La cohérence biologique du comportement des modèles de régulation a été évaluée par rapport à des études expérimentales extraites de la littérature scientifique à trois niveaux distincts (c'est-à-dire au niveau des voies génériques de régulation, de

métabolisme ainsi que du comportement cellulaire global), reproduisant principalement les observations expérimentales. L'un des avantages de ces modèles réside dans leur capacité à contribuer à l'identification des interactions réglementaires inconnues et d'effets directs ou indirects de composants ou de voies spécifiques les uns sur les autres. Globalement, la génération et le paramétrage d'un modèle logique à partir de la construction manuelle d'un réseau ainsi que l'analyse des données et la biocuration permettent d'éviter les problèmes associés aux méthodologies automatiques tels que la reconstruction incorrecte des réactions ou la compartimentation incorrecte conduisant à des représentations erronées. Dans le domaine de la PR, il s'agit de la deuxième tentative pour saisir la dynamique de l'activité pathogène des RASFs, mais de la première pour inclure le rôle clé du métabolisme. Dans le domaine du cancer, notre modèle Booléen exécutable représente la première tentative d'évaluation de l'activité pathogène dynamique des CAFs, d'autant plus de manière spécifique au cancer du sein ou en incluant les processus métaboliques. De tels modèles de régulation peuvent être analysés tels quels, en tirant parti de leur construction liée aux phénotypes cellulaires, pour identifier les nœuds ou les voies les plus importants dans chaque comportement cellulaire dynamique afin de répondre à des questions biologiques spécifiques de manière strictement qualitative.

Cependant, l'étude qualitative de l'impact des systèmes de régulation génique et de signalisation cellulaire sur les sous-processus métaboliques n'étant pas suffisante pour aborder la stœchiométrie des flux biochimiques, nous avons couplé nos modèles de régulation à une reconstruction générique et quantitative du métabolisme humain central, MitoCore **[250]**. Le choix du modèle métabolique a été basé sur deux facteurs : la fiabilité des réactions représentées, qui ont été sélectionnées manuellement pour MitoCore, plutôt qu'une reconstruction métabolique automatique, et le fait que notre sous-section métabolique d'intérêt soit le métabolisme central du carbone plutôt

que l'ensemble du métabolisme. Cependant, en principe, notre *framework* est adaptable à n'importe quel type de modèle métabolique basé sur des contraintes. Le *framework* proposé extrait des contraintes métaboliques supplémentaires à partir de composants métaboliques dont le comportement asymptotique « inactif » a été prouvé dans des conditions de régulation spécifiques à la cellule et à la maladie. Il permet de traiter automatiquement des modèles comportant des centaines de composants. Notre approche s'inspire de la doctrine centrale de l'immunométabolisme, à savoir les interconnexions étroites entre les processus de régulation immunitaire et la machinerie métabolique, et la nécessité d'intégrer l'étude dynamique de ces différentes couches biologiques pour comprendre la reprogrammation métabolique des RASFs et des CAFs.

Après avoir démontré l'adaptabilité de notre *framework* de modélisation hybride aux contextes des RASFs et des CAFs, nous l'avons compilé dans un outil python appelé MetaLo pour un plus large éventail d'applications. Cet outil *open-source* peut être utilisé par une grande variété d'utilisateurs ayant une formation pluridisciplinaire, par le biais de la ligne de commande ou de l'interface graphique. De plus, cet outil est interopérable avec d'autres outils de biologie systémique grâce au format standard des cartes d'interactions moléculaires et des modèles Booléens et métaboliques. À partir d'une carte d'interactions moléculaires standardisée et d'une reconstruction métabolique générique basée sur des contraintes, MetaLo applique automatiquement toutes les étapes de notre *framework* de couplage hybride (c'est-à-dire l'inférence du modèle Booléen de régulation, l'initialisation de ce dernier en fonction des conditions initiales définies par l'utilisateur, la computation des *trap-spaces* en tant que comportement régulatoire asymptotique, l'identification des composants métaboliques inactifs à long terme, la traduction en contraintes métaboliques et l'analyse de la distribution métabolique optimale). Dans l'ensemble, MetaLo a pour but d'aider à

l'identification de corrélations immunométaboliques dans diverses maladies complexes afin d'élucider les impacts régulatoires sur les processus métaboliques.

(2) La proposition d'un mécanisme potentiel expliquant la reprogrammation métabolique des fibroblastes dans des conditions spécifiques à la maladie en étudiant les impacts dynamiques régulatoires des RASFs et des CAFs sur leurs processus métaboliques, tout en identifiant le(s) régulateur(s) clé(s).

Les simulations de notre modèle hybride des RASFs dénote que les flux optimaux pour une production maximale d'ATP cellulaire sont glycolytiques, représentant 85% de la production d'ATP cellulaire. Elles illustrent également une augmentation des flux glycolytiques ainsi qu'une augmentation de l'absorption du glucose et de la sécrétion de lactate dans les RASFs, témoignant d'un métabolisme hautement glycolytique. Un métabolisme oxydatif faible est démontré par une diminution des flux TCA et OXPHOS et une diminution de la sécrétion des sous-produits mitochondriaux tels que le CO_2 et le H_2O. Un environnement hypoxique est illustrée par une diminution de l'absorption d'O_2 et une augmentation de la sécrétion de H^+, associée à l'acidité de l'environnement. Au-delà des voies métaboliques de production d'ATP, les résultats indiquent une reprogrammation de plusieurs autres voies métaboliques dans les RASFs. Une sécrétion accrue d'acides aminés et d'acides gras est mise en évidence, agissant potentiellement dans la PR comme substrats pour la production d'énergie, intermédiaires de biosynthèse, composants des phospholipides membranaires, ou support de l'érosion osseuse et de la dégradation du cartilage. Une augmentation de la carboxylation réductrice est également identifiée, nouvelle voie du métabolisme de la glutamine favorisant la croissance de cellules de type tumoral présentant des défauts mitochondriaux.

D’autres voies, notamment les réactions de transport mitochondrial, la synthèse de la cardiolipine ou le clivage de la glycine, semblent être affectées, probablement de manière indirecte, en raison de la réorientation des métabolites par le biais des autres voies métaboliques altérées.

Dans des conditions de régulation spécifiques aux CAFs, les flux optimaux pour la production d’ATP sont les flux glycolytiques, à l’origine de 85,05% de la production d’énergie cellulaire sous forme d’ATP. Un environnement hypoxique et un métabolisme anaérobie sont révélés par une diminution de l’absorption d’O_2 et une augmentation de la sécrétion de H^+, associées à l’acidité de l’environnement. Outre les voies métaboliques de production d’énergie, les voies de construction des macromolécules sont altérées. En particulier, l’absorption d’acides aminés par les CAFs est réduite, de même que leur dégradation et leur sécrétion. L’absorption des acides gras est également réduite tandis que leur sécrétion est augmentée. La synthèse de la cardiolipine est diminuée, ce qui est cohérent avec les résultats précédents, car ils sont connus pour réguler l’OXPHOS. D’autres voies, dont le folate cytosolique, la carboxylation réductrice et le métabolisme du butanoate, semblent être affectées, ce qui résulte très probablement indirectement de la réorientation des métabolites par d’autres voies altérées ou par l’application de nos contraintes métaboliques supplémentaires. Enfin, les transporteurs mitochondriaux sont affectés par la reprogrammation des voies mitochondriales évoquée ci-dessus.

Ainsi, la reprogrammation métabolique des fibroblastes semble être un élément crucial dans la pathogenèse de deux maladies complexes aussi différentes que le cancer du sein et la PR. En raison de la similitude du *framework* appliqué pour contextualiser le réseau métabolique générique MitoCore dans les deux maladies, une comparaison des voies métaboliques altérées peut être effectuée. Sur les sept enzymes métaboliques ayant un

comportement régulateur asymptotique égal à 0 et conduisant à contraindre les réactions métaboliques associées dans le modèle MitoCore dans les deux contextes biologiques, cinq sont partagées. En outre, six métabolites similaires dont le comportement réglementaire asymptotique est égal à 0 conduisent à contraindre des réactions métaboliques supplémentaires dans MitoCore. Afin d'identifier si ces contraintes communes sont suffisantes pour observer des altérations métaboliques similaires à celles des RASFs et des CAFs, une analyse métabolique supplémentaire a été entreprise incluant uniquement les contraintes métaboliques extraites des enzymes et des métabolites ayant un comportement asymptotique inactif dans les deux modèles de régulation. Les résultats décrivent un métabolisme reprogrammé avec un flux glycolytique élevé pour la production d'énergie, ainsi que des flux oxydatifs faibles. La sécrétion de lactate et de nutriments riches en énergie est élevée. La proportion de la production totale d'énergie sous forme d'ATP provenant de la glycolyse est calculée à 85,05%. Ces résultats, bien que légèrement différents au niveau des valeurs de certains flux, reproduisent assez fidèlement les altérations métaboliques observées dans les RASFs et les CAFs. Ceci nous amène déjà à suspecter un processus similaire de reprogrammation métabolique dans les RASFs et les CAFs. En outre, une analyse approfondie des voies métaboliques modifiées a été entreprise. Dans l'ensemble, les voies métaboliques directement liées à la production d'énergie sont modifiées de la même manière (augmentation de la glycolyse, diminution de l'OXPHOS et du TCA). Les sous-produits oxydatifs sont également altérés similairement dans les CAFs et les RASFs (augmentation du lactate et de la sécrétion, diminution de la sécrétion de CO_2 et de H_2O). L'environnement des fibroblastes, respectivement dans le microenvironnement tumoral et dans l'articulation de la PR, semble être modifié de façon similaire (diminution de l'absorption d'O_2 et augmentation de la sécrétion d'H^+).

Les voies métaboliques qui ne sont pas directement impliquées dans la production d'ATP sont également affectées. Par exemple, les conditions de régulation spécifiques aux deux maladies reprogramment de manière similaire les altérations des voies des acides aminés et des acides gras dans les fibroblastes, probablement en raison de leur importance dans la biosynthèse des macromolécules. En effet, la sécrétion des éléments constitutifs est également augmentée dans les deux situations. Certaines voies sont altérées de façon similaire mais posent la question de leur intérêt dans des conditions environnementales différentes. Par exemple, la carboxylation réductrice est augmentée de manière similaire dans les CAFs et les RASFs. Agissant comme une nouvelle voie de la glutamine, elle soutient la croissance des cellules présentant des déficiences mitochondriales. Warburg avait initialement émis l'hypothèse que les cellules cancéreuses présentaient un défaut mitochondrial **[395]**, mais des travaux ultérieurs ont réfuté cette hypothèse **[25]**. De telles études n'ont pas encore été menées dans ces deux types de fibroblastes. D'autres investigations expérimentales sont donc nécessaires pour déchiffrer leur statut mitochondrial et identifier un bénéfice potentiel des réactions de carboxylation réductrice. Dans l'ensemble, les transporteurs mitochondriaux et cytosoliques ainsi que les voies de transport sont affectés, pas nécessairement de la même manière, mais probablement toujours en raison de la reprogrammation des voies métaboliques en amont. Enfin, le métabolisme du butanoate n'est pas affecté de la même manière dans les CAFs et les RASFs. Cependant, il est typiquement impliqué dans des processus associés à la fermentation intestinale, ses altérations ne semblent donc pas significatives dans un contexte cancéreux ou auto-immun.

(3) La proposition de nouvelles cibles thérapeutiques pour les maladies à médiation immunitaire comme la PR ou le cancer du sein à partir de l'étude approfondie de la reprogrammation métabolique des RASFs et des CAFs.

Afin de déchiffrer le rôle des composés régulateurs dans les altérations métaboliques des RASFs, des *knock-ins* et *knock-outs* individuels des conditions initiales spécifiques aux RASFs ont d'abord été réalisés. Sur les 14 variantes de conditions initiales, seule la condition 3 a un impact significatif sur les voies de production d'ATP. En effet, lors de l'inhibition de HIF1 et du maintien des conditions initiales spécifiques à RASF pour les autres composants, la glycolyse a été considérablement réduite et l'OXPHOS a expliqué la majorité de la production d'ATP cellulaire. Cette situation, bien qu'extrême dans ses proportions, probablement en raison des règles d'extraction de contraintes de notre *framework*, est plus proche d'une situation saine. Ce résultat suggère que le ciblage de HIF1 pourrait participer à la restauration d'un profil métabolique sain chez les RASFs. De plus, il est cohérent avec des études expérimentales récentes démontrant que le *knock-out* de HIF1 réduit le métabolisme glycolytique dans les fibroblastes synoviaux humains **[363]**. D'autres combinaisons de *knock-ins* et *knock-outs* ont été générées et testées pour tenir compte de l'effet synergique potentiel des composants régulateurs sur les processus métaboliques. 2^{14} = 16 384 combinaisons ont été testées, représentant toutes les combinaisons possibles, en éliminant naturellement les *knock-outs* non biologiquement significatifs. Sur les 16 384 combinaisons, 1 984 ont été éliminées car elles généraient des comportements asymptotiques aberrants au niveau phénotypes cellulaires, par exemple une apoptose et une prolifération actives en même temps, prouvant les limites d'un modèle qui n'a pas été créé pour des *inputs* combinées mais pour reproduire un environnement spécifique à une cellule et à une maladie. 8 448 combinaisons ont été éliminées car le calcul des *trap-spaces* dépassait la limite de temps de trois minutes, très probablement en raison de l'impossibilité de réduire suffisamment la complexité du modèle avec l'algorithme de propagation des valeurs. Les 5 952 combinaisons restantes ont fait l'objet d'une analyse approfondie. Toutes les combinaisons ont montré un profil métabolique pathogène reprogrammé avec 96% de la

production d'ATP cellulaire assurée par les voies glycolytiques et 4% par OXPHOS. Afin d'identifier d'éventuels schémas associés à ce profil métabolique pathologique, une analyse de la valeur de chaque composant a été obtenue. Toutes les combinaisons de *knock-outs* et *knock-ins* liées à un profil métabolique pathologique incluent l'activation de HIF1. Le rôle régulateur clé de HIF1 avait déjà été identifié dans les *knock-outs* et *knock-ins* individuels. Son état d'activation constant dans toutes les combinaisons de conditions initiales spécifiques aux RASFs et associées à un profil métabolique pathogène démontre l'effet individuel prépondérant de HIF1 sur l'effet synergique de tout autre composant régulateur dans le modèle hybride des RASFs.

Après avoir reproduit la reprogrammation métabolique observée expérimentalement dans les CAFs, le défi consistait à en identifier les principaux moteurs de régulation. Les *knock-outs* et *knock-ins* individuels successifs des conditions initiales de régulation spécifiques aux CAFs ont donné lieu à 147 nouvelles combinaisons. Seul l'une d'entre elles dénote un profil métabolique sain pour la production d'énergie dans les CAFs, il s'agit de la condition 57 (C57). En effet, en supprimant HIF1, les voies métaboliques semblent retrouver une distribution saine, l'ATP cellulaire étant généré par des voies oxydatives plutôt que glycolytiques. Les aautres facteurs de régulation ne semblent pas affecter directement la distribution des flux métaboliques dans les CAFs. D'autres combinaisons de *knock-ins* et *de knock-outs* ont été générées et testées pour tenir compte de l'effet synergique potentiel des composants régulateurs sur les processus métaboliques. Compte tenu du nombre élevé de conditions initiales à tester et du nombre potentiel de 2^{147} = 1784059616E[44] combinaisons, une réduction du modèle a d'abord été entreprise. Cette dernière a été obtenue en se concentrant sur les voies moléculaires en amont des phénotypes cellulaires des CAFs impliqués dans les caractéristiques du cancer (c'est-à-dire la production de ROS, l'hypoxie,

la prolifération des fibroblastes, l'angiogenèse, la croissance tumorale, *etc*.). Le modèle CAFs extrait comportait 58 *inputs*, 51 si l'on exclut le glucose et tous les composants agissant en tant que « molécule simple ». Les 51 *inputs* restants ont ensuite été regroupés selon leur similitudes biologiques en 21 *inputs*. Ainsi, 2^{21} = 2 097 152 combinaisons ont été générées pour la suite des tests. Malheureusement, après près de 11 jours de simulation, « seulement » 308 159 combinaisons ont été calculées, qui ont toutes été éliminées de l'analyse ultérieure en raison de l'étape de calcul des *trap-spaces* qui a duré plus de trois minutes par combinaison. À ce stade, il n'est pas donc possible d'identifier un éventuel effet synergique des composés régulatoires sur les processus métaboliques dans le modèle des CAFs. Des stratégies alternatives pour atteindre cet objectif sont actuellement à l'étude.

Au-delà des nombreuses voies métaboliques altérées communes, le régulateur moléculaire clé a également été identifié comme étant HIF1 dans les RASFs et les CAFs. Déjà reconnu dans la PR comme un moteur de l'inflammation, de l'angiogenèse et de la destruction du cartilage **[323]**, le ciblage de HIF1 n'a pas encore été proposé dans le cadre d'une stratégie thérapeutique visant à résoudre la reprogrammation métabolique dans les fibroblastes. Dans le cancer du sein, les opportunités thérapeutiques ciblant HIF1 semblent limitées à ses activités métastatiques ou à son rôle de moteur de la prolifération tumorale. L'intérêt croissant pour le ciblage métabolique afin de s'attaquer aux caractéristiques pro-tumorales a donné lieu à quelques découvertes telles que l'Honokiol en tant qu'inhibiteur de la glycolyse médiée par HIF1 pour stopper la croissance des cellules du cancer du sein **[396]**. Cependant, son intérêt dans les CAFs n'a pas encore été étudié. Enfin, des études sur d'autres types de fibroblastes humains ont reconnu un rôle clé pour HIF1, par exemple dans l'antivieillissement et la régénération des fibroblastes dermiques **[397]** ou l'atténuation de la fibrose et le retardement du remodelage vasculaire dans les fibroblastes associés à la sclérose systémique **[398]**, mais son ciblage dans

la résolution de la reprogrammation métabolique des fibroblastes n'a pas encore été étudié.

Ainsi d'après nos résultats et compte tenu des altérations métaboliques communes, des avantages probables pour les cellules environnantes du microenvironnement pathogène et du moteur régulateur commun, nous proposons dans cette thèse l'existence d'un mécanisme commun dirigeant la transformation phénotypique des fibroblastes dans la polyarthrite rhumatoïde et le cancer du sein par le biais d'une reprogrammation métabolique induite par HIF1.

TABLE OF CONTENTS

LIST OF FIGURES

LIST OF TABLES

1 INTRODUCTION

1.1 IMMUNOMETABOLISM, AN EMERGING FIELD IN CELLULAR BIOLOGY

Introduced in 2011 as "the interface between the historically distinct disciplines of immunology and metabolism" **[1]**, the field of immunometabolism has emerged as a major area of research in cellular biology. It holds multiple facets and applications, notably in providing unique insights into complex pathological mechanisms with the ultimate goal of identifying novel therapeutic targets. A well-known topic in immunometabolism is the metabolic reprogramming of particular cellular actors acquiring an aggressive phenotype with crucial pathogenic features in immune-related diseases. Deciphering such complex and multilevel mechanisms, intertwining metabolic and regulatory immune processes, may broaden the therapeutic landscape of currently incurable diseases.

1.1.1 When immunity meets metabolism

To survive within their environment, organisms exhibit two fundamental features: the set of life-sustaining reactions, referred to as metabolism, and the ability to resist a harmful agent or process, known as immunity. Their dual implication in pathological processes is consequently not surprising. Yet, until very recently, immunological and metabolic subsystems were considered as totally independent and their interplay was widely neglected in treatment development. Immune disorders were, and remain for the greater part, treated through immunosuppressive therapies **[2]**, whereas treating metabolic disorders was focused on tackling associated conditions (*e.g.* high

blood pressure and blood sugar or unhealthy cholesterol levels) **[3]**. Despite their great strides in recent years, such therapies are essentially symptomatic and leave numerous diseases incurable. In this context, immunometabolism first emerged through the study of metabolic disorders and the observation of the associated immune disruptions. For instance, chronic metabolic inflammation, referred to as metaflammation, is now well acknowledged to be a significant hallmark of metabolic dysfunctions in insulin resistance and obesity **[4]**. Same goes for adipose tissue inflammatory cytokines involvement in metabolic disorders **[5]**. Unique metabolic alterations in key immune cells were also investigated and distinct activation states of macrophages were reported to be associated with distinct metabolic conditions, suggesting metabolic adaptations as a mediator of their phenotypic switch and cellular plasticity **[6]**, **[7]**. Further key breakthroughs paved the way of immunometabolism over the past two decades and are highlighted in **Figure 1**.

In light of these findings, immunometabolism claimed that besides the production of energy and biosynthetic precursors, cellular metabolic processes may also tightly regulate both innate and adaptive immune systems and exert a significant impact upon cellular phenotypes. Additionally, historically non-immune pathologies may result from the mobilization of immune regulatory pathways **[5]**, **[8]**. Immunometabolism further tailored the definitions of metabolism and immunity presented above. It suggested that the ability to resist a harmful agent or process is related to an efficient distribution of nutrients within cells and implies that metabolic processes outcome is governed by immune regulatory cascades (**Figure 2**).

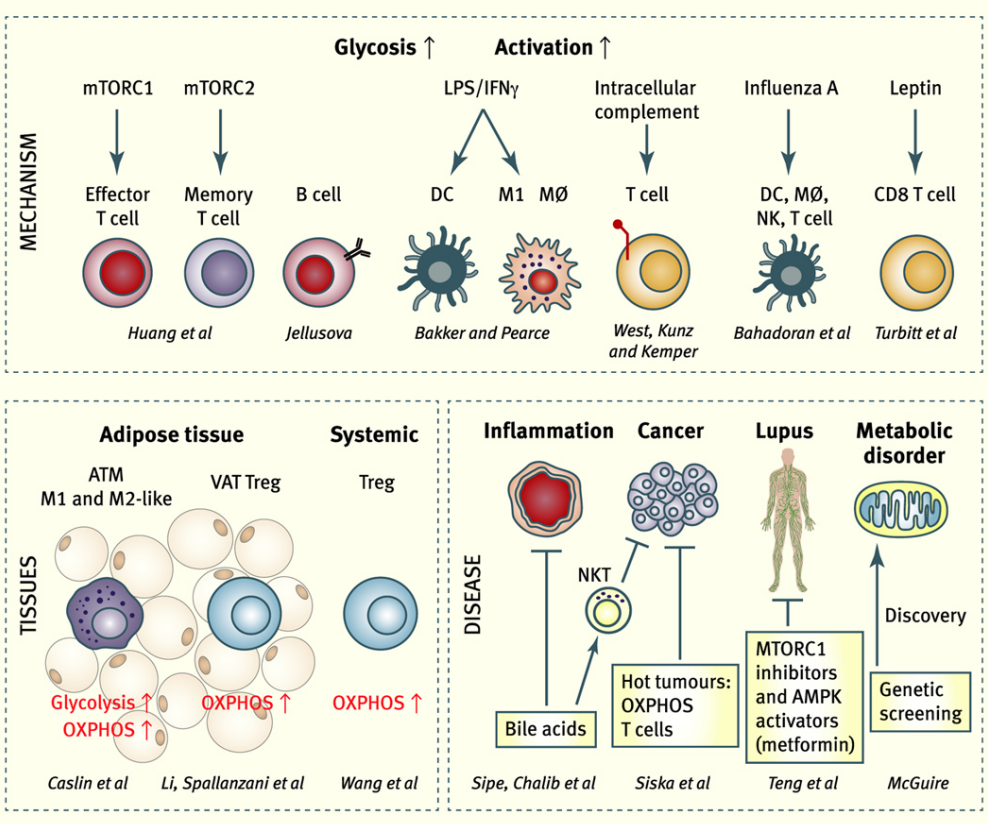

Figure 1. Graphical summary of recent findings demonstrating the mechanisms of immunometabolism and their impact on specific cells, tissues, and disease states [5]. From top to bottom and left to right: Huang *et al.* **[9]** highlighted the PI3K/Akt/mTORC1 and mTORC2 pathways as a central mechanism in T cells to sense and integrate nutrient availability and signaling. Jellusova **[10]** demonstrated the metabolic requirements of antibody-producing B cells to support high rates of protein synthesis and immune action. Bakker and Pearce **[11]** provided a detailed review of immuno-metabolic reprogramming in dendritic cells and macrophages after danger signal activation. West *et al.* **[12]** identified alternative metabolic ways to regulate T cell metabolism and physiology. Bahadoran *et al.* **[13]** worked on influenza-induced metabolic reprogramming of immune cells in the lung airway. Turbitt *et al.* **[14]** focused on the effect of obesity on T cell metabolism and function in the presence and absence of solid tumors through Leptin signaling. Caslin *et al.* **[15]**, Li *et al.* **[16]**, and Wang *et al.* **[17]**, highlighted the need to assess metabolic and cellular interactions in different tissues to identify macrophages or Treg cells polarization. Finally the role of immunometabolism in disease initiation was greatly highlighted with Sipe, Chaib *et al.* **[18]** tackling the role of host-microbial interactions on immunometabolism in anti-tumor immunity and other chronic diseases, Siska *et al.* **[19]** focusing on the Warburg effect in cancer cells, Teng *et al.* **[20]** studying distinct immune cell

populations metabolic programs in systemic lupus erythematosus, or McGuire **[21]** highlighting influence on immunity of Mendelian genetic metabolic disorders. *mTORC1/2: mammalian target of rapamycin complex 1/2; LPS: lipopolysaccharides; IFN: interferon; DC: dendritic cell; M1: macrophage M1; MØ: macrophages; NK: natural killer cells; ATM: adipose tissue macrophage; VAT: visceral adipose tissue; Treg: regulatory T cells; OXPHOS: oxidative phosphorylation; NKT: natural killer T cells; AMPK: adenosine monophosphate-activated protein kinase.*

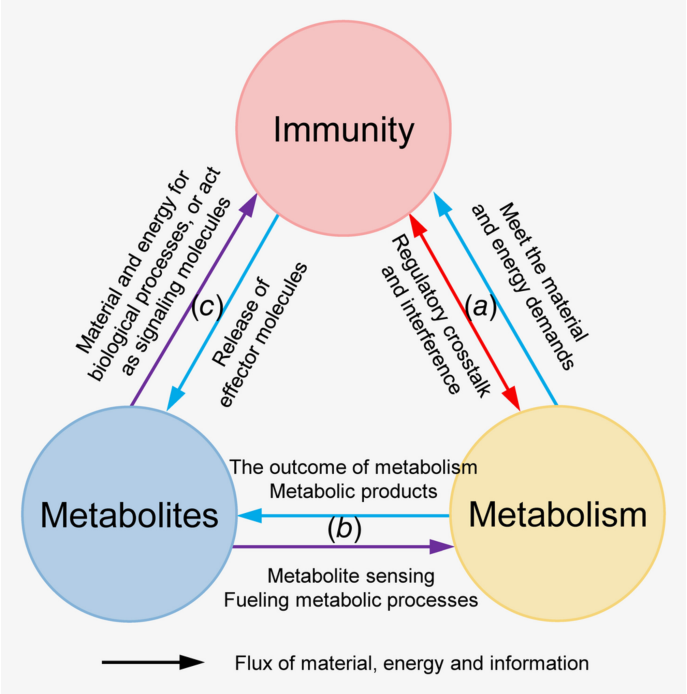

Figure 2. The various cross-talks of immunometabolism [22]. (a) Metabolic processes provide energy and materials to support immune processes. **(b)** The composition and levels of intracellular and extracellular metabolites may reflect and directly affect cellular metabolic status. Simultaneous metabolomic analysis of large numbers of metabolites can be useful for determining the metabolic status of cells. **(c)** Certain metabolites are closely related to immunity by their key signaling functions. Additionally, the levels of other metabolites can markedly affect the functions of immune cells.

In this context, unraveling the various cross-talks between immunity and metabolism in pathological contexts provides a promising avenue for drug and therapy development by considering specific cells metabolic subsystems as therapeutic targets. It is an even more important consideration in immune-mediated diseases since, rather than the current immunosuppressive approach, therapeutic targeting of immune cells metabolic processes may specifically antagonize target cells without affecting surrounding immune actors or pathways, potentially reducing adverse side effects associated with patients state of immunodeficiency **[8]**.

1.1.2 Metabolic reprogramming as an alternative pathway for cells with aggressive phenotypes

A key function of cellular metabolism is to generate energy in the form of adenosine triphosphate (ATP) to further build complex molecules (*e.g.* proteins, carbohydrates, fats, lipids) and generate biomass. In normal cells within healthy tissues, the most common way to generate energy for such anabolic processes is through oxidation of glycolytic pyruvate in the mitochondrial tricarboxylic acid cycle (TCA), further fueling mitochondrial oxidative phosphorylation (OXPHOS) and secreting low levels of lactate. Overall, 36 molecules of ATP are produced per molecule of glucose through electron transfer in the presence of oxygen. However, in 1927, Nobel Prize winner Otto Warburg reported for the very first time an alteration of metabolic pathways for energy production within cancer cells **[23]**, nowadays recognized as the “Warburg effect”. This metabolic reprogramming involved alterations in metabolic enzymes, metabolites, and metabolic pathways. The major one was identified as aerobic glycolysis through the generation of four molecules of ATP per molecule of glucose converted into pyruvate and lactate, significantly by-passing mitochondrial pathways of energy

production (**Figure 3**). Warburg initially suggested that this metabolic reprogramming promoted the adaptation of tumor cells to their cancerous surroundings, maintained their aggressive phenotype (*i.e.* high proliferation, continued growth, metastasis), and resulted from mitochondrial defects that prevented them from oxidizing carbon from glucose to CO_2. Although the Warburg effect is now fully recognized in cancer cells, with metabolic reprogramming considered as one of the 10 hallmarks of cancer **[24]**, certain features were later refuted. For instance, despite the initial hypothesis emitted by Warburg, a significant portion of cancer cells do not exhibit mitochondrial defects and are capable of undergoing oxidative energy production **[25]**. Indeed, mitochondrial metabolism is not shut down but greatly rewired to synthesize essential TCA-cycle intermediates for anabolic processes (*e.g.* amino acids, fatty acids, lipids).

Beyond the founding property of the Warburg effect, namely high glucose uptake fueling glycolysis and resulting in high lactate secretion even in presence of sufficient oxygen **[26]**, this metabolic reprogramming was later realized to cover additional bioenergetic changes. For instance, the pentose phosphate pathway (PPP) is largely fueled by glycolytic intermediates, as are amino acid synthesis pathways. The synthesis of lipids and glutaminolysis is additionally altered, along with modifications in mitochondrial bioenergetics as stated above. Finally, we now realize that such metabolic reprogramming is not limited to cancer cells. It can affect surrounding stromal cells of the tumor microenvironment (TME) which may undergo their own Warburg effect, usually to support adjacent cancer cells. This reciprocal relationship is known as the reverse Warburg effect **[27]**. It was also recently demonstrated that various non-cancerous cells of aggressive phenotype may experience a metabolic reprogramming to adapt and survive, such as macrophages, T cells or dendritic cells in various non-cancerous pathogenic conditions **[28]**.

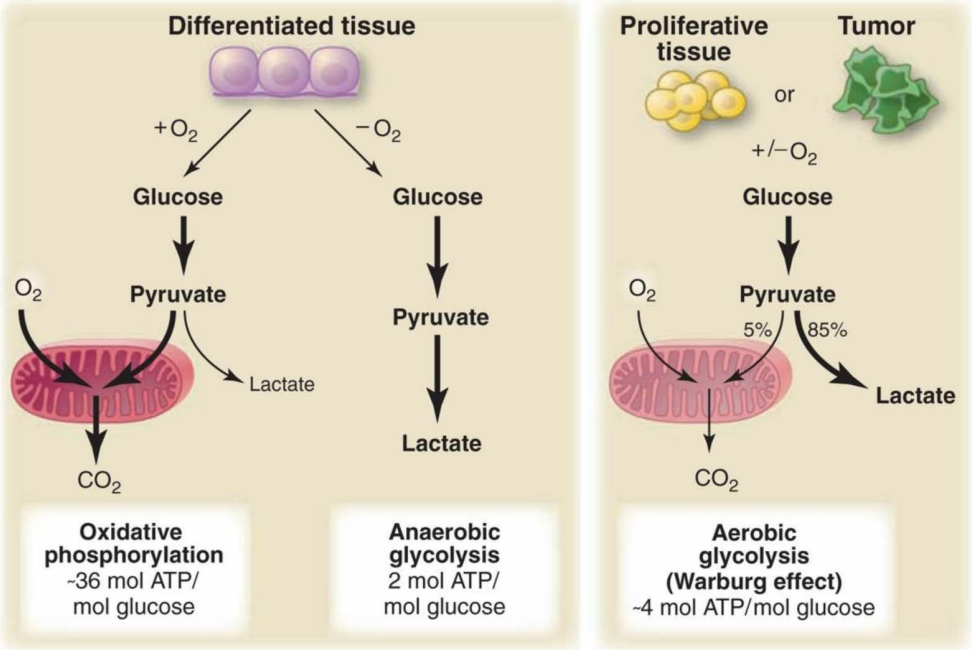

Figure 3. Understanding the Warburg effect [29]. In the presence of oxygen, non proliferating tissues metabolize glucose to pyruvate through glycolysis and completely oxidize most of it in the mitochondria to CO_2 during oxidative phosphorylation. Since O_2 is required as the final electron acceptor, this process must occur in an aerobic environment. When oxygen is limiting, cells can redirect the pyruvate generated by glycolysis away from mitochondrial oxidative phosphorylation by generating lactate through anaerobic glycolysis. This allows glycolysis to be pursued by cycling NADH back to NAD^+, but results in minimal ATP production when compared with oxidative phosphorylation. Warburg observed that proliferative tissues such as cancer cells tend to convert most glucose to lactate regardless of whether oxygen is present or not. Mitochondria remain functional and some oxidative phosphorylation continues in both cancer cells and normal proliferating cells.

The intricate mechanisms underlying the Warburg or reverse Warburg effects in cells with aggressive phenotype and their relevance to physiopathology are the focus of several recent studies **[29]**, **[30]**. Elucidating why oxygen-accessible cells would deprive themselves of the majority of ATP produced through mitochondrial oxidative pathways has been challenging. One hypothesis is based on the production rate of ATP, essential for such proliferative cells, which is higher through glycolysis than OXPHOS **[31]**. However, ATP production appears to be a concern only when resources are scarce, which is generally not the case for proliferating cells that are exposed to a continuous supply of glucose and nutrients *via* the bloodstream. Other hypotheses rely on the key role of metabolic intermediates, necessary for the biosynthetic needs of rapidly proliferating cells. For instance, this glycolytic switch provides ribose-5-phosphate and glycine for nucleotide biosynthesis, citrate for lipid synthesis, or TCA by-products to further produce fatty acids and amino acids **[32]**. Additionally, dumping the excess carbon as lactate, main by-product of glycolysis, may be effective to allow its quick incorporation into biomass, facilitating rapid cell division **[29]** and maintaining adequate levels of reduced forms of glutathione, enabling resistance to therapeutic agents **[8]**, **[33]**.

In other words, aggressive cells metabolic reprogramming may not only provide them with the necessary energy, but also the uptake and incorporation of high-energy nutrients into their biomass to support large-scale biosynthesis, rapid proliferation, survival, invasion, and other attributes associated with their pathogenic phenotype **[32]**. These metabolically reprogrammed cells with agressive phenotypes frequently contribute to pathogenic processes and unraveling their metabolic alterations driver may provide insights for better treatment.

1.2 METABOLIC REPROGRAMMING AT THE HEART OF COMPLEX DISEASES

Complex diseases are defined as diseases whose etiology and progression are determined by a combination of genetic, epigenetic, and environmental factors, challenging the development of proper curative treatments. It has recently been proven that a number of these complex pathological conditions may reshape metabolism and force particular cells to adapt through metabolic reprogramming. For instance, recent studies suggest that kidney cells may experience a glycolytic switch, contributing to disease progression **[34]**. Metabolic reprogramming of viruses allows them to increase their biomass to fuel viral genome replication and produce new virions **[35]**. On a more up-to-date topic, increasing insights into COVID-19-associated metabolic reprogramming have led to exploring metabolites with immunomodulatory properties as alternative therapeutic approaches to treat the associated inflammation **[36]**. In fact, excessive inflammation is the trademark of many complex diseases, notably cancer and rheumatoid arthritis (RA). Although quite different in their nature and operating mechanisms, these cancerous and autoimmune pathologies actually share many similarities. Beyond their global state of inflammation, they are characterized by common key cellular actors, namely fibroblasts, and their very similar metabolic reprogramming. As this phenomenon was initially observed in the context of cancer, progress in this field may be leveraged to further expand our understanding of RA. From a drug development perspective, as we learn more about the importance of rewiring metabolic processes to drive inflammation and disease physiopathology, novel therapeutic opportunities are likely to emerge for the treatment of such incurable disorders.

1.2.1 The use-case of cancerous diseases

Cancer is considered as a large group of over 100 different diseases and is characterized by the development of abnormal cells dividing uncontrollably and leading to the formation of a swelling, commonly known as a tumor **[37]**. According to the International Agency for Research on Cancer, the global incidence of cancer in 2020 was estimated at 18.6 million **[38]**. It is important to note that the standard mortality rate decreased by 33% between 1991 and 2023 **[39]**, probably due in part to earlier and earlier diagnosis and screening. However, as cancer still remains a leading cause of death worldwide, accounting for nearly 10 million deaths in 2020, or nearly one in six deaths **[38]**, it is considered a major public health issue **[37]** and numerous research projects are devoted to its curative treatment. Yet, a vast majority of proposed strategies are focused solely on cancer cells and greatly overlook surrounding cells of the TME, although they are increasingly recognized to play a major role in cancer initiation, development, and maintenance. Considering such cells when seeking for innovative therapeutic targets may prove highly beneficial in the treatment of still incurable cancers.

1.2.1.1 Physiopathology of cancer

Regardless of the type of cancer, there is a common physiopathological process of development **[40]** (**Figure 4**). The latter is a multi-step process occuring over four main stages involving mutation and selection for cells with progressively increasing capacity of proliferation, survival, invasion, and metastasis **[24]**, **[41]**. The first stage involves the primary mutation and initiation of the tumor. The initial genetic alteration leads to a mutation in a single cell, resulting in its abnormal proliferation: it is the first tumor cell. This is followed by cell proliferation and tumor progression as new mutations occur. Mutated cells present a selective advantage over normal cells as they

grow and divide rapidly. The offspring of a cell with such an additional mutation will therefore become dominant in the tumor population. Tumor cell proliferation progressively leads to the appearance of new tumor cell clones with increased growth rates and aggressive properties (*e.g.* survival, invasion, metastasis), a process called "clonal selection". The latter continues throughout tumor development. In addition, cancer cells invade blood and lymph vessels, allowing them to metastasize throughout the body. At the new sites, cells continue to multiply and eventually form new tumors. In this context, the interactions between cancer cells and the ecosystem of the TME (*e.g.* immune cells, stromal cells, extracellular matrix (ECM), vasculature) are active promoters of cancer progression **[42]**. Indeed, specific cells within the TME may release extracellular signals influencing metastasis, invasion, angiogenesis, or tumor growth. Additionally, the TME may transform into a niche for tumor cells to escape therapy.

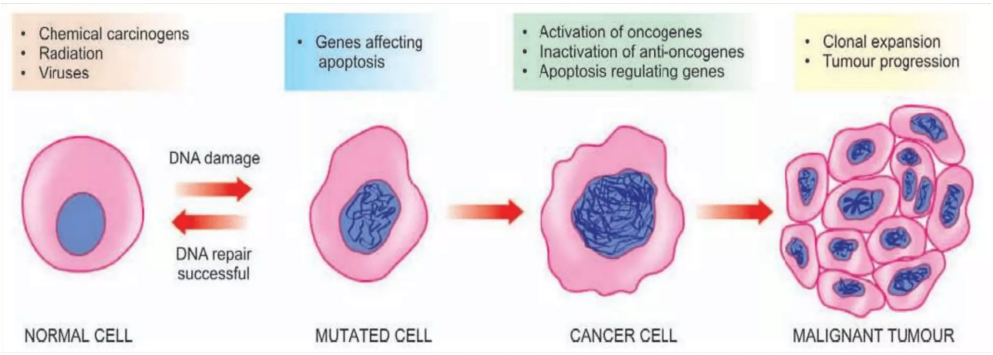

Figure 4. Molecular pathogenesis of cancer [40]. Cancers are caused by mutations whose damage failed to be successfully repaired. These mutations proliferate and invade tissues, leading to progressive clonal expansion of tumor cells.

In early 2000, Hanahan and Weinberg postulated that the evolution of healthy cells towards neoplastic tumors is accompanied by the acquisition of distinctive abilities, namely the "hallmarks of cancer" [24], [41]. Hallmarks are all underpinned by genome instability and mutation and were originally six biological capabilities acquired during the multistep development of human tumors. They have since been increased to eight capabilities and two enabling capabilities (**Figure 5**).

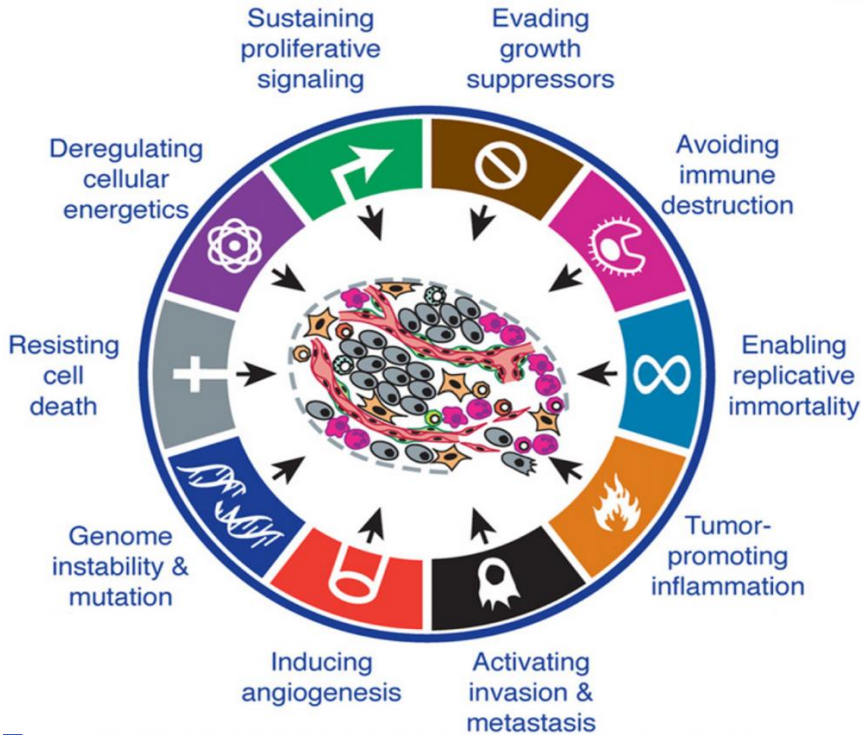

Figure 5. Graphical summary of the 10 hallmarks of cancer [24]. (1) Sustaining proliferative signaling: cancer cells do not need stimulation from external signals in the form of growth factors to multiply. This is rather driven by three main signaling pathways: Akt, MAPK/ERK, and mTOR. **(2)** Evading growth suppressors: to overcome growth inhibition from homeostatic signals, cancer cells lack response to external growth-inhibitory signals. **(3)** Avoiding immune destruction: despite cancer cells causing increased inflammation and angiogenesis, they also appear to be able to avoid interaction with the immune system through a loss of interleukin-33. **(4)** Enabling replicative immortality: tumor cells may

achieve unlimited replicative potential by synthesizing high telomerase enzyme levels or through a recombination-based mechanism, preventing telomere shortening, thus by-passing senescence and apoptosis. **(5)** Tumor-promoting inflammation: recent discoveries highlighted the role of local chronic inflammation in inducing cancer due to signaling within the tumor microenvironment. **(6)** Activating invasion and metastasis: the well-documented epithelial-to-mesenchymal transition is a key process in these mechanisms, allowing uninhibited cell division and metabolic adaptations enabling cell survival under nutrient-limiting and stress conditions. **(7)** Inducing angiogenesis: vascular network growth is important for metastasis as cancer cells require a sufficient supply of nutrients and oxygen, along with a means of waste removal. **(8)** Genome instability and mutation: cancer cells increased tendency for genomic changes and mutations affects cell division and tumor suppressor genes to further promote cancerous adaptations. **(9)** Resisting cell death: cancer cells prevent apoptosis through intrinsic mechanisms rather than a lack of response to external stimuli. **(10)** Deregulating cellular energetics: due to their excessive growth, cancer cells require high levels of energy and nutrients with the ability to survive in hypoxic environments, as tumors can be poorly vascularized. To meet these needs, many of the cellular metabolic pathways are altered in cancer.

1.2.1.2 Etiology and treatment of cancer

Cancer is considered as a complex disease arising from multiple factors in combination. However, each risk factor is more or less important in triggering specific cancer types. In any case, cancer and tumor development is initiated by a genetic mutation. The latter assumes two distinctive types: germline mutations or acquired mutations. Germline mutations occur in a sperm or egg cell and are passed from a parent to a child at the time of conception, the mutation being copied into every cell. Even if germline mutations have been associated with certain types of cancer, such as BRCA1 and BRCA2 for breast cancer, less than 10% of all cancers are associated with inherited genetic mutations **[43]**, **[44]**. On the other hand, acquired mutations occur from damage to genes in a particular cell during life and under the influence of environmental factors **[45]**. They are the most common cause of cancer and may be avoidable by reducing exposure to known factors. Particular agents,

known as carcinogens, have been linked to specific types of cancer, the most infamous being tobacco (accounting for 25–30% of cancer deaths) **[46]** along with alcohol (around 4%) **[47]**. Additionally, physical agents can lead to cancer through their physical, rather than chemical, effects on cells **[48]**. Usually, physical carcinogens must get inside the body and require years of exposure to develop cancer. For instance, environmental exposures to pesticides or fertilizers have been linked to childhood cancers **[49]**. Finally, an estimated 15% of human cancers are attributable to virus infections including human DNA or RNA viruses **[50]**. Together, diet and obesity are linked to approximately 30–35% of cancer deaths **[51]**, **[52]**. Physical inactivity is also thought to contribute to cancer risk, not only through its effect on body weight, but also through its negative effects on the immune and endocrine systems **[51]**.

Given the broad range of cancer diseases, the treatment options may vary depending on the type of cancer. In all cases, a multitude of treatment options are available including surgical interventions, chemotherapies, radiotherapies, immunotherapies, hormone therapies, targeted drug treatments, *etc*. Regarding the latter, they are either small-molecule drugs or monoclonal antibodies. Small-molecule drugs are low molecular weight molecules targeting intracellular processes to kill cancer cells (*e.g.* epidermal growth factor receptor (EGFR), vascular endothelial growth receptor (VEGFR), reactive oxygen species (ROS), phosphoinositide 3-kinases (PI3K) inhibitors) **[53]** while monoclonal antibodies are much larger molecules usually binding at the surface of cancer cells and interacting with specific targets **[54]**. Such treatments, while very successful in certain types of cancer, essentially target specific genes and proteins involved in cancer cells survival, growth or invasion, and do not consider cancer cells wide interactions within the TME.

1.2.1.3 Cancer-associated fibroblasts, key players of the tumor microenvironment

Despite their great strides in recent decades, a significant proportion of drug-based therapeutic approaches in cancer still fails, mainly due to drug resistance **[55]**. The latter represents the main challenge of researchers to date. Resistance may occur when cancer cells present molecular alterations driving insensitivity to drugs before treatment, called intrinsic resistance, or when cancer cells adapt to a drug while its administration, known as extrinsic resistance **[56]**. The latter is suspected to arise from changes in the TME, as its interplay with cancer cells is often partially or totally overlooked in the development of cancer therapy. Yet, the importance of the TME in cancer initiation and progression has been widely recognized for years **[57]**–**[59]**. While cancer develops through genetic and epigenetic alterations, tumor growth, survival, and metastasis are regulated through complex interactions with stromal cells of the TME **[58]**, **[60]**, **[61]**. Among them, multiple studies in various cancers have demonstrated the key role of cancer-associated fibroblasts (CAFs) **[62]**–**[64]**.

Overall, the presence and high density of CAFs in the TME is indicative of a poor prognosis for the patient, thus they are considered as pro-tumor agents **[65]**. Indeed, CAFs present a tumor-like phenotype through engagement in cancer cell proliferation and invasion by sending pro-tissue fibrosis signals **[62]**. They are considered as primary drivers of angiogenesis in the TME as they are known to secrete vascular endothelial growth factor (VEGF), stromal cell-derived factor 1 (SDF-1), fibroblast growth factor (FGF), and platelet-derived growth factor (PDGF) to drive the growth of new blood vessels **[66]**. CAFs secrete major inflammatory cytokines, maintaining an inflammatory state around cancer cells through immune system modulation **[62]**–**[64]**. They are further involved in ECM remodeling through the production of ECM-

degrading proteases [67] (**Figure 6**). CAFs additionally support cancer cells by modulating their epithelial-to-mesenchymal transition (EMT) and secrete growth factors, cytokines, and chemokines [62]–[64]. They have been found to promote tumor metastasis by up-regulating genes involved in pro-tumorigenic pathways and/or down-regulating tumor suppressor genes. Finally, by creating a stromal niche for cancer stem cells, CAFs may enable them to escape therapy [62]–[64].

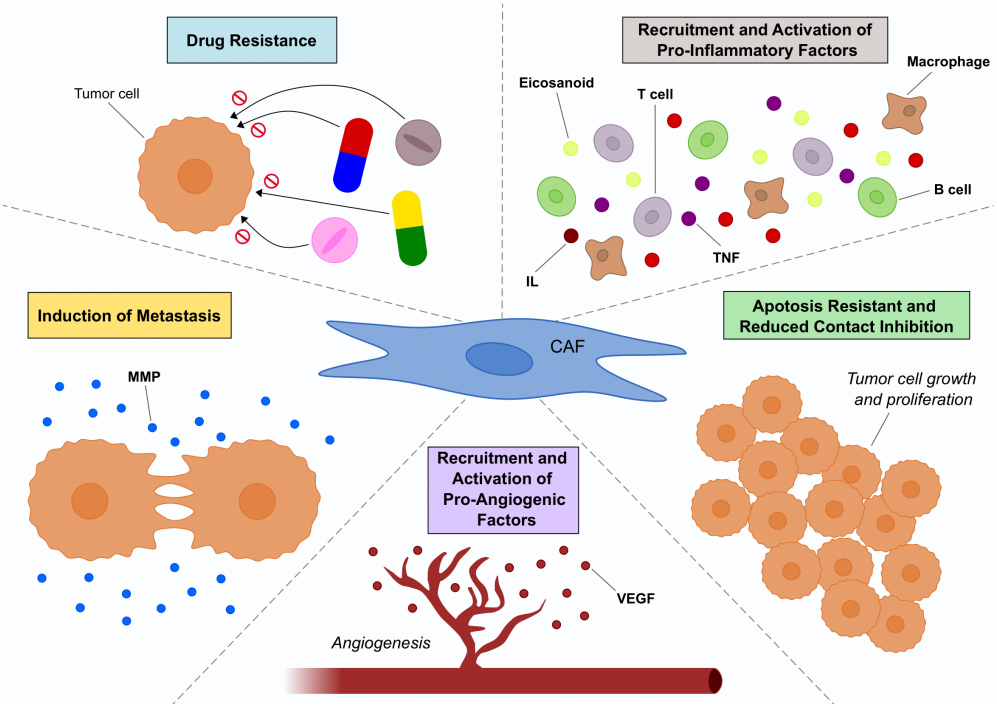

Figure 6. Key roles of cancer-associated fibroblasts (CAFs) in cancer pathogenesis and progression. CAFs are involved in a wide range of pathogenic mechanisms including recruitment and activation of pro-angiogenic, pro-inflammatory factors, apoptosis resistance and reduced contact inhibition, along with metastasis, proliferation, and drug resistance, overall perpetuating cancer maintenance and progression. *TNF: tumor necrosis factor; IL: interleukin; VEGF: vascular endothelial growth factor; MMP: matrix metalloproteinase.*

The precise origin of CAFs is a debated subject. The obvious hypothesis lies in an alteration of local precursors, *i.e.* healthy fibroblasts, following excessive exposure to cancer cells **[68], [69]**. Nevertheless, the TME being composed of both epithelial and endothelial cells, the latter are also considered to be a potential source of CAFs **[70], [71]**. Several reports additionally support the assumption that mesenchymal stem cells, apart from aggravating tumor proliferation, invasion and metastasis **[72]**, are a potential origin for CAFs **[73], [74]**.

Understanding the heterogeneity of cells belonging to the TME is essential for elucidating complex mechanisms and designing novel strategies for precision medicine. CAFs constitute a heterogeneous population **[75]** and concomitant analysis of multiple surface markers across several cancers and species demonstrated the existence of at least four different well-recognized CAFs sub-populations, namely CAFs-S1 to S4 **[76]**. Each CAFs subtype was shown to correlate with characteristic functional processes, suggesting that biomarker signatures of each subpopulation could be achievable. CAFs-S1 and CAFs-S4 are both myofibroblastic activated CAFs whose expressions are strictly restricted to cancer whereas CAFs-S2 and CAFs-S3 are also detected in healthy tissues and could be reminiscent of normal fibroblasts. However, CAFs-S1 are mainly involved in tumor-like phenotypes (*e.g.* immunosuppression, tumor growth and proliferation, inflammation, ECM remodeling), whereas CAFs-S4 are responsible for generic core signaling, motility, and perivascular signatures **[77]**.

1.2.1.4 Metabolic reprogramming of cancer-associated fibroblasts in the tumor microenvironment

As mentioned above, Otto Warburg initially depicted an altered metabolism in cancer cells, epitomizing the first observation of metabolic reprogramming, later recognized in other cells of the TME. It is notably the case of CAFs, which undergo a reverse Warburg effect crosstalk with cancer cells. Indeed, CAFs experience a metabolic switch from OXPHOS to glycolysis for energy production **[78]**, allegedly fueling biosynthetic pathways of cancer cells and contributing to tumor development, invasion, metastasis, and resistance to therapy **[79]**. This glycolytic shift seems driven by transcriptional alterations of glycolytic genes (*e.g.* pyruvate kinase muscle isozyme M2 (PKM2), lactate dehydrogenase (LDH) **[79]**) along with high expression of glycolytic-related transporters (*e.g.* monocarboxylate transporters (MCTs), glucose transporters (GLUTs) **[80]**). Downregulation of isocitrate dehydrogenase 3α (IDH3α), a rate-limiting enzyme of the TCA **[81]**, is also a major driver of the bypass of mitochondrial oxidative pathways. Lipid metabolism seems further correlated with CAFs activation and pathological characteristics. For instance, fatty acid synthase (FASN), a crucial enzyme in fatty acid synthesis, was found to be significantly increased in CAFs, whereas their migration was blocked by knockdown of FASN in colorectal cancer **[82]**. Amino acid metabolism **[83]**, and in particular glutamine metabolism **[84]**, is altered in CAFs, and associated with an increased autophagy of fibroblasts, a potential energy source for promoting the activity of mitochondria in cancer cells. In light of these metabolic alterations observations, various metabolic components have been therapeutically targeted in cancer-associated fibroblasts and show promising results (**Table 1**).

Table 1. List of drugs and compounds targeting cancer-associated fibroblasts metabolism. *HK2: hexokinase 2; GLUT:glucose transporter; MCT: monocarboxylate transporter; LDH: lactate dehydrogenase; PGK: phosphoglycerate kinase; PK: pyruvate kinase; PFK: phosphofructokinase; GAPDH: glyceraldehyde-3-phosphate dehydrogenase; SDH: succinate dehydrogenase*

Metabolic target	Drug or component
HK2	3-Bromopyruvate **[85]** 2-Deoxyglucose **[86], [87]** Lonidamine **[86], [88]** T-Lipo-3-BP **[85]**
GLUT	WZB117 **[89]** Fasentin **[90]** Phloretin **[86]**, **[91]**–**[93]**
MCT	Metformin **[86]**, **[94]**–**[96]** Quercetin **[97], [98]** NAC **[98]**–**[103]** α-Cyano-4-hydroxycinnamic **[96], [104], [105]** Acetylcysteine combined with Topotecan **[99], [106]**
LDH	FX11 **[86], [100], [107]** Oxamate **[103], [108]** Quinoline 3-sulfonamides **[109]** Gossypol **[110]**–**[114]** Galloflavin **[115], [116]** NHI **[117]**–**[119]**
PGK	Adenovirus-shPGK1 **[120]**
PK	Shikonin and analogs **[121]** Alkannin **[82]** PKM2-siRNA **[122]**9/25/2023 7:45:00 AM
PFK	3 PO **[123]**
GAPDH	3-Bromopyruvate **[124], [125]**
SDH	3-Bromopyruvate **[124]**

CAFs further participate in cancer cells metabolic reprogramming through the transfer of metabolites, proteins, and lipids, thereby contributing to sustain their high proliferation rate (**Figure 7**) **[99]**. Several pathways and mechanisms have been suggested to allow CAFs to sustain this high glycolytic flux, including paracrine signals emitted by the cancer cell itself within the TME, but further studies are needed to shed light on this topic. Thus, the development of drug-based therapies for cancer should focus on this reciprocal relationship between cancer cells and fibroblasts.

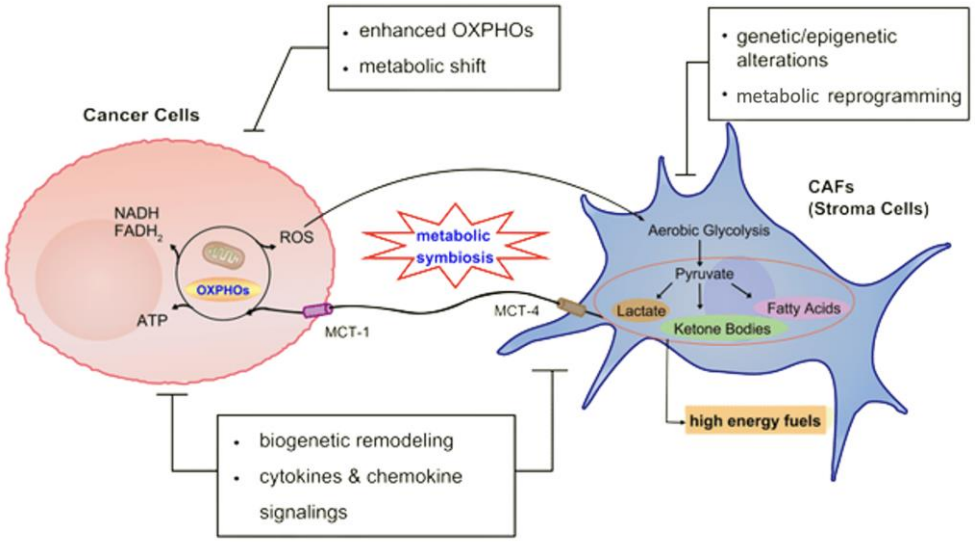

Figure 7. The reverse Warburg effect [99]. Cancer cells may induce oxidative stress in neighboring cancer-associated fibroblasts and secrete reactive oxygen species (ROS), triggering aerobic glycolysis and production of high energy metabolites which are transported to adjacent cancer cells to sustain their anabolic need. In this process, many events occur such as loss of Caveolin-1 in stroma cells, upregulation of mono-carboxylate transporters (MCTs) in both.

As breast cancer (BC) has overtaken lung cancer as the most frequently diagnosed cancer worldwide since 2020 **[38]**, the study of CAFs in this specific cancer has been initiated and some biological data are available. Therefore, we will mainly focus on this type of cancer for the future of this work.

1.2.2 The use-case of an autoimmune disease: rheumatoid arthritis

Rheumatoid arthritis (RA) is the most common type of autoimmune arthritis in the world. It affects approximately 0.46% of the worldwide population **[126]** with geographical disparities attributed to different risk factors exposure, demographic variations, or under-reporting in some regions **[127]**. Resulting from a dysregulated immune system damaging articular structures, RA causes pain, swelling, and stiffness in the joints, ultimately leading to a partial or total loss of function of the affected limbs. Given the increasing proportion of people affected, the over-mortality associated with the disease, and its impact on the patients quality of life through functional, psychological, social, and professional repercussions, RA is considered as a major public health concern **[128]–[130]**. However, this auto-immune disease is still incurable. Current treatments are only symptomatic and restricted to dysregulated immune pathways, characterized by high levels of non-response to treatment and highlighting the need for a broader understanding of RA actors and pathogenesis to propose new therapeutic targets.

1.2.2.1 Physiopathology of rheumatoid arthritis

We commonly identify three stages of disease progression in RA: preclinical RA, early RA, and established RA **[131]** (**Figure 8**). In most patients, the disease pathogenesis begins several years before the appearance of the first symptoms *via* a non-specific inflammatory response to a (yet) unidentified stimulus. The pre-clinical phase of RA is illustrated by a genetic predisposition exacerbated by environmental factors responsible for amino acids post-transcriptional conversion in a wide range of proteins. Such altered peptides are recognized by antigen-presenting cells of the innate immune system and further bind to their surface through the major histocompatibility complex. This phenomenon leads to antigen presentation to T cells, simulating B cells to synthesize a range of antibodies recognizing self-proteins, including rheumatoid factors. Early RA is characterized by synovial inflammation based on mononuclear cell infiltration, dominated by $CD4^+$ T cells and macrophages, together with early stromal cell activation initiated in the preclinical phase. At this point, synovial hyperplasia is the main hallmark of RA and the key contributor to the invasive pannus formation. In a healthy joint, the inner layer of the joint capsule, the synovial membrane (or synovium), is a thin lining serving as a source of nutrients for cartilage and synthesizing joint lubricants. It consists of two main sub-layers: the synovial lining or intimal layer, primarily composed of rheumatoid arthritis synovial fibroblasts (RASFs) and macrophages, and the subintimal area of the synovium including mainly the vascular system of the joint. In RA, the synovial lining is greatly hypertrophied, forming a hyperplastic pannus, and the subintimal zone is heavily infiltrated with inflammatory cells (*e.g.* T cells, B cells, lymphocytes, macrophages, mast cells, mononuclear cells), elevating cytokines secretions and ultimately eroding surrounding cartilage and bone **[132]**.

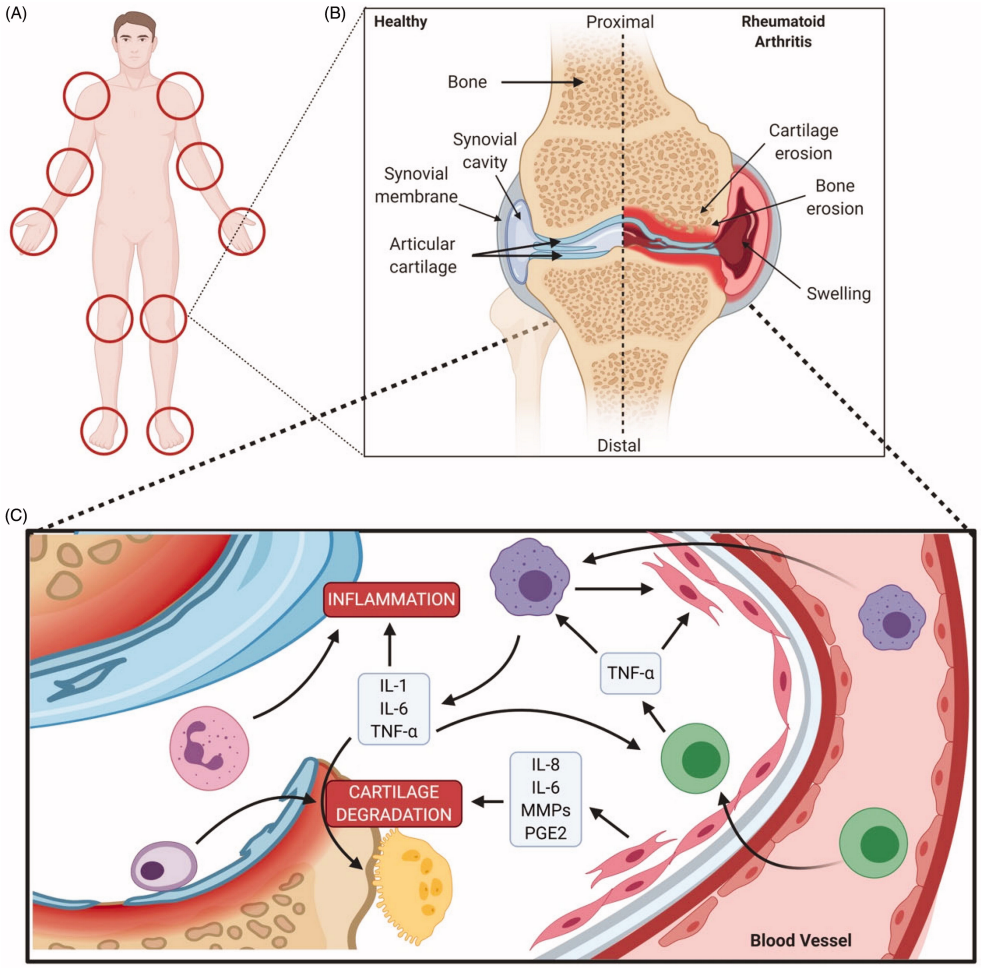

Figure 8. Physiopathology of rheumatoid arthritis (RA) [133]. (A) Locations of mainly impacted articulations in RA. Unlike other arthritic conditions, joints are affected symmetrically. **(B)** A healthy synovial joint and the impact of RA: in a healthy joint (left), there is no swelling in the synovial joint capsule, cartilage and bone are intact. Whereas in RA (right), there is swelling, cartilage and bone erosion. **(C)** Mechanism of RA within the joint capsule. TNF alpha impacts synoviocytes, macrophages/monocytes and osteoclasts; initiating RA pathogenesis. Synoviocytes line the capsule and T-cells infiltrate the synovial membrane, initiating inflammation *via* TNF alpha. Joint degradation occurs *via* recruitment of macrophages and secretion of inflammatory cytokines. Bone erosion occurs by osteoclasts and inhibition of collagen secretion by synoviocytes. *IL-1: interleukin 1; IL-6: interleukin 6; TNF-α: tumor necrosis factor alpha; MMPs: matrix metalloproteinases; PGE2: prostaglandin E2.*

The effusion of synovial fluid in the joint due to the thinning of the synovial capsule gradually leads to swelling and pain **[131]**. RASFs are recognized as key coordinators of this phase as they recruit cytokines and proteases to maintain the inflammatory state along with enzymes responsible for the degradation of the ECM. Established RA refers to the result of sustained immune infiltration in a chronic inflammation of the synovial membrane leading to deformation and destruction of the joints. RASFs maintain this phase by spreading to neighboring tissues, greatly propagating the disease.

1.2.2.2 Etiology and treatment of rheumatoid arthritis

Although the last decades were filled with remarkable progress on our knowledge of RA and it is now widely recognized that the disease is triggered by a dysfunction of the immune system, its precise etiology is not yet fully established. Similarly to cancer, RA is considered to be a complex disease as it is suspected to arise, develop, and be maintained through complex interactions between multiple factors throughout the different stages of the disease (**Figure 9**). First identified factors were susceptibility genes such as the HLA-DRB1 motif, encoding the P4 peptide-binding pocket, known as the shared epitope **[134], [135]** laterly followed by non-HLA-associated relevant genes **[136]**. Epigenomics studies further identified three main epigenetic alterations factors associated with RA, namely aberrant DNA methylation, abnormal histone modification, and unusual expression of small non-coding RNAs (mainly microRNAs) **[137]**. Beyond coding and non-coding gene alterations, the impact of environmental factors on the disease onset and development is now widely recognized **[138]**, including smoking **[139]**, air pollution and exposure to dust **[140]**, or excessive body weight **[141]**. Additionally, RA female-to-male prevalence ratio having consistently been established at 3:1 **[142]** along with modifications in disease activity during

pregnancy **[143]**, hormonal factors have been suspected to play a role **[144]**. Finally, two more controversial risk factors for RA are microbial infections **[145]** or the psychological cause **[146]** such as a traumatic event as a trigger for the disease.

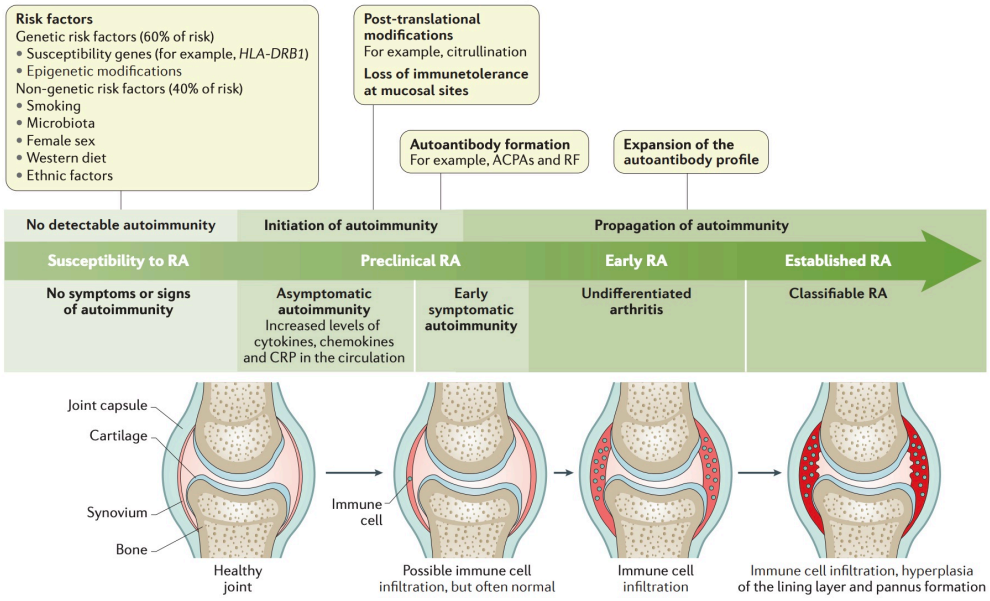

Figure 9. Development and progression of rheumatoid arthritis according to its different risk factors [131]. Both genetic and non-genetic risk factors contribute to the disease and multiple risk factors are likely required before a threshold is reached above which RA is triggered. *ACPA: anti-citrullinated protein antibody; CRP: C-reactive protein; RF: rheumatoid factor.*

The etiological complexity and fragmented knowledge regarding the disease physiopathology directly contribute to the lack of cure for RA. Although various treatment options are available, they all aim to reduce symptoms (*e.g.* inflammation, chronic pain) or slow down joint damage in order to improve the overall patients quality of life. Disease-modifying antirheumatic drugs (DMARDs) can be used to promote remission by slowing or stopping disease

progression **[147]**. They are immunosuppressive and immunomodulatory agents each having a unique mechanism of action but overall interfering with critical pathways of the inflammatory cascade. They are commonly classified into conventional DMARDs (*e.g.* methotrexate, leflunomide, hydroxychloroquine, and sulfasalazine), targeting the entire immune system, and biological DMARDs (*e.g.* infliximab, etanercept, adalimumab, abatacept, tofacitinib), targeting specific sub-processes. Nonsteroidal anti-inflammatory drugs (NSAIDs) such as acetylsalicylate, naproxen, or ibuprofen are also commonly administered to RA patients to relieve chronic pain and decrease inflammation. Their mode of action is more comprehensive as they inhibit the enzymatic activity of COX molecules and reduce inflammation by targeting prostaglandin synthesis **[148]**. Finally, steroids, also called corticosteroids, have powerful anti-inflammatory effects in RA as they quickly improve chronic pain, stiffness, and decrease joint swelling by addressing leukocytes functioning **[149]**. They are typically prescribed for short-term use to reduce flare-ups and mainly include prednisone, prednisolone, hydrocortisone, methylprednisolone acetate, and triamcinolone.

Beyond the inherent toxicity of each prescribed drug, the most concerning adverse side effect of currently administered RA treatments is an increased risk of common and serious infections, including bacterial, fungal, and viral infections, generally due to the patients state of immunodeficiency **[150]**. Additionally, despite the various options presented above, 30–40% of RA patients do not respond significantly to treatment and are in a state of therapeutic distress **[151], [152]**, emphasizing the need for alternative therapeutic strategies. Such innovations require a better understanding of the disease and its various cellular actors to broaden the therapeutic fields of application beyond the sole immune system.

1.2.2.3 Rheumatoid arthritis synovial fibroblasts, key players of the rheumatic joint

RASFs are the primary constituents of the hyperplastic pannus and play a key role in its formation and maintenance, and consequently, in RA pathogenesis **[153]**. In healthy joints, fibroblasts create a one-or-two-cells thick layer, punctuated by tissue-resident macrophages, and guarantee the structural integrity of the intimal layer along with its nutrient supply. However, in RA, they tend to exhibit very distinct characteristics in terms of phenotype, morphology, and gene expression patterns as they become key drivers of the disease **[154]** (**Figure 10**). Fassbender first described the distinct morphological features of RASFs in the early 1980s, which were later confirmed by morphofunctional analysis, namely abundant cytoplasm, dense endoplasmic reticula, and large and pale nuclei with several prominent nucleoli **[155], [156]**. Additionally, RASFs exhibit several tumor-like behaviors, such as reduced contact inhibition and resistance to apoptosis, demonstrating a continuous growth process **[153]**. Their increased ability to migrate and invade periarticular tissues, including bone and cartilage, contributes to the destruction of the latter **[154], [157]**. Indeed, they express highly altered levels of adhesion molecules, cytokines, chemokines, and matrix-degrading enzymes, causing cartilage damage and mediating the interaction with neighboring inflammatory and endothelial cells **[158]**. Finally, RASFs can be considered as primary drivers of inflammation and angiogenesis **[154]**. Overall, they disturb the homeostatic balance between leukocyte recruitment, proliferation, emigration, and death, leading to a persistent leukocyte infiltration, maintaining synovial inflammation. In this way, RASFs are no longer considered as passive bystanders, but as active players in RA pathogenesis and sustained chronicity. However, currently administered therapies in RA greatly overlook their crucial role.

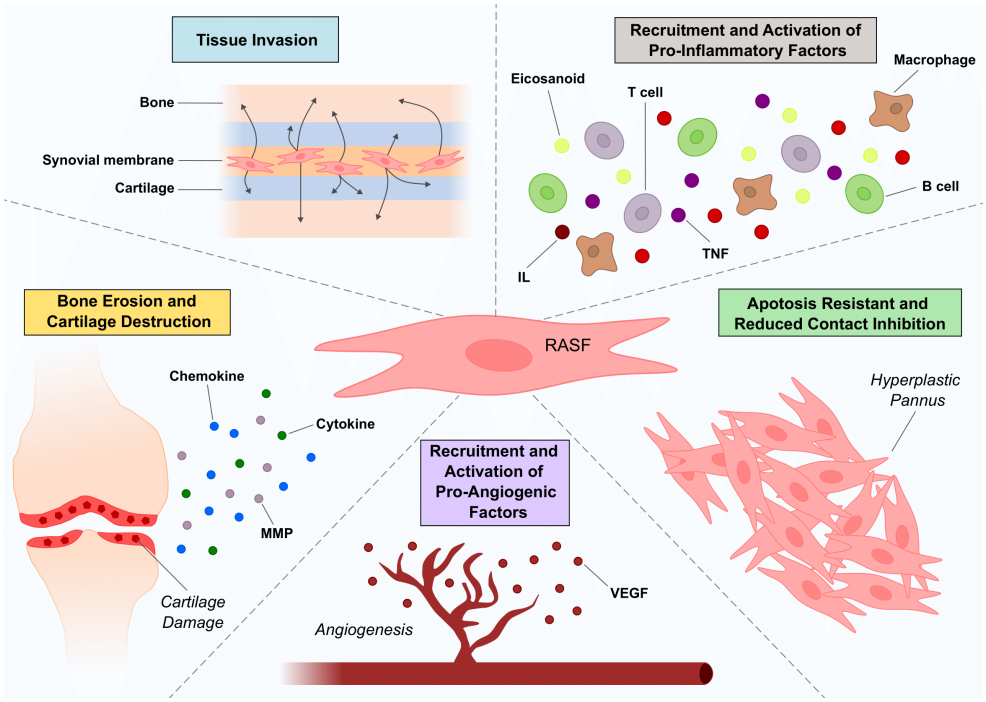

Figure 10. Key roles of rheumatoid arthritis synovial fibroblasts (RASFs) in rheumatoid arthritis pathogenesis and progression. RASFs are involved in a wide range of pathogenic mechanisms including recruitment and activation of pro-angiogenic, pro-inflammatory factors, bone erosive and cartilage destructive factors, apoptosis resistance and reduced contact inhibition, along with tissue invasion and proliferation, overall perpetuating inflammation and responsible for cartilage destruction, exacerbating joint damage. *TNF: tumor necrosis factor; IL: interleukin; VEGF: vascular endothelial growth factor; MMP: matrix metalloproteinase.*

The origin of RASFs remains quite elusive and numerous hypotheses have been considered. Despite early assumptions suggesting differentiation of RASFs from $CD34^+$ bone marrow cells in RA patients **[159]**, the main theory to date relies on a global mesenchymal stem cell descent for RASFs **[160]**. RASFs are recognized to express certain common fibroblasts markers, including expression of collagens (type IV and V), fibroblast activating protein, vimentin, and CD90 along with unique RASF-specific surface markers. The latter may vary between multiple RASF populations and predict

different localization, function, and role in RA pathogenesis **[161]**. They are further being investigated as potential therapeutic targets in RA **[162]**.

1.2.2.4 Metabolic reprogramming of rheumatoid arthritis synovial fibroblasts in the rheumatic joint

RA disease activity scores, inflammatory markers, and extra-articular manifestations have repeatedly shown significant associations with metabolic disorders **[163], [164]**. Moreover, fibroblasts activation within an RA-affected immune system have been associated with metabolic disruptions (**Figure 11**) **[165]**. Energy production pathways appear significantly altered with an increase in glucose metabolism, hallmark of cells of aggressive phenotype. Indeed, an increase in RA patients serum glucose along with elevated glucose consumption are reported **[165]** while the very breakdown of glucose is altered in RASFs. A significant decrease in mitochondrial energy production is depicted **[166]** along with enhancement of glycolytic genetic activity, notably its main effectors, hexokinase 2 (HK2), 6-phosphofructo-2-kinase/fructose-2,6-bisphosphatase 3 (PFKFB3), pyruvate kinase isozyme M2 (PKM2), and glucose transporter 1 (GLUT1) **[165]**. RASFs increase in glycolytic activity may also be reflected by the increase of lactate in patients serum, its main by-product **[167]**.

Besides the glycolytic increase, RASFs metabolic profiling illustrates major alterations in other classes of macromolecules with contributions to the maintenance of their aggressive phenotype. Mitochondrial genes associated with apoptosis, redox balance, and protein transport are disturbed **[168]**. A high glutamine metabolism is depicted while the enzyme glutaminase 1 (GLS1) is involved in RASFs proliferation **[169]**. Free fatty acids (FFA) are increased, which may directly contribute to articular inflammation and

degradation in inflammatory joint diseases. Choline metabolism is highly active **[170]**, linked to malignancy, invasion, and metastasis in multiple cancers **[171], [172]**. Impaired metabolic pathways reprogram energy production but their by-products also benefit RASFs. For instance, lactate, glutamine, and succinate are involved in the maintenance of inflammation along with RASFs invasive phenotype **[173]**.

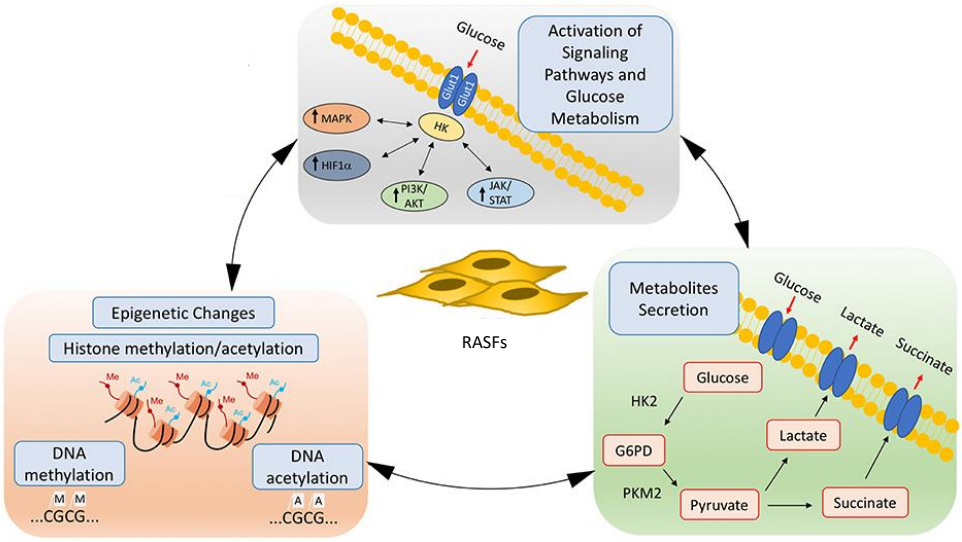

Figure 11. Rheumatoid arthritis synovial fibroblasts (RASFs) glucose metabolism and chronic activation in rheumatoid arthritis [165]. Chronic glucose metabolic changes induced by inflammatory mediators in RASFs will activate many signaling pathways, including HIF, MAPK, PI3K/Akt, and JAK/STAT pathways, which also increases the expression of key glucose metabolism related genes such as GLUT1, HK2, or LDH. Intermediate glucose metabolites including pyruvate, lactate, succinate, a-ketoglutarate, fumarate, and acetyl-coenzyme will create a chronic and sustained RASFs activation, either by being secreted extracellularly and triggering profound effects on the biology of other cells, or by inducing a new epigenetic landscape that results in a stable RASFs activation that is maintained even without continuous stimulation. *HK2: hexokinase 2; G6PD: glucose 6 phosphate dehydrogenase; PKM2: pyruvate kinase muscle isozyme M2.*

As these metabolic alterations are involved in various of RASFs aggressive phenotypes, experimental studies investigated specific components inhibition and reported promising findings (**Table 2**).

Table 2. List of drugs and compounds targeting rheumatoid arthritis synovial fibroblasts metabolism. *HK2: hexokinase 2; GLUT: glucose transporter; MCT: monocarboxylate transporter; LDH: lactate dehydrogenase; PGK: phosphoglycerate kinase; PK: pyruvate kinase; PFK: phosphofructokinase; GAPDH: glyceraldehyde-3-phosphate dehydrogenase; SDH: succinate dehydrogenase.*

Metabolic target	Drug or component
HK2	3-Bromopyruvate **[174]–[179]** 2-Deoxyglucose **[174]** Lonidamine **[175]** Tofacitinib **[180]**
GLUT	WZB117 **[8]** Tumor Necrosis Factor-α inhibitor **[181]**9/25/2023 7:45:00 AM
MCT	Metformin **[174], [181], [182]** MCT4-siRNA **[183]**
LDH	Tofacitinib **[180]**
PGK	PGK1-SiRNA **[176]**
PK	TEPP-46 **[8]** Tumor Necrosis Factor-α inhibitor **[181]**
PFK	3 PO **[181]** PFK15 **[184], [185]** PFKFB3-SiRNA **[183]**
GAPDH	Heptelidic Acid **[8]** Tumor Necrosis Factor-α inhibitor **[181]**
SDH	Saponin **[92]** Dimethyl Malonate **[186]**

In light of the various observations of immunometabolic crosstalks and alterations, focused and targeted therapy against certain metabolic components in one of RA key players, namely RASFs, represents a promising lead in the treatment of this disease. However, few hypotheses still exist regarding the activating signal of RASFs metabolic reprogramming. The main one is obviously a response to a wide range of paracrine signals (*e.g.* cytokines, chemokines, growth factors) emitted in the RA joint, but the exact signaling cascade and emitting party are still under investigation. Indeed, once RASFs metabolic alterations are identified, it is necessary to understand their initiation and precise origin to successfully address them therapeutically.

1.3 CONTRIBUTIONS OF COMPUTATIONAL APPROACHES IN UNRAVELING MULTILAYER BIOLOGICAL MECHANISMS

Biological processes rely on complex interactions between thousands of molecules at different scales and with their environment, creating complex interaction networks whose disruption can lead to pathologies. Although increasingly studied and clearly demonstrating the joint involvement of metabolism and immunity in pathological mechanisms, the applications of immunometabolism in therapy development remain poorly exploited. In particular due to the difficulty to unravel an integrated overview of the various biological mechanisms involved, of which the principals are pathogenic gene regulation, cellular signaling, and metabolism. To decipher the key mechanisms and actors driving fibroblasts metabolic reprogramming in diseases as complex as rheumatoid arthritis and breast cancer, an integrative and comprehensive overview is necessary. Computational methods can help address this issue and contribute to the progress of biological discoveries.

1.3.1 Molecular interaction maps as static knowledge bases

The mapping and accurate mechanistic representation of implicated pathways is an essential step to study the various mechanisms underlying disease pathogenesis. In addition, the increased interest in biological interactions has generated a large influx of biological data to process, highlighting the need for visualization and simplification of complex information to obtain clear insights on cellular functioning.

In this context, molecular interaction maps emerged as high-quality representations of disease-associated processes acting as comprehensive knowledge bases. First introduced in 1999 by Kurt W. Kohn **[187]**, they are organized, unambiguous, and curated representations of known biological and biochemical interactions in a visual form spanning across various types of reactions (*e.g.* formation of multi-subunit complexes, chemical modification of proteins, movement in cellular compartments) and biological processes (*e.g.* extra- and intra-cellular signaling, transcription, translation, metabolism) while removing the noise that may arise from automatically inferred interaction networks. Such standardized networks can be constructed either employing top-down approaches, including reverse engineering using machine learning algorithms and omics data or a bottom-up approach, starting with text mining and literature curation **[188]**. Initially introduced with their own notation (*i.e.* system of symbols and syntactic conventions), the construction of molecular interaction maps was later formalized with the Systems Biology Graphical Notation (SBGN) **[189]**, an international effort to standardize diagrams depicting biochemical and cellular processes studied in systems biology. Molecular interaction maps have been massively developed to study both biological mechanisms (*e.g.* P53 and MDM2 relationship **[190]**, mTOR signaling **[191]**, gastrin and cholecystokinin receptors functioning **[192]**, MAPK network influence on cancer cell fate **[193]**) and diseases (*e.g.*

COVID-19 **[194]**, asthma **[195]**, cystic fibrosis **[196]**, Parkinson's disease **[197]**). The latter may serve as stand-alone knowledge bases, comprehensive templates for visualization and analysis of omics datasets, or can be analyzed in terms of the underlying network structure to identify distinct biological clusters or highly connected nodes.

In 2010, a comprehensive RA-specific map was published **[198]** based on high-throughput experiments, literature, publicly available datasets, and KEGG pathway database **[199]**. A decade later, in 2020, a second effort to formalize RA knowledge was published using the first map as a basis, the RA-map **[200]** (**Figure 12**). It is a fully annotated, expert validated, state-of-the-art molecular interaction map illustrating the major molecular and signaling pathways involved in disease pathogenesis in an SBGN-compliant format. The RA-map was manually curated for each component and reaction, with defined cellular pathways and molecular signatures under thorough expert validation. In addition to manual curation of the scientific literature, other sources such as the Ingenuity Pathway Analysis (IPA) **[201]** or KEGG pathway **[199]** databases were used to obtain RA molecular pathways and phenotypic signatures information. While this RA-map offers a formalized representation of the major pathways implicated in the disease, it does not cover metabolic processes. Additionally, the map was built as a global map using information from multiple human RA studies, focusing on small-scale experiments in various cell and tissue types (*e.g.* fibroblasts, macrophages, synovial tissue, peripheral blood mononuclear cells), and is not RASF-specific.

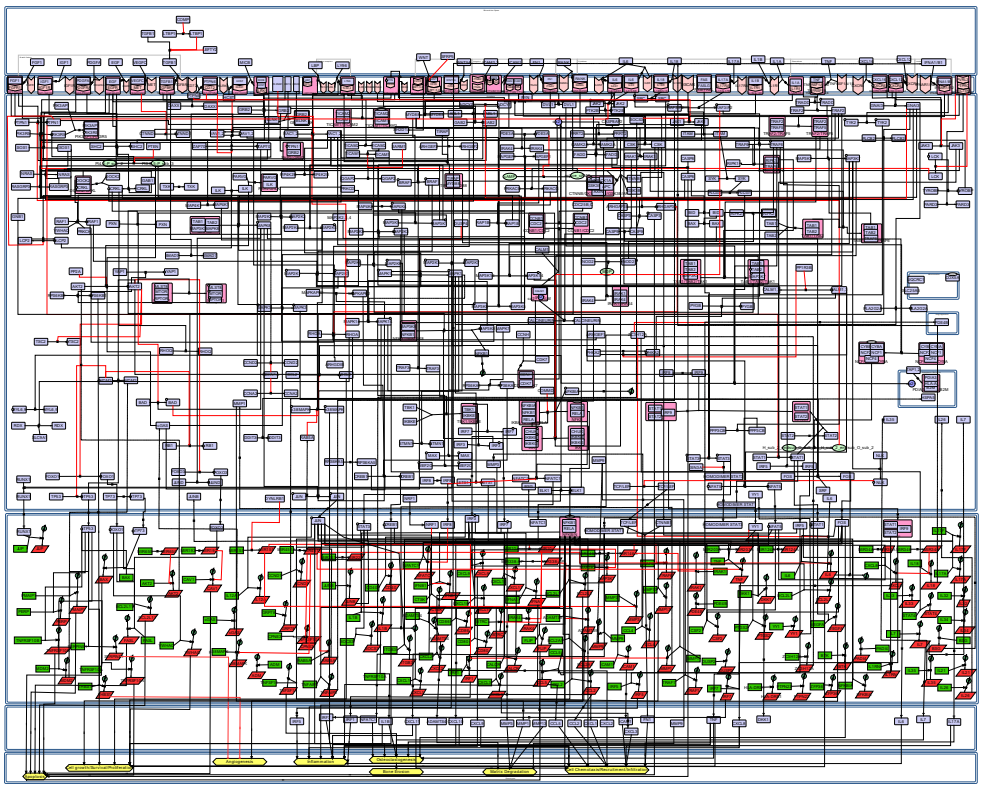

Figure 12. Snapshot of the RA-map [200]. The map is color-coded with proteins in purple, genes in green, RNAs in red and phenotypes in yellow. State transitions and catalysis reactions are displayed in black, and the inhibitions are in red. Compartments are distinguished as bounding boxes.

Regarding cancer-related mechanisms, several attempts to create graphical representations have emerged, such as the Cancer Cell Map Initiative **[202]** or the human tumor atlas network **[203]**, regrouping several detailed molecular and cellular maps. Although the latter molecular interaction maps focus essentially on the TME, fibroblasts are poorly represented. The Atlas of Cancer Signaling Networks (ACSN) **[204]**, a web-based resource of biological maps depicting molecular processes in cancer cells and TME, tried to address this issue. It uses Google Maps™ engine to navigate through different altered pathways, species, and disease mechanisms in diverse

biological systems responsible for cancer progression (*e.g.* angiogenesis, TME, adaptive immune response). The ACSN includes a SBGN-compliant CAF-map (**Figure 13**), representing the molecular interactions between TME and CAFs along with their role within carcinogenesis. All nodes and interactions are derived from biomining of the literature and cross references of species thanks to several databases such as HGNC **[205]**, Uniprot **[206]**, or Genecards **[207], [208]**. However, the ACSN CAF-map poorly covers metabolic processes and their impact upon CAFs aggressive behaviors. Additionally, it is not cancer-specific but rather gathers information from multiple types of cancer.

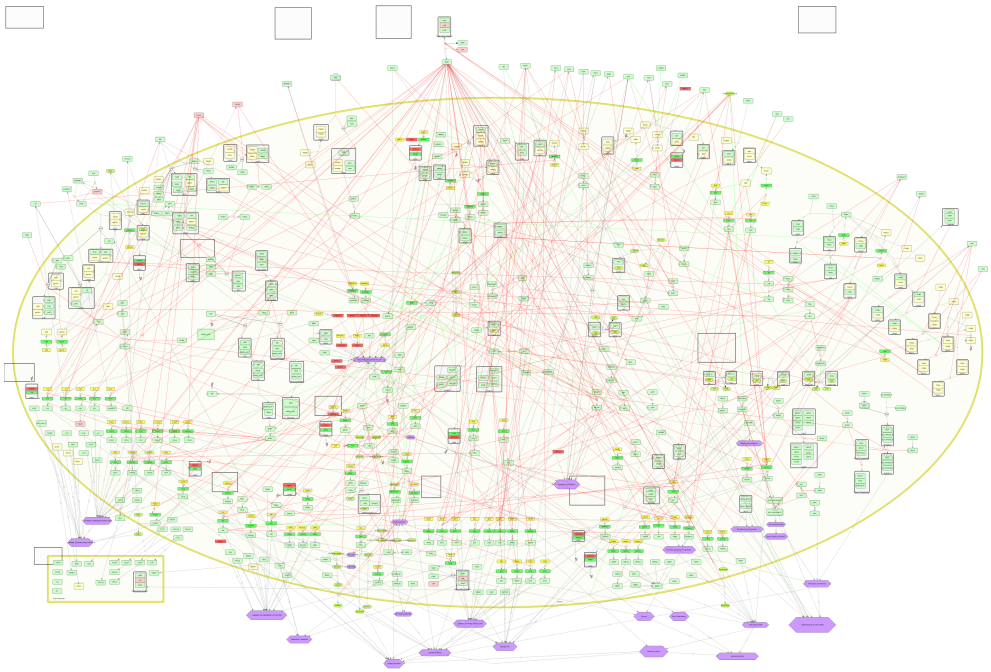

Figure 13. The CAF-map within the Atlas of Cancer Signaling Network [204]. This CAF-specific comprehensive map, manually curated from the literature, represents CAFs molecular interactions in tumors. The map is color-coded with proteins in light green, genes in yellow, RNAs in dark green, antisense RNAs in red, and phenotypes in purple. State transitions and catalysis reactions are displayed in black, and the inhibitions are in red.

Such molecular interaction maps represent great resources, however, they are mainly focused on signaling processes and the corresponding metabolic pathways are often absent or underrepresented. To the best of our knowledge, efforts to reconstruct a generic human cell metabolic network have been ongoing with the creation of the ReconMap **[209]** (**Figure 14**) based on the human metabolic atlas **[210]**. Its access through the virtual metabolic human (VMH) database allows easy navigation and search of information on human and gut microbial metabolism along with links to hundreds of diseases and nutritional data. However, these metabolic reconstructions are often greatly focused on downstream events and completely lack upstream regulators linking these networks to signaling cascades and gene regulation processes.

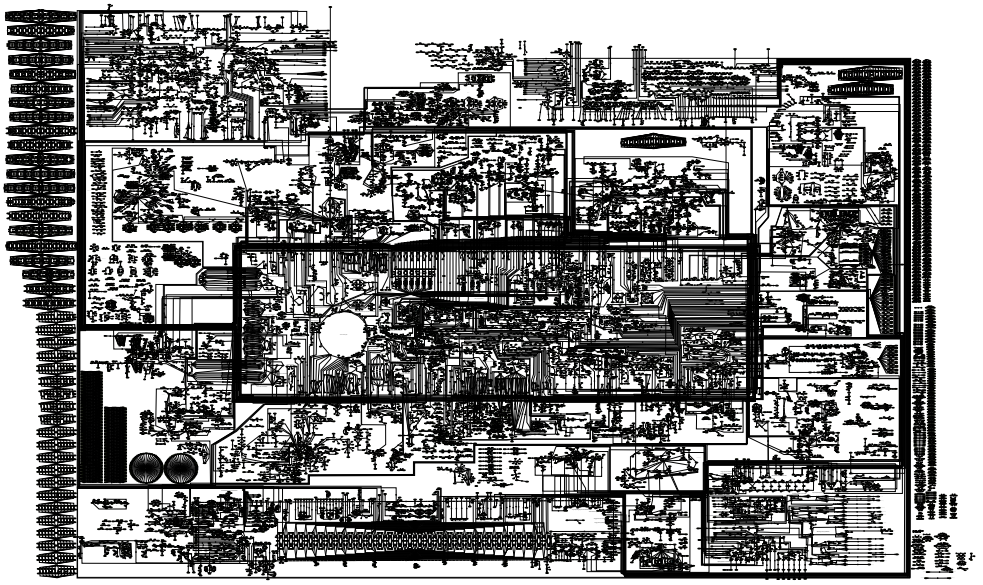

Figure 14. The ReconMap interactive visualization of human metabolism [209]. The ReconMap is a comprehensive visual reconstruction of Recon 2, a genome-scale reconstruction of human metabolism.

1.3.2 Computational modeling to unravel dynamic properties

Molecular interaction maps have emerged as a meaningful way of representing biological mechanisms in a comprehensive and systematic manner. However, all living systems are by definition dynamic. Thus, static graphical representations of molecular and cellular networks can provide useful but limited information on the mechanisms underlying disease pathogenesis, progression, severity, or even response to treatment. In this context, dynamical studies and modeling can reveal critical information about the global behavior of the system under various conditions by performing *in-silico* simulations, perturbation experiments, hypotheses-testing, and predictions. Various modeling formalisms exist, more or less adapted to account for different biological processes.

Qualitative models based on logical relationships among components provide an appropriate description for systems with unknown mechanistic foundations or lacking precise quantitative data **[211]**. In this context, logical models are the most powerful tools to decipher complex biological processes in a qualitative way, especially Boolean models **[212], [213]**. Boolean models (**Figure 15**) allow the parameter-free study of large-size biological pathways underlying dynamic properties. In the Boolean formalism, nodes represent regulatory components and arcs represent their interactions. Each node is associated with a Boolean value (0 or 1), indicating its qualitative concentration (*i.e.* absent or present) or activity level (*i.e.* inactive or active). The state of each node depends on the combination of its upstream regulators state and is described by a Boolean rule defined by the logical operators "AND", "OR", and "NOT". Boolean models can be updated in the "synchronous" mode, where all nodes are updated simultaneously, or in the "asynchronous" mode, where nodes are updated one by one. Such formalism is particularly suited for influence networks depicting cellular signaling or

gene regulation pathways carrying signal flow. Within our scope, it would enable us to investigate the dynamic regulatory and genetic mechanisms driving the pathogenesis of RASFs in the RA joint or breast CAFs in the TME.

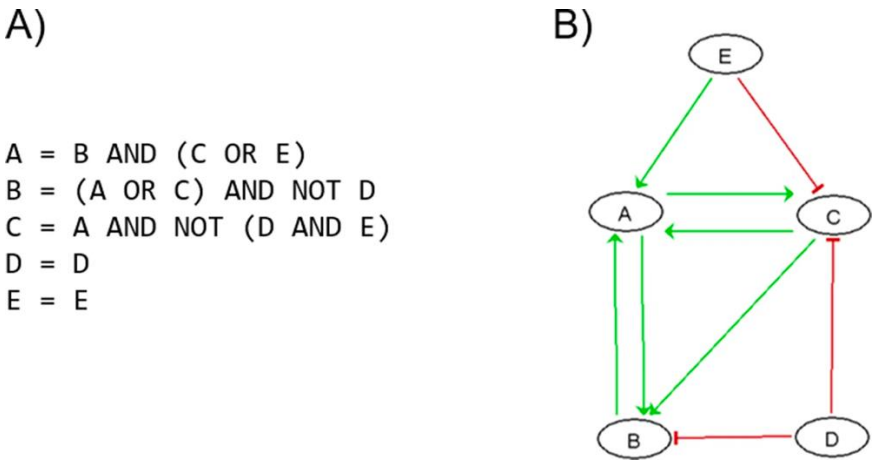

Figure 15. Example of a Boolean toy model. (A) Boolean rules associated with the **(B)** Boolean network where arcs (interactions) between nodes (components) are subdivided in activations, in green, and inhibitions, in red.

Although quite powerful, qualitative computational modeling approaches have not been widely applied to improve understanding of RA, with the notable exception of a recently published large-scale Boolean model of RASFs **[214]**. Covering the major phenotypes of apoptosis, cell proliferation, matrix degradation, bone erosion, and inflammation, its main purpose was to reproduce the effect of single or combined treatments and predict new molecular targets and drug candidates. Including the major pathways of signaling and gene regulation involved in RA pathogenesis, this model is however limited by its lack of coverage of metabolic pathways. In the cancer field, Boolean models have been widely used to study abnormal

tumor signaling pathways with patient-specific models of signaling networks for personalized treatments **[215]** along with impact of EMT transition in cancer-associated phenotypes **[216]**. However, the role of CAFs in the TME have not been studied, let-alone in a cancer specific manner.

Despite being well-suited to account for the modeling of signaling and gene regulation mechanisms, qualitative modeling is not appropriate to assess quantitative metabolic properties. Where signaling and gene regulation carry signal flow, metabolism generates mass flow, requiring a specific modeling formalism. In this biological context, a widely used approach for analyzing metabolic networks is a constraint-based method, namely Flux Balance Analysis (FBA). The latter is a mathematical method used in large-scale reconstructions of metabolic networks to analyze the flow of metabolites **[217]**. Its main advantage lies in the need for little information regarding enzymes kinetic parameters and metabolites concentrations as it calculates the flow of metabolites by assuming steady state conditions (**Figure 16**). Thus, FBAs are computationally inexpensive and very suitable for genome-wide reconstructions of human metabolism.

Metabolic profiling has gained significant attention in the RA joint, however, to our knowledge, there is no modeling effort to construct RA-specific metabolic networks or assess metabolic dynamics in the RA joint, regardless of the cell type of interest. Some attempts were carried out in the field of cancer, to predict selective drug targets in cancer through metabolic network analysis **[218]**, to study cancer cells Warburg effect **[219]**, or for drug development purposes **[220]**. However, there is no metabolic reconstruction covering the functioning of CAFs and their involvement in the TME.

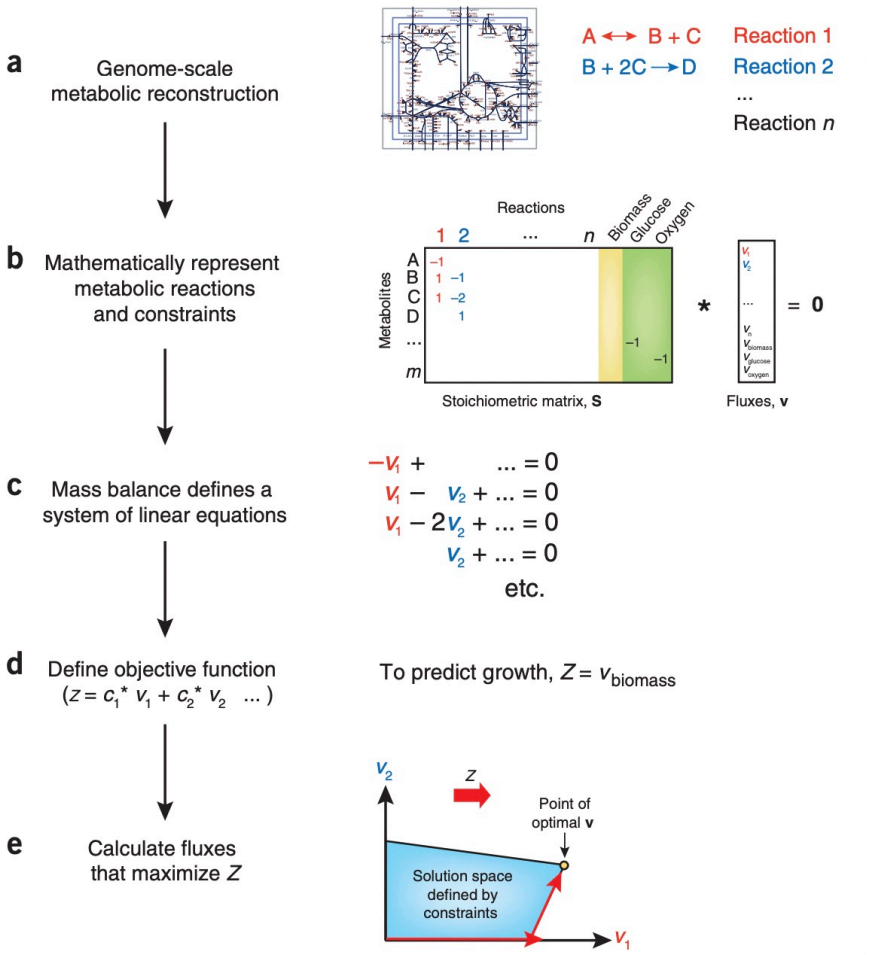

Figure 16. Graphical summary of the formulation of an FBA problem [217]. **(a)** First, a metabolic network reconstruction is built, consisting of a list of stoichiometrically balanced biochemical reactions. **(b)** Next, this reconstruction is converted into a mathematical model by forming a matrix (labeled S) in which each row represents a metabolite and each column represents a reaction. **(c)** At steady state, the flux through each reaction is given by the equation Sv = 0. Since there are more reactions than metabolites in large models, there is more than one possible solution to this equation. **(d)** An objective function is defined as Z = cTv, where c is a vector of weights (indicating how much each reaction contributes to the objective function). In practice, when only one reaction is desired for maximization or minimization, c is a vector of zeros with a one at the position of the reaction of interest. When simulating growth, the objective function will have a 1 at the position of the biomass reaction. **(e)** Finally, linear programming can be used to identify a particular flux distribution that maximizes or minimizes this objective function while observing the constraints imposed by the mass balance equations and reaction bounds.

1.3.3 Hybrid modeling to decipher integrated processes

According to the central doctrine of immunometabolism, namely the tight interconnections between immune regulatory processes and metabolic machinery, leveraging qualitative and quantitative modeling formalisms independently is not suitable to assess the dynamic impact of signaling and genetic pathways upon metabolism, let alone in cell- and disease-specific contexts. It is rather necessary to integrate the dynamic study of these various biological layers to unravel RASFs and breast CAFs metabolic reprogramming.

In this sense, a few tools and frameworks have been developed in the last decade. The probabilistic integrative modeling of genome-scale metabolic and regulatory networks (PROM) method **[221]** attempts to combine transcriptional regulatory networks with the corresponding metabolic network by integrating high-throughput data into constraint-based modeling. This tool, ideal for constructing genome-scale regulatory-metabolic network models for less-studied organisms, might suffer from the limitations of automatic reconstructions, namely not-curated reconstruction of improper gene-protein-reactions rules leading to incorrect compartmentalization of reactions or directionality constraints along with incorrect metabolic rates. The FlexFlux tool **[222]** further tries to bridge the gap between regulatory and metabolic networks analysis through the combination of FBA and qualitative simulations by seeking regulatory steady states through synchronous updates of multi-state qualitative initial values to constrain FBA fluxes. Although covering multiple types of regulatory and metabolic analysis, FlexFlux requires initial values and qualitative states to user-defined continuous intervals equivalences for every component of large-scale regulatory models, a daunting task when trying to tackle large-scale and complex pathogenic mechanisms. A more recent framework is the regulatory dynamic enzyme-

cost flux balance analysis method (r-deFBA) **[223]**, which combines dynamic modeling of metabolism and transcriptional regulation to account for regulatory events in a discrete-continuous setting. Again, this strategy is limited by the need for pre-defined transcription factors to target gene relationships for components of large-scale networks. Other approaches combining regulation and metabolic analysis have been proposed but, to our knowledge, none of them is able to successfully combine reliability on the interactions depicted in large-scale networks, lack of omics data in poorly addressed biological fields such as RASFs and breast CAFs, along with powerful regulatory analysis, all necessary features for the proper analysis of RASFs and breast CAFs metabolic reprogramming. This observation highlights a need for an innovative computational framework allowing simultaneous simulations of signal (*i.e.* cellular signaling and gene regulation) along with mass (*i.e.* metabolic processes) flow to decipher complex and multi-layer biological mechanisms.

Associated scientific communication, details here

The state-of-the-art in metabolic reprogramming of RASFs and CAFs along with computational approaches of interest were published in a review of literature:

Aghakhani, S; Zerrouk, N; Niarakis, A. Metabolic reprogramming of fibroblasts as therapeutic target in rheumatoid arthritis and cancer: deciphering key mechanisms using computational systems Biology Approaches. *Cancers* **2021**, 13, 35. https://doi.org/10.3390/cancers13010035

2 OBJECTIVES OF THE PHD THESIS

Metabolic alterations in fibroblasts appear to exert a determining role in the acquisition of an aggressive phenotype and their pathogenic activity in RA and BC. Transformations of healthy fibroblasts into RASFs, characterized by increased proliferation and resistance to apoptosis, contribute to the chronicity of RA and sustained joint inflammation. Same goes with breast CAFs and their interaction with cancer cells contributing to tumor growth, invasion, and resistance to therapy.

Immunometabolic targeting suggests that repolarization of immune-related cells, such as RASFs and breast CAFs, to healthy and non-aggressive phenotypes through manipulation of their metabolism might represent a promising approach to decrease their key pathogenic activity. This therapeutic opportunity might additionally allow for cellular selectivity in the regulation of immune responses through the differential metabolic requirements of these cells of aggressive phenotypes.

To address RASFs and breast CAFs metabolic requirements, it is necessary to unravel their complex processes and identify their master regulatory driver(s). In view of the similarity of cellular actors in these two complex diseases and the metabolic alterations they seem to undergo, their joint study seems beneficial to explore new opportunities.

Computational methods appear well suited to drive new biological knowledge in complex and still uncured diseases by integrating various biological layers and exploiting their static and dynamic features. A hybrid modeling formalism, covering the various biological features of pathogenic gene regulation, signaling, and metabolism may account for RASFs and breast CAFs dynamic immuno-metabolic interconnections.

In this context, the main objective of this PhD thesis is to leverage computational approaches to decipher the mechanisms underlying the transformation of RASFs and breast CAFs, key players in the associated disease pathogenesis, through their metabolic reprogramming and further propose innovative therapeutic targets (**Figure 17**). This objective will be achieved by:

(1) Leveraging static and dynamic computational approaches in the cell- and disease-specific contexts of RASFs and breast CAFs covering cellular signaling, gene regulation, and metabolism to decipher fibroblasts emerging behavior under disease-specific conditions integrating multiple biological machineries.

(2) Proposing a potential mechanism (common or not) explaining fibroblasts metabolic reprogramming in disease-specific conditions by studying the dynamic impacts of RASFs and breast CAFs gene regulation and signaling pathways upon their metabolic processes along with identifying key regulator(s).

(3) Suggesting new therapeutic targets in drug development for RA and BC immune-mediated diseases from insights into RASFs and CAFs metabolic reprogramming.

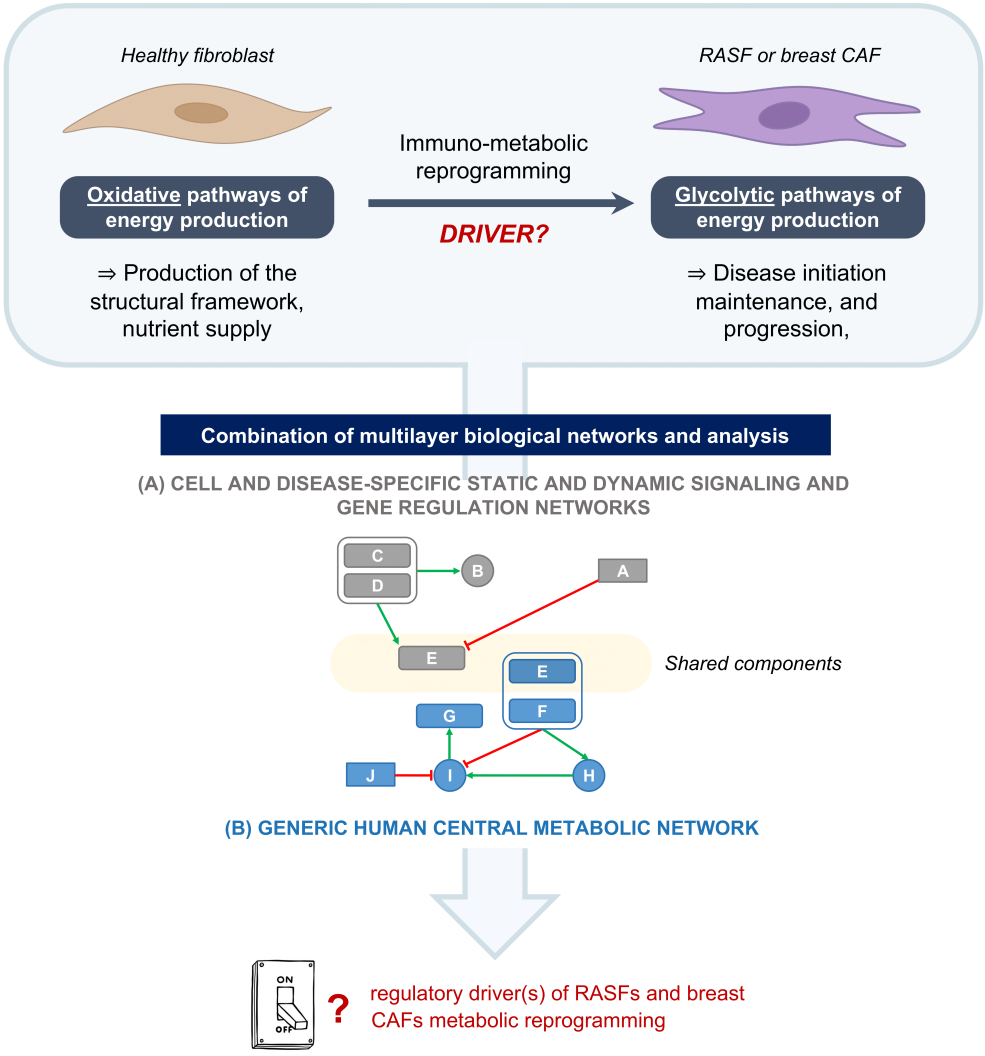

Figure 17. Graphical abstract summarizing the different PhD objectives.

3 METHODS

3.1 CONSTRUCTION OF MOLECULAR INTERACTION MAPS

The first step of this work is to gather state-of-the-art mechanistic information regarding the pathogenic processes related to fibroblasts in RA and BC in the form of molecular interaction maps. The latter are conceptual representations of biological mechanisms intended for knowledge-driven data interpretation and modeling **[224], [225]**. They may encode molecular disease mechanisms for intuitive exploration and comprehensive overview. As discussed above, some efforts have already been made to assemble the available knowledge in RA and cancer diseases within molecular interaction maps, respectively with the RA-map **[200]** and the CAF-map from the ACSN **[204]**. Nevertheless, such molecular interaction maps cannot be used as is due to a number of limitations: the RA-map gathers information from multiple cell types and tissues within the RA joint and is not RASF-specific. Moreover it completely lacks metabolic representations. On the other-hand, the CAF-map poorly represents metabolic pathways and is not specific to BC but is rather a generic representation of CAFs involvement in the TME. Thus, both original RA- and CAF-maps will be used as basis and further improved to meet our needs. Molecular interaction map being organized, unambiguous, and curated knowledge bases displaying biological and biochemical interactions in a visual form, each step of our maps construction requires clear community-driven standards to be followed to ensure findability, accessibility, interoperability, and reproducibility, known as FAIR principles **[226]**. The construction of these static representations shares common features and standards as well as specificities that will be discussed below.

3.1.1 Common strategy and standards for the construction of the RA-map V2 and CAF-map V2

3.1.1.1 Molecular interaction map layout

The Systems Biology Graphical Notation (SBGN) **[189]** was introduced in 2009 as a community effort to propose a standardized visual language for representation of biochemical interactions networks. It further fosters efficient and accurate representation, visualization, storage, exchange, and reuse of information. SBGN is subdivided into three complementary languages **[227]** covering different levels of information (**Figure 18**).

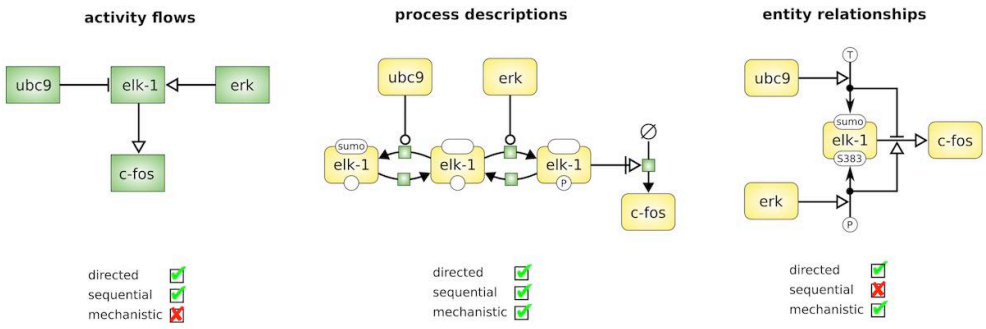

Figure 18. Systems Biology Graphical Notation (SBGN) and its different languages [227]. Among activity flow, entity relationship, and process description, the latter is the most exhaustive in its coverage of various biological mechanisms.

The activity flow (AF) language represents interaction networks including influence directions and modes of regulation (*e.g.* activation, inhibition). The entity relationship (ER) language representation further includes mechanistic details and the direction of influences but no sequential information. The process description (PD) language, the most detailed one, includes specifics

regarding the direction of influences, mechanism of action, and order of events. We chose the SBGN PD langage for the creation of our molecular interaction maps for its level of precision. Thus, all non-compliant reactions and representations in the original RA-map and CAF-map were adapted to SBGN PD standards and the latter language was used for all additions in the molecular interaction maps.

As a modeling software that draws SBGN PD biochemical networks, we used the CellDesigner software **[228]**, a structured diagram editor, in version 4.4. In CellDesigner, the various components of the molecular interaction maps (*e.g.* compartment, phenotype, protein, gene, RNA, simple molecule, ion, complex) and interactions (*e.g.* state transition, catalysis, inhibition, transcription, translation, transport) are distinguished in the form of specific glyphs and notations according to SBGN PD standards (**Figure 19**). CellDesigner further encodes all molecular interaction maps in the Systems Biology Markup Language (SBML) **[229]**, a computer-readable format facilitating exchange and reuse of biochemical networks representations.

To ensure a better visual understanding, molecular interaction maps were biologically compartmentalized. Cellular compartments featured in each molecular interaction map were designed to reflect the molecular architecture of the biological entity of interest (*e.g.* extracellular space, plasma membrane, cytoplasm, nucleus, mitochondrion, endoplasmic reticulum, phenotypes, secreted compartment, and transmembrane domain).

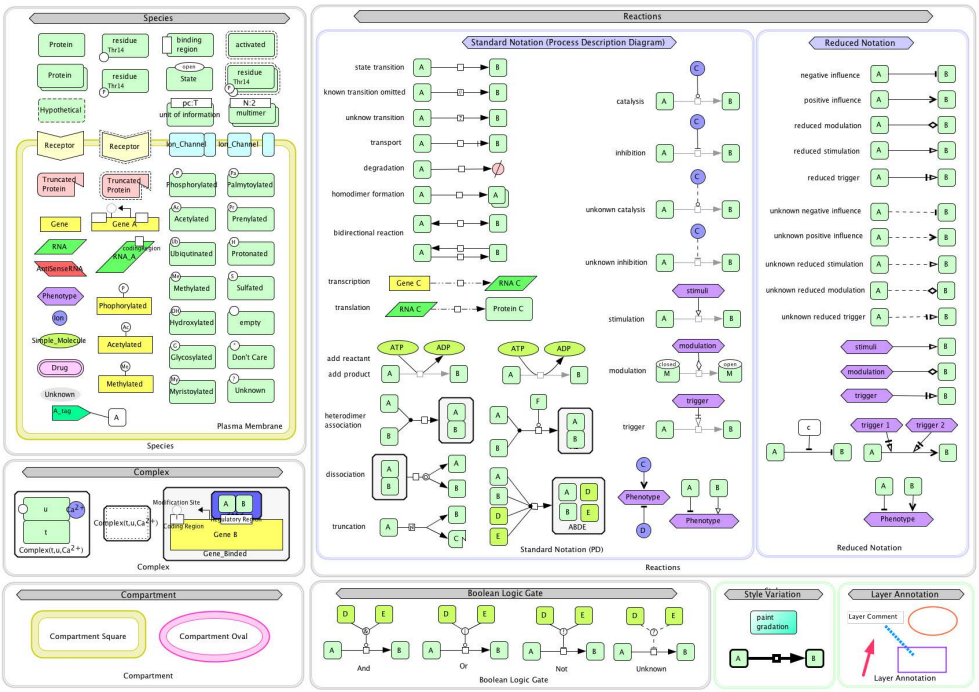

Figure 19. Current graphical notation of CellDesigner [228]. Each round-cornered box represents a state of a molecular species. Species are reacting entities independent of location. These include simple ions (e.g. protons, calcium), simple molecules (*e.g.* glucose, ATP), large molecules (*e.g.* RNA, polysaccharides, and proteins), and other molecules in biochemical and gene regulatory networks. The closed arrows (arrow head filled) represent changes in the state of modification (or allostericity), rather than indicating activation. The graphical notations avoid using symbols that directly point to the molecule to indicate activation and inhibition. Instead, the diagram directly indicates a transition from an inactive to an active state for activation, and a transition from an active state to an inactive state for inhibition. When these transitions are promoted or inhibited by other mediating molecules, these reactions are represented by circle-headed lines for activation and bar-headed lines for inhibition, respectively. An open arrow (arrow head not filled) indicates the translocation of a molecule.

With the help of specialized literature and external pathway databases (*e.g.* KEGG [199], PANTHER [230]), clear attribution of species to each compartment was obtained for both molecular interaction maps. This representation allows for a clear and precise illustration of signal flow from the top of the molecular interacton map (displaying extracellular ligands

complexation with plasmic receptors), through the cytoplasm (signaling and metabolic machineries), nucleus (gene regulation processes), to the bottom compartments (molecules secretion in the extracellular space and phenotype activation).

3.1.1.2 Molecular interaction map curation

The original RA-map and CAF-map underwent a first step of manual curation based on a broad study of literature and pathway databases (*i.e.* KEGG **[199]**, PANTHER **[230]**) to validate the depicted information and search for new components and interactions involved in the associated disease pathogenesis. Relevant keywords and phrases in each pathological context were used to filter the literature on PubMed and Google Scholar (*e.g.* "RASFs signaling pathways", "CAFs in the TME", "fibroblasts aggressive behaviors in RA/cancer"). Only human-based studies were included in each molecular interaction maps according to Curation and Annotation of Logical Models (CALM) standards **[231]**. Including a component or a reaction in a map followed precise curation criteria: first, we included all components experimentally proven to be expressed fibroblast-specifically in the disease pathogenesis. Then, we included all fibroblast-specific reactions and interactions experimentally proven to occur in the disease pathogenesis. General and non-disease specific interactions were further added to complete representations where cell- and disease-specific information was unavailable or incomplete. Such strict curation rules allowed us to increase the overall confidence level of the molecular interaction maps and limit false positives.

All included components were named in accordance with HUGO Gene Nomenclature Committee (HGNC) identifiers **[205]** for signaling and gene regulatory pathways and BiGG IDs **[232]** for metabolic components.

3.1.1.3 Molecular interaction map annotation

Annotations were added to provide reliable references for all species and reactions present in the molecular interaction maps in accordance with Minimal Information Requested In the Annotation of Models (MIRIAM) **[233]** standards for annotating and curating computational networks. According to the authors, MIRIAM standard aims to "enable users to (i) have confidence that curated models are an accurate reflection of their associated reference descriptions, (ii) search collections of curated models with precision, (iii) quickly identify the biological phenomena that a given curated model or model constituent represents and (iv) facilitate model reuse and composition into large subcellular models". MIRIAM annotations were added through the dedicated section of CellDesigner with the relation "bqbiol: is describedby", (**Figure 20**) which is used to link a component or a reaction to the literature or data that describes it (*e.g.* PubMed references (PMIDs), DOI, GEO, KEGG identifier).

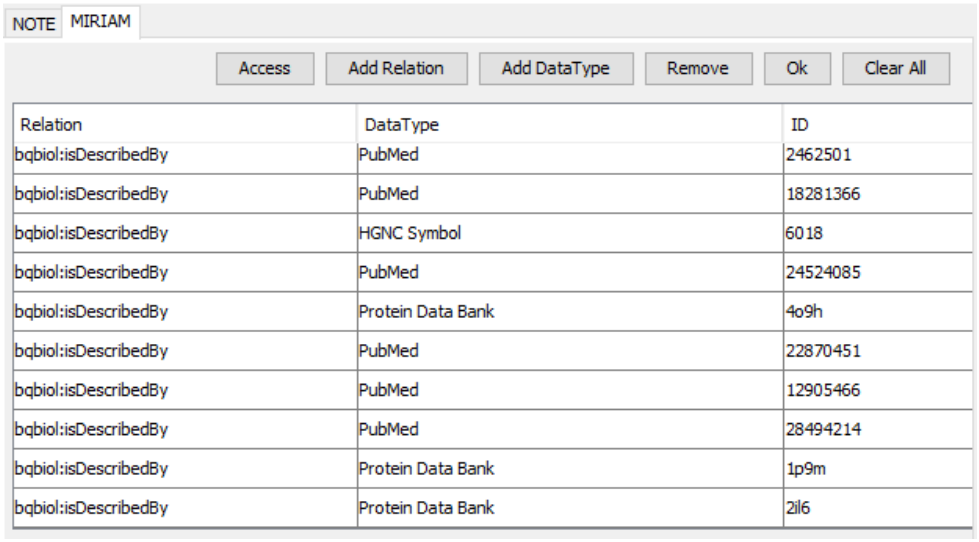

Figure 20. Snapshot of the MIRIAM section in CellDesigner. Annotations used to curate the IL6 component in the original RA-map are shown: they cover various types of information ranging from PubMed IDs to HGNC symbol and Protein Data Bank data.

3.1.1.4 Molecular interaction map visualization and accessibility

The increasing structuring of molecular mechanisms calls for a need to ensure their proper storage and accessibility. The Molecular Interaction NEtwoRks VisuAlization (MINERVA) **[234]** repository of molecular interaction maps was developed for the visual exploration, analysis, and management of networks encoded in systems biology formats, including CellDesigner **[228]**, SBML **[229]**, and SBGN **[189]**. The MINERVA platform is based on the Google Maps™ API and provides automated content annotation and verification along with mapping of drug targets through DrugBank **[235]** or CHEMBL **[236]**, and overlaying experimental data (**Figure 21**). Our molecular interaction maps were all made publicly available as online interactive maps on the standalone MINERVA web server.

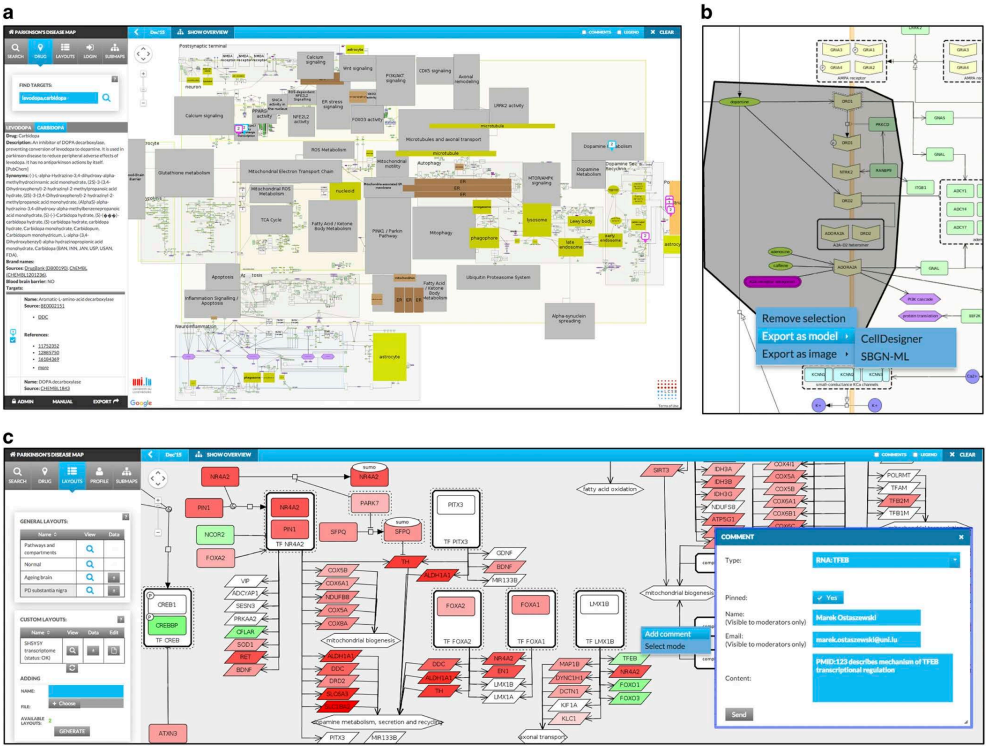

Figure 21. MINERVA interface and functionalities [234]. **(a)** Main interface, displaying drug target search results for terms "levodopa" and "carbidop"'. Information fetched from DrugBank and ChEMBL are displayed in the left panel, while targets of queried drugs are shown in the display area as markers. **(b)** Export of the selected content. A portion of the diagram is selected and exported as a model (CellDesigner or SBGN formats). **(c)** Display of experimental data and content commenting. Publicly available datasets (left panel, "General overlays") or user-provided datasets (left panel, "User-provided overlays") can be visualized on top of the displayed content. Users can pin comments to elements or interactions of the displayed network directly from the display area.

3.1.1.5 Molecular interaction maps evaluation

Standardized and annotated molecular interaction maps help assess both the network specificity (*i.e.* cellular and/or disease-specificity) and confidence in the depicted information. First, both maps cell- and/or disease-specific signatures were assessed based on specific lists of components, referred to as "overlays" in MINERVA. The latter were extracted from specialized

literature and omics datasets. They allowed us to visualize specific pathways within the molecular interaction maps in MINERVA and calculate the maps precise coverage. Indeed, the percentage of the map components present in the cell- and/or disease-specific overlay were obtained. The higher the percentage, the higher the specificity of the molecular interaction map for that cell type or disease. Secondly, an additional annotation score was generated for all components of the molecular interaction maps based on the number of bibliographic references (*i.e.* PMIDs) describing them within the CellDesigner MIRIAM dedicated tab. The higher the literature-based annotation score, the greater the experimental reliability and confidence in the inclusion of the component within the molecular interaction map.

3.1.1.6 Molecular interaction maps topological analysis

Molecular interaction maps provide standalone knowledge bases but may also be analyzed in terms of their underlying network structure. The latter may reveal key features and enable a better understanding of the connectivity and interactions between components. To do so, we used the Cytoscape open-source software **[237]** in version 3.8.2 for network analysis and visualization. Basic network topology analysis was undertaken with the built-in NetworkAnalyzer tool on our molecular interaction maps in the XML format. For every node of the network, NetworkAnalyzer computes its degree (in- and out-degrees for directed networks), its clustering coefficient, the number of self-loops, and a variety of other parameters. NetworkAnalyzer also computes edge betweenness for each edge in the network. Note that this plug-in may compute said parameters for both directed (*i.e.* containing only directed interactions) and undirected networks (*i.e.* containing only undirected interactions). If the respective options are enabled, NetworkAnalyzer stores the computed values as attributes of the

corresponding nodes and edges. This enables the users to apply different visualizations or to filter nodes or edges based on the values of the computed attributes. Such basic topological analysis enables us to identify highly-connected clusters of nodes which may share similar biological features.

3.1.2 Construction of the RA-map V2

We used the original RA-map **[200]** as a basis for the construction of the state-of-the-art RA-map V2. The original RA-map is a mechanistic representation of existing knowledge related to the onset and progression of RA. It includes 506 components connected through 446 reactions, is based on the manual curation of 353 peer-reviewed articles, and is compliant with SBGN PD **[189], [227]** standards. While it offers a formalized representation of the major signaling and gene regulation pathways implicated in the disease, it does not cover metabolic pathways and is a global RA rather than a RASF-specific molecular interaction map. The RA-map was downloaded from the MINERVA platform (https://ramap.uni.lu/minerva/) in the standard XML format for further modifications in CellDesigner **[228]**.

Beyond the general upgrades presented above, the main addition of the RA-map V2 concerned the inclusion of metabolic pathways which were not represented at all. Metabolic pathways of interest in the context of RASFs metabolic reprogramming were identified based on specialized literature with queries including “RASF metabolic reprogramming” or “metabolic pathways altered in RASFs”, extracted from the PANTHER pathway database **[230]**, adapted to SBGN PD **[189], [227]** standards when required, and included in the original RA-map. In addition, considerable bibliographical work was conducted to find evidence linking the newly added metabolic pathways to the already present signaling and gene regulatory pathways, along with

adding new ones. The latter may include inhibition/activation of an enzyme activation/transcription by signaling or genetic pathways, metabolites acting as transcription factors, or metabolites involved in signaling pathways or activating a phenotype.

Already existing biological compartments (*i.e.* extracellular space, plasma membrane, cytoplasm, mitochondrion, endoplasmic reticulum, golgi apparatus, nucleus, secreted compartments, and phenotypes) were kept. Biological processes taking place in the mitochondria and endoplasmic reticulum were detailed (*i.e.* apoptotic pathway and the calcium pathway). Already existing cellular phenotypes were kept and the hypoxic phenotype was added due to its known importance in cellular metabolism.

The cell-specific coverage and confidence of the RA-map V2 was further calculated. Regarding the specificity of the network, we leveraged the "overlay" function of MINERVA **[234]** to assess it. Overlays are user-provided lists of components, overlaid on the network, that may be specific to a cell, disease, or any type of biological contexts and are extracted from data or manual literature curation. We provided nine different sample-specific overlays, namely fibroblasts, macrophages, synovial fluid, synovial tissue, peripheral blood mononuclear cells (PBMC), blood, serum, chondrocytes, and Th1 to assess the coverage of the RA-map V2. First two are updated versions of the overlays provided in the initial RA-map paper **[200]** and were obtained by aggregating single-cell omics data and literature mining. Remaining sample-type specific lists were obtained solely through literature mining. Regarding RASFs, said omics data include differentially expressed genes from GSE109449 **[238]**, a RASF-specific single cell RNA-seq analysis dataset. The serum overlay was created to account for a new source of information used in the maps. The annotation score of the RASF-map V2 was further calculated to evaluate the confidence in the depicted information.

3.1.3 Construction of the CAF-map V2

Similarly, the CAF molecular interaction map was not built from scratch but rather based on previous work from the ACSN online database of multi-scale biological maps **[204]**. The CAF-map was downloaded from the ACSN 2.0 website (https://acsn.curie.fr) in the standard XML format and imported in CellDesigner **[228]**. It represents the major molecular interactions depicting the role of CAFs in the TME. However, the CAF-map displays generic CAF-specific interactions and is not specific to a certain type of cancer. It includes 681 components connected through 581 reactions and is based on the manual curation of 358 peer-reviewed articles. It is consistent with SBGN standards **[188]** and thoroughly annotated with pertinent information and references.

The layout of the CAF-map was edited to shift from a round cell with functional modules (*e.g.* "integrin signaling pathways", "motility", "growth factors production", "cytokines and chemokines production", "core signaling") to a compartmentalized map with biological compartments (*i.e.* extracellular space, cytosol, nucleus, mitochondria, endoplasmic reticulum, secreted compartment, and phenotypes). It allowed us to depict a straight flow of information within biologically-relevant compartments of the map.

Phenotypes were deleted either to allow for a detailed description of the pathways of interest (*i.e.* "TCA", "glycolysis", and "ketone bodies degradation" phenotypes), when they lacked added value in CAFs involvement in TME and cancer development (*i.e.* "microtubule polymerization", "actin polymerization", and "septine polymerization" phenotypes), or when their only interactions were to be activated by another phenotype (*i.e.* "stress fibril formation" and "matrix effects" phenotypes).

Semantics were greatly updated to comply with SBGN PD standards **[189], [227]** for graphical visualization when not fully respected. It included

adorning macromolecules with their residue (*e.g.* “phosphorylated”, “acetylated”) or state of modification (*i.e.* “active”, “inactive”). Incorrect representation of biochemical reactions such as ligand binding its receptor, were further corrected. Non-standardized reactions including the RNA complex formation were corrected. Autocrine and paracrine signaling described as an internal element that would activate its own receptor were deleted and replaced in a more comprehensive pathway by transporting the component in the secreted compartment and making it available to bind its own receptors of proximal cell receptors.

Relevant annotations regarding components and reactions (*e.g.* PubMed IDs (PMID), HUGO identifiers **[205]**, pathways of interest) were previously stored in the note section of CellDesigner. Consistent with MIRIAM standards **[233]**, such notes were automatically retrieved and inserted in the dedicated MIRIAM section of CellDesigner **[228]** with the qualifier “bqbiol: isDescribedBy”.

In the case of the CAF-map V2, it was not cellular specificity that had to be assessed, since the ACSN CAF-map was built only with CAF-specific information, and all additions to the CAF V2 map have been as well, but rather the cancer-specificity of the network. Due to the difficulty of obtaining healthy samples to compare with diseased samples to extract differential signatures, only two datasets were available for cancer-specific analysis: the public non-small cell lung cancer (NSCLC) GSE22874 dataset **[239]** from the National Center for Biotechnology Information **[240]** and the private breast cancer EGAD00001003808 dataset from the European Genome-phenome Archive **[241]**. GSE22874 is a microarray analysis including, among other stroma cell-types, 15 NSCLC CAFs samples and 15 healthy control fibroblasts samples established from primary cultures. Its differential gene expression was analyzed using the GEO2R interactive web tool

(https://www.ncbi.nlm.nih.gov/geo/geo2r/) script code on R version 4.2.2. Refining of the latter was performed with selection of adjusted p-value > 0.05 and absolute fold change (FC) > 1.5. Next, EGAD00001003808 was analyzed. It is a RNA-Seq dataset of 47 CAF samples sorted from fresh BC including 28 CAFs-S1 and 19 CAFs-S4 subtypes. Both CAFs-S1 and CAFs-S4 subpopulations are myofibroblastic activated CAFs whose expressions are strictly restricted to cancer and characterized by high levels of fibroblast activating protein **[77]**. However, CAFs-S1 are mainly involved in tumor-like phenotypes (*e.g.* immunosuppression, tumor growth and proliferation, inflammation, ECM remodeling), whereas CAFs-S4 are responsible for generic core signaling, motility, and perivascular signatures. Thus, CAFs-S4 represented the control group against the aggressive CAFs-S1 group of interest. The tissue harvesting protocol, as well as the data mapping, alignment, quality control, and normalization processes are detailed in **[67]**. Differential expression analysis (DEA) was performed afterwards using the Limma package **[242]** in R version 4.2.2 to identify differentially expressed genes (DEG) between breast CAFs-S1 and CAFs-S4. Standard significance threshold of adjusted p-value > 0.05 and absolute FC > 1.5 were applied.

For each DEA, results were first plotted on the CAF-map V2 in the MINERVA platform with a color-code corresponding to the over- or under-expression of specific components of the map within the datasets. The annotation score of the CAF-map V2 was further calculated to evaluate the confidence in the depicted information.

3.2 INFERENCE OF CELL- AND DISEASE-SPECIFIC REGULATORY BOOLEAN MODELS

Beyond their static knowledge base function, both RA-map V2 and CAF-map V2 were used to infer cell- and disease-specific Boolean regulatory models to study RASFs and breast CAFs dynamic features in pathogenic environments. However, these two molecular interaction maps, even greatly updated, still have limitations in this objective. Despite its RASF-specific enrichment, the RA-map V2 remains a global map, gathering information from several cell types, tissues, fluids, and is not RASF-specific. Similarly, despite its updates and corrections, the CAF-map V2 remains a global map, gathering information from multiple types of cancer and is not specific to BC. A number of measures, similar or not, were undertaken to tackle these challenges.

3.2.1 Common strategy for inference of the RASFs and breast CAFs regulatory Boolean models

3.2.1.1 The CaSQ map-to-model framework

A molecular interaction map and a dynamic Boolean model are two distinct entities which may serve different purposes and are generally created independently. Nevertheless, both constructions share some common features, namely the topology of the network or the mode of influence. In this context, the CellDesigner as SBML-*qual* (CaSQ) tool **[243]** attempts to bridge the gap between static representations in the form of molecular interaction maps and dynamic Boolean models. CaSQ automatically infers large-scale Boolean models in the standard SBML-*qual* format **[244]** from SBGN PD **[189], [227]** molecular interaction maps in the CellDesigner **[228]** XML format. The logical rules of the regulatory model are based on the

topology of the static network. Note that CaSQ allows to retain all references, annotations, and layout of the molecular interaction map in the associated model, facilitating interoperability. The tool is used through the command line with specific positional and optional arguments, the parameters of interest in our work are presented as follows : casq <infile> -c -s -u <specific node(s)> -d <specific node(s)> where :

- -c (--csv) stores species information into a separate CSV file;
- -s (--sif) stores the influence information into a separate SIF file;
- -u (--upstream) only infers a model from species upstream of this specific node;
- -d (--downstream) only infers a model from species downstream of this specific node.

3.2.1.2 Boolean regulatory model visualization and accessibility

Regulatory models were made available on the Cell Collective **[245]** and BioModels **[246], [247]** repositories of biological models. Cell Collective is a web-based platform enabling researchers to collaboratively build and share qualitative large-scale models of various biological systems (*e.g.* gene regulation, signal transduction, cell-cell interaction networks) without having to enter or modify complex mathematical equations (**Figure 22**). Models may be annotated with published references that support the depicted information. The platform further allows to interactively simulate, perturb, and analyze models by running system-wide *in-silico* experiments and visualize cellular responses under different conditions. Cell collective hosts and provides export features of biological models encoded in the standard SBML format **[229]**. Additionally, BioModels gathers freely-available published mathematical models of biological systems in diverse modeling formats.

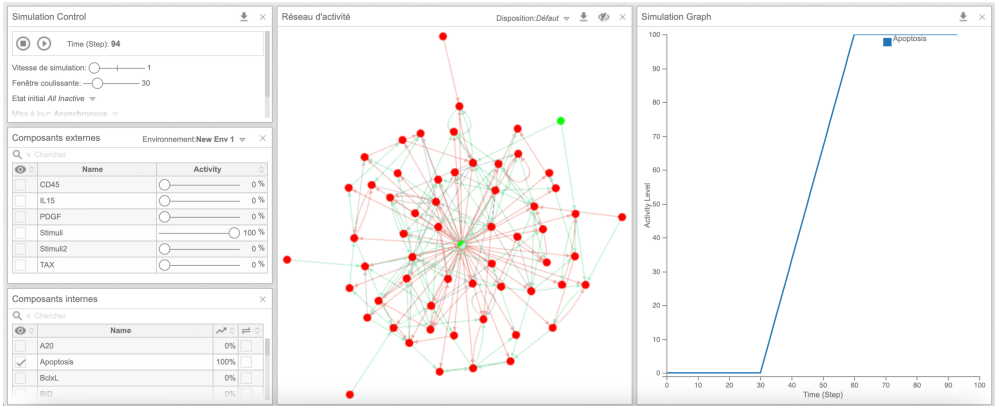

Figure 22. Overview of the Cell Collective simulation platform [245]. The left-hand panel first represents the simulation parameters: the simulation speed corresponds to the plot rate of simulations and has no impact on results; the sliding window is the number of steps over which the fraction of activity/inactivity of each node is calculated and displayed (*e.g.* if the sliding window is 100, and the node is active in 20 steps over the last 100 steps, the activity level displayed on the graph will be 20%); the update can be synchronous or asynchronous depending on the characteristics of the simulation. The external components are those not regulated by any upstream components, unlike the internal components which are. The value of external components can be initialized, but being in a binary qualitative study, we will always set it to 0% (inactive or absent component) or 100% (active or present component). The internal components can be qualitatively on (active or present) or off (active or absent) representing biological mutations to simulate loss- or gain-of-function experiments. The evolution of activity of internal and external components according to the initialization of the model can be followed on the activity network on the middle panel (green for active, red for inactive) or on the simulation graph on the right panel with the activity level of each node according to the logical time step.

3.2.1.3 Regulatory behavior validation

The Boolean regulatory models dynamic behavior were thoroughly assessed to confirm their biological relevance through three different approaches.

First, a generic validation approach was carried out to confirm the involvement of individual components into RASFs or breast CAF-specific signaling or gene regulatory pathways. In greater detail, a literature review was undertaken and experimental evidence for RASF- and breast CAF-specific activity were retrieved from *in-vitro* and *in-vivo* studies in both humans and murine models of RA and BC (*e.g.* single or multiple knock-out and knock-in experiments, genetic recombination experiments). The latter studies experimental conditions were used to initialize the RASF- or breast CAF model (*e.g.* a gene knock-out experiment was translated as an initial value of 0 for said gene in the regulatory model and a gene knock-in was translated as an initial value of 1). This mechanistic verification was performed in a synthetic state of the model where remaining nodes were set to 0 (*i.e.* absent or inactive). Specific components to test values were then switched from 0 to 1 or 1 to 0 depending on the experimental scenario to assess their particular contributions to the pathway. Simulations were performed on the Cell Collective interactive platform **[245]** in the asynchronous updating mode, with a simulation speed of one, and a sliding window of 30.

Secondly, the global behavior of the model was assessed. This comprehensive analysis, conducted at the level of RASFs or breast CAFs regulatory cellular phenotypes allowed us to compare the overall behavior of the model to biologically known RASFs or breast CAFs cellular dynamics. This time, the long-term behavior of the model was evaluated through analysis of its trap-spaces under RASFs or breast CAF-specific initial conditions. Trap-spaces are regions of the state-space from which the system cannot escape **[248],**

[249] (**Figure 23**). By definition, each trap-space contains at least one attractor of the model. However, trap-spaces may overlap with each other. Thus, minimal trap-spaces (later referred to as "trap-spaces"), *i.e.* trap-spaces which do not include smaller trap-spaces, offer a good approximation of Boolean models attractors by faithfully capturing its asymptotic behavior. Trap-spaces were computed using BioLQM [250] and the biolqm.trapspace function, using binary decision diagrams or an ASP-based solver. Their computation relies on the identification of positive and negative prime implicants for each components function without performing simulation but rather through a symbolic approach implementing a constraint-solving method. In this context, each trap-space reflects a different subspace of RASFs or breast CAFs cellular phenotypes. The latter were compared with known RASFs or breast CAF overall cellular behavior extracted from specialized literature to confirm the asymptotic behavior of the model.

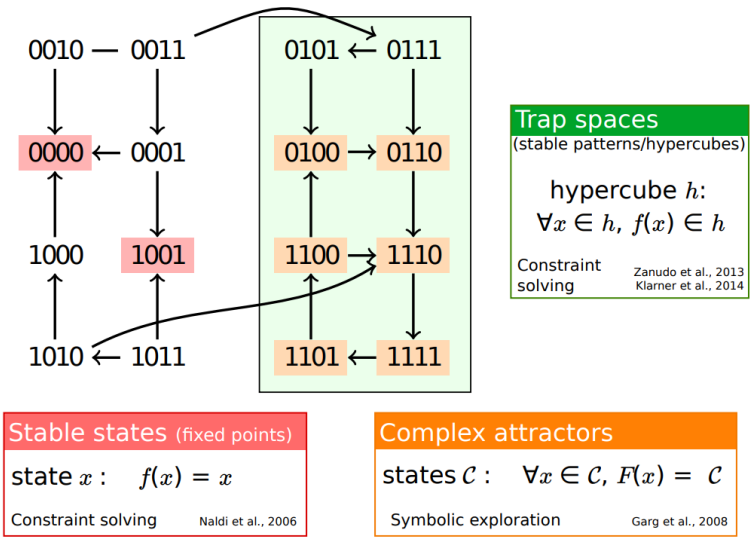

Figure 23. Attractors in Boolean models. Stable states are where the system reaches a stable configuration that does not change over time. Complex attractors are where the system oscillates between multiple states in a periodic manner. Trap-spaces are where the system gets trapped in a subset of states from which it cannot escape.

Finally, the global impact of regulatory pathways (*e.g.* signaling and gene regulation) upon metabolic subprocesses was evaluated to confirm its proper reproduction in a pathological cellular context. It was done by projecting the trap-spaces of the regulatory model on metabolic components and comparing the latter asymptotic behavior with specialized literature.

3.2.2 Inference of the regulatory Boolean RASF model

CaSQ (version 1.1.0) **[243]** was used to infer a Boolean model from the RA-map V2 in the standard SBML-*qual* **[244]** format. Its latest functionality enables extraction and translation into a model, not of an entire molecular map, but only a subpart of interest. This feature allowed us to overcome the lack of cellular-specificity of the RA-map V2 by only extracting pathways associated with RASF-specific inputs. Inputs, in the sense of components that are not regulated by any other upstream components, are supposed to exert an important role on the behavior of the model due to the linearity of the map and the associated-inferred model. Given our molecular interaction map construction, in the vast majority of cases, the inputs of our model are extracellular ligands or microRNAs. To identify RASF-specific inputs, a comprehensive list of all regulatory inputs was obtained and their fibroblastic specificity was confirmed or refuted one by one based on a thorough assessment of specialized literature.

Initial conditions for all regulatory model inputs were retrieved from specialized literature. They allowed us to simulate the regulatory model in a RASF-specific environment and validate its behavior. In greater detail, we sought to assign a Boolean value to each input based on its state (*i.e.* level of expression or presence) in RASFs. This was achieved in two ways based on the *in-vitro* or *in-vivo* origin of the study. In an *in-vivo* setting, this qualitative

observation must necessarily be obtained relatively to the same observation in a fibroblast in another biological state. Ideally, it should be compared to a healthy fibroblast. However, expression data rarely exist in healthy fibroblasts as healthy patients are not usually willing to provide synovial samples due to the invasiveness of the procedure (few samples after accidents and joint replacement may be available). Samples are more easily recovered from patients suffering from other joint diseases. Therefore, in the context of data analysis, the control for RA is commonly osteoarthritis (OA) because of the similarity of the affected areas but fairly different features (*i.e.* OA is a degenerative, non-autoimmune, and non-inflammatory disease). Thus, expression data comparison in fibroblasts between RA and OA were retrieved from specialized literature and if a specific component was over-regulated in RA compared to OA, a value of 1 was assigned to the component. A value of 0 was assigned if it was under-regulated in RA compared to OA. In an *in-vitro* context, synovial fibroblasts are cultured according to particular settings and the state of specific components is compared before and after RASFs differentiation to assign it a Boolean value (*i.e.* 1 if over-expressed in cultured RASFs compared to normal fibroblasts and 0 if under-expressed).

3.2.3 Inference of the regulatory Boolean breast CAF model

We used the CaSQ tool (version 1.1.0) **[243]** and its default parameters to generate a Boolean model from the global CAF-map V2 in the standard SBML-*qual* format **[244]**.

A data-driven breast cancer-specific contextualization of the CAF model V2 was conducted to overcome the lack of cancer-specificity. To this purpose, the already-analyzed dataset EGAD00001003808 from the European Genome-phenome Archive **[241]** was leveraged. In addition to the previous

analyses, most significant DEG were depicted with an absolute FC > 1. Biological processes related to the most significant DEG were assessed by enrichment analysis on the GO Resource powered by PANTHER **[251]**. If pathways related to biological processes driven by highly significant DEG were not represented in the CAF-map V2, an additional step of literature search was conducted to include them and cover most of breast CAF-related pathways. Identified DEGs were discretized to fix the initial conditions of the CAF model in accordance with BC-specific biology. Up-regulated DEG present in the regulatory model were set to an initial value of 1. Similarly, down-regulated DEG present in the regulatory model were set to an initial value of 0. Finally, the inputs of a logical model being the nodes which do not present any upstream regulators, they are suspected to exert a significant control on the dynamics of the model due to the linearity of signal transduction. Thus, fixing their initial values is crucial to reproduce breast CAF-specific conditions. For inputs that would not have been fixed by the DEA, initial conditions may be extracted from BC-specific peer-reviewed literature similarly to RASFs. Overall, this effort to combine data-driven and manually curated breast CAF-specific information to initialize the regulatory CAF model allows to confidently contextualize it to reproduce, as closely as possible, breast CAF-specific conditions for further behavior validation.

3.3 COUPLING OF CELL- AND DISEASE-SPECIFIC REGULATORY MODELS WITH A GENERIC HUMAN METABOLIC NETWORK

Construction of cell- and/or disease-specific metabolic networks or existing computational frameworks to parametrize metabolic networks in disease-specific context are greatly limited by the lack of data in poorly studied biological fields such as RASFs and breast CAFs and issues associated with

improper automatic network reconstructions. According to one of the principles of immunometabolism, namely the distribution of metabolic fluxes arising from the upstream immune-related signaling network, we aim to contextualize a generic metabolic model from the asymptotic dynamic behavior of its regulatory system represented by the associated Boolean regulatory model. By doing so, we aim to obtain hybrid models of RASFs and breast CAFs covering multiple biological layers and allowing an integrated overview of immunometabolic dynamics.

3.3.1 Metabolic network of choice

The metabolic network used in this work is the MitoCore model **[252]**, a manually curated constraint-based model of human central metabolism. It includes two compartments (*i.e.* cytosol and mitochondria), 74 metabolites, 324 metabolic reactions, and 83 transport reactions and covers all parts of central metabolism directly or indirectly involved with energy production. This core model, although smaller in size compared to recently published huge human genome-scale metabolic models, allows to avoid many large models associated issues (*e.g.* unrealistic ATP production rates, automatic and not-curated reconstruction of improper gene-protein-reactions rules leading to incorrect compartmentalization of reactions or directionality constraints). Additionally, considering its manual curation, users can have great confidence in each depicted reaction and have a better insight on the behavior of the system, allowing for an easier evaluation of the results. The default parameters of MitoCore simulate normal cardiomyocyte metabolism. However, the default simulation settings can be applied to various biological contexts without necessarily implying cell-specific features. Indeed, cardiomyocytes can metabolize a wide range of substrates, have reactions common to many other cell types, and represent the metabolism of the human

heart, an organ of utmost importance in human health, disease, and toxicology. Moreover, MitoCore includes processes that are inactive in cardiomyocytes but that can be activated to represent other cell-types metabolic features (*e.g.* gluconeogenesis, ketogenesis, β-alanine synthesis and folate degradation). As a proof of concept regarding the generalization of their model, MitoCore modelers were able to successfully simulate the fumarase deficiency, a nervous system condition, using the default cardiomyocyte parameters.

3.3.2 Framework for hybrid modeling

The objective of our hybrid modeling framework is to contextualize the MitoCore generic reconstruction of human metabolism through the signaling and gene regulation impact of cell- and disease-specific networks. Thus, we will constrain the metabolic fluxes of MitoCore based on the cell- and disease-specific regulatory trap-spaces. The latter contextualized metabolic model will further be analyzed to evaluate the impact of regulatory subsystems upon metabolic processes in these particular contexts.

The general architecture of the framework for hybrid modeling is provided in **Figure 25** and its various steps are discussed below:

(1) Value propagation **[253], [254]**, a method implemented in the CoLoMoTo notebook **[255]**, is applied to the cell- and disease-specific Boolean regulatory model to facilitate its analysis. Indeed, when given a set of logical rules (*i.e.* the regulatory model Boolean rules) and a cellular context (*i.e.* the regulatory model cell- and disease-specific initial conditions), this iterative algorithm allows the computation of specific components dynamical consequences on the overall behavior of the model. It reveals the influence specific

components may exert on the dynamics of the network and reduce its complexity. Note that this method does not impact the asymptotic behavior of the model: all dynamical consequences calculated in this manner would occur regardless. In greater details, the cellular context is first formalized by assigning the cell- and disease-specific initial conditions. Next, a model reduction technique is applied where for each constant node, the corresponding value is inserted into the logical rule associated with each of its target nodes. Each logical rule is then simplified using Boolean algebra. If the rule simplifies to a constant, this fixed value is further propagated into the logical rules of its own downstream nodes. This process is iterated until no further propagation can be applied (**Figure 24**).

(2) Evaluating the influence of cell- and disease-specific components upon the global regulatory behavior of the model through the value propagation algorithm allows to decrease its complexity to identify trap-spaces. Trap-spaces are considered as approximations of attractors and faithfully capture the asymptotic behavior of Boolean models. To identify the regulatory trap-spaces, the outputs of value propagation (*i.e.* value of all nodes of the model after complete propagation of initial conditions) are considered as a new set of initial conditions of the regulatory model and the already presented biolqm.trapspace function is applied. Indeed, without decreasing the complexity of the regulatory Boolean models, computation of traps-spaces with BioLQM is hardly achievable for large-scale networks due to computational reasons as they are commonly computed based on prime implicants which can be of a great number when increasing model size.

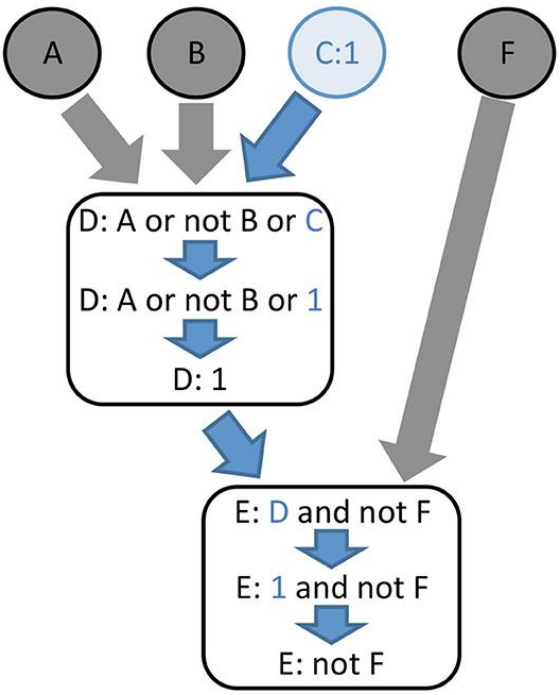

Figure 24. The principle of logical value propagation analysis [252]. A simple example involving two core nodes: D and E, and four input nodes: A, B, C, and F. The value 1 is initially assigned to the node C and further propagated through the model. The assignment C:1 implies the evaluation of D to 1. Consequently, the function assigned to node E becomes "not F." In other words, assigning the value 1 to node C activates node D independently from the value of its other inputs A and B, while node E becomes completely dependent on the value of node F.

(3) Once the asymptotic behavior of the Boolean regulatory model is obtained, *i.e.* its trap-spaces, our interest lies in the impact of the asymptotic behavior of regulatory subsystems upon the metabolic subsystem, *i.e.* trap-spaces projected on metabolic components. However, it is worth noticing that the Boolean regulatory model rules do not allow to differentiate a protein with a signaling function from a metabolic enzyme or any simple molecule from a metabolite. To overcome this limitation, all components of the regulatory model are extracted as a list, as well as enzymes and metabolites from MitoCore,

which are identifiable. Both regulatory and MitoCore metabolic components being consistently named with BiGG IDs **[232]**, the regulatory components are compared to MitoCore metabolites and a list of the regulatory metabolites is extracted. This matching is limited by excluding a list of manually predefined compounds considered by MitoCore as metabolites but actually are common metabolic intermediates (**Table 3**). Similarly, a list of the regulatory enzymes is extracted. Said lists are used to project previously identified regulatory trap-spaces on the metabolic enzymes and metabolites. The latter reflect the cell- and disease-specific signaling and gene regulation processess impact upon cellular metabolism, *i.e.* cellular phenotype.

(4) Metabolic components state within regulatory trap-spaces may oscillate depending on the simulation conditions. In order to interpret these trap-spaces and constrain associated metabolic fluxes in MitoCore, we will restrict ourselves to the maximum values of trap-spaces for metabolic components. A metabolic enzyme-associated maximal trap-space value strictly superior to 0 means this metabolic enzyme might be activated or present according to the outcome of the regulatory model. An enzyme being qualitatively activated or present does not give any information regarding the feasibility nor the kinetics of the metabolic reactions it is supposed to catalyze. Similarly, a metabolite-relative maximal trap-space value strictly superior to 0 shows the metabolite is produced in some of these regulatory conditions. However, it does not give any information regarding its producing reactions high or low flux. Thus, it is impossible, without any further user-provided information, to influence the reaction flux of metabolic components associated with maximal trap-spaces values strictly superior to 0. On the other hand, a metabolic enzyme with a

projected maximal trap-space value equal to 0 (*i.e.* trap-spaces always equal to 0) expresses the inactivation or absence of the said enzyme by signaling or gene regulation pathways. The catalyzed metabolic reactions will not happen. A metabolite-associated maximal trap-space value of 0 denotes the non-production of the said metabolite. Its producing reactions did not occur. Hence, for every metabolic enzyme or metabolite with projected maximal regulatory trap-spaces values equal to 0, we constrain the flux of its associated MitoCore metabolic reaction (*i.e.* catalyzed reactions or producing reactions) to 0.

(5) Once the generic MitoCore metabolic model is cell- and disease-specifically contextualized by the outcomes of the regulatory model, Flux Balance Analysis (FBA) is performed using CobraPy **[256]** to evaluate the metabolic flux distribution. Actually, two FBAs are conducted to highlight a potential change in metabolic fluxes distribution under cell- and disease-specific conditions. The first FBA is conducted without any additional constraints, reflecting the generic and healthy control state. The second FBA is conducted with the additional metabolic flux constraints extracted from regulatory trap-spaces, reflecting the cell- and disease-specific condition. The objective function is set to maximum cellular ATP production to reflect the primary energy production role of central metabolism. It is manually defined as the sum of the three cellular ATP-producing reactions (*i.e.* the seventh and tenth reactions of glycolysis, and the complex V of OXPHOS or ATP synthase).

Table 3. Common metabolic intermediates considered as metabolites in the MitoCore model.

Identifier	Detailed name
M_atp_c	Cytosolic Adenosine Triphosphate
M_adp_c	Mitochondrial Adenosine Diphosphate
M_adn_c	Cytosolic Adenosine
M_adp_m	Cytosolic Adenosine Diphosphate
M_amp_c	Cytosolic Adenosine Monophosphate
M_amp_m	Mitochondrial Adenosine Monophosphate
M_atp_m	Mitochondrial Adenosine Triphosphate
M_cdp_m	Mitochondrial Cytidine Diphosphate
M_cmp_c	Cytosolic Cytidine Monophosphate
M_co_c	Cytosolic Carbon Monoxide
M_co_e	Extracellular Carbon Monoxide
M_co2_c	Cytosolic Carbon Dioxide
M_co2_e	Extracellular Carbon Dioxide
M_co2_m	Mitochondrial Carbon Dioxide
M_coa_c	Cytosolic Coenzyme A
M_coa_m	Mitochondrial Coenzyme A
M_ctp_c	Cytosolic Cytidine Triphosphate
M_fe2_c	Cytosolic Ferrous Ion
M_fe2_e	Extracellular Ferrous Ion
M_fe2_m	Mitochondrial Ferrous Ion
M_ficytC_c	Cytosolic Ferricytochrome c
M_ficytC_e	Extracellular Ferricytochrome c
M_ficytC_m	Mitochondrial Ferricytochrome c
M_gdp_c	Cytosolic Guanosine Diphosphate
M_gdp_m	Mitochondrial Guanosine Diphosphate
M_gtp_c	Cytosolic Guanosine Triphosphate
M_gtp_m	Mitochondrial Guanosine Triphosphate
M_h_c	Cytosolic Hydrogen Ion
M_h_e	Extracellular Hydrogen Ion
M_h_m	Mitochondrial Hydrogen Ion
M_h2o_c	Cytosolic water
M_h2o_m	Mitochondrial water
M_h2o2_c	Cytosolic Hydrogen Peroxide

M_h2o2_m	Mitochondrial Hydrogen Peroxide
M_hco3_c	Cytosolic Bicarbonate
M_hco3_e	Extracellular Bicarbonate
M_hco3_m	Mitochondrial Bicarbonate
M_nad_c	Cytosolic Nicotinamide Adenine Dinucleotide
M_nad_e	Extracellular Nicotinamide Adenine Dinucleotide
M_nad_m	Mitochondrial Nicotinamide Adenine Dinucleotide
M_nadh_c	Cytosolic Nicotinamide Adenine Dinucleotide
M_nadh_e	Extracellular Nicotinamide Adenine Dinucleotide
M_nadh_m	Mitochondrial Nicotinamide Adenine Dinucleotide
M_nadp_c	Cytosolic Nicotinamide Adenine Dinucleotide Phosphate
M_nadp_m	Mitochondrial Nicotinamide Adenine Dinucleotide Phosphate
M_nadph_c	Cytosolic Nicotinamide Adenine Dinucleotide Phosphate
M_nadph_m	Mitochondrial Nicotinamide Adenine Dinucleotide Phosphate
M_no_c	Cytosolic Nitric Oxide
M_no_e	Extracellular Nitric Oxide
M_o2_c	Cytosolic Oxygen
M_o2_e	Extracellular Oxygen
M_o2_m	Mitochondrial Oxygen
M_o2s_m	Mitochondrial Superoxide Anion
M_pheme_c	Cytosolic Heme
M_pheme_m	Mitochondrial Heme
M_pi_c	Cytosolic Orthophosphate
M_pi_e	Extracellular Orthophosphate
M_pi_m	Mitochondrial Orthophosphate
M_q10_m	Mitochondrial Ubiquinone
M_q10h2_m	Mitochondrial Ubiquinol

The MitoCore metabolic model lacking cellular and tissular specificity, a numerical interpretation of metabolic flux values was not possible. FBA results were only interpreted in terms of flux distribution. For instance, the ratios of ATP production from glycolytic or OXPHOS reactions relative to total ATP production (represented by the objective function) were calculated. Analysis of uptake and secretion of carbon fluxes (C-flux) was also carried out to account for the turnover of carbonated molecules. The C-flux of an uptake reaction represents the total cellular carbon influx from this specific uptake reaction. Similarly, the C-flux of a secretion reaction represents the proportion of total cellular carbon efflux coming from this specific secretion reaction. Finally, a comparison of both FBAs internal fluxes was conducted and a difference in metabolic fluxes was identified from a greater than 2-fold variation in both contexts.

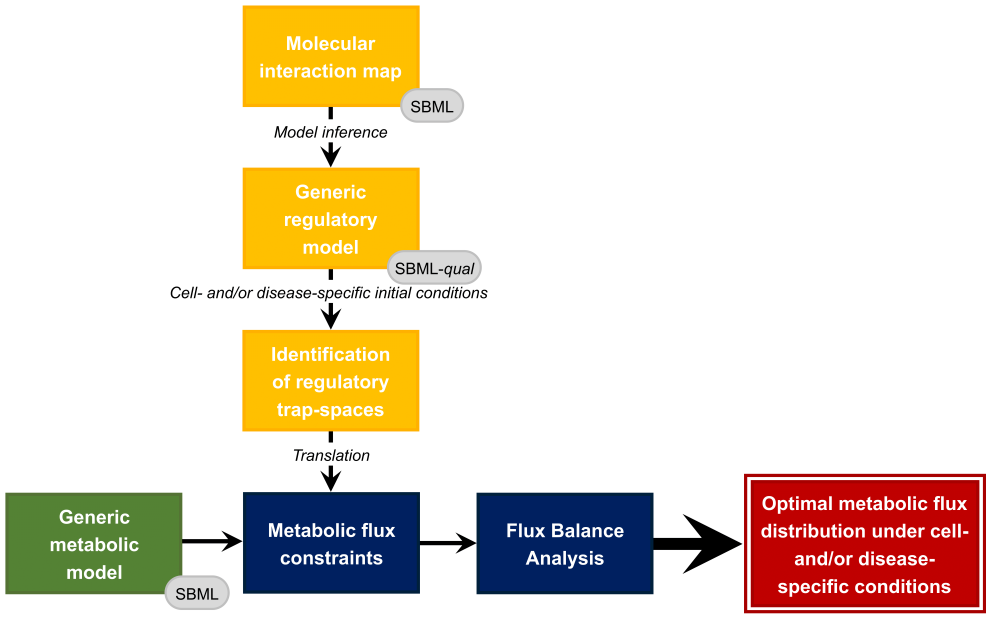

Figure 25. General architecture of the hybrid modeling framework. The generic metabolic model is contextualized by the asymptotic behavior of the cell- and disease-specific regulatory model and the impact of signaling and gene regulation systems upon metabolism, resulting in additional metabolic constraints.

3.3.3 Identification of regulatory driver(s)

To identify regulatory components potentially responsible for metabolic alterations in RASFs and breast CAFs, a knock-out/knock-in strategy of the regulatory initial conditions was conducted on both models. All initial regulatory conditions set to 1 in the RASF or breast CAF-specific configuration were successively set to 0 while the other remained at RASF or breast CAF-specific values. Similarly, all regulatory components initial conditions set to 0 in the RASF or breast CAF-specific configuration were successively set to 1 while the other remained at RASF or breast CAF-specific values. Subsequent value propagation, metabolic compounds-projected regulatory trap-spaces identification and extraction of metabolic constraints were conducted to perform FBA and evaluate metabolic fluxes distribution in these new conditions. To depict the key metabolic function of energy production, the proportion of total cellular ATP production from glycolysis and OXPHOS were compared in the various FBAs.

However, this type of combination only allows us to study the effect of single components knock-out or knock-in at a time as they are tested individually, and therefore eliminates any synergistic effects of regulatory components upon metabolic processes. To overcome this limitation, we additionally adopted a second, more comprehensive strategy of combined knock-outs and knock-ins. This time, all possible combinations of regulatory initial conditions were automatically generated and further tested, *i.e.* 2^n combinations (n being the number of initial conditions). A few exceptions were implemented to cope with the exponential increase in the number of combinations to be tested as a function of the number of initial conditions and for computational power reasons arising therefrom. First, after reaching the trap-space computation step of our framework, all initial conditions combinations exhibiting aberrant trap-spaces projected onto cellular

ontological phenotypes (*e.g.* both apoptosis and proliferation or negative and positive regulators being active at the same time) were eliminated. Secondly, a number of initial conditions knock-out or knock-in were not included in the combinations for biological significance reasons. For instance, glucose knock-out was eliminated as its absence prevents all our metabolic reactions of interest from taking place. The effect of "simple molecules" as referred to in CellDesigner (*e.g.* Ca^{2+}, phosphatidylinositol 4,5-bisphosphate, lysophosphatidic acid) was additionally eliminated as they are signaling intermediates shared by many regulatory pathways and do not directly play a key role. Finally, a time out function was implemented on the search for trap-space step of our pipeline. Indeed, depending on the initial condition combination tested, the latter may not reduce the complexity of the regulatory model enough through value propagation to obtain its trap-spaces in an acceptable timeframe. The trap-space search was limited to three minutes per combination to avoid wasting precious computing time. Three additional measures were implemented specifically for the CAF model due to the very high number of components fixed in the initial conditions. First, only an extraction of the CAF-map V2 and not the whole map was inferred in Boolean regulatory model, by focusing on all molecular pathways upstream of CAFs cellular phenotypes involved in the hallmarks of cancer. This was intended to reduce the complexity of the model as a function of the number of nodes, while maintaining biological consistency. Secondly, only inputs combinations were tested. Indeed, as highlighted before, the regulatory models inputs (*i.e.* nodes not regulated upstream) are suspected to exert a critical role over the global behavior of the model and may represent potential therapeutic targets. Remaining internal components were excluded from the combinations and remained at their fixed breast CAF-specific initial condition value. Even when focusing solely on the effect of input combinations, the number of the latter may still be too high. Thus, a final step of grouping inputs based on their type or biological role was undertaken to

reduce their number. Finally, in both biological contexts and for all remaining combinations, the framework was applied as displayed previously and ATP production rates from glycolytic and oxidative pathways were assessed. Combinations were associated with a healthy metabolic profile if cellular ATP production originated over 60% from OXPHOS and with a pathogenic profile if cellular ATP production originated over 60% from glycolysis. In each category, identification of specific patterns of components was undertaken. To optimize calculations, the framework code was adapted as displayed above and parallelized to run on 64 cores simultaneously on a virtual machine from the french bioinformatics institute (IFB) cloud service.

By doing so, all individual and combined effects of regulatory components upon metabolic sub-processes and, above all, upon the preferential metabolic pathway for energy production in the form of ATP, were fully assessed within the limits of biological coherence.

3.3.4 Python packaging of the hybrid modeling framework

For a broader application to a wide range of dynamic study of the cellular impact of gene regulation and signaling upon metabolic processes, and particularly upon its central function of energy production, we provided the packaging of our hybrid modeling framework within a pip-installable Python tool of the name MetaLo for Metabolic analysis of Logical models extracted from maps. A multiplatform graphical user interface (GUI) was implemented using the wxPython toolkit **[257]** and the Gooey parser **[258]**.

The MetaLo package automatically applies the previously presented hybrid modeling framework and further covers the Boolean network inference from a standardized molecular interaction map. A few adjustments were implemented as compared to the hybrid modeling framework, notably for

packaging and distribution (*i.e.* bioLQM is not Python-compliant) along with performance reasons (*i.e.* computation of trap-spaces may be achieved faster and without decreasing the complexity of the network). Such revisions exclusively concern the search for regulatory trap-spaces. Indeed, our framework previously required a preliminary step of application of the value propagation algorithm **[254]** from CoLoMoTo **[255]** to reduce the complexity of the regulatory model before identifying its trap-spaces through the Java bioLQM toolkit **[250]**. The latter is no longer necessary as the search for trap-spaces is now handled by Trappist **[259]**, an open-source Python tool for computing minimal trap-spaces of Boolean models. Trappist replaces the need for prime-implicants with the enumeration of maximal siphons in the Petri net encoding the Boolean regulatory model. Beyond that slight difference replacing steps **(1)** and **(2)**, and the addition of the step model inference by CaSQ **[243]**, the various steps pursued by MetaLo to couple a regulatory Boolean model inferred from a molecular interaction map with a generic constraint-based metabolic reconstruction are exactly identical to those presented above. Thus, MetaLo relies on four external packages (*i.e.* CaSQ **[243]**, CobraPy **[256]**, Pandas, and Trappist **[259]**). Note that it allows to cover all specificities of the integrated tools and packages (*e.g.* leverage the ability of CaSQ to infer only a subpart of a molecular interaction map, the ability of CobraPy to run FVAs instead of FBAs).

To confirm the correct packaging of our framework and demonstrate how the few adjustments displayed above had no impact upon the coupling process of regulatory and metabolic models, the results of RASFs and breast CAFs FVAs by MetaLo were compared to the results of the hybrid framework. Note that results of FVAs were compared, not FBAs, since the latter only returns one of the possible solutions, whereas FVAs cover the range of optimized fluxes. Evaluating if the framework FBA results lies within MetaLo FVAs ranges of fluxes confirms the homogeneity of the results.

4 RESULTS

4.1 STATE-OF-THE-ART KNOWLEDGE BASES IN THE FORM OF MOLECULAR INTERACTION MAPS

4.1.1 The RA-map V2, a comprehensive graphical representation of RA pathogenesis

After major updates and corrections, the RA-map V2 is a state-of-the-art graphical representation illustrating the major signaling, gene regulation, and metabolic pathways, along with molecular mechanisms and phenotypes involved in RA pathogenesis (**Figure 26**). It is available as a standalone molecular interaction map on the MINERVA platform **[234]** at https://ramap.uni.lu/minerva/.

The RA-map V2 is fully compliant with SBGN PD standards for graphical representation **[189], [227]**, MIRIAM for annotation **[233]**, CALM for biocuration **[231]**, SMBL for format interoperability **[229]**, and overall FAIR principles **[226]**. It is compartmentalized with biologically relevant compartments for cellular representation (*i.e.* extracellular space, plasma membrane, mitochondrion, endoplasmic reticulum, nucleus, secreted compartments, extracellular space). It includes 720 species (*i.e.* 329 proteins, 135 genes, 136 RNAs, 54 simple molecules, 1 ion and 65 molecular complexes, 9 phenotypes) and 602 reactions (*i.e.* transport, translation, transcription, heterodimer association, dissociation, state activation, reduced physical stimulation). Phenotypes depicted in the RA-map V2 are specific nodes describing different biological states and behavior. They can describe specific cellular actors outcome or reproduce signals emitted by various cellular actors into the RA joint. All of the RA-map V2 phenotypes are clearly defined in **Table 4**.

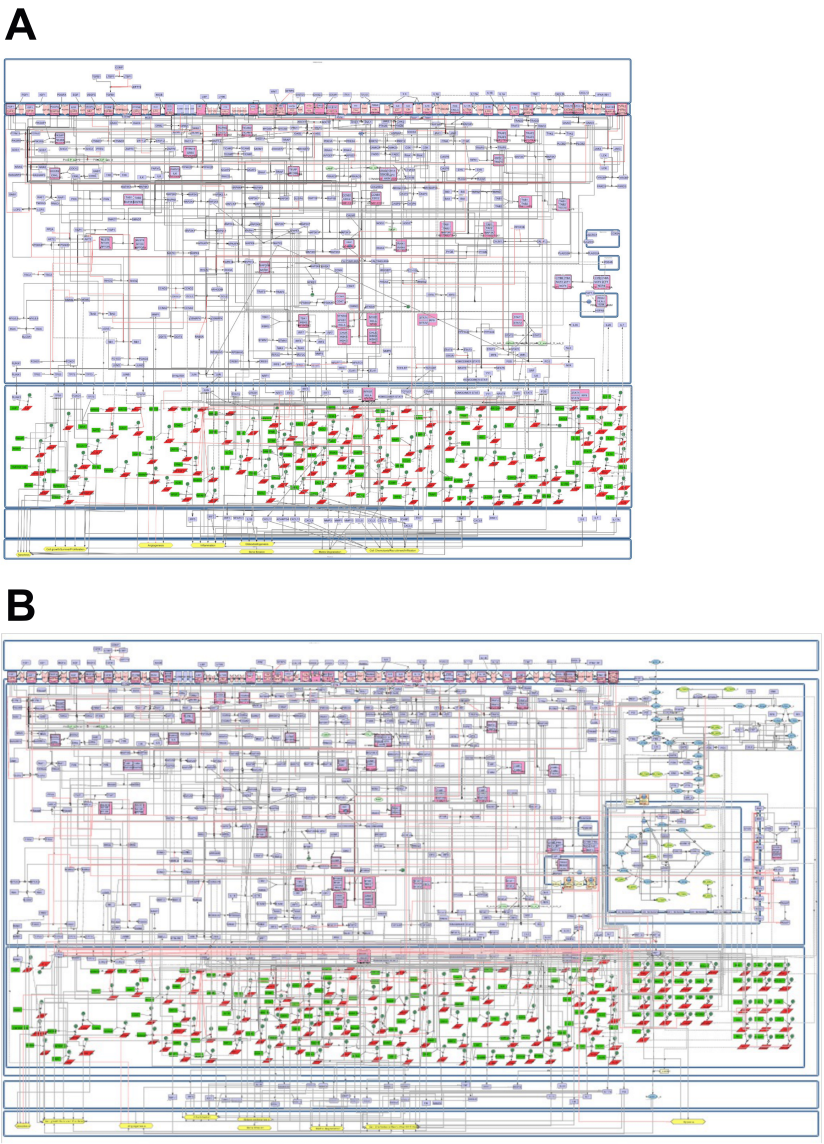

Figure 26. Upgrade of the original RA-map into the RA-map V2. CellDesigner visualization of **(A)** the original RA-map and **(B)** the RA-map V2. The RA-map V2 depicts a standard-compliant formal representation with addition of metabolic pathways, hypoxia phenotype, and expansion of mitochondria and endoplasmic reticulum compartments. The map is color-coded with proteins in purple, genes in green, RNAs in red and phenotypes in yellow. State transitions and catalysis reactions are displayed in black, and the inhibitions are in red. Compartments are distinguished as bounding boxes.

Table 4. RA-map V2 coverage in biological phenotypes and definition.

Phenotype	Specificity	Definition
Angiogenesis	Signal in the environment	Angiogenesis refers to the formation of new blood vessels. By carrying aggressive cells to the site of inflammation and supplying nutrition and O_2 to proliferating inflamed tissue, new blood vessels help maintain the RA chronic inflammatory state **[260]**.
Apoptosis	Cellular outcome	Apoptosis is the process of controlled self-destruction. In RA, apoptosis may be dysregulated, leading to an accumulation of immune cells and the release of pro-inflammatory factors, contributing to the perpetuation of inflammation. Synovial cell apoptotic changes have been linked to RA etiology as a crucial mechanism controlling tissue composition and homeostasis **[261]**.
Bone erosion	Signal in the environment	Bone erosion refers to the loss or destruction of bone tissue. In RA, chronic inflammation and activation of immune cells (*e.g.* osteoclasts) from the hypertrophied synovial membrane lead to the erosion and cartilage destruction of bone in affected joints **[262]**.
Cell chemotaxis, recruitment, infiltration	Cellular outcome	Cell chemotaxis is the directed movement of cells in response to chemical signals. In RA, various immune cells (*e.g.* monocytes, neutrophils, lymphocytes) are recruited and infiltrate the synovial tissue, perpetuating the inflammatory response. For instance, leukocyte infiltration of the synovial compartment is due to increased production of adhesion molecules and chemokines in the endothelium **[263]**.
Cell growth, survival, proliferation	Cellular outcome	Cell growth, survival, and proliferation refer to the processes by which cells increase in number and maintain their viability. In RA, abnormal cell signaling and dysregulation of growth factors can contribute to the expansion and survival of immune cells involved in the inflammatory response **[264]**.
Hypoxia	Signal in the environment	Hypoxia refers to a condition characterized by inadequate oxygen supply to tissues. In RA, chronic inflammation can cause hypoxia in the synovial tissue, leading to the production of pro-inflammatory factors and contributing to disease progression through disordered apoptosis and metabolism, cartilage degradation, and oxidative damage **[265]**.

Inflammation	Signal in the environment	Inflammation is the immune response to injury, infection, or tissue damage. In RA, inflammation occurs in the synovial tissue of joints, leading to swelling, pain, and stiffness. Chronic inflammation can cause joint damage and deformity over time **[266]**.
Matrix degradation	Cellular outcome	Matrix degradation refers to the breakdown of the extracellular matrix, which provides structural support to tissues. In RA, enzymes released by immune cells, such as matrix metalloproteinases, contribute to the degradation of the synovial tissue and cartilage, leading to joint damage **[267]**.
Osteoclastogenesis	Cellular outcome	Osteoclastogenesis is the process of differentiation and activation of osteoclasts, specialized cells responsible for bone resorption. In RA, abnormal activation of osteoclasts contributes to bone erosion and destruction of the affected joints **[268]**.

This new version of the RA-map represents an upgrade regarding the number of components through the addition of 214 species, primarily involved in metabolic pathways along with apoptotic and endoplasmic reticulum compartment, 156 reactions, primary interconnecting metabolic pathways with signaling and gene regulation pathways, and the hypoxic phenotype. We included 222 additional bibliographical references (*i.e.* experimental studies and literature reviews) both validating components and interactions already present in the original RA-map along with illustrating RA-map V2 additions, for a total of 575 PMIDs.

Statistical analysis conducted for cellular-specificity and confidence evaluation are publicly available on a GitLab repository at https://gitlab.com/genhotel/rasf-hybrid-model. The high number of references enhances confidence in the depicted mechanisms as 87% of the components included in the RA-map V2 are supported with more than one experimental evidence and 65% with more than two (**Figure 27**).

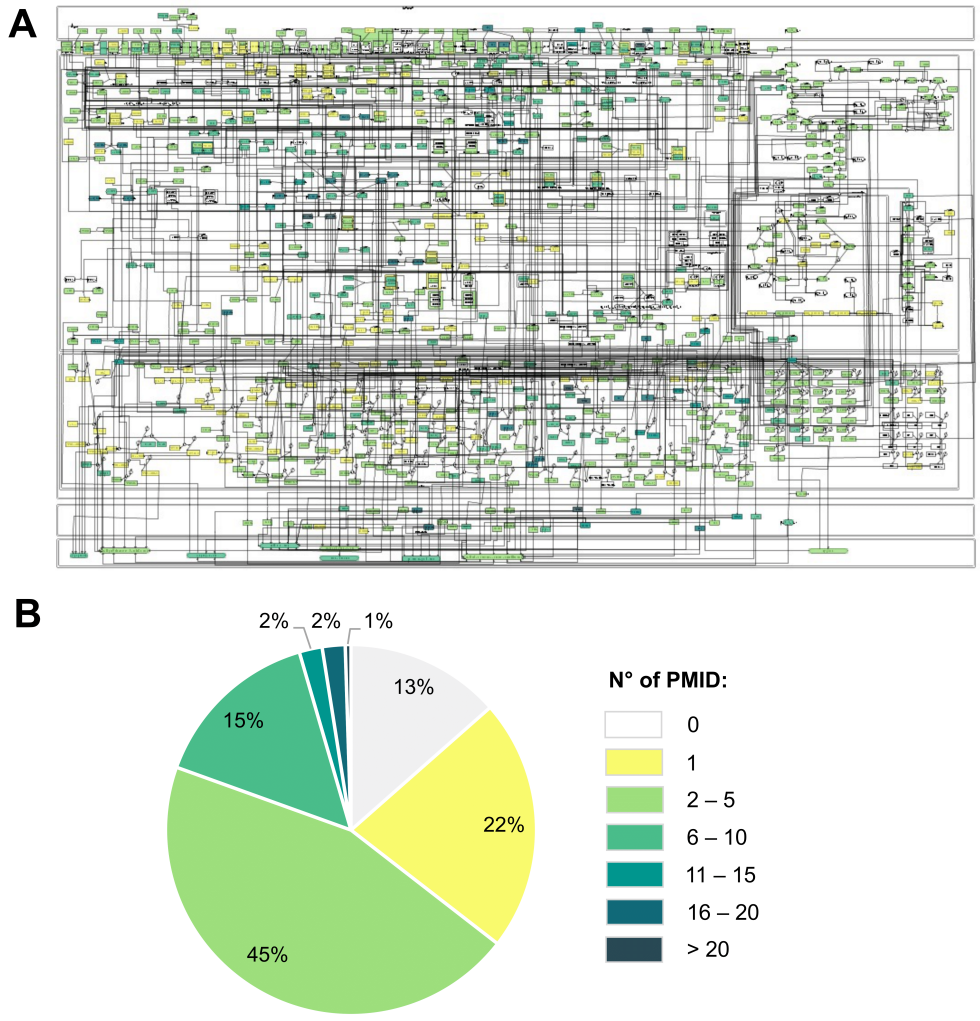

Figure 27. Annotation score of the RA-map V2. (A) Overlay on MINERVA of the annotation scores upon the RA-map V2. Each component of the molecular interaction map is colored according to its annotation score. **(B)** Pie-chart of the annotation scores distribution among the RA-map V2 components.

However, one should note that, as shown in **Figure 27**, 13% of the RA-map V2 components are not supported by any bibliographic reference. This may be due to a variety of reasons. For instance, many "simple molecules", as referred to in CellDesigner, (*e.g.* ATP, ADP, NADH, NADPH, H_2O, O_2, CoA, FADH) act as products or reactants of well-known biological reactions.

Thus, their expressions are rarely highlighted in disease-specific experimental studies as it is rather inherently recognized. Also, molecules that act as intermediates in specific metabolic pathways may not present bibliographical references. In this case, we have evidence that the metabolic pathway is expressed in a cell- and/or disease-specific manner, but not all intermediates have been studied experimentally and confirmed one by one. For instance, specific metabolic pathways such as the PPP are found to be expressed in RASFs, however, experimental evidence may not be available for each and every PPP metabolic component. Similarly, certain intermediates are required for an efficient signal transduction in gene regulation or intracellular signaling which may not yet have been widely documented yet.

Beyond the considerable effort of the initial RA-map to include the main disease hallmarks (*e.g.* cytokines, chemokines, growth factors, toll-like receptors) and molecular pathways (*e.g.* JAK-STAT pathway, NF-KB pathway, MAPK pathway, interleukin pathways), we aimed to expand the coverage in disease-specific metabolic dysregulated pathways. In particular, we focused on adding glycolysis, TCA, PPP, and OXPHOS pathways as their interplay with inflammation and immunity mechanisms, among others, have been proven in RA **[269], [270]**. In addition, non-metabolic functions of metabolites and metabolic enzymes were illustrated, such as their transcription regulation function (*e.g.* Hexokinase 2 or Phosphoglycerate Kinase 1 **[271]**) or their involvement in disease-specific signaling pathways or phenotypes (*e.g.* Lactate **[272]**, Glucose-6-Phosphate Isomerase **[273]** or Pyruvate **[274]**).

The RA-map V2 integrates information from several sources and cellular actors within the RA joint. The user can take advantage of its extensive annotation and assess the coverage of the molecular interaction map by opting for the specific representation of a particular cell type in MINERVA. As

shown in **Figure 28**, the RA-map V2 is mainly composed of fibroblast specific information (73%) but other cell types, tissues, and fluids involved in RA pathogenesis **[275]** are also represented, including synovial tissue, synovial fluid, blood components, serum components, PBMC, chondrocytes and macrophages. However, when interpreting those results, one must consider that a specific component can be common to several cell types and not always specific to only one.

Topological analysis of the RA-map V2 network was further conducted on Cytoscape **[237]** to explore the topology of the associated network and reveal hidden properties. The network was first visualized in the default style with the edge-weighted spring-embedded layout. The latter represents the connections between the nodes as metal springs attached to the pair of nodes. Such springs repel or attract their ends according to a force function. The layout algorithm defines node positions so as to minimize the sum of forces in the network. As shown in **Figure 29**, the RA-map V2 network is shown as a large connected core with a few unconnected subsystems. The connected core corresponds to the connected subgraphs (*i.e.* parts of the network in which any node can be reached from any other node). Its large size may be interpreted as the inherent interconnectedness of signaling, gene regulation, and metabolic pathways involved in RA pathogenesis. On the other hand, 26 unconnected subgraphs of one to eight components are depicted. These unconnected subparts of the network may represent nodes that have been described as involved in RA, explaining their inclusion in the RA-map V2, but that have not been yet replaced in the complexity of its pathogenesis and may reflect the still highly fragmented knowledge about the disease. Indeed, a number of unconnected subparts correspond to microRNAs experimentally proven to be altered in RA (*e.g.* MIR34A, MIR221, MIR203A, MIR124 **[276]**) whose mode of action may remain undeciphered. A more striking example is the HLA-DRB1 component, the first genetic factor identified in

RA pathogenesis **[134], [135]**, whose precise mode of action is still unknown. Another explanation for the non-connectivity of such subgraphs could rely on the strictness of our curation criteria which may have eliminated a few components and interactions in the RA-map V2.

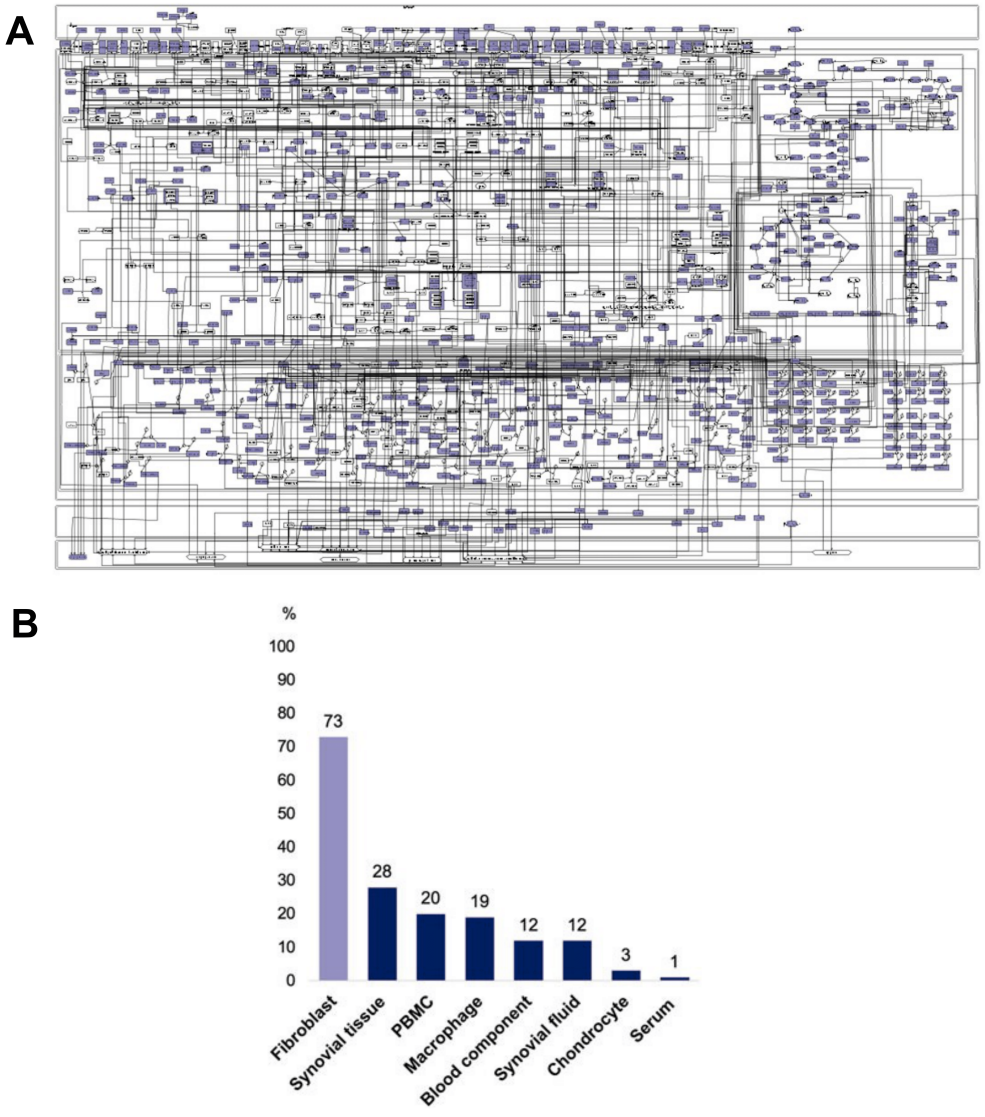

Figure 28. Cell-specificity of the RA-map V2 components. (A) Visualization of the fibroblast-specific overlay on the RA-map V2. **(B)** Distribution of the RA-map V2 cellular specificity.

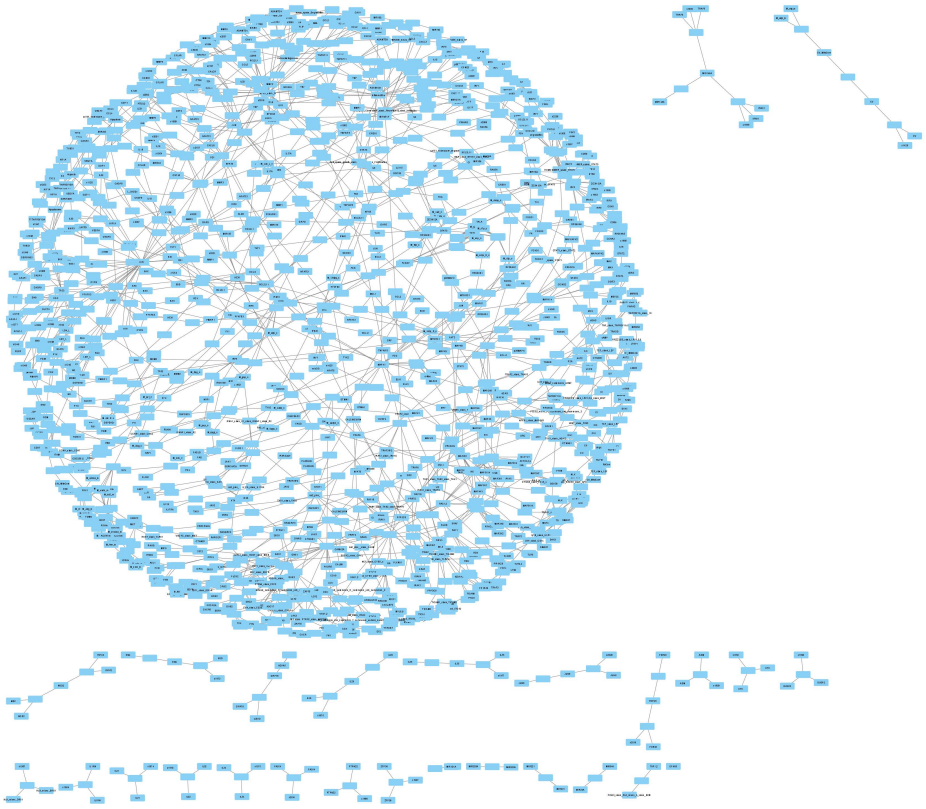

Figure 29. Visualization of the RA-map V2 in Cytoscape. The default style is applied along with the edge-weighted spring-embedded layout. We distinguish a large highly-connected core network, characterizing the variety of intertwined regulatory and metabolic pathways in RA pathogenesis, as well as 26 unconnected subsystems, reflecting the still fragmented knowledge in the disease pathogenesis.

Proper topological analyses were further performed on the RA-map V2 network in the undirect setting to provide insights into the connectivity or interaction patterns within the network (**Table 5**).

Table 5. Results of the default topological analysis performed by Cytoscape NetworkAnalyzer plugin on the RA-map V2. Number of nodes: number of different entities; number of edges: number of different interactions between nodes; average number of neighbors: average connectivity of a node in the network; network diameter: maximum length of shortest paths between two nodes; network radius: minimum among the non-zero eccentricity of the nodes in the network; characteristic path length: expected distance between two connected nodes; clustering coefficient: average of the clustering coefficients for all nodes in the network. The clustering coefficient is a ratio N/M, where N is the number of edges between the neighbors of n, and M is the maximum number of edges that could possibly exist between the neighbors of n (between 0 and 1); network density: shows how densely the network is populated with edges (between 0 and 1); Network heterogeneity: diversity or variation in properties or characteristics of nodes or edges within a network; Network centralization: quantifies the degree to which network connectivity or control is concentrated in a subset of nodes within a network; Connected components: connected components are subsets of nodes within a network where each node is directly or indirectly connected to every other node within the same subset.

Statistic	Value
Number of nodes	1673
Number of edges	1989
Average number of neighbors	2.4
Network diameter	26
Network radius	14
Characteristic path length	9.785
Clustering coefficient	0
Network density	0.002
Network heterogeneity	0.832
Network centralization	0.018
Connected components	27

In the RA-map V2 network, each node has an average of 2.4 neighbours. This value provides information about the overall span or reachability of the network and is not very high. It suggests a rather sparse and spread-out or decentralized network, where nodes are relatively distant from each other. A network diameter of 26 refers to the longest shortest path length between any two nodes in the network. The network radius of 14 represents the minimum number of edges required to reach the farthest node from a specific node in the network, again suggesting that the network has a wide spread. A characteristic path length of 9.8 is a measure of how efficiently information or signals can travel within the network suggests a dispersed network, where it may take more steps to transmit information across the network. Network heterogeneity refers to the degree of diversity or variation in properties or characteristics of nodes or edges within a network. A value of 0.832 indicates a relatively high level of heterogeneity and diversity in the network. This means that the network contains nodes or edges that differ significantly in their attributes, resulting in a non-uniform distribution of these properties across the network. The network density refers to the proportion of actual connections or edges in a network compared to the total number of possible connections. A value of 0.002 means that only 0.2% of the possible connections between nodes in the network actually exist. This value indicates a sparse or low-density network, where only a small fraction of potential connections are present. The clustering coefficient for the RA network being equal to zero suggests that there are no particular links between the neighbours of a node, giving space to more star-like shapes (*i.e.* node with several edges connected to it) than cliques (*i.e.* node that its neighbours have also edges in common) in the network. Networks whose topologies resemble a star have a centralization close to 1, whereas decentralized networks are characterized by having a centralization close to 0. Here, we have a network centralization value of 0.018, confirming the latter observations. Overall, the RA-map V2 network seems fairly sparse, decentralized and heterogeneous.

Beyond default topological analyses, Cytoscape allowed us to identify the most important hubs in our large-scale RA-map V2 network by sorting them according to their degree. Note that highly connected nodes depicting cellular phenotypes were removed from this classification as they represent an outcome of the various biological pathways. Hubs are nodes with higher degree of connectivity and may represent distinct biological clusters highly involved in RA pathogenesis whose therapeutic targeting may be promising in altering the pathogenic phenotype. As shown in **Table 6**, HIF1 is the most connected component within the RA-map V2 network. It seems to interact with a variety of regulatory and metabolic components, thus exerting a probable central role in RA pathogenesis, as suggested before **[181]**. In addition to HIF1, other components appear to play a hub role within the RA-map V2 network: they are all key regulators in RA pathogenesis with a precise mode of action attributed (*e.g.* NFKB is a transcription factor involved in regulating the expression of numerous genes involved in inflammation and immune responses in RA **[277]**; TP53 is a tumor suppressor gene that regulates cell cycle progression, DNA repair, apoptosis, and contribute to the abnormal proliferation of synovial fibroblasts **[278]**; AKT2 is a serine/threonine protein kinase involved in cell survival, growth, and metabolism leading to increased survival and proliferation of synovial fibroblasts and immune cells **[279]**). Their central role is hardly surprising. However, two of the remaining hub nodes are metabolic components (*i.e.* M_g3p_c, M_f6p_c), clearly highlighting the immuno-metabolic pathways interconnections and crosstalks within the RA-map V2 with a central role of metabolism for regulation of RA pathogenic signaling and gene regulation.

Table 6. Top 10 hubs of the RA-map V2 network. Hubs are highly connected nodes of the network which may exert a key role in the associated pathogenesis.

Node	Type	Degree
HIF1	Protein	30
NFKB/N	Complex	29
TP53	Protein	18
AKT2	Protein	14
MAPK1	Protein	14
JUN	Protein	13
RAC1,2	Protein	11
M_g3p_c	Metabolite	10
FOS	Protein	8
M_f6p_c	Metabolite	8

4.1.2 The CAF-map V2, a comprehensive graphical representation of CAFs involvement in the TME

After major updates and corrections, the CAF-map V2 is an extensive knowledge base illustrating the major cellular signaling, gene regulation, and metabolic pathways, as well as molecular mechanisms and phenotypes involving CAFs in cancer initiation and progression. It is available as a standalone molecular interaction map on the MINERVA platform **[234]** at https://pathwaylab.elixir-luxembourg.org/CAF-map_V2. Visualizations of both the original CAF-map and CAF-map V2 are provided in **Figure 29**.

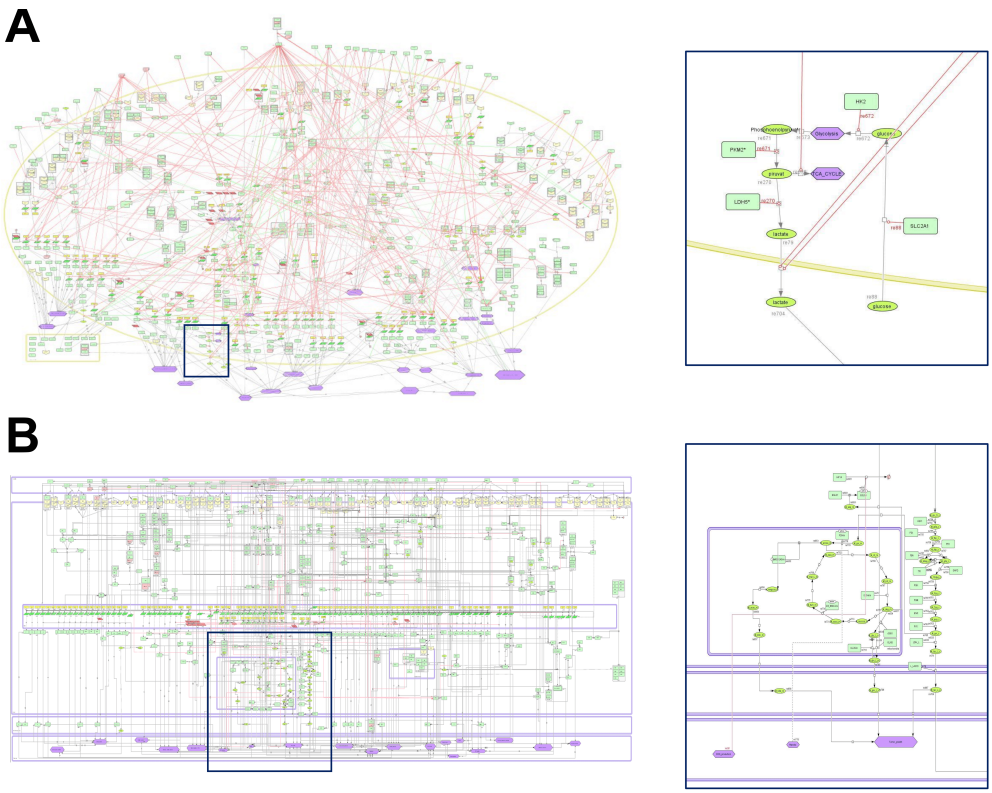

Figure 30. CellDesigner visualization of the (A) original CAF-map from ACSN and (B) CAF-map V2 with associated zoom-ins on glucose-related pathways. The CAF-map V2 depicts a standard-compliant formal representation and layout revision with a clear signal flow. Components are precisely attributed to newly created biologically-relevant compartments. Glucose pathways are compartmentalized and are no longer represented only as phenotypes but properly detailed. Up-to-date mechanistic information was further added.

The CAF-map V2 is fully compliant with SBGN PD standards for visualization **[189], [227]**, MIRIAM for annotation **[233]**, CALM for biocuration **[231]**, SMBL for format interoperability **[229]**, and overall FAIR principles **[226]**. It includes 649 species (*i.e.* 308 proteins, 95 genes, 114 RNAs, 43 simple molecules, and 89 molecular complexes, 19 phenotypes) and 544 reactions (*i.e.* transport, translation, transcription, dissociation, heterodimer association, state activation, reduced physical stimulation, negative and positive influence). Phenotypes of the CAF-map V2 are specific

nodes describing different biological states and behavior. They can describe fibroblasts outcome or reproduce cellular signals emitted by the latter within the TME. All of the CAF-map V2 phenotypes are clearly defined in **Table 7**. Biological compartments depicting extracellular space, cytosol, nucleus, mitochondrion, endoplasmic reticulum, secreted compartments were further added in the map to account for biological compartmentalization and cell transport. Beyond the considerable effort of the initial CAF-map to include major cancer functional modules (*e.g.* "growth factors production", "cytokines", "chemokines production", "matrix regulation") and molecular pathways (*e.g.* "growth factors signaling pathways", "inflammatory signaling pathways", "integrin signaling pathways"), coverage in disease-specific mechanisms was expanded in the CAF-map V2. For instance, metabolic pathways initially only considered as phenotypes were fully detailed, along with addition of the calcium ion signaling pathway in the new endoplasmic reticulum compartment.

Table 7. CAF-map V2 coverage in biological phenotypes and definition.

Phenotype	Specificity	Definition
Actomyosin contractility	Cellular outcome	Actomyosin contractility refers to the ability of cells to generate force and contract through the interaction of actin filaments and myosin motor proteins. In CAFs, increased actomyosin contractility can contribute to the remodeling of the extracellular matrix and promote tumor cell invasion and migration **[280]**.
Angiogenesis	Signal in the TME	Angiogenesis refers to the formation of new blood vessels. In the TME, CAFs play a role in angiogenesis by secreting various growth factors, cytokines, and proteases that promote the formation of new blood vessels to supply nutrients and oxygen to the growing tumor **[66]**.
Cytokine production	Cellular outcome	CAFs are known to produce a variety of cytokines, regulating immune responses and cell behavior promoting tumor cell survival, proliferation, and invasion **[281]**.

ECM regulation	Signal in the TME	CAFs are involved in synthesis, remodeling, and degradation of the extracellular matrix. CAFs can deposit excessive amounts of ECM components, leading to fibrosis and tissue stiffening in the TME or produce enzymes degrading the ECM, facilitating tumor invasion and metastasis **[282]**.
Fibroblast markers	Cellular outcome	Fibroblast markers are proteins or molecules expressed by fibroblast cells used to identify and distinguish CAFs from other cell types within the TME **[283]**.
Fibroblast proliferation	Cellular outcome	Fibroblast proliferation refers to the process by which fibroblast cells divide and increase in number. In cancer, CAFs can exhibit increased proliferation compared to normal fibroblasts, leading to their accumulation within the TME **[284]**.
Fibrosis	Signal in the TME	Fibrosis refers to the excessive deposition of collagen and other components of the ECM, resulting in the formation of fibrous tissue. In the TME, CAFs can contribute to fibrosis, leading to increased tissue stiffness and the formation of a reactive stroma supporting tumor growth and invasion **[285]**.
Formation of basement membrane	Signal in the TME	The basement membrane is a specialized ECM structure that separates epithelial or endothelial cells from underlying connective tissue. CAFs can participate in the formation or remodeling of the basement membrane in the TME, affecting cell adhesion, migration, and invasion **[286]**.
Growth factors production	Cellular outcome	CAFs can produce various growth factors promoting tumor cell growth, survival, angiogenesis, and metastasis **[287]**.
Hypoxia	Signal in the TME	Hypoxia refers to a condition of low oxygen levels. In the TME, regions of hypoxia can induce the activation and recruitment of CAFs which may exhibit altered behavior and secrete specific factors contributing to tumor progression and angiogenesis **[288]**.
Immune system modulation	Signal in the TME	CAFs can influence the immune system in the TME by suppressing immune cell function or promoting the recruitment of immunosuppressive cells, thereby contributing to tumor immune evasion **[289]**.
Markers of fibroblast activation	Cellular outcome	Markers of fibroblast activation are proteins or molecules that are expressed by activated fibroblasts, including CAFs. Their expression indicates the transition of fibroblasts into an activated state with enhanced functions and altered phenotypes **[283]**.

Matrix degradation	Cellular outcome	Matrix degradation refers to the breakdown or remodeling of the extracellular matrix components by various enzymes, such as matrix metalloproteinases. CAFs can secrete MMPs and other proteases that contribute to the degradation of the ECM, allowing tumor cells to invade and metastasize **[290]**.
Migration into the tumor	Cellular outcome	CAFs can migrate from surrounding normal tissues into the tumor stroma. This migration is often driven by signals from tumor cells and the TME. Once in the tumor, CAFs may contribute to tumor growth and progression through various mechanisms **[291]**.
Negative regulators of CAFs	Cellular outcome	Negative regulators of CAFs are factors or signaling pathways that can inhibit or suppress the activation and functions of CAFs, playing a role in maintaining tissue homeostasis and limiting excessive fibroblast activation and ECM remodeling **[283]**.
ROS production	Cellular outcome	CAFs can produce increased levels of ROS, which can have diverse effects on tumor cells and the TME by influencing signaling pathways, promoting DNA damage, and contributing to the pro-inflammatory and pro-tumorigenic effects **[97]**.
Reactive stroma	Signal in the TME	Reactive stroma refers to the altered and activated state of the stromal tissue in the TME. CAFs are a major component of the reactive stroma, characterized by increased ECM deposition, fibrosis, and altered signaling **[57]**.
Tumor growth	Signal in the TME	CAFs play a significant role in promoting tumor growth by providing growth factors, remodeling the ECM, facilitating angiogenesis, and creating a supportive tumor microenvironment **[292]**.
Tumor invasion	Signal in the TME	CAFs contribute to tumor invasion by facilitating tumor cell migration, ECM remodeling, and promoting EMT. CAFs can create tracks and provide guidance cues for tumor cells, promoting their invasion into surrounding tissues and facilitating metastasis **[293]**.

A dozen additional peer-reviewed articles (*i.e.* experimental studies and literature reviews) enabled us to correct and extend the mechanical processes depicted in the map for a total of 368 PMIDs. Statistical analysis conducted for specificity and confidence are publicly available at https://gitlab.com/genhotel/breast-cafs-reverse-warburg-effect. High number of references enhances confidence in presented mechanisms as 76% of the components are supported with more than one experimental evidence and 70% more than 2 (**Figure 30**).

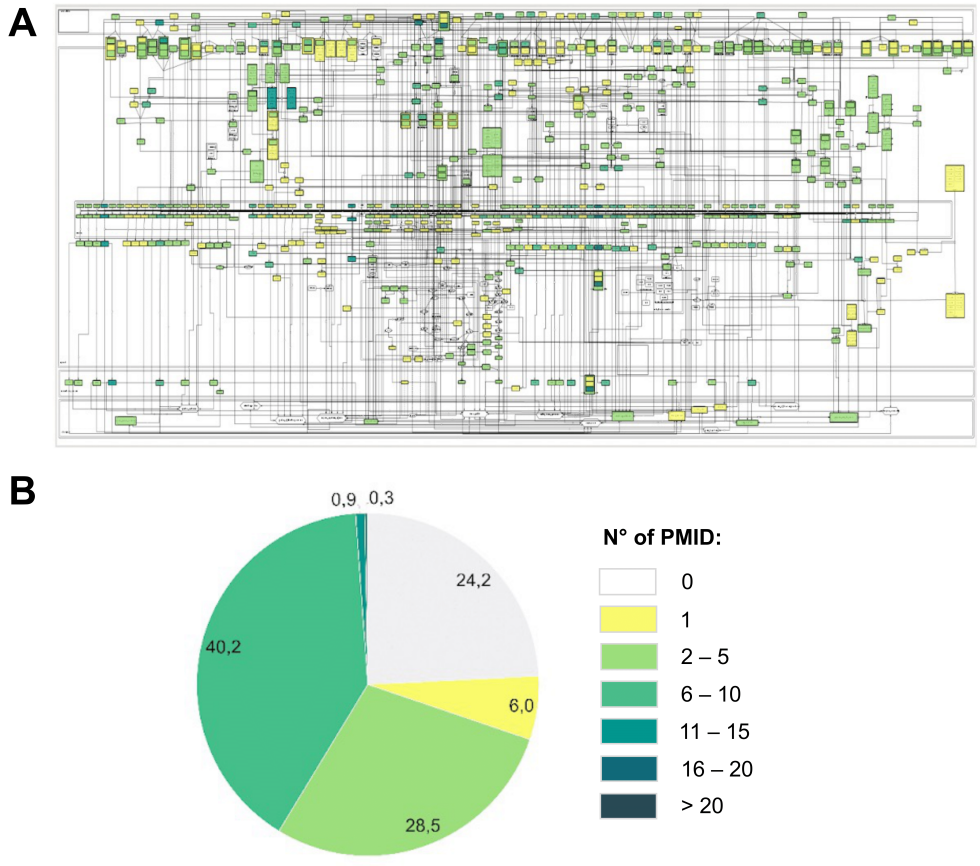

Figure 31. Annotation score of the CAF-map V2. (A) Overlay on MINERVA of the annotation scores upon the CAF-map V2. **(B)** Pie-chart of the annotation scores distribution among the CAF-map V2 components.

Similarly to the RA-map V2, a number of components depicted in the CAF-map V2 are not supported by any bibliographic reference, due to the same variety of reasons: expression of simple molecules acting as products or reactants of well-known biological reactions are often not highlighted in experimental studies, metabolic or signaling intermediates necessary for proper signal transduction may additionally not be described.

The CAF-map V2 network is totally specific to CAFs as all included components were extracted from data manually curated from CAF-specific studies. Thus, it is the cancer-specificity that was further assessed through DEA. Results of NSCLC and BC-specific DEAs are presented in **Figure 31**.

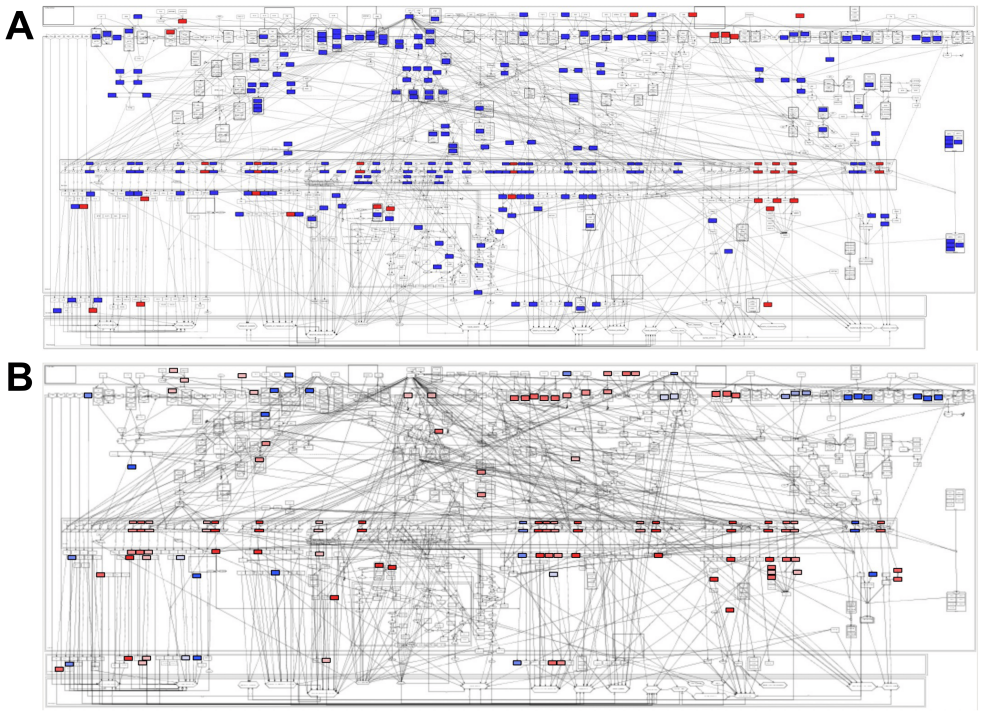

Figure 29. Visualization of cancer-specific differential expression analysis as overlays on the CAF-map V2 in MINERVA. (A) Results of cultured non-small cell lung cancer-associated fibroblasts *vs.* healthy fibroblasts analysis. **(B)** Results of breast cancer CAFs-S1 *vs.* CAFs-S4.

Topological analysis of the CAF-map V2 network was further conducted on Cytoscape **[237]** to explore the topology of the associated network and reveal hidden properties. The network was first visualized in the default style and the edge-weighted spring-embedded layout. The latter represents the connections between the nodes as metal springs attached to the pair of nodes. Such springs repel or attract their ends according to a force function. The layout algorithm defines node positions so as to minimize the sum of forces in the network. As shown in **Figure 32**, the CAF-map V2 network is shown as a single large connected core (*i.e.* parts of the network in which any node can be reached from any other node through a specific path). Its large size may be interpreted as the inherent interconnectedness of components and signaling, gene regulation, and metabolic pathways involving CAFs within the TME and further in cancer pathogenesis.

Proper topological analyses were further performed on the CAF-map V2 network in the undirect setting to provide insights into the connectivity or interaction patterns within the network (**Table 8**). In the CAF-map V2 network, each node has an average of 2.6 neighbours. This value is not very high, suggesting a rather sparse and fragmented network. A network diameter of 20 refers to the longest shortest path length between any two nodes in the network. This value provides information about the overall span or reachability of the network and suggests a spread-out network where nodes are relatively distant from each other. The network radius of 11 represents the minimum number of edges required to reach the farthest node from a specific node in the network, again suggesting that the network has a wide spread, with nodes relatively distant from each other.

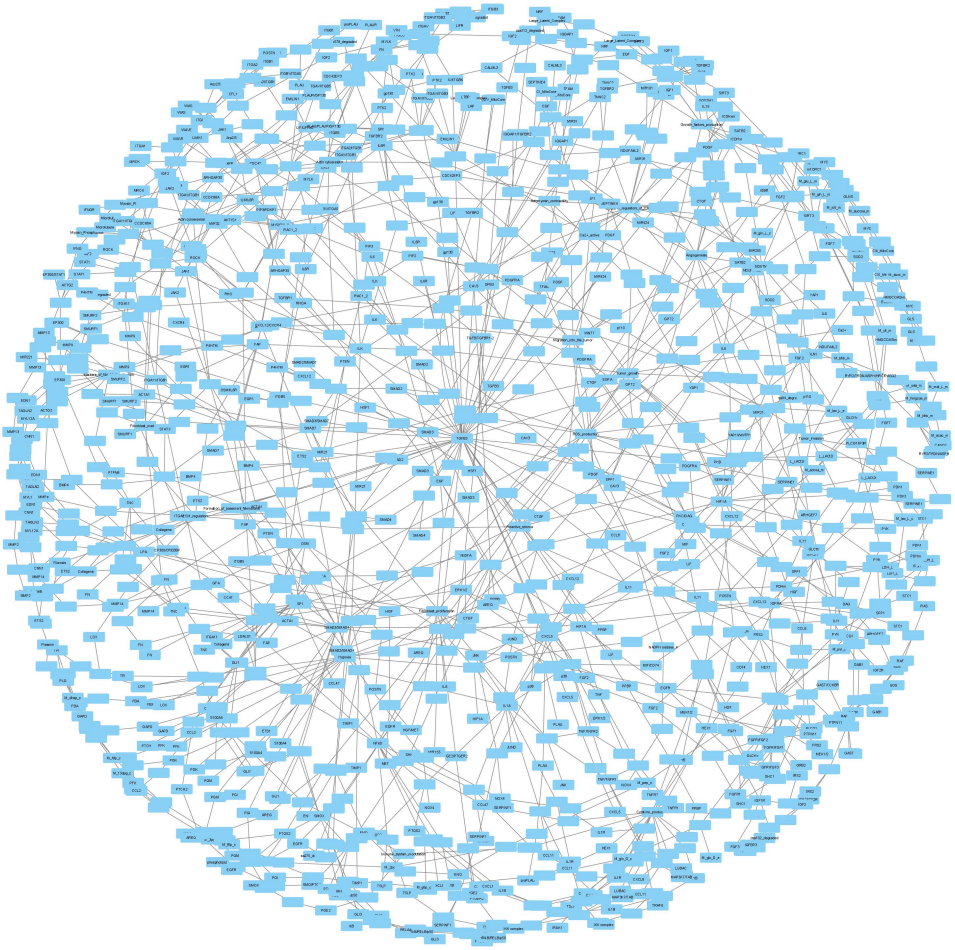

Figure 30. Visualization of the CAF-map V2 on Cytoscape. The default style is applied along with the edge-weighted spring-embedded layout. We can distinguish a large highly-connected core network, characterizing all intertwined regulatory and metabolic pathways in CAFs involvement in cancer pathogenesis.

Table 8. Results of the default topological analysis performed by Cytoscape NetworkAnalyzer plugin on the CAF-map V2. Number of nodes: number of different entities; number of edges: number of different interactions between nodes; average number of neighbors: average connectivity of a node in the network; network diameter: maximum length of shortest paths between two nodes; network radius: minimum among the non-zero eccentricity of the nodes in the network; characteristic path length: expected distance between two connected nodes; clustering coefficient: average of the clustering coefficients for all nodes in the network. The clustering coefficient is a ratio N/M, where N is the number of edges between the neighbors of n, and M is the maximum number of edges that could possibly exist between the neighbors of n (between 0 and 1); network density: shows how densely the network is populated with edges (between 0 and 1); Network heterogeneity: diversity or variation in properties or characteristics of nodes or edges within a network; Network centralization: quantifies the degree to which network connectivity or control is concentrated in a subset of nodes within a network; Connected components: connected components are subsets of nodes within a network where each node is directly or indirectly connected to every other node within the same subset.

Statistic	Value
Number of nodes	1218
Number of edges	1554
Average number of neighbors	2.6
Network diameter	20
Network radius	11
Characteristic path length	8.198
Clustering coefficient	0
Network density	0.002
Network heterogeneity	0.771
Network centralization	0.029
Connected components	1

A characteristic path length of 8.2 is a measure of how efficiently information or signals can travel within the network suggests a dispersed network, where it may take more steps to transmit information across the network. Network heterogeneity refers to the degree of diversity or variation in properties or characteristics of nodes or edges within a network. A value of 0.771 indicates a relatively high level of heterogeneity or diversity in the network. This means that the network contains nodes or edges that differ significantly in their attributes, resulting in a non-uniform distribution of these properties across the network. The network density refers to the proportion of actual connections or edges in a network compared to the total number of possible connections. A value of 0.002 means that only 0.2% of the possible connections between nodes in the network actually exist. This value indicates a sparse or low-density network, where only a small fraction of potential connections are present. The clustering coefficient for the CAF network being equal to zero suggests that there are no particular links between the neighbours of a node, giving space to more star-like shapes (*i.e.* node with several edges connected to it) than cliques (*i.e.* node that its neighbours have also edges in common) in the network. Networks whose topologies resemble a star have a centralization close to 1, whereas decentralized networks are characterized by having a centralization close to 0. Here, we have a network centralization value of 0.029, confirming the latter observations. Overall, the CAF-map V2 network seems fairly sparse, decentralized and heterogeneous.

Beyond default topological analyses, Cytoscape allowed us to identify the most important hubs in our large-scale CAF-map V2 network by sorting them according to their degree. Note that highly connected nodes depicting cellular phenotypes were removed from this classification as they represent an outcome of the various biological pathways. Hubs are nodes with higher degree of connectivity and may represent distinct biological clusters highly involved in RA pathogenesis whose therapeutic targeting may be promising

in altering the pathogenic phenotype. As shown in **Table 9**, TGFB, the SMAD complex, and HIF1A are the most connected component within the CAF-map V2 network. They seem to interact with a variety of regulatory and metabolic components, thus exerting a probable central role in CAFs involvement in the TME and cancer pathogenesis. In addition, other components appear to play a hub role within the CAF-map V2 network: they are all key regulators in CAFs pathogenesis with a precise mode of action attributed (*e.g.* CAV1, involved in promoting the activation and differentiation of CAFs **[294]**; IL1A, promoting the activation of fibroblasts into CAFs **[295]**; NFKB, inducing the production of cytokines, chemokines, and growth factors by CAFs, thereby promoting tumor cell proliferation, survival, angiogenesis, and immune evasion **[296]**). Their central role is hardly surprising.

Table 9. Top 10 hubs of the CAF-map V2 network. Hubs are highly connected nodes of the network which may exert a key role in the associated pathogenesis.

Node	Type	Degree
TGFB	Protein	37
SMAD3/SMAD4	Complex	17
HIF1A	Protein	14
CAV1	Protein	10
IL1A	Protein	10
NFkB	Protein	10
LPA	Simple molecule	8
SMAD7	Protein	8
OSM	Protein	7
PDGF/PDGFRA	Complex	7

The work presented in this section enabled us to tackle part of the first objective of the thesis, namely creating standalone static knowledge bases for RA and CAFs covering cellular signaling, gene regulation, and metabolism. The RA-map V2 and CAF-map V2 manually curated and validated graphical knowledge bases in the form of molecular interaction maps, totally standardized in their construction, layout, annotation, and format represent the first efforts to reconstruct disease-specific static molecular networks covering interactions between regulatory and metabolic processes. With a high level of confidence in the depicted mechanistic information, the RA-map V2 and CAF-map V2 were used as online up-to-date knowledge bases gathering curated mechanistic information, templates for overlaying multiple omics datasets and highlight cellular- or disease-specificity, and were analyzed in terms of topology to highlight potential hubs with considerable regulatory influence.

Associated scientific communication, details here

The construction of the RA-map V2 was published in an original research article and presented at two international scientific conferences:

Zerrouk, N*; **Aghakhani, S*;** Singh, V; Augé, F; Niarakis, A. A mechanistic cellular atlas of the rheumatic joint. *Frontiers in Systems Biology* **2022** 2:925791. https://doi.org/10.3389/fsysb.2022.925791

Zerrouk, N*; **Aghakhani, S*;** Singh, V; Augé, F; Niarakis, A. A multicellular atlas of the rheumatic joint. *European Conference on Computational Biology*; September 18-21, **2022**; Sitges — Spain (poster)

The construction of the CAF-map V2 was published in an original research paper and presented at an international scientific conference:

Aghakhani, S; E Silva Saffar, S; Soliman, S; Niarakis, A. Hybrid computational modeling highlights reverse Warburg effect in breast cancer-associated fibroblasts. *Computational and Structural Biotechnology Journal* **2023**. https://doi.org/10.1016/j.csbj.2023.08.015

Aghakhani, S; E Silva Saffar, S; Soliman, S; Niarakis, A. **A large-scale hybrid model to study metabolic reprogramming in cancer-associated fibroblasts.** *ONCOLille Days*; November 2-4, **2022**, Lille — France (poster)

4.2 LARGE-SCALE BOOLEAN REGULATORY MODELS FOR DYNAMIC ANALYSIS

4.2.1 The RASF model, an executable model of RASFs pathogenic activity in the RA joint

Inference of the RASF model was conducted by CaSQ based on the RA-map V2 by focusing solely on RASF-specific molecular pathways (**Figure 33**). The latter are determined as pathways associated with the RA-map V2 RASF-specific inputs as determined from peer-reviewed specialized literature (**Table 10**).

Table 10. Characteristics of the RA-map V2 export for inferring the RASF Boolean model with CaSQ. Export direction and bibliographical reference for each component are provided.

Export	Component	Class	Reference
Upstream	HIF1	Protein	[297]
Downstream	IL6	Extracellular ligand	[298]
Downstream	IL18	Extracellular ligand	[299]
Downstream	FGF1	Extracellular ligand	[300]
Downstream	PDGFA	Extracellular ligand	[301]
Downstream	TGFB1	Extracellular ligand	[302]
Downstream	WNT5A	Extracellular ligand	[303]
Downstream	SFRP5	Extracellular ligand	[304]
Downstream	RANKL	Extracellular ligand	[305]
Downstream	IL17A	Extracellular ligand	[306]
Downstream	FASLG	Extracellular ligand	[307]
Downstream	IKBA NFKB1 RELA	Extracellular ligand	[308]
Downstream	TNF	Extracellular ligand	[309]
Downstream	GLC	Extracellular metabolite	[177]
Downstream	MIR192	microRNA	[310]

```
casq RA_map-V2.xml -d FGF1 PDGFA TGFB1 WNT5A RANKL IL6_Ex-
tracellular_space_Space   IL18   FASLG   IL17A_Extracellu-
lar_space_Space              TNF_Extracellular_space_Space
M_glc_D_e_simple_molecule                Hypoxia_phenotype
IKBA/NFKB1/RELA_complex MIR192_rna SFRP5 -u Hypoxia_pheno-
type
```

Figure 34. CaSQ command line to infer the RASF model from the RA-map V2by focusing on RASF-specific pathways. The optional arguments -d (--downstream) only export species downstream of this specific node and -u (--upstream) only export species upstream of this specific node.

The obtained RASF model is a dynamic Boolean model of 359 nodes, including 14 inputs, and 642 interactions. The RASF model is accessible online within BioModels repositories of biological models **[246], [247]** with the identifier MODEL2212220001 and the Cell Collective platform **[245]** at https://research.cellcollective.org/human-rheumatoid-arthritis-synovial-fibroblast. Statistical analysis conducted are publicly available on a GitLab repository at https://gitlab.com/genhotel/rasf-hybrid-model.

The latter RASF-specific model inference step enabled us to increase the cellular specificity of our dynamic model. Indeed, although the RA-map V2 is a collection of information from several cell types, tissues, and fluids, the inferred model is mostly RASF-specific (82%) (**Figure 34A**). When interpreting those results, one must consider that a specific component can be common to several cell types. If only exclusive components are considered, the model is 91% RASF-specific (**Figure 34B**). This high level of cellular specificity, achieved through RASF-specific pathway inference, along with the phenotypes and extracellular ligands specificity, allows referring to this regulatory Boolean model as the RASF model. In addition, the annotation score of the model enables high confidence in the depicted information. Indeed, 97% of components present more than one manually curated experimental evidence and 74% present more than 2 (**Figure 34C**).

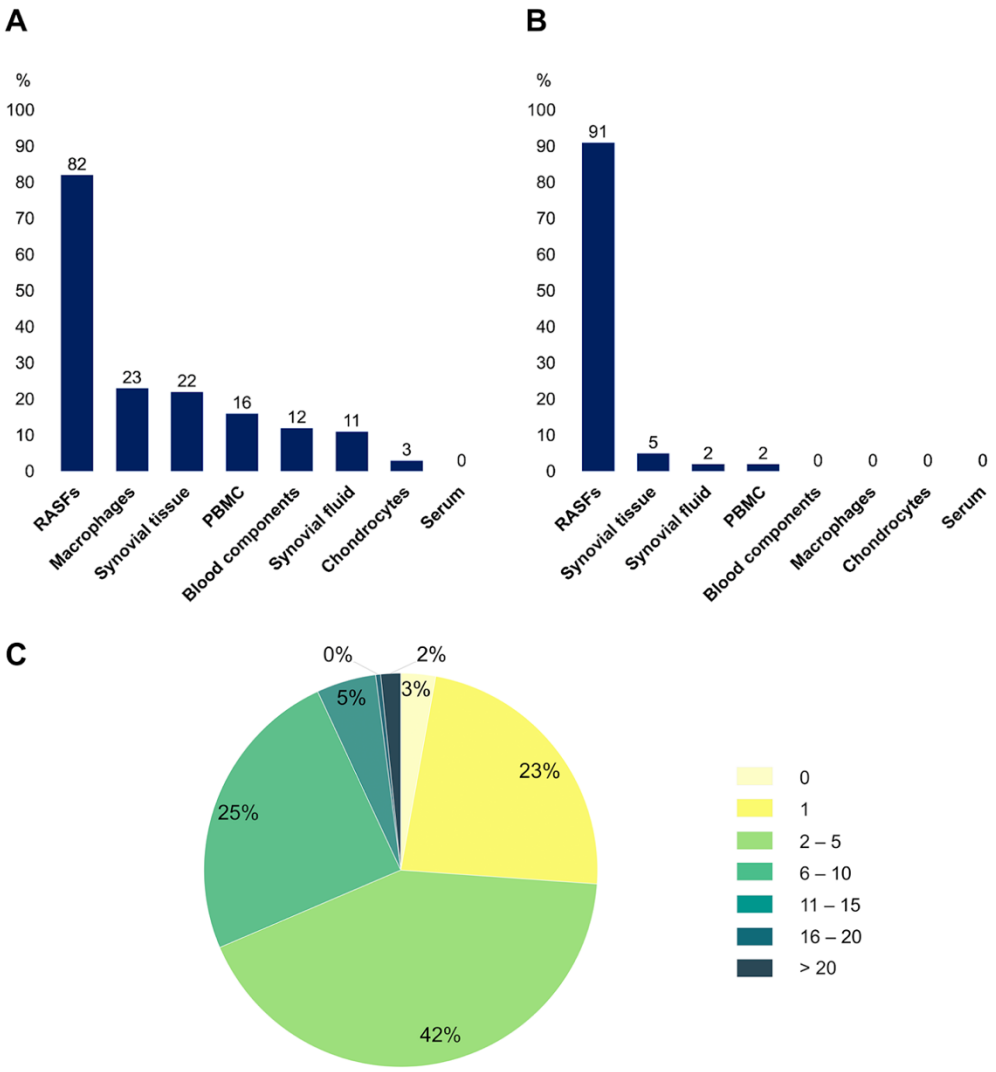

Figure 35. Statistical analysis of the RASF model. (A) Distribution of the cellular specificity of the RASF model. **(B)** Distribution of the RASF the cellular specificity of the RASF model when only exclusive components are considered. **(C)** Annotation scores distribution among the components of the RASF model.

Various situations can be considered regarding the 3% of components for which no bibliographic reference is given. Many are simple molecules acting as products or reactants of well-known biological reactions whose expressions are rarely highlighted in disease-specific experimental studies

(*e.g.* ATP, ADP, NADH, NADPH, H_2O, O_2, FADH, Ca^{2+}). A further distinction is made regarding pathway intermediates. For instance, a specific pathway might be experimentally proven to be expressed in a disease-specific manner, but not all intermediates are necessarily studied. It is the case for several metabolic pathways that are found to be expressed in RASFs but experimental evidence is not available for every component.

To validate the behavior of the RASF model, generic *in-silico* simulations conducted on the Cell Collective platform were first compared with experimental scenarios extracted from the specialized literature. For instance, we identified an experimental scenario whereby MicroRNA-192 expressed in RASFs is involved in the activation of apoptosis by down-regulating Caveolin-1 **[310, p. 1]**. We translated such experimental qualitative observation in terms of an *in-silico* experiment by subsequently activating and inactivating the expression of MicroRNA-192 and visualizing the state of the apoptotic phenotype along with Caveolin-1 (**Figure 35**). The simulation displays the activation of apoptosis through the down regulation of Caveolin-1 and vice-versa, thus validating the experimental scenario. Remaining scenarios were tested and validated in the same manner. Regarding this evaluation, 23 experimental scenarios were confirmed out of 30 (**Table 11**). Scenarios that were not reproducible were due to multiple reasons. First, mechanistic information regarding certain interactions may be lacking in the literature, leading to a missing or incomplete representation in the RA-map V2 and the associated RASF model. Additionally, the validation of some scenarios involved stoichiometric information that was not possible to reproduce with a strictly Boolean formalism. Finally, some generic scenarios were not validated since other pathways already activated or inactivated said phenotype under the same initial conditions.

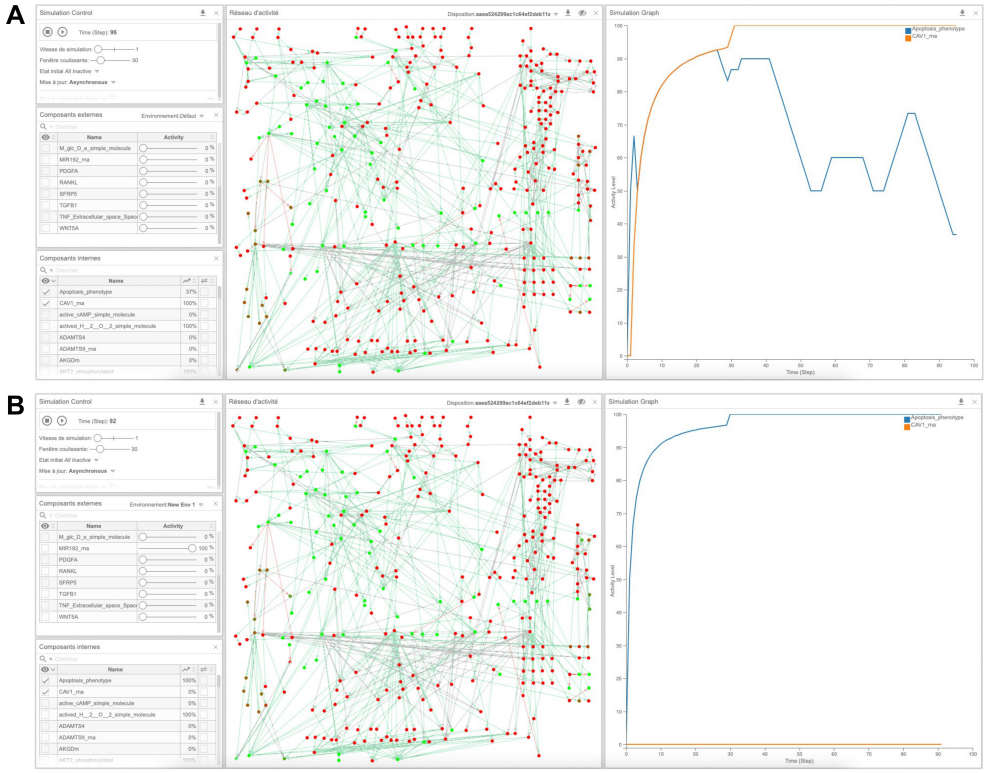

Figure 36. Assessment of the reproduction of an experimental scenario by the RASF model through an *in-silico* simulation on the Cell Collective interactive modeling platform. Simulation parameters are displayed on the left panel with a simulation speed of one, a sliding window of 30 and an asynchronous updating mode. The experimental observation that MicroRNA-192 induces apoptosis in RASFs *via* down-regulation of Caveolin-1 **[310, p. 1]** is reproduced on the RASF model with **(A)** inactivation and **(B)** activation of "MIR192_rna" (within the external components tab) along with visualization of "apoptosis_phenotype" and "CAV1_rna" (within the internal components tab). Signal tracking is displayed on the middle panel to monitor the regulatory signal flux under both simulation conditions. Simulation graphical results are shown on the right panel and confirm experimental observation: MicroRNA-192 is necessary to induce RASFs apoptosis through down-regulation of Caveolin-1.

Table 11. Biological scenarios identified from literature used for generic validation of the behavior of the RASF model in the Cell Collective platform. Experimental conditions were used as the input of the model and its outputs were compared to the biological outcome to confirm or refute the validation of a scenario.

Phenotype	Experimental observation	Reference	Input of the RASF model	Output of the RASF model	Coherence
Angiogenesis	PAI-1/SERPINE-1 strongly supports angiogenic activity in RASFs	[311]	SERPINE-1 ON	Angiogenesis ON	YES
			SERPINE-1 OFF	Angiogenesis oscillating	
	Hypoxia upregulates angiogenesis in RASFs	[312]	Hypoxia ON	Angiogenesis ON	YES
			Hypoxia OFF	Angiogenesis oscillating	
	Glucose-6-Phosphate Isomerase mediates hypoxia-induced angiogenesis in RASFs	[313]	GPI ON	Angiogenesis oscillating	NO
			GPI OFF	Angiogenesis oscillating	
	SDF-1 acts as a pro-angiogenic factor in RASFs	[314]	SDF-1 ON	Angiogenesis ON	YES
			SDF-1 OFF	Angiogenesis oscillating	
	IL-8/CXCL8 is considered as a pro-angiogenic factor in RASFs	[315]	CXCL8 ON	Angiogenesis ON	YES
			CXCL8 OFF	Angiogenesis oscillating	
Apoptosis	MicroRNA-192 induces apoptosis in RASFs through down-regulation of Caveolin 1	[310, p. 1]	MIR192 ON	Apoptosis ON, CAV1 OFF	YES
			MIR 192 OFF	Apoptosis OFF, CAV1 ON	
	TNF can induce apoptosis in RASFs only, when NFKB was inhibited	[316]	TNF ON, NFKB OFF	Apoptosis OFF	NO
			TNF ON, NFKB ON	Apoptosis OFF	

Bone erosion, osteoclastogenesis	AP-1, consisting of c-Fos and c-Jun, is key in signaling pathways ultimately leading to bone degradation	[317]	JUN ON, FOS ON	Bone erosion ON	**YES**
			JUN OFF, FOS OFF	Bone erosion OFF	
	RASFs RANKL expression is responsible for bone erosion	[318]	RANKL ON	Bone erosion ON	**NO**
			RANKL OFF	Bone erosion ON	
Cell chemotaxis, recruitment, infiltration	Citrullination of fibronectin alters RASFs ability to adhere and invade the RA joint and travel through the bloodstream	[319]	FN1 ON	Cell chemotaxis, recruitment, infiltration ON	**YES**
			FN1 OFF	Cell chemotaxis, recruitment, infiltration OFF	
Cell growth, survival, proliferation	Local fibroblast proliferation but not cellular influx is responsible for synovial hyperplasia in collagen antibody-induced arthritis	[320]	No initial conditions	Cell growth, survival, proliferation ON	**YES**
Hypoxia	Hypoxia, through HIF1α, promotes the expression of IL-33, SDF-1, MMP-3, IL-6, and VEGF	[321]	HIF1A ON	IL33 ON	**YES**
			HIF1A OFF	IL33 OFF	
			HIF1A ON	SDF1 ON	**YES**
			HIF1A OFF	SDF1 OFF	
			HIF1A ON	MMP3 ON	**YES**
			HIF1A OFF	MMP3 OFF	
			HIF1A ON	VEGF ON	**YES**
			HIF1A OFF	VEGF OFF	
			HIF1A ON	IL-6 OFF	**NO**
			HIF1A OFF	IL-6 OFF	
		[322]	PHD2 ON	HIF1A_a OFF	**NO**

	Knockdown of PHD-2 in RASFs dramatically augmented HIF1α expression and hypoxia		PHD2 OFF	HIF1A_a OFF	
Inflammation	HIF1α promotes inflammation in RASFs	[323]	HIF1A ON	Inflammation ON	YES
			HIF1A OFF	Inflammation OFF	
	Silencing PGK1 in RASFs reduces the secretion of IL-1β	[176]	PGK1 ON	IL-1β OFF	NO
			PGK1 OFF	IL-1β OFF	
	Synovial inflammatory cells were significantly decreased after the anti-TNF treatment	[324]	TNF ON	Inflammation ON	YES
			TNF OFF	Inflammation OFF	
	Activated NF-κB key components in RASFs contribute to persistent inflammation	[308]	IKBA NFKB1 RELA ON	Inflammation ON	YES
			IKBA NFKB1 RELA OFF	Inflammation OFF	
	Treatment with a neutralizing anti-IL-17 antibody suppressed joint inflammation	[325]	IL17A ON	Inflammation ON	YES
			IL17A OFF	Inflammation OFF	
	IL6 signaling induces an inflammatory response in RASFs	[326]	IL6 ON	Inflammation ON	YES
			IL6 OFF	Inflammation OFF	
	Suppression of JAK2/STAT3 signaling is involved in the anti-inflammatory effect	[327]	JAK2, STAT3 ON	Inflammation ON	YES
			JAK2, STAT3 OFF	Inflammation OFF	
	IL17A induces production of IL6 from RASFs	[328]	IL17A ON	IL6 OFF	NO
			IL17A OFF	IL6 OFF	
		[277]	NFKB ON	MMP13 ON	YES

Matrix degradation	NF-κB activation was found necessary for the induction of MMP-13 expression, implicated in the degradation of extracellular matrix		NFKB OFF	MMP13 OFF	
	HK2 ablation decreased RASFs bone and cartilage damage	[178]	HEX1 ON	Matrix degradation ON	**YES**
			HEX1 OFF	Matrix degradation OFF	
	The expression of MMP-3 was markedly enhanced in RASFs cultured under hypoxia	[329]	Hypoxia ON	MMP3 ON	**YES**
			Hypoxia OFF	MMP3 OFF	
	CCL5 induces collagen degradation by activating MMP-1 and MMP-13 expression in RASFs	[330]	CCL5 ON	MMP-1, MMP-13	**NO**
			CCL5 OFF	MMP-1, MMP-13	
	MMP-9 stimulates RASF-mediated degradation of cartilage	[331]	MMP-9 ON	Matrix degradation ON	**YES**

Subsequent global regulatory behavior evaluation under RASF-specific initial conditions (**Table 12**), *i.e.* identification of its complete asymptotic behavior, depicted eight different trap-spaces.

Table 12. RASF-specific initial conditions extracted from literature. Inputs of the regulatory model are marked with an asterisk.

Component	RASF-behavior	Source	Value
FASLG*	Activated	[307]	1
IL6*	Activated	[298]	1
IL18*	Activated	[299]	1
RANKL*	Activated	[305]	1
MIR192*	Down-regulated	[310]	0
TNF*	Activated	[309]	1
FGF1*	Activated	[300]	1
PDGFA*	Activated	[301]	1
WNT5A*	Activated	[303]	1
IL17A*	Activated	[306]	1
TGFB1*	Activated	[302]	1
IKBA NFKB1 RELA*	Activated	[308]	1
SFRP5*	Down-regulated	[304]	0
GLC*	Present	[178]	1
HIF1	Activated	[297]	1

Each trap-space reflects a different subspace of RASFs cellular phenotypes. Most components values are stable within all trap-spaces (always fixed at 0 or 1) but others vary within trap-spaces. The projection of trap-spaces restricted to the ontological phenotypes (*i.e.* distinct cellular outcome) are displayed in **Table 13**. The phenotypes of angiogenesis, bone erosion, cell chemotaxis, cell growth, inflammation, matrix degradation, and osteoclastogenesis exhibit an asymptotic stable active state when the model is simulated under RASF-specific conditions. These results are consistent with known RASFs biological aggressive behavior as described in specialized scientific literature [332].

Table 13. Projection of the trap-spaces of the RASF model restricted to its ontological phenotypes.

Ontological phenotype	Trap-space							
	0	**1**	**2**	**3**	**4**	**5**	**6**	**7**
Angiogenesis	1	1	1	1	1	1	1	1
Apoptosis	0	0	0	0	0	0	0	0
Bone Erosion	1	1	1	1	1	1	1	1
Cell Chemotaxis, Recruitment, Infiltration	1	1	1	1	1	1	1	1
Cell Growth, Survival, Proliferation	1	1	1	1	1	1	1	1
Hypoxia	1	0	1	0	0	0	1	1
Inflammation	1	1	1	1	1	1	1	1
Matrix Degradation	1	1	1	1	1	1	1	1
Osteoclastogenesis	1	1	1	1	1	1	1	1

The asymptotic state of ontological phenotypes is the result of the combined regulation exerted by their upstream regulators, as described in the logical formulas. Thus, the behavior of biomarker groups associated with each ontological phenotypes can be identified in the different trap-spaces and be used for comparison against experimental evidence. For instance, all interleukins (*e.g.* IL121, IL18, IL1B, IL33, IL6) being active under RASF-specific conditions accounts for the asymptotic active state of the ontological inflammatory phenotype and confirms their experimentally observed function of inflammation drivers **[333]**. Likewise for matrix metalloproteinases (*e.g.* MMP3, MMP9, MMP13) leading to matrix degradation **[334]** or cytokines (*e.g.* TNF, IL17) activating bone erosion and osteoclastogenesis **[335]**. A pattern of growth factors (*e.g.* PDGFA, FGF1, VEGFA) activation is observed within the eight different trap-spaces and is associated with activation of the cell growth and proliferation phenotype. These findings are consistent with experimental evidence **[336]**. This proliferative behavior is

confirmed in parallel by an asymptotic inactive state of the apoptotic phenotype, reproducing fibroblasts resistance to programmed cell death in RA **[261]**. Accordingly with biological knowledge, it is due to the active state of anti-apoptotic components (*e.g.* CAV1) and the inactivity of pro-apoptotic ones (*e.g.* Bak, Bax) in all eight trap-spaces under RASF-specific conditions. Finally, the hypoxic phenotype varies within trap-spaces, reflecting a biologically relevant feed-back loop. Trap-spaces where hypoxia is active are associated with active HIF1 and inactive PHD2. On the contrary, trap-spaces where hypoxia is inactivated are associated with inactive HIF1 and active PHD2. It reflects the well-known regulation of the cellular response to hypoxia by PHD2 through HIF1 **[337]**. The variations of fixed values within the eight trap-spaces can also be interpreted at the level of the RASF regulatory pathways. For instance, in trap-spaces 0, 1, 5, and 7, MAPK1 is active in parallel with BCL2. The latter are inactive in trap-spaces 2, 3, 4, and 6. It confirms the regulation of BCL2 through the MAPKs pathway **[338]**.

Subsequent metabolic process evaluation under RASF-specific initial conditions (**Table 12**), *i.e.* projection of its trap-spaces restricted to the metabolic components are displayed in **Table 14**. These observations allow us to assess the adequacy of the regulatory impact on metabolic systems under cell- and disease-specific conditions, by comparing them with specialized literature. Asymptotic behavior of the four metabolic processes of interest in RASFs (*i.e.* glycolysis, OXPHOS, TCA and PPP) under cell- and disease-specific regulatory initial conditions is stable within all trap-spaces. It reflects the consistency of RASFs regulatory impact upon metabolic subprocesses. Without going into the details of each metabolic component, we observe an overall activity of all metabolic components involved in glycolytic processes, inactivity of all OXPHOS and TCA components, along with both oscillations in activity of PPP components. The latter *in-silico* observations reproduce experimental findings of RASFs significant decrease in mitochondrial energy

production through OXPHOS fueled by TCA, enhancement of glycolytic activity, along with the glucose shunt to specific subparts of the PPP **[165], [173], [177]**, **[274]**. The same applies to the trap-space activity of glucose and lactate transporters (*i.e.* GLCt1r, LACt2r) which are also very active in response to high glycolytic activity **[274]**.

Table 14. Projection of the trap-spaces of the RASF model restricted to its metabolic components.

Component	Type	Trap-space	Pathway
AKGDm	Enzyme	0	TCA
ALDO_rna	RNA	1	Glycolysis
CI_MitoCore	Enzyme	0	OXPHOS
CI_rna	RNA	0	OXPHOS
CII_MitoCore	Enzyme	0	OXPHOS
CII_rna	RNA	0	OXPHOS
CIII_MitoCore	Enzyme	0	OXPHOS
CIII_rna	RNA	0	OXPHOS
CIV_MitoCore	Enzyme	0	OXPHOS
CIV_rna	RNA	0	OXPHOS
ENO_Cytoplasm	Enzyme	1	Glycolysis
ENO_Cytoplasm_active	Enzyme	1	Glycolysis
ENO_rna	RNA	1	Glycolysis
F26BP_simple_molecule	Metabolite	1	Glycolysis
FBA_Cytoplasm	Enzyme	1	Glycolysis
FBA_Cytoplasm_active	Enzyme	1	Glycolysis
G6PDH2r_Cytoplasm	Enzyme	1	PPP
G6PDH2r_Cytoplasm_active	Enzyme	0	PPP
G6PDH2r_rna	RNA	1	PPP
GAPD_Cytoplasm	Enzyme	1	Glycolysis
GAPD_Cytoplasm_active	Enzyme	1	Glycolysis
GAPD_rna	RNA	1	Glycolysis

GLCt1r	Transporter	1	/
GLCt1r_rna	RNA	1	/
HEX1_Cytoplasm	Enzyme	1	Glycolysis
HEX1_Cytoplasm_active	Enzyme	1	Glycolysis
HEX1_rna	RNA	1	Glycolysis
ICDHxm	Enzyme	0	TCA
L_LACt2r	Transporter	1	/
L_LACt2r_rna	RNA	1	/
LDH_L	Enzyme	1	Glycolysis
LDH_L_rna	RNA	1	Glycolysis
M_13dpg_c_simple_molecule	Metabolite	1	Glycolysis
M_2pg_c_simple_molecule	Metabolite	1	Glycolysis
M_3pg_c_simple_molecule	Metabolite	1	Glycolysis
M_6pgc_c_simple_molecule	Metabolite	0	PPP
M_6pgl_c_simple_molecule	Metabolite	0	PPP
M_accoa_m_simple_molecule	Metabolite	0	TCA
M_adp_c_simple_molecule	Metabolite	1	/
M_akg_m_simple_molecule	Metabolite	0	TCA
M_atp_c_simple_molecule	Metabolite	1	/
M_cit_m_simple_molecule	Metabolite	0	TCA
M_co2_m_simple_molecule	Metabolite	0	/
M_coa_m_simple_molecule	Metabolite	0	/
M_dhap_c_simple_molecule	Metabolite	1	/
M_e4p_c_simple_molecule	Metabolite	1	PPP
M_f6p_c_simple_molecule	Metabolite	1	Glycolysis
M_fdp_c_simple_molecule	Metabolite	1	Glycolysis
M_fum_m_simple_molecule	Metabolite	0	TCA
M_g3p_c_simple_molecule	Metabolite	1	Glycolysis
M_g6p_c_simple_molecule	Metabolite	1	Glycolysis
M_glc_D_c_simple_molecule	Metabolite	1	Glycolysis
M_glc_D_e_simple_molecule	Metabolite	1	/
M_gtp_m_simple_molecule	Metabolite	0	/

M_h2o_c_simple_molecule	Metabolite	1	/
M_h2o_m_simple_molecule	Metabolite	0	/
M_icit_m_simple_molecule	Metabolite	0	TCA
M_lac_L_c_simple_molecule	Metabolite	1	Glycolysis
M_Lac_L_e_simple_molecule	Metabolite	1	/
M_mal_L_m_simple_molecule	Metabolite	0	TCA
M_nadh_c_simple_molecule	Metabolite	1	/
M_nadh_m_simple_molecule	Metabolite	0	/
M_nadph_c_simple_molecule	Metabolite	0	/
M_oaa_m_simple_molecule	Metabolite	0	TCA
M_pep_c_simple_molecule	Metabolite	1	Glycolysis
M_pyr_c_simple_molecule	Metabolite	1	Glycolysis
M_r5p_c_simple_molecule	Metabolite	1	PPP
M_ru5p_D_c_simple_molecule	Metabolite	0	PPP
M_s7p_c_simple_molecule	Metabolite	1	PPP
M_succ_m_simple_molecule	Metabolite	0	TCA
M_succoa_m_simple_molecule	Metabolite	0	TCA
M_xu5p_D_c_simple_molecule	Metabolite	1	PPP
PDHm	Enzyme	0	TCA
PDK_rna	RNA	1	Glucose
PDK1_Mitochondrion_inner_mb	Enzyme	1	Glucose
PDK1_Mitochondrion_inner_mb_active	Enzyme	1	Glucose
PFKFB3_Cytoplasm	Enzyme	1	Glycolysis
PFKFB3_Cytoplasm_active	Enzyme	1	Glycolysis
PFKFB3_rna	RNA	1	Glycolysis
PGI_Cytoplasm	Enzyme	1	Glycolysis
PGI_Cytoplasm_active	Enzyme	1	Glycolysis
PGI_rna	RNA	1	Glycolysis
PGK_Cytoplasm	Enzyme	1	Glycolysis
PGK_Cytoplasm_active	Enzyme	1	Glycolysis
PGK_rna	RNA	1	Glycolysis
PGM_Cytoplasm	Enzyme	1	Glycolysis

PGM_Cytoplasm_active	Enzyme	1	Glycolysis
PGM_rna	RNA	1	Glycolysis
PYK_Cytoplasm	Enzyme	1	Glycolysis
PYK_Cytoplasm_active	Enzyme	1	Glycolysis
PYK_rna	RNA	1	Glycolysis
TKT1_Cytoplasm	Enzyme	1	PPP
TKT1_Cytoplasm_active	Enzyme	1	PPP
TKT1_rna	RNA	1	PPP

4.2.2 The breast CAF model, an executable model of CAFs pathogenic activity in the breast TME

Translation of the CAF-map V2 using CaSQ default parameters generated a dynamic Boolean model of 463 nodes, including 62 inputs, and 793 interactions. The latter is publicly available on the Cell Collective platform **[245]** at https://research.cellcollective.org/human-breast-cancer-associated-fibroblasts and BioModels repository **[246], [247]**: MODEL2307090001.

However, components and interactions depicted in the model are not cancer-specific but generic to CAFs in the TME. The DEA conducted to contextualize the model in a BC-specific manner is publicly available at https://gitlab.com/genhotel/breast-cafs-reverse-warburg-effect. It identified 3678 DEG in CAFs-S1 *vs.* CAFs-S4 among the 18252 mapped genes (**Figure 36**). 1866 DEG were significantly up-regulated in CAFs-S1 *vs.* CAFs-S4, leading to fixing an initial condition of 1 for 71 nodes of the CAF model. Most significantly up-regulated DEG in CAFs-S1 are mainly involved in chemotaxis, ECM organization, locomotion, response to growth factors, cell adhesion, migration, motility, differentiation, and proliferation (**Figure 37A**).

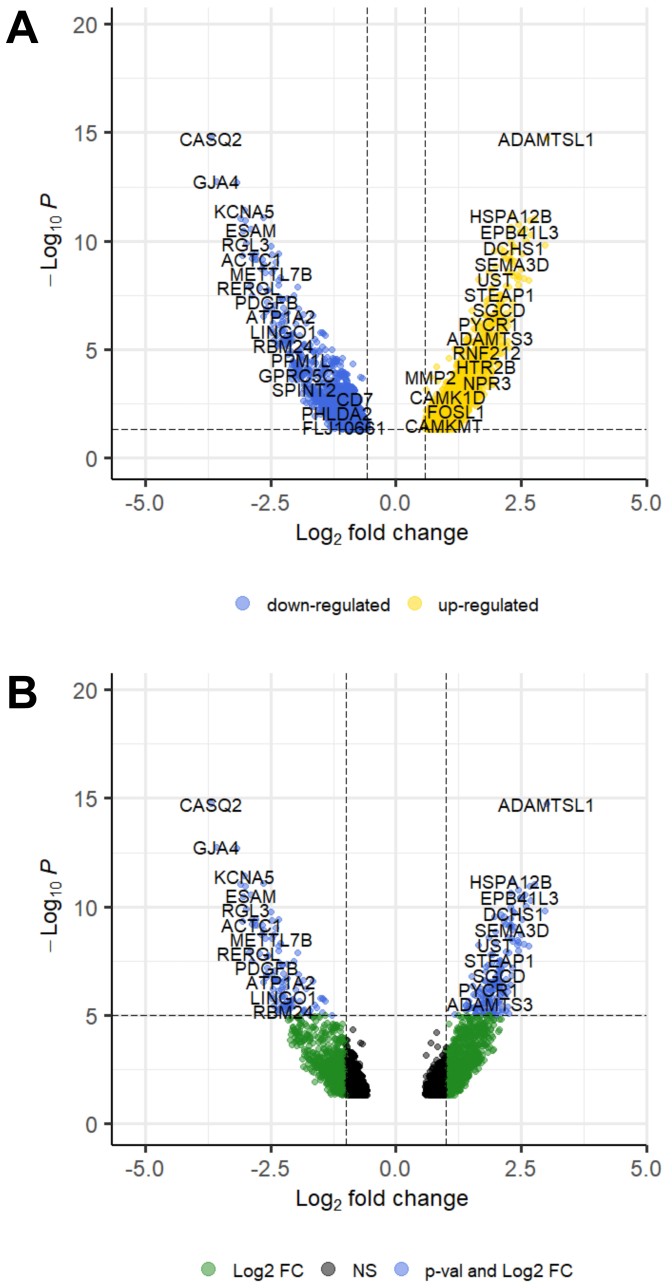

Figure 31. Results of the differential expression analysis performed on the EGAD00001003808 dataset from the European Genome-phenome Archive. (A) Visualization of the differentially expressed genes between CAFs-S1 vs. CAFs-S4 with standard significance threshold of adjusted p-value > 0.05 and absolute fold change > 1.5. **(B)** Visualization of the most-significantly differentially expressed genes between CAFs-S1 vs. CAFs-S4 with standard significance threshold of adjusted p-value > 0.05 and an absolute FC > 1.

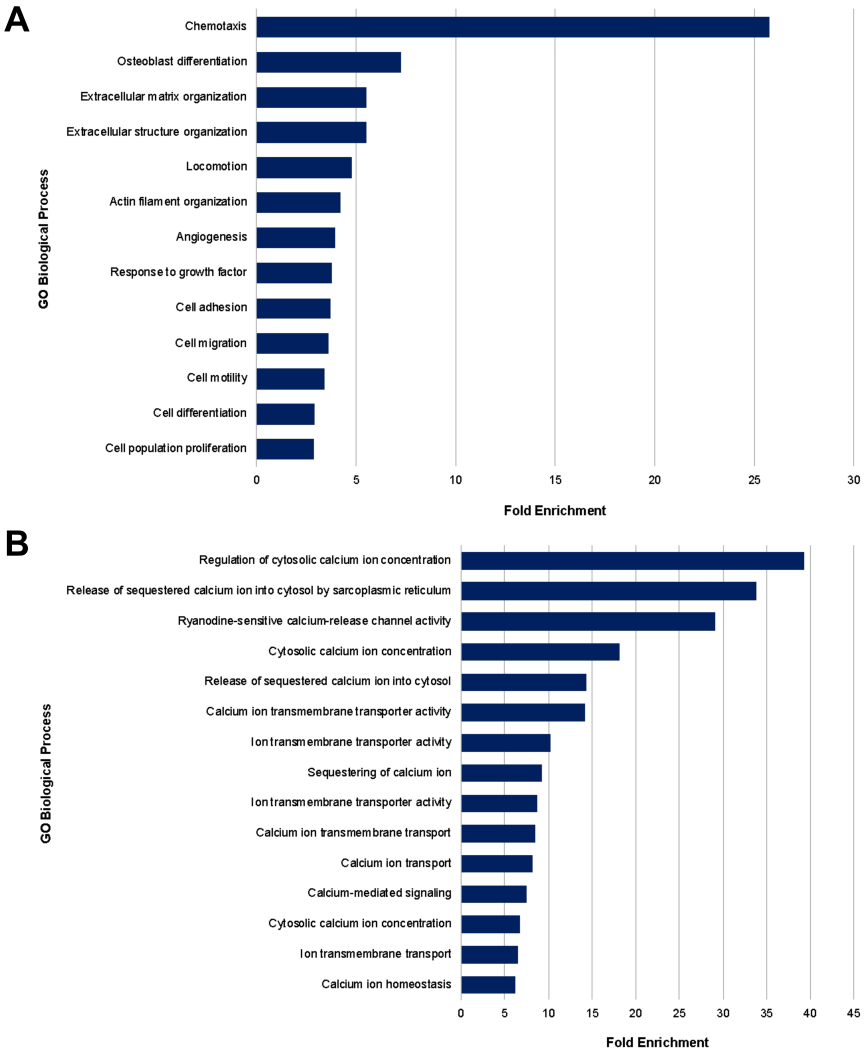

Figure 38. Visualization of biological processes related to the most significantly differentially expressed genes in CAFs-S1 *vs.* CAFs-S4 after enrichment analysis classified by Fold Enrichment. (A) Biological processes associated with the most significant up-regulated differentially expressed genes. **(B)** Biological processes associated with the most significant down-regualted differentially expressed genes. Fold enrichment is calculated by comparing the proportion of genes in our differentially expressed genes subset that belong to a specific category with the expected proportion of genes in the latter category in the reference set.

Such observations support the classification of CAFs-S1 as the subpopulation of CAFs carrying key aggressive functions. 1812 DEG were significantly down-regulated in CAFs-S1 vs. CAFs-S4, leading to fix an initial condition of 0 for 34 nodes of the CAF model. Most significantly down-regulated DEG in CAFs-S1 are involved in ion transport and signaling, specifically calcium ions (**Figure 37B**).

Finally, 41 inputs of the CAF model remained unfixed, leading to assign their values through manual curation of peer-reviewed breast CAF-specific literature. The complete list of breast CAF-specific initial conditions along with their source of attribution is outlined in **Table 15**.

Table 15. Breast CAFs-specific initial conditions generated from data-driven differential expression.

Component	Function	Initial value	Source
ACTA1	Internal node	0	DEA
ACTA1_rna	Internal node	0	DEA
ACTG2	Internal node	0	DEA
ACTG2_rna	Internal node	0	DEA
AKT1S1_phosphorylated	Internal node	1	DEA
AREG_Cytosol	Internal node	0	DEA
AREG_extracellular	Input node	0	DEA
AREG_rna	Internal node	0	DEA
AREG_Secreted_compartment	Internal node	0	DEA
ARHGEF7	Internal node	1	DEA
BMP4	Internal node	1	DEA
BMP4_rna	Internal node	1	DEA
CALML3	Internal node	0	DEA
CASQ2	Input node	0	DEA
CAV3	Internal node	0	DEA
CAV3_rna	Internal node	0	DEA
CCL11	Internal node	1	DEA

CCL11_rna	Internal node	1	DEA
CCL8	Internal node	0	DEA
CCL8_rna	Internal node	0	DEA
CFL1	Input node	1	22954256
Collagens_extracellular	Input node	1	31521169
CTGF_extracellular	Input node	1	34108441
CXCL1	Internal node	1	DEA
CXCL1_rna	Internal node	1	DEA
CXCL12_extracellular	Input node	1	DEA
CXCL12_rna	Internal node	1	DEA
CXCL12_Secreted_compartment	Internal node	1	DEA
CXCL12CXCR4_complex	Internal node	1	DEA
CXCL2	Internal node	1	DEA
CXCL2_rna	Internal node	1	DEA
EGF_extracellular	Input node	1	35267539
EGFR	Internal node	1	DEA
EGFR_complex	Internal node	1	DEA
EGFR_rna	Internal node	1	DEA
EMILIN1	Internal node	1	DEA
FAP	Internal node	1	DEA
FAP_rna	Internal node	1	DEA
FGF1	Input node	1	33568624
FGF2_extracellular	Input node	1	32557854
FGF3	Input node	1	35267539
FGF4	Input node	1	33081025
FGF7	Internal node	1	DEA
FGF7_rna	Internal node	1	DEA
FGFRFGF1_complex	Internal node	1	DEA
FGFRFGF2_complex	Internal node	1	DEA
FGFRFGF3_complex	Internal node	1	DEA
FGFRFGF4_complex	Internal node	1	DEA
FN_extracellular	Input node	1	35481621
GAST	Input node	1	28560291
GASTCCKBR_complex	Internal node	0	DEA
GLI2	Internal node	1	DEA
GLI2_rna	Internal node	1	DEA

GLNS	Input node	1	27829138
M_glc_D_e_simple_molecule	Input node	1	DEA
HGF_extracellular	Input node	1	22282252
HIF1A	Internal node	1	DEA
HRC	Input node	0	DEA
IFNG	Input node	1	33005420
IGF1_extracellular	Input node	1	DEA
IGF1_rna	Internal node	1	DEA
IGF1_Secreted_compartment	Internal node	1	DEA
IGF2_extracellular	Input node	1	DEA
IGF2_rna	Internal node	1	DEA
IGF2_Secreted_compartment	Internal node	1	DEA
IGFBP3	Input node	1	DEA
IGFBP4	Input node	1	19536088
IHH	Input node	1	35224148
IL12	Input node	0	DEA
IL18	Input node	0	31231372
IL1A	Input node	1	31231372
IL1B_extracellular	Input node	1	31231372
IL1R_complex_Cytosol	Internal node	0	DEA
IL1R_complex_Cytosol_2	Internal node	0	DEA
IL6_extracellular	Input node	1	35267539
IRS2_phosphorylated	Internal node	1	DEA
ITGA11	Internal node	1	DEA
ITGA11_rna	Internal node	1	DEA
ITGA11ITGB1_complex_Cytosol	Internal node	1	DEA
ITGA11ITGB1_complex_Cytosol_active	Internal node	1	DEA
ITGA1ITGB1_complex_Cytosol	Internal node	0	DEA
ITGA1ITGB1_complex_Cytosol_active	Internal node	0	DEA
ITGAVITGB6_complex_Cytosol	Internal node	0	DEA
ITGAVITGB6_complex_Cytosol_active	Internal node	0	DEA
Large_Latent_Complex_extracellular	Input node	1	DEA
Large_Latent_Complex	Internal node	1	DEA

_Secreted_compartment			
LGALS1	Input node	1	24229053
LIF_extracellular	Input node	1	34947829
LIMK1_phosphorylated	Internal node	1	DEA
LOX	Internal node	1	DEA
LOX_rna	Internal node	1	DEA
LPA_simple_molecule	Input node	0	DEA
MAP3K7TAB_complex	Internal node	1	DEA
MIF	Input node	0	24939415
MIR101_antisense_rna	Input node	0	28289080
MIR141_antisense_rna	Input node	0	28289080
MIR155_antisense_rna	Input node	1	23171795
MIR200B_antisense_rna	Input node	0	28289080
MIR205_antisense_rna	Input node	0	28289080
MIR211_antisense_rna	Input node	1	31702390
MIR214_antisense_rna	Input node	0	23171795
MIR221_antisense_rna	Input node	1	28289080
MIR31_antisense_rna	Internal node	1	28289080
MMP13	Internal node	1	DEA
MMP13_rna	Internal node	1	DEA
MMP14	Internal node	1	DEA
MMP14_rna	Internal node	1	DEA
MMP2	Internal node	1	DEA
MYLK_phosphorylated	Internal node	0	DEA
NDUFA4L2	Internal node	0	DEA
NOX4	Internal node	1	DEA
NOX4_rna	Internal node	1	DEA
OSM	Input node	1	35192545
PDGF_extracellular	Input node	1	34272173
PDGFPDGFRA_complex	Internal node	1	DEA
PDGFRA	Internal node	1	DEA
PDGFRA_rna	Internal node	1	DEA
PGE2_simple_molecule	Input node	1	33271839
phospholipid_simple_molecule	Input node	1	
PI45P2_simple_molecule	Input node	1	34108441
PLAU	Internal node	1	DEA

PLAU_rna	Internal node	1	DEA
PLG	Input node	1	33921488
POSTN_extracellular	Input node	1	35267539
PPBP	Internal node	0	DEA
PPBP_rna	Internal node	0	DEA
proPLAU_extracellular	Input node	1	24229053
PTCH2_rna	Internal node	1	DEA
PTGS2	Internal node	1	DEA
PTGS2_rna	Internal node	1	DEA
PTPN6	Input node	0	DEA
RYR2TRDNASPH_complex	Input node	0	DEA
RYR2TRDNASPHHRCCASQ2	Internal node	0	DEA
SEPTINE4	Internal node	0	DEA
SERPINE1	Internal node	1	DEA
SERPINE1_rna	Internal node	1	DEA
SHH	Input node	1	28496132
SMOPTCH_complex	Internal node	1	DEA
SMOX	Internal node	1	DEA
TGFB3_Cytosol	Internal node	1	DEA
TGFB3_extracellular	Internal node	1	DEA
TGFB3_rna	Internal node	1	DEA
TNF	Input node	0	DEA
VTN	Input node	1	33211735
WAS_phosphorylated	Internal node	0	DEA
WNT7	Input node	1	34108441
WWTR1	Input	1	DEA

To validate the behavior of the model, generic model simulations were first compared to breast CAF-specific experimental scenarios extracted from the literature. For instance, we identified an experimental scenario whereby MicroRNA-155 promotes proliferation of human breast CAFs **[339]**. We translated such experimentally observed scenario in terms of an *in-silico*

experiment by subsequently activating and inactivating the expression of MicroRNA-155 and visualizing the fibroblast proliferative phenotype (**Figure 38**). The simulation displays the activation of fibroblast proliferation depending on the activation of MicroRNA-155, thus validating the experimental scenario. Remaining scenarios were tested and validated in the same manner: details of each experimental scenario, associated CAF model initialization, and dynamic results are presented in **Table 16**. Overall, regarding this generic evaluation, 29 experimental scenarios were confirmed by the CAF model out of 41 biological scenarios. Ten scenarios were not reproducible mostly due to a lack of mechanistic detail regarding specific interactions in the literature, leading to a missing or incomplete representation in the CAF-map V2 and the associated breast CAF model. Finally, two generic scenarios were not validated as other pathways were needed concomitantly.

Subsequent global behavior evaluation of the model under breast CAF-specific initial conditions, *i.e.* identification of its complete asymptotic behavior, depicted 128 trap-spaces. Each trap-space reflects a different subspace of breast CAFs cellular phenotypes. Most components values are stable within all trap-spaces (always fixed at 0 or 1) but others vary within trap-spaces. The projection of trap-spaces restricted to ontological phenotypes (*i.e.* distinct cellular outcome) identifies a single trap-space (**Table 17**). It illustrates activity of aggressive phenotypes in breast CAFs, *e.g.* angiogenesis, fibroblast proliferation, hypoxia, matrix degradation, tumor growth and invasion, while negative regulators are inactive. These findings are consistent with the behavior of breast CAFs as described in scientific literature **[340]**.

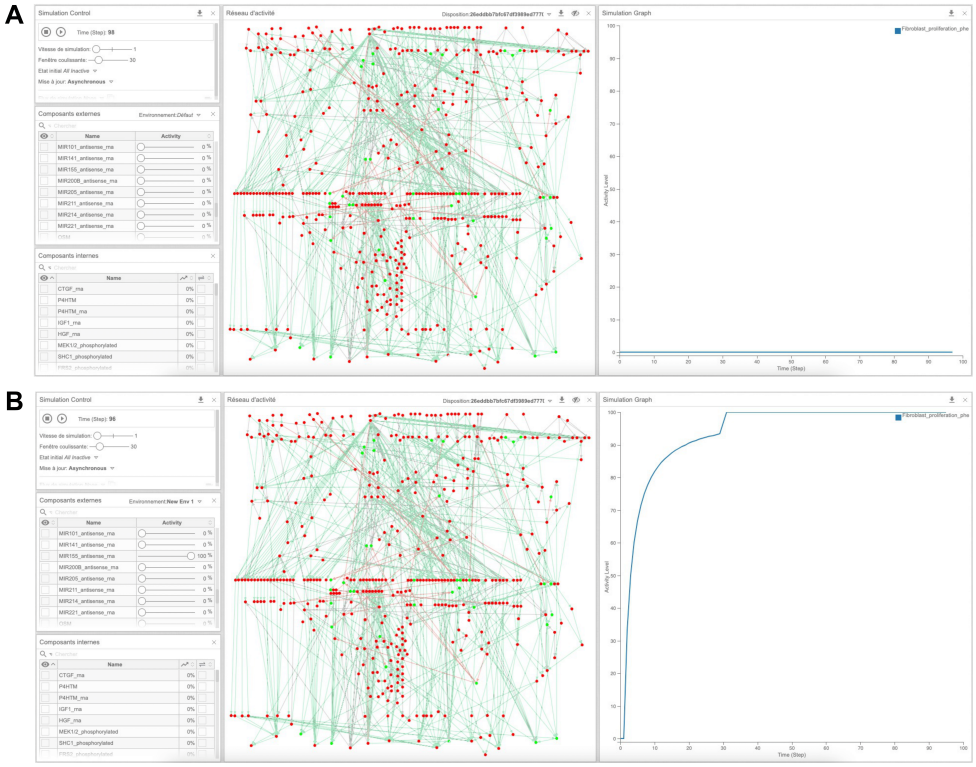

Figure 39. Assessment of the reproduction of an experimental scenario by the breast CAF model through an *in-silico* simulation on the Cell Collective interactive modeling platform. Simulation parameters are displayed on the left panel with a simulation speed of one, a sliding window of 30 and an asynchronous updating mode. The experimental observation that MicroRNA-155 induces breast CAFs proliferation **[339]** is reproduced on the RASF model with **(A)** inactivation and **(B)** activation of "MIR155" (within the external components tab) along with visualization of "fibroblast_proliferation_phenotype" (within the internal components tab). Signal tracking is displayed on the middle panel to track the regulatory signal flux under both simulation conditions. Simulation graphical results are shown on the right panel and confirm experimental observation: MicroRNA-155 is necessary to induce breast CAFs proliferation.

Table 16. Biological scenarios identified from literature used for generic validation of the behavior of the breast CAF model in the Cell Collective platform. Experimental conditions were used as the input of the model and its outputs were compared to the biological outcome to confirm or refute the validation of a scenario.

Experimental observation	Reference	Input of the CAF model	Output of the CAF model	Coherence
A loss of Caveolin induces the metabolic reprogramming of breast CAFs by increasing mitochondrial dysfunction.	[341]	CAV-3 OFF/ON	CI, CIV OFF/ON	**YES**
Breast CAFs recombinantly expressing TGF-β show upregulation of myofibroblast markers β-actin.		TGFB3 OFF/ON	Actin cytoskeletal OFF/ON	**YES**
Breast CAFs recombinantly expressing TGF-β show a loss of Cav-1/3 expression.		TGFB3 OFF/ON	CAV3_rna ON/OFF	**YES**
Tumors derived from TGF-β ligand overexpressing breast CAFs display increased extracellular matrix deposition and increased secretion of: a. Collagens, b. Tenascin C.		TGFB3 ON/OFF	COLLAGENS OFF/OFF	**NO**
			TNC OFF/OFF	**NO**
Breast CAFs promote tumor growth, in an angiogenesis-independent manner when overexpressing TGF-β3.		TGFB3 OFF/ON	Tumor growth OFF/ON	**YES**
Upregulation of miR-221 in breast CAFs affects growth and migration by CTGF signaling pathway.	[342]	miR-221 ON	Tumor growth OFF/OFF	**NO**
Downregulation of miR-320 in breast CAFs promotes tumor angiogenesis.	[343]	miR-320 OFF/ON	Angiogenesis OFF/ON	**YES**
miR-155 promotes proliferation of human breast CAFs.	[339]	miR-15 OFF/ON	Fibroblast proliferation OFF/ON	**YES**
Blockage of MAPK/p38 pathway diminished IL-32-induced tumor growth.	[344]	MAPK, p38 OFF/ON	Tumor growth OFF/ON	**YES**
Enhanced WNT expression in breast CAFs contributes to invasion and migration of breast cancer cells.	[345]	WNT7 OFF/ON	Migration into tumor OFF/ON	**YES**
In breast CAFs, IL-1β promotes cell invasion through IL-1R.	[346]	IL-1β OFF	Tumor invasion OFF/OFF	**NO**

CAFs PDGF signaling has an active role in breast tumor progression.	[347]	PDGF OFF/ON	Tumor growth, migration OFF/ON	**YES**
In breast CAFs, CXCL12 promotes cell invasion through TGF-β pathway.	[348]	CXCL12 OFF/ON	Tumor invasion OFF/ON	**YES**
In breast CAFs, FGF2 promotes cancer growth and progression.	[349]	FGF2 OFF/ON	Tumor growth, growth factors OFF/ON	**YES**
CXCL1 is considered as a pro-inflammatory gene signature of breast CAFs.	[350]	CXCL1 OFF/ON	Cytokine production, immune system modulation OFF/ON	**YES**
Breast CAFs promote tumor growth through secretion of HGF.	[351]	HGF OFF/ON	Tumor growth OFF/ON	**YES**
miR-21 and miR-200B target TGF-β signaling and impact tumor progression and promotion in breast CAFs.	[352]	miR-21 OFF		**NO**
		miR-200B OFF		**NO**
Myeloid-derived OSM reprograms breast CAFs to a more tumorigenic phenotype by eliciting the secretion of VEGF.	[353]	OSM OFF/ON	VEGF OFF/ON	**YES**
OSM promoted tumor growth through breast CAFs.			Tumor growth OFF/ON	**YES**
OSM induced the expression of classical CAF markers such as FAP, POSTN, VEGF, and IL6 in breast CAFs.			FAP, POSTN, VEGF, IL6 OFF/ON	**YES**
OSM induced signatures related to fibroblast activation and JAK/STAT3 signaling, in agreement with increased STAT3 phosphorylation by OSM in breast CAFs.			STAAT3 OFF/OFF	**NO**
Plasmin expression affects tumor cell invasion.	[354]	Plasmin OFF/ON	Matrix degradation, matrix effects OFF/ON	**YES**
Plasmin expression is required for activation of EMT in breast cancer.	[355]	Plasmin ON/OFF	Matrix effect OFF/OFF	**NO**
TGF-β promotes CXCL5 secretion in breast CAFs.	[356]	TGF-β ON/OFF	CXCL5 ON/OFF	**YES**
Lactate production in breast CAFs promotes breast cancer tumor growth.	[357]	Lactate OFF/ON	Tumor growth OFF/ON	**YES**

TFAM-deficient breast CAFs showed evidence of mitochondrial dysfunction.		TFAM OFF/ON	CI, CV OFF/ON	**YES**
SIRT3 in breast CAFs was found to: a. Suppress HIF1α and its target genes; b. Suppress tumor growth and proliferation; c. Suppress ROS production.	**[358], [359]**	SIRT3 OFF/ON	HIF1A OFF/OFF	**NO**
			Tumor growth, tumor fibroblast proliferation OFF/ON	**YES**
			ROS production OFF/ON	**YES**
Breast CAFs promote tumor growth and angiogenesis through elevated CXCL12 secretion.	**[360]**	CXCL12 OFF/ON	Tumor growth, Angiogenesis OFF/ON	**YES**
LOX family members are considered as ECM-modifying enzymes in breast CAFs by remodeling the extracellular matrix.	**[361]**	LOX OFF/ON	ECM regulation phenotype and matrix effects OFF/ON	**YES**
Downregulation of MiR-205 in breast CAFs promotes VEGF-independent angiogenesis through activation of IL-11/IL-15 signaling by YAP1.	**[362]**	MiR-205 OFF		**NO**
In breast cancer, HIF1α transcriptionally upregulates glycolytic enzymes and lactate production.	**[363]**	HIF1A OFF/ON	Glycolytic enzymes, lactate OFF/ON	**YES**
Lactate generated by hypoxic breast CAFs promotes cell invasion.	**[364]**	Lactate OFF/ON	Tumor invasion OFF/ON	**YES**
Inhibiting NF-κB signaling in fibroblasts was shown to reduce inflammatory cytokine secretion.	**[365]**	NFkB OFF/ON	Cytokine production phenotype OFF/ON	**YES**
Ets2 inactivation through depletion of Pten in breast CAFs was sufficient to decrease tumor growth and progression.	**[366]**	PTEN OFF		**NO**
SERPINE1 promotes cellular invasion in breast CAFs.	**[367]**	SERPINE1 OFF/ON	Tumor invasion OFF/ON	**YES**
CASQ2 overexpression accelerated tumorigenesis, induced collagen structure remodeling, and increased distant metastasis.	**[368]**	CASQ2 OFF/ON	Collagens OFF/OFF	**NO**
Hypoxic breast CAFs led to sustained elevation of HIF1α.	**[79]**	Hypoxia OFF/ON	HIF1A OFF/ON	**YES**

The asymptotic state of ontological phenotypes is the result of their regulators combined effect exerted through their Boolean rules. Thus, the behavior of groups of biomarkers associated with each ontological phenotype can be identified to further validate the behavior of the breast CAF model. For instance, the constant activation of matrix metalloproteinases (*e.g.* MMP2, MMP9), known to lead to matrix degradation **[369]**, within all trap-spaces, accounts for the asymptotic activation of the associated phenotype. Their role in the coordination of ECM is also well established **[370]**, which supports the consistency of their trap-space with the "ECM regulation" phenotype. Likewise, most interleukins (*e.g.* IL1A, IL1B, IL11 IL6) being active under breast CAF-specific conditions confirms their experimentally observed function of immune system modulation and cytokine production drivers **[371]**. The asymptotic activated state of the hypoxic phenotype is explained by the sustained activation of its main molecular driver, Hypoxia-Inducible Factor 1 (HIF1) **[372]**. The latter is further involved with ROS production **[372]**, confirmed in the trap-spaces analysis. Likewise with the angiogenic and reactive stroma phenotypes and their key player, VEGF **[373]**. Migration, tumor growth, and invasion appear to be driven by growth factors and Wnt signaling pathway, consistent with literature **[374]**.

Table 17. Projection of the trap-spaces of the breast CAF model restricted to its ontological phenotypes.

Ontological phenotype	Trap-space
Actomyosin contractility	1
Angiogenesis	1
Cytokine production	1
ECM regulation	1
Fibroblast markers	1
Fibroblast proliferation	1
Fibrosis	1
Formation of basement membrane	1
Growth factors production	1
Hypoxia	1
Immune system modulation	1
Markers of fibroblast activation	1
Matrix degradation	1
Migration into the tumor	1
Negative regulators of CAFs	0
Reactive stroma	1
ROS production	1
Tumor growth	1
Tumor invasion	1

Furthermore, activation of key fibroblastic markers (*e.g.* FAP, PDGF) in parallel with inactivation of known negative regulators of breast CAFs (*e.g.* miR101, miR141, CAV3, SIRT3) under initial disease-specific conditions explain the state of both related phenotypes. Finally, fibroblast proliferation requires EGF and TGFB signaling pathways **[375]**. Fibrosis and basement membrane formation seems governed by collagens **[376]**. Actin, myosin, and TNC drive actomyosin contractility **[377]**, all confirming experimental observations in breast CAFs.

Subsequent metabolic process evaluation under breast CAF-specific initial conditions (**Table 15**), *i.e.* projection of its trap-spaces restricted to the metabolic components are displayed in **Table 18**. These observations allow us to globally assess the adequacy of the regulatory impact on metabolic systems under cell- and disease-specific conditions, by comparing them with the specialized literature.

Table 18. Projection of the trap-spaces of the breast CAF model restricted to its metabolic components.

Component	Trap-space	Type	Metabolic pathway
L_LACt2r	1	Transporter	Lactate
lac_L_e	1	Metabolite	/
lac_L_c	1	Metabolite	Glycolysis
GLCt1r	1	Transporter	Glucose
glc_D_e	1	Metabolite	Glucose
glc_D_c	1	Metabolite	Glucose
LDH_L	1	Enzyme	Glycolysis
PYK	1	Enzyme	Glycolysis
ICDHxm	0	Enzyme	TCA
GLCt1r	1	Transporter	Glucose
HEX1	1	Enzyme	Glycolysis
HEX1_rna	1	RNA	Glycolysis
glu_L_m	0	Metabolite	TCA
r0081	1	Enzyme	Glutamine
HMGCOASim	0	Enzyme	Ketogenesis
gln_L_m	0	Metabolite	Glutamine
gln_L_c	0	Metabolite	Glutamine
GLUNm	0	Enzyme	Glutamine
g6p_c	1	Metabolite	Glycolysis
f6p_c	1	Metabolite	Glycolysis
fdp_c	1	Metabolite	Glycolysis
dhap_c	1	Metabolite	Glycolysis
g3p_c	1	Metabolite	Glycolysis
3pg_c	1	Metabolite	Glycolysis
2pg_c	1	Metabolite	Glycolysis
pyr_c	1	Metabolite	Glycolysis

pep_c	1	Metabolite	Glycolysis
13dpg_c	1	Metabolite	Glycolysis
pyr_m	1	Metabolite	Glycolysis
cit_m	0	Metabolite	TCA
icit_m	0	Metabolite	TCA
akg_m	0	Metabolite	TCA
succoa_m	0	Metabolite	TCA
succ_m	0	Metabolite	TCA
fum_m	0	Metabolite	TCA
mal_L_m	0	Metabolite	TCA
accoa_m	0	Metabolite	TCA
CI_MitoCore	0	Enzyme	OXPHOS
akg_m	0	Metabolite	TCA
PYK	1	Enzyme	Glycolysis
LDH_L	1	Enzyme	Glycolysis
oaa_m	0	Metabolite	TCA
PGI	1	Enzyme	Glycolysis
FBA	1	Enzyme	Glycolysis
TPI	1	Enzyme	Glycolysis
GAPD	1	Enzyme	Glycolysis
PGK	1	Enzyme	Glycolysis
PGM	1	Enzyme	Glycolysis
ENO	1	Enzyme	Glycolysis
hmgcoa_m	0	Metabolite	Ketogenesis
acac_m	0	Metabolite	Ketogenesis
bhb_m	0	Metabolite	Ketogenesis
PFK	1	Enzyme	Glycolysis
PFK_rna	1	RNA	Glycolysis
PGI_rna	1	RNA	Glycolysis
FBA_rna	1	RNA	Glycolysis
TPI_rna	1	RNA	Glycolysis
PGK_rna	1	RNA	Glycolysis
GAPD_rna	1	RNA	Glycolysis
ENO_rna	1	RNA	Glycolysis
GLNS	1	Enzyme	Glutamine
PDHm	0	Enzyme	TCA
CIV_MitoCore	0	Enzyme	OXPHOS
PDK1	1	Enzyme	Glucose
PDK1_rna	1	RNA	Glucose
CIII_MitoCore	0	Enzyme	OXPHOS

Asymptotic behavior of the five metabolic processes of interest in breast CAFs (*i.e.* glycolysis, OXPHOS, TCA, ketogenesis and glutamine metabolism) under cell- and disease-specific regulatory initial conditions is stable within all trap-spaces. It reflects the consistency of breast CAFs regulatory impact upon metabolic subprocesses. Without going into the details of each metabolic component, we observe an overall activity of all metabolic components involved in glycolytic processes, inactivity of all OXPHOS, TCA, and ketogenesis components, along with both activity and inactivity of glutamine pathway components. These *in-silico* observations reproduce experimental reverse Warburg effect findings in CAFs, namely significant decrease in mitochondrial energy production through OXPHOS fueled by TCA **[97]** along with glutamine shunt and enhancement of glycolytic activity **[378]**. The same applies to the trap-space activity of glucose and lactate transporters (*i.e.* GLCt1r, LACt2r) which are also very active in response to high glycolytic activity **[379]**. As regards the metabolic pathways involved in ketogenesis, the process of generating ketone bodies primarily occurs in the liver during periods of prolonged fasting or low carbohydrate availability. As the main focus of ketogenesis is in hepatocytes, few studies have studied ketogenesis in CAFs and the understanding of ketogenesis in CAFs is not as well-established as in liver cells.

This second part addresses our efforts to infer cell- and disease-specific executable Boolean regulatory models for RASFs and breast CAFs covering dynamic regulatory processes from the previously constructed up-to-date molecular interaction maps. Regulatory models were automatically inferred and further parameterized leveraging both data-driven and manual curation processes to ensure high confidence in the depicted information. After thorough behavior validation according to multiple criteria, we obtained the first two large-scale cell- and disease-specific regulatory Boolean models for RASFs and breast CAFs. The latter are completely standardized in their construction, annotation, and format and publicly available on multiple biological model repositories. They enable us to decipher the dynamic emergent behaviors of fibroblasts under disease-specific conditions.

Associated scientific communication, details here

The construction of the RASF model was published in an original research article and presented at an international scientific conference:

Aghakhani, S; Soliman, S; Niarakis, A. Metabolic reprogramming in rheumatoid arthritis synovial fibroblasts: a hybrid modeling approach. *PLOS Computational Biology* **2022** 18(12): e1010408. https://doi.org/10.1371/journal.pcbi.1010408

Aghakhani, S; Soliman, S; Niarakis, A. Metabolic Reprogramming in Rheumatoid Arthritis Synovial Fibroblasts (RASFs): a Hybrid Modeling Approach. *European Conference on Computational Biology*; September 18-21, **2022**; Sitges — Spain (poster)

The construction of the breast CAF was published in an original research article and presented at an international scientific conference:

Aghakhani, S; E Silva Saffar, S; Soliman, S; Niarakis, A. Hybrid computational modeling highlights reverse Warburg effect in breast cancer-associated fibroblasts. *Computational and Structural Biotechnology Journal* **2023**. https://doi.org/10.1016/j.csbj.2023.08.015

Aghakhani, S; E Silva Saffar, S; Soliman, S; Niarakis, A. A large-scale hybrid model to study metabolic reprogramming in cancer-associated fibroblasts. *ONCOLille Days*; November 2-4, **2022**, Lille — France (poster)

4.3 CELL- AND DISEASE-SPECIFIC HYBRID MODELS TO COVER AN ADDITIONAL BIOLOGICAL LAYER

4.3.1 The RASF hybrid model, an integrated dynamic overview of cell-specific pathogenic signaling, gene regulation and metabolism in the RA joint

Application of the complete framework to obtain the model RASF is shown within the Jupyter notebook in **Figure S1**. All necessary scripts and files to generate results depicted below are available on a GitLab repository at https://gitlab.com/genhotel/rasf-hybrid-model and in a Zenodo permanent archive at https://doi.org/10.5281/zenodo.7181588.

In greater details, the value propagation method was applied to the regulatory Boolean model under RASF-specific initial conditions identified earlier (**Table 12**) to decrease its complexity. Out of the 359 components, 313 were fixed by the value propagation algorithm (*i.e.* 100 were fixed at 0 and 213 at 1) (**Figure 39**). Evidently, the RASF-specific initial conditions, including 14 inputs and 2 intermediary nodes, exert an important control over the whole network.

Using the results of value propagation as a new set of initial conditions enabled us to decrease the complexity of the RASF model to obtain its trap-spaces, including the complete asymptotic behavior of the system. As described within the hybrid modeling framework, only metabolic components with proven inactive states are considered to extract additional metabolic constraints. Using RASF-specific regulatory conditions, the maximal trap-spaces associated with seven metabolic enzymes and 12 metabolites were equal to 0. According to the hybrid modeling framework, this led to constraint 52 metabolic reaction of MitoCore to 0 (**Table 19** and **Table 20**). For instance, the maximal trap-space value relative to the metabolic enzyme AKGDm (2-Oxoglutarate Dehydrogenase) was equal to 0. Thus, the

metabolic flux of the reaction it catalyzes (*i.e.* R_AKGDm) was constrained to 0 in MitoCore. Similarly, the maximal trap-space value associated with the metabolite fum_m (mitochondrial fumarate) was equal to 0. Such dually extracted constraints reflect the consistency of RASFs signaling and gene regulation processes impact upon their metabolic pathways.

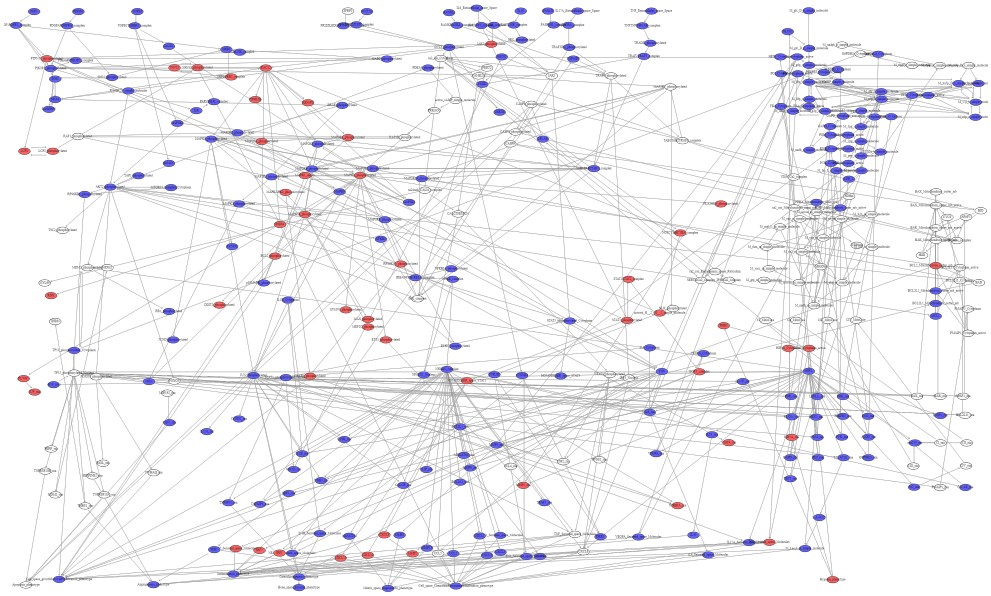

Figure 40. Visualization of the value propagation algorithm upon the RASF model network under RASF-specific initial conditions. This iterative algorithm allows the computation of specific components dynamical consequences on the overall behavior of the model. Under RASF-specific initial conditions, 313 components of the RASF model were fixed by value propagation, including 100 fixed at 0 (in white) and 213 at 1 (in blue). The remaining 46 components values were not fixed, they are displayed in red.

Table 19. Metabolic enzymes with projected maximal regulatory trap-space equal to 0 under RASF-specific initial conditions and their associated catalyzed reaction constrained to 0 in MitoCore.

Enzyme	Complete Name	Metabolic subsystem	Catalyzed reaction
AKGDm	2-Oxoglutarate Dehydrogenase	Tricarboxylic acid cycle	R_AKGDm
CI_MitoCore	NADH Dehydrogenase	Electron transport chain	R_CI_MitoCore
CII_MitoCore	Succinate Dehydrogenase	Electron transport chain	R_CII_MitoCore
CIII_MitoCore	Cytochrome C Reductase	Electron transport chain	R_CIII_MitoCore
CIV_MitoCore	Cytochrome C Oxidase	Electron transport chain	R_CIV_MitoCore
ICDHxm	Isocitrate Dehydrogenase	Tricarboxylic acid cycle	R_ICDHxm
PDHm	Pyruvate Dehydrogenase	Tricarboxylic acid cycle	R_PDHm

Table 20. Metabolites with projected maximal regulatory trap-space equal to 0 under RASF-specific initial conditions and their associated producing reactions constrained to 0 in MitoCore.

Metabolite	Complete name	Metabolic subsystem	Producing reaction
6pgc_c	6-Phospho-D-gluco-nate	Pentose phosphate pathway	R_PGL
6pgl_c	D-Glucono-1,5-lac-tone 6-phosphate	Pentose phosphate pathway	R_G6PDH2r
accoa_m	Acetyl-CoA	Isoleucine degrada-tion	R_ACACT10m
		FA and ketone body metabolism, ketogen-esis	R_ACACT1rm
		TCA periphery	R_ACITLm_Mito-Core
		Alcohol metabolism	R_ACSm
		Ketogenesis / Leucine degradation	R_HMGLm

		Beta-alanine degradation	R_MMSAD3m
		Beta-alanine degradation	R_MMSAD3m2_MitoCore
		Fatty acid metabolism	R_MTPC14_MitoCore
			R_MTPC16_MitoCore
			R_r0287
			R_r0634
			R_r0724
			R_r0732
		Glycolysis, gluconeogenesis	R_PDHm
akg_m	2-Oxoglutarate	Lysine degradation	R_2AMADPTmC_MitoCore
		Tryptophan Metabolism	R_2OXOADPTmC_MitoCore
		Malate aspartate shuttle	R_ASPTAm
		Glutamate degradation/synthesis	R_GLUDxm
			R_GLUDym
		Tricarboxylic acid cycle	R_ICDHxm
			R_ICDHyrm
cit_m	Citrate	Mitochondrial transporters	R_CITtamB
			R_CITtbm
			R_r0917
			R_r0917b_MitoCore
		Tricarboxylic acid cycle	R_CSm
fum_m	Fumarate	Electron transport chain	R_CII_MitoCore
		Mitochondrial transporters	R_FUMtmB_Mitocore
icit_m	Isocitrate	Tricarboxylic acid cycle	R_ACONTm
mal_L_m	L-Malate	Malate aspartate shuttle	R_AKGMALtm
			R_MALSO3tm

		Mitochondrial transporters	R_MALSO4tm
			R_MALTSULtm
			R_r0913
		Tricarboxylic acid cycle	R_FUMm
oaa_m	Oxaloacetate	Tricarboxylic acid cycle periphery	R_ACITLm_MitoCore
			R_MDHm
			R_PCm
ru5p_D_c	D-Ribulose 5-phosphate	Pentose phosphate pathway	R_GND
succ_m	Succinate	Ketone bodies - degradation	R_OCOAT1m
		Mitochondrial transporters	R_SUCCt2m
			R_SUCCt3m_MitoCore
			R_r0829
			R_r0830
			R_r0830B_MitoCore
		Tricarboxylic acid cycle	R_SUCOAS1m
			R_SUCOASm
		GABA shunt	R_r0178
succoa_m	Succinyl-CoA	Tricarboxylic acid cycle	R_AKGDm
		Propanoate metabolism	R_MMMm

A first FBA was carried out to enable the assessment of metabolic fluxes distribution in a control situation. In addition, it allowed comparison with the second FBA, including metabolic constraints extracted from the RASF regulatory model. Results of both FBAs can be visualized in **Figure 40**. Details of all uptake and secretion C-fluxes results for both FBAs can be found in **Table 21** and **Table 22**. Complete metabolic flux distribution in control and RASF-specific conditions is displayed in **Table S1** and **Table S2**.

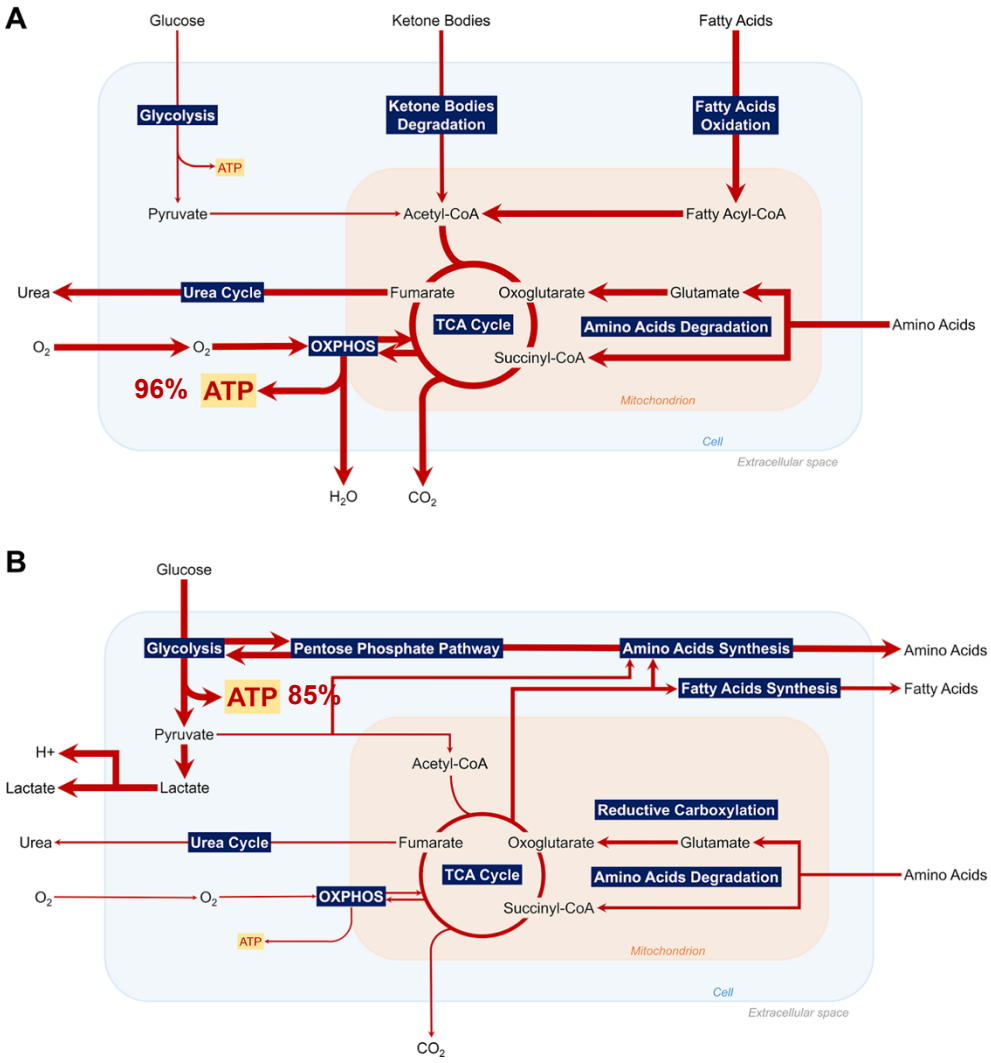

Figure 41. Summary of the major active pathways of central metabolism according to Flux Balance Analysis in (A) control (B) and RASF-specific conditions. The objective function was set at maximum cellular ATP production. The ratio of cellular ATP production from glycolysis to total cellular ATP production from glycolysis and oxidative phosphorylation is calculated at 96% in healthy cells and 85% in rheumatoid arthritis synovial fibroblasts.

Table 21. Main uptake and secretion reactions according to the objective function of maximum ATP production in a control (healthy) cellular situation.

Uptake

Metabolite	Reaction	Flux	C-number	C-flux
acac_e	EX_acac_e	0.114	4	2.49%
ala_L_e	EX_ala_L_e	0.01	3	0.16%
arg_L_e	EX_arg_L_e	0.007	6	0.23%
asn_L_e	EX_asn_L_e	0.01	4	0.22%
asp_L_e	EX_asp_L_e	0.154	4	3.36%
bhb_e	EX_bhb_e	0.048	4	1.05%
but_e	EX_but_e	0.006	4	0.13%
cyan_e	EX_cyan_e	0.001	1	0.01%
cys_L_e	EX_cys_L_e	0.001	3	0.02%
glc_D_e	EX_glc_D_e	0.9	6	29.48%
gly_e	EX_gly_e	0.009	2	0.10%
glyc_e	EX_glyc_e	0.01	3	0.16%
h_e	EX_h_e	3.458	0	0.00%
hco3_e	EX_hco3_e	1.71	1	9.34%
hdca_e	EX_hdca_e	0.4684	16	40.92%
his_L_e	EX_his_L_e	0.01	6	0.33%
lie_L_e	EX_lie_L_e	0.004	6	0.13%
lac_L_e	EX_lac_L_e	0.575	3	9.42%
leu_L_e	EX_leu_L_e	0.016	6	0.52%
lys_L_e	EX_lys_L_e	0.03	6	0.98%
o2_e	EX_o2_e	19.8	0	0.00%
pro_L_e	EX_pro_L_e	0.004	5	0.11%
ser_L_e	EX_ser_L_e	0.017	3	0.28%
thr_L_e	EX_thr_L_e	0.012	4	0.26%
val_L_e	EX_val_L_e	0.011	5	0.30%

Secretion

Metabolite	Reaction	Flux	C-number	C-flux
co2_e	EX_co2_e	-18.31	1	99.96%
h2o_e	EX_h2o_e	-16.7	0	0.00%
nh4_e	EX_nh4_e	-0.362	0	0.00%
tcynt_e	EX_tcynt_e	-0.001	1	0.01%
urea_e	EX_urea_e	-0.007	1	0.04%

Table 22. Main uptake and secretion reactions according to the objective function of maximum ATP production in a rheumatoid arthritis synovial fibroblast-specific situation.

Uptake

Metabolite	Reaction	Flux	C-number	C-flux
asn_L_e	EX_asn_L_e	0.01	4	0.65%
asp_L_e	EX_asp_L_e	0.154	4	10.01%
glc_D_e	EX_glc_D_e	0.9	6	87.72%
gly_e	EX_gly_e	0.005	2	0.16%
glyc_e	EX_glyc_e	0.01	3	0.49%
h2o_e	EX_h2o_e	0.055	0	0.00%
his_L_e	EX_his_L_e	0.01	6	0.97%

Secretion

Metabolite	Reaction	Flux	C-number	C-flux
ac_e	EX_ac_e	-0.01	2	0.32%
ala_L_e	EX_ala_L_e	-0.164	3	7.99%
co2_e	EX_co2_e	-0.169	1	2.75%

h_e	EX_h_e	-1.636	0	0.00%
lac_L_e	EX_lac_L_e	-1.82	3	88.69%
nh4_e	EX_nh4_e	-0.04	0	0.00%
ser_L_e	EX_ser_L_e	-0.005	3	0.24%

As biologically expected, the optimal fluxes for maximum cellular ATP production in a control situation are TCA and OXPHOS fluxes. They are responsible for 96% of total ATP production. In a control situation, the main uptaken carbonated molecules are hexadecanoate (40.92% of total C-flux), glucose (29.48%), lactate (9.42%), and HCO_3 (9.34%), primary energy sources for most cells. The main secreted carbonated molecule is CO_2 (99.96%) as it is the principal product of oxidative metabolism along with H_2O. In RASF-specific regulatory conditions, the optimal fluxes for maximum cellular ATP production are glycolytic, accounting for 85% of cellular ATP production. Metabolic uptake and secretion fluxes are also affected. The main uptaken carbonated molecules are glucose (85.69% of total C-flux) and aspartate (9.77%). The main secreted carbonated molecules are lactate (86.12%) and alanine (8.33%).

In addition, a comparison of internal metabolic fluxes (**Table S1** and **Table S2**) in both situations illustrates increased glycolytic fluxes along with increased glucose uptake and lactate secretion in RASFs, accounting for a highly glycolytic metabolism. Low oxidative metabolism is demonstrated through decreased (almost null) TCA and OXPHOS fluxes and decreased secretion of OXPHOS by-products such as CO_2 and H_2O. A hypoxic environment is displayed with decreased O_2 uptake and increased H^+ secretion associated with environment acidity. Beyond metabolic pathways of ATP production, results denote reprogramming of several other metabolic

pathways in RASFs. An increased amino acids and fatty acids secretion is shown, potentially acting in RA as substrates for energy production, biosynthesis intermediates, components of membrane phospholipids, or support for bone erosion and cartilage degradation. Increased reductive carboxylation is also identified, a novel glutamine metabolism pathway supporting the growth of tumor-like cells with mitochondrial defects. Further pathways including mitochondrial transport reactions, cardiolipin synthesis, or glycine cleavage, appear to be impacted, most likely indirectly as a result of metabolites redirection through up-regulated metabolic pathways.

To decipher the role of regulatory components in RASFs metabolic alterations, individual knock-ins and knock-outs of RASF-specific initial conditions were first performed. In greater details, 14 FBAs were conducted following different sets of initial regulatory conditions. As shown in **Table 23**, out of the 14 RASF-specific initial conditions variants, only condition 3 (C3) significantly impacted ATP production pathways. Indeed, when inhibiting Hypoxia-Inducible Factor 1 (HIF1) and keeping RASF-specific initial conditions for the remaining components, glycolysis was dramatically decreased and OXPHOS explained the cellular ATP production. This situation, although extreme in its proportions due to the constraint extraction rules of the framework, is closer to a control situation. This finding suggests that targeting HIF1 could participate in restoring a healthy metabolic profile in RASFs. Moreover, it is coherent with recent experimental studies demonstrating that HIF1 knockdown reduces glycolytic metabolism in human synovial fibroblasts **[363]**.

Table 23. Regulatory knock-out/knock-in simulations set of initial conditions along with their FBA results in terms of total cellular ATP production from glycolysis and OXPHOS. All components value initially set to 1/0 in RASF-specific conditions were alternatively set to 0/1 while the others remained at RASF-specific values.

Component	Set of Initial Conditions													
	C1	**C2**	**C3**	**C4**	**C5**	**C6**	**C7**	**C8**	**C9**	**C10**	**C11**	**C12**	**C13**	**C14**
FASLG	0	1	1	1	1	1	1	1	1	1	1	1	1	1
FGF1	1	0	1	1	1	1	1	1	1	1	1	1	1	1
HIF1	1	1	0	1	1	1	1	1	1	1	1	1	1	1
IKBA/NFKB1/RELA	1	1	1	0	1	1	1	1	1	1	1	1	1	1
IL17A	1	1	1	1	0	1	1	1	1	1	1	1	1	1
IL18	1	1	1	1	1	0	1	1	1	1	1	1	1	1
IL6	1	1	1	1	1	1	0	1	1	1	1	1	1	1
MIR192	0	0	0	0	0	0	0	1	0	0	0	0	0	0
PDGFA	1	1	1	1	1	1	1	1	0	1	1	1	1	1
RANKL	1	1	1	1	1	1	1	1	1	0	1	1	1	1
SFRP5	0	0	0	0	0	0	0	0	0	0	1	0	0	0
TGFB1	1	1	1	1	1	1	1	1	1	1	1	0	1	1
TNF	1	1	1	1	1	1	1	1	1	1	1	1	0	1
WNT5A	1	1	1	1	1	1	1	1	1	1	1	1	1	0
GLC	1	1	1	1	1	1	1	1	1	1	1	1	1	1
Glycolysis	85.1	85.1	**0**	85.1	85.1	85.1	85.1	85.1	85.1	85.1	85.1	85.1	85.1	85.1
OXPHOS	14.9	14.9	**100**	14.9	14.9	14.9	14.9	14.9	14.9	14.9	14.9	14.9	14.9	14.9

Further combinations of knock-ins and knock-outs were generated and tested to account for the potential synergistic effect of regulatory components upon metabolic processes. $2^{14} = 16384$ combinations were tested, representing all possible combinations of knock-ins and knock-outs of the RASF-specific initial conditions (**Table 12**), naturally eliminating glucose knockouts that are not biologically meaningful. Out of the 16384 knock-ins and knock-outs combinations of RASF-specific initial conditions, 1984 were eliminated as they generated aberrant asymptotic behaviors of ontological phenotypes (*i.e.* apoptosis and proliferation active at the same time), proving the limits of a model that was not created for combined inputs but to reproduce a cell- and disease-specific environment. 8448 combinations were eliminated as the computation of trap-spaces exceeded the time limit of three minutes, most likely due to the impossibility of reducing the complexity of the model enough with the value propagation algorithm. The remaining 5952 combinations were thoroughly analyzed. All combinations demonstrated a reprogrammed pathogenic metabolic profile with 96% of cellular ATP production provided by glycolytic pathways and 4% from OXPHOS. To identify eventual patterns associated with such diseased metabolic profile, the average value of each component was obtained. As shown in **Table 24**, all combinations of RASF-specific knock-outs and knock-ins related to a diseased metabolic profile included the activation of HIF1. As for the other components, the averages do not allow us to identify a distinctive signature. The key regulatory role of HIF1 had already been identified within individual knock-outs and knock-ins. Its constant activated state in all combinations of RASF-specific initial conditions associated with a pathogenic metabolic profile demonstrates the overriding individual effect of HIF1 over the synergistic effect of any other regulatory components in the RASF hybrid model.

Table 24. Average value of each regulatory component within all combinations of RASF-specific knock-outs and knock-ins associated with a diseased metabolic profile.

Regulatory component	Averaged value within all combinations
FASLG	0.33333333
FGF1	0.51612903
HIF1	**1**
IKBA/NFKB1/RELA	0.5
IL17	0.5
IL18	0.51612903
IL6	0.5
MIR192	0.33333333
PDGFA	0.48387097
RANKL	0.5
SFRP5	0.48387097
TGFB1	0.5
TNF	0.5
WNT5A	0.51612903
GLC	1

4.3.2 The breast CAF hybrid model, an integrated dynamic overview of cell-specific pathogenic signaling, gene regulation and metabolism in the TME

All necessary scripts and files to generate results depicted below are available on a GitLab repository at https://gitlab.com/genhotel/breast-cafs-reverse-warburg-effect and in a Zenodo permanent archive at https://doi.org/10.5281/zenodo.7874614.

The value propagation method was applied to the regulatory Boolean model under breast CAF-specific initial conditions identified earlier (**Table 15**). Out of the 463 components present in the breast CAF model, 434 were fixed by

value propagation (127 were fixed at 0 and 307 at 1) (**Figure 41**). Evidently, the breast CAF-specific initial conditions, including 56 inputs and 91 intermediary nodes, exert an important control over the whole network.

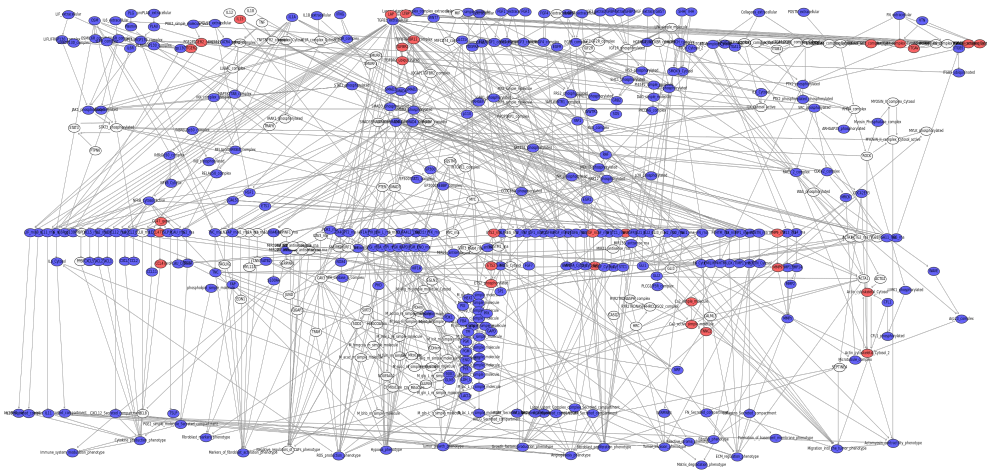

Figure 42. Visualization of the value propagation algorithm upon the breast CAF model network under breast CAF-specific initial conditions. This iterative algorithm allows the computation of specific components dynamical consequences on the overall behavior of the model. Under breast CAF-specific initial conditions, 434 components of the CAF model were fixed by value propagation, including 127 fixed at 0 (in white) and 307 at 1 (in blue). 29 components values were not fixed, they are displayed in red.

Using the results of value propagation as a new set of initial conditions enabled us to decrease the complexity of the breast CAF model to obtain its trap-spaces, including the complete asymptotic behavior of the system. A single trap-space is identified. It is a stable state, which indicates that, under influences from breast CAF-specific cellular signaling and gene regulation networks, the asymptotic behavior of all metabolic components is fully stable. As described in the hybrid modeling framework, additional metabolic constraints were extracted from metabolic compounds with a proven inactive asymptotic behavior. This concerns 7 metabolic enzymes and 15 metabolites

leading to constrain the flux of 66 unique metabolic reactions to 0 (**Table 25** and **Table 26**). The high number of constrained reactions is explained by enzymes commonly catalyzing a single metabolic reaction whereas metabolites were produced by numerous reactions. Additionally, certain metabolic reactions (*e.g.* R_PDHm, R_ICDHxm, R_GLUNm) were constrained both through their catalyzing enzymes and their produced metabolites. It reflects the consistency of breast CAF-specific cellular signaling and gene regulation machinery upon its metabolic processes. This approach allows to contextualize MitoCore, a generic core metabolic network, in the cell- and disease-specific context of breast CAFs.

Table 25. Metabolic enzymes with projected maximal regulatory trap-space equal to 0 under breast CAF-specific initial conditions and their associated catalyzed reaction constrained to 0 in MitoCore.

Enzyme	Complete Name	Metabolic subsystem	Catalyzed reaction
GLUNm	Mitochondrial Glutaminase	Glutamine degradation	R_GLUNm
CI_MitoCore	NADH Dehydrogenase	Electron transport chain	R_CI_MitoCore
HMGCOASim	Hydroxymethylglutaryl Coenzyme A Synthase	Ketogenesis	R_ HMGCOA-Sim
CIII_MitoCore	Cytochrome C Reductase	Electron transport chain	R_CIII_MitoCore
CIV_MitoCore	Cytochrome C Oxidase	Electron transport chain	R_CIV_MitoCore
ICDHxm	Isocitrate Dehydrogenase	Tricarboxylic acid cycle	R_ICDHxm
PDHm	Pyruvate Dehydrogenase	Tricarboxylic acid cycle	R_PDHm

Table 26. Metabolic enzymes with projected maximal regulatory trap-space equal to 0 under breast CAF-specific initial conditions and their associated catalyzed reaction constrained to 0 in MitoCore.

Metabolite	Complete name	Metabolic subsystem	Producing reaction
gln_L_c	L-Glutamine [cytoplasmic]	Glutamine synthesis	R_GLNS
		L-Glutamine transport	R_r2525
hmgcoa_m	3-Hydroxy-3-methylglutaryl-CoA [mitochondrial]	Leucine degradation	R_MGCHrm
		Ketogenesis	R_ HMGCOA-Sim
accoa_m	Acetyl-CoA [mitochondrial]	Isoleucine degradation	R_ACACT10m
		FA and ketone body metabolism, ketogenesis	R_ACACT1rm
		TCA periphery	R_ACITLm_MitoCore
		Alcohol metabolism	R_ACSm
		Ketogenesis / Leucine degradation	R_HMGLm
		Beta-alanine degradation	R_MMSAD3m
		Beta-alanine degradation	R_MMSAD3m2_MitoCore
		Fatty acid metabolism	R_MTPC14_MitoCore
			R_MTPC16_MitoCore
			R_r0287
			R_r0634
			R_r0724
			R_r0732
		Glycolysis, gluconeogenesis	R_PDHm
akg_m	2-Oxoglutarate [mitochondrial]	Lysine degradation	R_2AMADPTmC_MitoCore
		Tryptophan Metabolism	R_2OXOADPTmC_MitoCore
		Malate aspartate shuttle	R_ASPTAm
		Glutamate degradation and synthesis	R_GLUDxm
			R_GLUDym
		Tricarboxylic acid cycle	R_ICDHxm

			R_ICDHyrm
cit_m	Citrate [mitochondrial]	Mitochondrial transporters	R_CITtamB
			R_CITtbm
			R_r0917
			R_r0917b_MitoCore
		Tricarboxylic acid cycle	R_CSm
fum_m	Fumarate [mitochondrial]	Electron transport chain	R_CII_MitoCore
		Mitochondrial transporters	R_FUMtmB_Mitocore
icit_m	Isocitrate [mitochondrial]	Tricarboxylic acid cycle	R_ACONTm
mal_L_m	L-Malate [mitochondrial]	Malate aspartate shuttle	R_AKGMALtm
		Mitochondrial transporters	R_MALSO3tm
			R_MALSO4tm
			R_MALTSULtm
			R_r0913
		Tricarboxylic acid cycle	R_FUMm
oaa_m	Oxaloacetate [mitochondrial]	Tricarboxylic acid cycle periphery	R_ACITLm_MitoCore
			R_MDHm
			R_PCm
gln_L_m	L-Glutamine [mitochondrial]	Mitochondrial transporters	R_GLNtm
succ_m	Succinate [mitochondrial]	Ketone bodies degradation	R_OCOAT1m
		Mitochondrial transporters	R_SUCCt2m
			R_SUCCt3m_MitoCore
			R_r0829
			R_r0830
			R_r0830B_MitoCore
		Tricarboxylic acid cycle	R_SUCOAS1m
			R_SUCOASm
		GABA shunt	R_r0178
succoa_m	Succinyl-CoA [mitochondrial]	Tricarboxylic acid cycle	R_AKGDm
		Propanoate metabolism	R_MMMm

acac_m	Acetoacetic acid [mitochondrial]	Mitochondrial transporters	R_ACACt2mB_MitoCore
		Ketone bodies degradation	R_BDHm
		Ketogenesis, leucine degradation	R_HMGLm
glu_L_m	L-Glutamate [mitochondrial]	GABA shunt	R_ABTArm
		Beta-alanine degradation	R_APAT2rm
		Malate asparte shuttle	ASPGLUmB_MitoCore
		Malate aspartate shuttle	R_ASPTAm
		Cysteine degradation	R_CYSTAm
		Mitochondrial transporters	R_GLUt2mB_MitoCore
		Isoleucine degradation	R_ILETAm
		Leucine degradation	R_LEUTAm
		Ornithine degradation	R_ORNTArm
		Valine degradation	R_VALTAm
		Proline, ornithine degradation	R_r0074
		Tricarboxylic acid cycle periphery	R_r0081
		Lysine degradation	R_r0450
		Lysine degradation	R_r0525
bhb_m	3-Hydroxybutyric acid [mitochondrial]	Mitochondrial transporters	R_BHBtmB_MitoCore

Visualization of both control and breast CAF-specific FBA results are provided in **Figure 42**. Details of all uptake and secretion C-fluxes results for both FBAs can be found in **Table 27** and **Table 28**. Complete metabolic flux distribution in control and RASF-specific conditions is displayed in **Table S1** and **Table S3**.

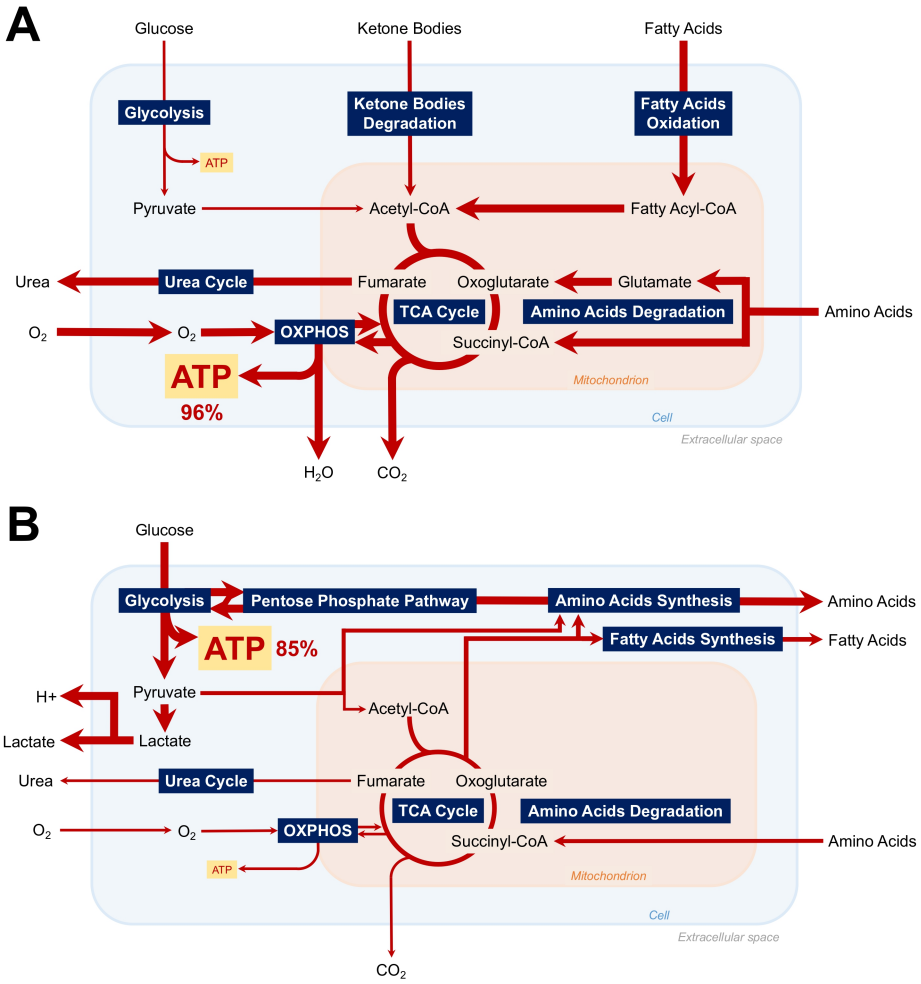

Figure 43. Summary of the major active pathways of central metabolism according to Flux Balance Analysis in (A) control (B) and breast CAF-specific conditions. The objective function was set at maximum cellular ATP production. The ratio of cellular ATP production from glycolysis to total cellular ATP production from glycolysis and oxidative phosphorylation is calculated at 96% in healthy cells and 85% in rheumatoid arthritis synovial fibroblasts.

Optimal fluxes for ATP production in a healthy fibroblast are OXPHOS fluxes, accounting for 96% of cellular ATP production. Main uptaken carbonated molecules are hexadecanoate (40.92% of total C-flux), glucose (29.48%), lactate (9.42%), and HCO_3 (9.34%), primary energy sources for most cells. Main secreted carbonated molecule is CO_2 (99.96%). Under breast CAF-specific regulatory conditions, optimal fluxes for ATP production are glycolytic fluxes, as they now explain 85.05% of cellular energy production in the form of ATP. Main uptaken carbonated molecules are glucose (87.72% of total C-flux) and aspartate (10.01%). Main secreted carbonated molecules are lactate (88.69%) and alanine (7.99%). Comparison of internal metabolic fluxes revealed reprogramming of major metabolic pathways for ATP production. Globally increased glycolytic fluxes along with increased lactate secretion in breast CAFs reflect a highly glycolytic metabolism. Low oxidative metabolism is demonstrated by decreased OXPHOS and TCA-associated fluxes along with decreased secretion of oxidative by-products (*e.g.* CO_2 and H_2O).

Table 27. Main uptake and secretion reactions according to the objective function of maximum ATP production in a control (healthy) cellular situation.

Uptake

Metabolite	Reaction	Flux	C-number	C-flux
acac_e	EX_acac_e	0.114	4	2.49%
ala_L_e	EX_ala_L_e	0.01	3	0.16%
arg_L_e	EX_arg_L_e	0.007	6	0.23%
asn_L_e	EX_asn_L_e	0.01	4	0.22%
asp_L_e	EX_asp_L_e	0.154	4	3.36%
bhb_e	EX_bhb_e	0.048	4	1.05%
but_e	EX_but_e	0.006	4	0.13%
cyan_e	EX_cyan_e	0.001	1	0.01%
cys_L_e	EX_cys_L_e	0.001	3	0.02%
glc_D_e	EX_glc_D_e	0.9	6	29.48%
gly_e	EX_gly_e	0.009	2	0.10%
glyc_e	EX_glyc_e	0.01	3	0.16%
h_e	EX_h_e	3.458	0	0.00%
hco3_e	EX_hco3_e	1.71	1	9.34%
hdca_e	EX_hdca_e	0.4684	16	40.92%
his_L_e	EX_his_L_e	0.01	6	0.33%
lie_L_e	EX_lie_L_e	0.004	6	0.13%
lac_L_e	EX_lac_L_e	0.575	3	9.42%
leu_L_e	EX_leu_L_e	0.016	6	0.52%
lys_L_e	EX_lys_L_e	0.03	6	0.98%
o2_e	EX_o2_e	19.8	0	0.00%
pro_L_e	EX_pro_L_e	0.004	5	0.11%
ser_L_e	EX_ser_L_e	0.017	3	0.28%
thr_L_e	EX_thr_L_e	0.012	4	0.26%
val_L_e	EX_val_L_e	0.011	5	0.30%

Secretion

Metabolite	Reaction	Flux	C-number	C-flux
co2_e	EX_co2_e	-18.31	1	99.96%
h2o_e	EX_h2o_e	-16.7	0	0.00%
nh4_e	EX_nh4_e	-0.362	0	0.00%
tcynt_e	EX_tcynt_e	-0.001	1	0.01%
urea_e	EX_urea_e	-0.007	1	0.04%

Table 28. Main uptake and secretion reactions according to the objective function of maximum ATP production in a breast cancer-associated fibroblast-specific situation.

Uptake

Metabolite	Reaction	Flux	C-number	C-flux
asn_L_e	EX_asn_L_e	0.01	4	0.65%
asp_L_e	EX_asp_L_e	0.154	4	10.01%
glc_D_e	EX_glc_D_e	0.9	6	87.72%
gly_e	EX_gly_e	0.005	2	0.16%
glyc_e	EX_glyc_e	0.01	3	0.49%
h2o_e	EX_h2o_e	0.055	0	0.00%
his_L_e	EX_his_L_e	0.01	6	0.97%

Secretion

Metabolite	Reaction	Flux	C-number	C-flux
ac_e	EX_ac_e	-0.01	2	0.32%
ala_L_e	EX_ala_L_e	-0.164	3	7.99%
co2_e	EX_co2_e	-0.169	1	2.75%
h_e	EX_h_e	-1.636	0	0.00%

lac_L_e	EX_lac_L_e	-1.82	3	88.69%
nh4_e	EX_nh4_e	-0.04	0	0.00%
ser_L_e	EX_ser_L_e	-0.005	3	0.24%

A hypoxic environment along with anaerobic metabolism is revealed through decreased O_2 uptake and increased H+ secretion, associated with environmental acidity. Besides metabolic pathways for energy production, macromolecular building blocks pathways are altered in breast CAFs. Particularly, amino acids uptake by breast CAFs is decreased (*e.g.* proline, glycine), along with their decreased degradation (*e.g.* proline), and increased secretion (*e.g.* serine, lysine). Fatty acids uptake is further decreased (*e.g.* butanoic acid) while their secretion is increased (*e.g.* palmitic acid). Cardiolipin synthesis is decreased in breast CAFs, coherently with former findings as they are known to regulate OXPHOS. Further pathways including folate cytosolic, reductive carboxylation, and butanoate metabolism, appear to be impacted, most likely resulting indirectly from metabolites redirection through other altered pathways or through the application of our additional metabolic constraints. Finally, mitochondrial transporters are affected due to the reprogramming of mitochondrial pathways discussed above.

After computationally reproducing the experimentally observed metabolic reprogramming in breast CAFs, the challenge consists in identifying its main regulatory drivers. Successive individual knock-outs and knock-ins of breast-CAF specific regulatory initial conditions resulted in 147 new sets, and therefore 147 new FBAs. A complete list of FBA results per set of initial conditions by ratio of total cellular ATP produced through glycolytic or oxidative pathways is provided in **Table 29**. Among the performed FBA, only one set of regulatory initial conditions reproduces a healthy metabolic profile

for energy production in breast CAFs, it is condition 57 (C57). Indeed, by knocking-out HIF1, metabolic pathways seem to recover a healthy-like distribution with cellular ATP being generated from oxidative rather than glycolytic pathways. Other regulatory inputs do not seem to directly affect metabolic fluxes distribution in breast CAFs.

Further combinations of knock-ins and knock-outs were generated and tested to account for the potential synergistic effect of regulatory components upon metabolic processes. In view the high number of initial conditions to be tested and potentially resulting in 2^{147} = 1784059616E^{44} combinations, a reduction of the model was first undertaken. The latter was obtained by focusing on the molecular pathways upstream of CAFs cellular phenotypes involved in hallmarks of cancer (*i.e.* ROS production, hypoxia, fibroblast proliferation, angiogenesis, tumor growth, tumor invasion, matrix degradation, migration into the tumor, ECM regulation, reactive stroma, immune system modulation) (**Figure 43**).

```
casq CAF_map-V2.xml -u ROS_production_phenotype Hypoxia_phenotype Fibroblast_proliferation_phenotype Angiogenesis_phenotype Tumor_growth_phenotype Tumor_invasion_phenotype Matrix_degradation_phenotype Migration_into_the_tumor_phenotype ECM_regulation_phenotype Reactive_stroma_phenotype Immune_system_modulation_phenotype
```

Figure 44. CaSQ command line to infer the extracted CAF model from the CAF-map V2 by focusing on hallmarks of cancer-specific pathways. The optional arguments -u (--upstream) only export species upstream of this specific node.

Table 29. Regulatory knock-out/knock-in FBA simulation results in terms of percentage of total cellular ATP production from glycolytic and oxidative pathways. Each components value initially set to 1/0 in breast CAF-specific conditions was alternatively set to 0/1 while the others remained unchanged (the details of each set of initial conditions is provided in the GitLab). Condition C57 corresponds to the knock-out of HIF1 (other regulatory inputs do not seem to directly affect metabolic fluxes distribution in breast CAFs).

GLYC	**OXPHOS**		C34	85.05	14.95	C68	85.05	14.95
C1	85.05	14.95	C35	85.05	14.95	C69	85.05	14.95
C2	85.05	14.95	C36	85.05	14.95	C70	85.05	14.95
C3	85.05	14.95	C37	85.05	14.95	C71	85.05	14.95
C4	85.05	14.95	C38	85.05	14.95	C72	85.05	14.95
C5	85.05	14.95	C39	85.05	14.95	C73	85.05	14.95
C6	85.05	14.95	C40	85.05	14.95	C74	85.05	14.95
C7	85.05	14.95	C41	85.05	14.95	C75	85.05	14.95
C8	85.05	14.95	C42	85.05	14.95	C76	85.05	14.95
C9	85.05	14.95	C43	85.05	14.95	C77	85.05	14.95
C10	85.05	14.95	C44	85.05	14.95	C78	85.05	14.95
C11	85.05	14.95	C45	85.05	14.95	C79	85.05	14.95
C12	85.05	14.95	C46	85.05	14.95	C80	85.05	14.95
C13	85.05	14.95	C47	85.05	14.95	C81	85.05	14.95
C14	85.05	14.95	C48	85.05	14.95	C82	85.05	14.95
C15	85.05	14.95	C49	85.05	14.95	C83	85.05	14.95
C16	85.05	14.95	C50	85.05	14.95	C84	85.05	14.95
C17	85.05	14.95	C51	85.05	14.95	C85	85.05	14.95
C18	85.05	14.95	C52	85.05	14.95	C86	85.05	14.95
C19	85.05	14.95	C53	85.05	14.95	C87	85.05	14.95
C20	85.05	14.95	C54	85.05	14.95	C88	85.05	14.95
C21	85.05	14.95	C55	100.0	0	C89	85.05	14.95
C22	85.05	14.95	C56	85.05	14.95	C90	85.05	14.95
C23	85.05	14.95	**C57**	**0.00**	**100**	C91	85.05	14.95
C24	85.05	14.95	C58	85.05	14.95	C92	85.05	14.95
C25	85.05	14.95	C59	85.05	14.95	C93	85.05	14.95
C26	85.05	14.95	C60	85.05	14.95	C94	85.05	14.95
C27	85.05	14.95	C61	85.05	14.95	C95	85.05	14.95
C28	85.05	14.95	C62	85.05	14.95	C96	85.05	14.95
C29	85.05	14.95	C63	85.05	14.95	C97	85.05	14.95
C30	85.05	14.95	C64	85.05	14.95	C98	85.05	14.95
C31	85.05	14.95	C65	85.05	14.95	C99	85.05	14.95
C32	85.05	14.95	C66	85.05	14.95	C100	85.05	14.95
C33	85.05	14.95	C67	85.05	14.95	C101	85.05	14.95

C102	85.05	14.95	C118	85.05	14.95	C134	85.05	14.95
C103	85.05	14.95	C119	85.05	14.95	C135	85.05	14.95
C104	85.05	14.95	C120	85.05	14.95	C136	85.05	14.95
C105	85.05	14.95	C121	85.05	14.95	C137	85.05	14.95
C106	85.05	14.95	C122	85.05	14.95	C138	85.05	14.95
C107	85.05	14.95	C123	85.05	14.95	C139	85.05	14.95
C108	85.05	14.95	C124	85.05	14.95	C140	85.05	14.95
C109	85.05	14.95	C125	85.05	14.95	C141	85.05	14.95
C110	85.05	14.95	C126	85.05	14.95	C142	85.05	14.95
C111	85.05	14.95	C127	85.05	14.95	C143	85.05	14.95
C112	85.05	14.95	C128	85.05	14.95	C144	85.05	14.95
C113	85.05	14.95	C129	85.05	14.95	C145	85.05	14.95
C114	85.05	14.95	C130	85.05	14.95	C146	85.05	14.95
C115	85.05	14.95	C131	85.05	14.95	C147	85.05	14.95
C116	85.05	14.95	C132	85.05	14.95			
C117	85.05	14.95	C133	85.05	14.95			

The extracted CAF model featured 58 inputs, 51 if excluding glucose and all components acting as “simple molecule” as referred to in CellDesigner. The 51 remaining inputs were subsequently grouped into 21 inputs as shown in **Table 30**.

Table 30. Grouping nodes acting as inputs in the extracted breast CAF model.

Initial inputs of the extracted CAF model	Group of inputs of the updated extracted CAF model	Reason for grouping
AREG EGF CTGF HGF PDGF	Growth factor	Components of the growth factor family
CASQ2 HRC RYR2/TRDN/ASPH	Ca2+_binding_proteins	Involved in the calcium binding to the endoplasmic reticulum
IL12 IL18	IL12/18	Proinflammatory cytokines of the interleukin family responsible for cell-mediated inflammation
miR101 miR141 miR200B miR205 miR214	MIRs_0	Negative regulators of CAFs
FGF1 FGF2 FGF3 FGF4	FGFs	Components of the fibroblast growth factor family
IGF1 IGF2 IGFBP3 IGFBP4	IGFs	Components of the insulin growth factor family
IHH SHH	Hedgehog_proteins	Components of the cellular signaling Hedgehog pathway
IL1A IL1B IL6	IL6/1A/1B	Proinflammatory cytokines of the interleukin L1 family
HIF1	HIF1	/
miR155 miR211 miR221	MIRs_1	Up-regulated micro-RNAs
proPLAU PLG	Proteases	Proteases signaling components
WNT7 WWRT1	WNT_proteins	Components of the WNT signaling pathway

MIF IFNγ LIF OSM	Cytokines	Up-regulated cytokines
TNF	TNF	/
VTN Collagens POSTN FN Large Latent Complex	ECM_proteins	Proteins involved in the regulation of the ECM
GAST	GAST	/
LGALS1	LGALS1	/
CFL1	CFL1	/
GLNS	GLNS	/
CXCL12	CXCL12	/

Thus, 2^{21} = 2 097 152 combinations were generated for further testing, accounting for all possible combinations of knock-ins and knock-outs of the extracted breast CAF-specific inputs (**Table 30**). Unfortunately, after nearly 11 days of simulation, "only" 308 159 combinations were calculated, all of which were eliminated of further analysis due to the trap-space computation step lasting more than three minutes per combination. At this point, the identification of a possible synergetic effect of regulatory inputs upon metabolic processes in the hybrid breast CAF model is not possible. Alternative strategies to meet this objective are currently being considered.

4.3.3 MetaLo, a Python package for metabolic analysis of logical models infered from molecular interaction maps

Written in Python, MetaLo is a pip-installable package for coupling cell- and/or disease-specific regulatory Boolean models inferred from standardized molecular interaction maps with generic metabolic networks (https://pypi.org/project/metalo/). It is an open-source tool published under the GNU General Public License version 3.0. MetaLo allows assessment of the impact of gene regulation and cellular signaling pathways upon metabolic processes under cell- and/or disease-specific conditions, and more specifically upon its central function of energy production through the calculation of the ratio of ATP produced through glycolysis and, by extension, OXPHOS.

MetaLo is interoperable with a wide range of systems biology tools as its inputs and outputs are in standard formats. Indeed, two input files are required: a cell-specific molecular interaction map in CellDesigner **[228]** XML format and a generic metabolic network in the SBML format **[229]**. Note that molecular interaction maps must be compliant with SBGN PD standards **[189], [227]** for representation and that metabolic components must be named consistently in both the molecular interaction map and the metabolic network. Users do not need to be proficient in the Python programming language as MetaLo can be operated in two forms, namely through the command line or *via* its graphical interface (**Figure 44**).

MetaLo results displays both control and cell- and/or disease-specific FBA results along with ratio of ATP produced through glycolytic or oxidative pathways and further generates several output files:

- A CaSQ-generated CSV file including all regulatory components names, logic formulae and aliases from CellDesigner;

- A CaSQ-generated SBML file encoding the regulatory logical model in the standard SBML-qual format;
- A CaSQ-generated BNET file encoding the regulatory logical model for further use by Trappist;
- A Trappist-generated CSV file covering all computed trap-spaces of the regulatory model;
- A MetaLo-generated CSV file displaying control FBA results;
- A MetaLo-generated CSV file displaying cell- and/or disease-specific FBA results.

Additional options are further available in MetaLo to i) not infer a Boolean model from the global molecular interaction map but only from specific sub-parts downstream and/or upstream of specific components, ii) provide an additional CSV file including initial conditions to forcefully initialize the regulatory model and reproduce cell- and/or disease-specific environments, and iii) display flux variability (FVA) results instead of FBA results. The goal of FVA is to compute the maximal and minimal values, *i.e.* intervals of reaction fluxes, when the objective function is optimized rather than unique flux values.

A

```
$ metalo --help

usage: metalo [-h] [-v] [-D] [-f] [-i INIT] [-c CASQ] MAP METABOLISM

Metabolic analysis of Logical models extracted from maps. Copyright (C) 2023 Sahar.Aghakhani@i
GPLv3

positional arguments:
MAP                   CellDesigner file containing the mechanistic map
METABOLISM            MitoCore style metabolic model

options:
-h, --help            show this help message and exit
-v, --version         show program's version number and exit
-D, --debug           display some debug information
-f, --fva             run FVA to get interval of values
-i INIT, --init INIT  CSV file with forced initial values for the Logic model
-c CASQ, --casq CASQ  Additional arguments for CaSQ like -u, -d or -r
```

B

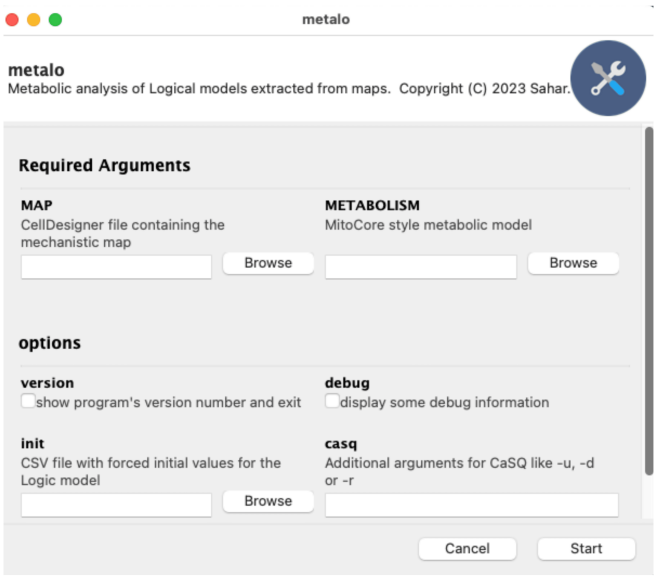

Figure 45. Usage of MetaLo through (A) the command line or (B) the graphical interface. Minimal inputs required are a cell- and/or disease-specific molecular interaction map in the CellDesigner XML file format and a generic constraint-based metabolic network in the SBML format. Additional arguments may be specified including initial conditions for the simulation of the regulatory model, specification for model inference through CaSQ or conduction of flux variability analysis instead of flux balance analysis.

We compared the results of MetaLo (version 0.5.2) RASFs (**Figure 45**) and breast CAFs (**Figure 46**) FVAs to the initial hybrid coupling framework FBA results. In both cases, MetaLo FVA results in terms of all metabolic reactions flux intervals cover the reaction flux value indicated by the FBA results of the initial framework. Moreover, the objective functions and ratios of ATP production through glycolysis are totally similar between both analyses. The packaging of MetaLo was successful and the few modifications implemented did not impact the cell-and disease-specific regulatory and metabolic network coupling nor the subsequent metabolic analysis.

A

```
(base) sahar@sahar-VirtualBox:~/Bureau/MetaLo/RASF$ metalo RA_map_V2.xml mitocore_v1.01.x
ml -i RASF_IC.csv -c "-d FGF1 PDGFA TGFB1 WNT5A RANKL IL6_Extracellular_space_Space IL18
FASLG IL17A_Extracellular_space_Space TNF_Extracellular_space_Space M_glc_D_e_simple_mole
cule Hypoxia_phenotype IKBANFKB1RELA_complex MIR192_rna SFRP5 -u Hypoxia_phenotype" -f
```

B

```
Objective
=========
1.0 PGK + 1.0 PYK + 1.0 CV_MitoCore = 4.460666666666667

Uptake
------
Metabolite   Reaction  Flux           Range  C-Number C-Flux
   asn_L_e EX_asn_L_e  0.01    [0.01; 0.01]         4  0.51%
   asp_L_e EX_asp_L_e 0.154  [0.154; 0.154]         4  7.80%
   glc_D_e EX_glc_D_e   0.9      [0.9; 0.9]         6 68.39%
    glyc_e  EX_glyc_e  0.01    [0.01; 0.01]         3  0.38%
       h_e     EX_h_e 0.074 [-1.652; 0.075]         0  0.00%
    hco3_e  EX_hco3_e  1.71       [0; 1.71]         1 21.66%
   his_L_e EX_his_L_e  0.01    [0.01; 0.01]         6  0.76%
   thr_L_e EX_thr_L_e  0.01       [0; 0.01]         4  0.51%

Secretion
---------
Metabolite      Reaction   Flux            Range  C-Number C-Flux
     2hb_e      EX_2hb_e  -0.01       [-0.01; 0]         4  0.51%
 HC00250_e  EX_HC00250_e      0      [-0.001; 0]         0  0.00%
      ac_e       EX_ac_e  -0.01   [-0.01; -0.01]         2  0.25%
   ala_L_e    EX_ala_L_e -0.174   [-0.175; 0.01]         3  6.61%
   arg_L_e    EX_arg_L_e      0       [0; 0.007]         6  0.00%
  citr_L_e   EX_citr_L_e      0      [-0.007; 0]         6  0.00%
     co2_e      EX_co2_e -1.884 [-1.896; -0.169]         1 23.86%
    cyan_e     EX_cyan_e      0       [0; 0.001]         1  0.00%
   cys_L_e    EX_cys_L_e      0       [0; 0.001]         3  0.00%
     gly_e      EX_gly_e      0  [-0.012; 0.005]         2  0.00%
     h2o_e      EX_h2o_e  -1.66  [-1.677; 0.236]         0  0.00%
   lac_L_e    EX_lac_L_e  -1.81 [-2.005; -1.809]         3 68.77%
mercplac_e EX_mercplac_e      0      [-0.001; 0]         3  0.00%
     nh4_e      EX_nh4_e  -0.04  [-0.225; -0.03]         0  0.00%
      no_e       EX_no_e      0      [-0.007; 0]         0  0.00%
      o2_e       EX_o2_e      0       [0; 0.025]         0  0.00%
   phe_L_e    EX_phe_L_e      0        [0; 0.01]         9  0.00%
   ser_L_e    EX_ser_L_e      0  [-0.005; 0.017]         3  0.00%
     so3_e      EX_so3_e      0  [-0.001; 0.001]         0  0.00%
   tcynt_e    EX_tcynt_e      0      [-0.001; 0]         1  0.00%
    tsul_e     EX_tsul_e      0      [-0.001; 0]         0  0.00%
   tyr_L_e    EX_tyr_L_e      0       [-0.01; 0]         9  0.00%

The proportion of global ATP production through glycolysis in the trap-spaces conditions
 is [0.8505, 0.8505].
```

Figure 46. MetaLo analysis of RASF regulatory impact upon metabolic processes. (A) Specification of analysis parameters with the generic RA-map V2, CaSQ arguments for inference of the RASF model, RASF-specific initial conditions, and running flux variability analysis instead of flux balance analysis. **(B)** Flux variability analysis results for main uptake and secretion metabolic reaction fluxes and in terms of overall ratio of ATP produced through glycolytic pathways.

A

```
(base) sahar@sahar-VirtualBox:~/Bureau/MetaLo/CAF$ metalo CAF-map_V2_MitoCore_ID.xml
mitocore_v1.01.xml -i Breast_CAF_initial_conditions.csv -f
```

B

```
Objective
=========
1.0 PGK + 1.0 PYK + 1.0 CV_MitoCore = 4.460666666666622

Uptake
------
Metabolite   Reaction  Flux           Range  C-Number C-Flux
   asn_L_e EX_asn_L_e  0.01    [0.01; 0.01]         4  0.51%
   asp_L_e EX_asp_L_e 0.154  [0.154; 0.154]         4  7.83%
   glc_D_e EX_glc_D_e   0.9      [0.9; 0.9]         6 68.65%
     gly_e   EX_gly_e 0.005 [-0.012; 0.005]         2  0.13%
    glyc_e  EX_glyc_e  0.01    [0.01; 0.01]         3  0.38%
       h_e     EX_h_e 0.074 [-1.652; 0.075]         0  0.00%
    hco3_e  EX_hco3_e  1.71       [0; 1.71]         1 21.74%
   his_L_e EX_his_L_e  0.01    [0.01; 0.01]         6  0.76%

Secretion
---------
Metabolite      Reaction   Flux            Range  C-Number C-Flux
     2hb_e      EX_2hb_e      0       [-0.01; 0]         4  0.00%
 HC00250_e  EX_HC00250_e      0     [-0.001; 0]         0  0.00%
      ac_e       EX_ac_e  -0.01   [-0.01; -0.01]         2  0.25%
   ala_L_e    EX_ala_L_e      0   [-0.175; 0.01]         3  0.00%
   arg_L_e    EX_arg_L_e      0       [0; 0.007]         6  0.00%
  citr_L_e   EX_citr_L_e      0     [-0.007; 0]         6  0.00%
     co2_e      EX_co2_e -1.879 [-1.896; -0.169]         1 23.89%
    cyan_e     EX_cyan_e      0       [0; 0.001]         1  0.00%
   cys_L_e    EX_cys_L_e      0       [0; 0.001]         3  0.00%
     h2o_e      EX_h2o_e -1.491  [-1.677; 0.236]         0  0.00%
   lac_L_e    EX_lac_L_e -1.984 [-2.005; -1.809]         3 75.67%
mercplac_e EX_mercplac_e      0     [-0.001; 0]         3  0.00%
     nh4_e      EX_nh4_e -0.204  [-0.225; -0.03]         0  0.00%
      no_e       EX_no_e      0     [-0.007; 0]         0  0.00%
      o2_e       EX_o2_e      0       [0; 0.025]         0  0.00%
   phe_L_e    EX_phe_L_e      0        [0; 0.01]         9  0.00%
   ser_L_e    EX_ser_L_e -0.005  [-0.005; 0.017]         3  0.19%
     so3_e      EX_so3_e      0  [-0.001; 0.001]         0  0.00%
   tcynt_e    EX_tcynt_e      0     [-0.001; 0]         1  0.00%
   thr_L_e    EX_thr_L_e      0       [0; 0.01]         4  0.00%
    tsul_e     EX_tsul_e      0     [-0.001; 0]         0  0.00%
   tyr_L_e    EX_tyr_L_e      0       [-0.01; 0]         9  0.00%

The proportion of global ATP production through glycolysis in the trap-spaces conditions
 is [0.8505, 0.8505].
```

Figure 47. MetaLo analysis of breast CAFs regulatory impact upon metabolic processes. (A) Specification of analysis parameters with: the generic CAF-map V2, breast CAF-specific initial conditions, and running flux variability analysis instead of flux balance analysis. **(B)** Flux variability analysis results for main uptake and secretion metabolic reaction fluxes and in terms of overall ratio of ATP produced through glycolytic pathways.

This final section tackles our efforts to integrate the dynamic behavior of multiple biological machinery (*e.g.* cellular signaling, gene regulation and metabolism) by studying the dynamic impacts of RASFs and breast CAFs regulatory pathways upon their metabolic subprocesses and identifying key regulator(s). We addressed this challenge by developing an innovative hybrid modeling framework further packaged in an open-source Python tool of the name MetaLo. The latter was applied to our cell- and disease-specific contexts and enabled us to generate the two first large-scale hybrid models of RASFs and breast CAFs leveraging both data-driven and manual approaches. MetaLo combines the previous RASFs and breast CAFs regulatory Boolean models automatically inferred from up-to-date molecular interaction maps with the MitoCore generic reconstruction of human metabolism. They allowed us to propose a potential commong mechanism of fibroblasts metabolic reprogramming in RA and BC, driven by HIF1, initiating their aggressive behavior.

Associated scientific communication, details here

The construction of the RASF hybrid model was published in an original research article and presented at an international scientific conference:

Aghakhani, S; Soliman, S; Niarakis, A. Metabolic reprogramming in rheumatoid arthritis synovial fibroblasts: a hybrid modeling approach. *PLOS Computational Biology* **2022** 18(12): e1010408. https://doi.org/10.1371/journal.pcbi.1010408

Aghakhani, S; Soliman, S; Niarakis, A. Metabolic Reprogramming in Rheumatoid Arthritis Synovial Fibroblasts (RASFs): a Hybrid Modeling Approach. *European Conference on Computational Biology*; September 18-21, **2022**; Sitges — Spain (poster)

The construction of the breast CAF hybrid ws published in an original research article and presented at an international scientific conference:

Aghakhani, S; E Silva Saffar, S; Soliman, S; Niarakis, A. Hybrid computational modeling highlights reverse Warburg effect in breast cancer-associated fibroblasts. *Computational and Structural Biotechnology Journal* **2023**. https://doi.org/10.1016/j.csbj.2023.08.015

Aghakhani, S; E Silva Saffar, S; Soliman, S; Niarakis, A. **A large-scale hybrid model to study metabolic reprogramming in cancer-associated fibroblasts.** *ONCOLille Days*; November 2-4, **2022**, Lille — France (poster)

The packaging of the hybrid coupling framework within the MetaLo tool will be submitted for publication very shortly in an applications note and was presented at an international scientific conference:

Aghakhani, S; Soliman, S; Niarakis, A. Metabolic analysis of logical models infered from molecular interaction maps. *Building Immune Digital Twins*; May 15th to June 2nd, **2023**; Orsay — France (oral presentation)

5 DISCUSSION

Immunometabolism refers to the tight interconnections between the historically distinct disciplines of immunology and metabolism **[1]**. It covers the regulation of immune responses by metabolic processes and nutrient distribution along with immune systems regulatory impact upon metabolism. The relevance of immunometabolism in physiopathology is increasingly recognized, particularly as one of its key features is the metabolic response to pathogenic immune dysregulation. Immune-related cells may adapt, rewire, and adopt specific metabolic subprograms, driving disease initiation or maintenance by determining specific cellular behavior, namely metabolic reprogramming **[5], [380]**. The latter refers to the alterations in cellular bioenergetics occuring in response to changes in environmental conditions or cellular requirements, both of which are very likely to occur in disease conditions. These adaptations are regulated by various processes along with gene regulation, response to the cellular signals, and energetic demands. Understanding metabolic reprogramming is crucial in the quest for novel therapeutic targets for incurable diseases where the impact of metabolism has historically been overlooked. In addition to opening up new avenues for drug development, immunometabolic targeting can reduce the adverse side effects of a number of therapies by enabling cellular specificity rather than shutting down all or part of the immune system and resulting in a potentially hazardous state of immunosuppression for patients.

Leveraging immunometabolic processes seems particularly relevant to us in the context of complex diseases whose etiologies are not yet fully understood, resulting in an absence of curative therapies. It is the case of RA or BC where the majority of current treatments are mainly intended to alleviate symptoms. These two diseases, although quite different in nature (*i.e.* autoimmune and

cancerous), share a great number of similarities, starting with the immunometabolic reprogramming of one of the key actors in their respective pathogenesis: the synovial fibroblasts of the RA joint **[165]** and the fibroblasts of the TME **[379]**. Such metabolic reprogramming is largely associated with the transformation of both types of fibroblasts, initially involved in the structural integrity of tissues or efficient nutrient distribution, in cells of aggressive phenotype with specific behaviors and characteristics. In particular, the cartilage and bone destruction occurring in RA is largely initiated and sustained by RASFs **[332]** while CAFs are greatly involved in cancer initiation, progression, and resistance to therapy **[68]**. It should be noted that CAFs metabolic reprogramming within the TME (*i.e.* their reverse Warburg effect) has long been studied experimentally, whereas observations of metabolic alterations in fibroblasts of the RA joint are relatively recent. Therefore, we undertook in this PhD thesis a joint study of the role of metabolic reprogramming in these two pathologies. Our aim was to capitalize on progress made in one context (*i.e.* cancer) in order to move forward in the other (*i.e.* RA). It enabled us to gain a better understanding of the integrated mechanisms of pathological immunometabolism and identify probable therapeutic targets.

While RASFs and CAFs share many similarities, we were compelled to consider the different pathological characteristics and the distinct micoenvironments that drive their metabolic reprogramming. Moreover, as fibroblasts are complex systems with a variety of biological processes intertwined, an additional focus was given on integrating multiple layers of information that would allow the interconnections between extracellular stimuli, intracellular signaling cascades, transcription factor activity, gene expression regulation and, last but not least, metabolic processes. This is not a trivial task **[381]** and has largely limited the applications of immunometabolism in therapy development due to the absence of an

integrated overview. Numerous factors may be responsible, arising from the need to integrate numerous heterogeneous data to cover multiple biological layers (*e.g.* inherent complexity of interactions and feedback loops between the different biological layers, traditional experimental techniques focusing on individual components or pathways, making it difficult to obtain a holistic overview) or the dynamic nature of biological systems (*e.g*. diverse outcomes depending on the cellular context and environment). Hence, by considering the variety of cellular actors and biological processes involved in RASFs and breast CAFs metabolic reprogramming, along with their interactions, we aimed at leveraging computational approaches. Indeed, we tackled the latter challenges by developing an integrated framework for the study of immunometabolism through advances in high-throughput technologies, computational biology and systems biology approaches. Our main objective was to decipher the intracellular cascades responsible for RASFs and breast CAFs metabolic alterations and their regulation.

Our innovative hybrid modeling framework covers the various biological layers of signaling, gene regulation, and metabolism. It allows us to couple a generic core metabolic network with a cell- and disease-specific regulatory Boolean model automatically inferred from a molecular interaction map in both RASFs and breast CAFs-specific contexts. The coupling is ensured through the translation of Boolean regulatory trap-spaces into metabolic constraints. Thus, we obtain contextualized metabolic networks allowing us to assess the impact of fibroblasts regulatory behavior upon their metabolic flux distribution in disease-specific contexts. It further allows us to capture potential metabolites exchanges within their microenvironment and link them to downstream metabolic pathways. This functional coupling opens new avenues on targeting and modulating the immune system to reverse metabolic reprogramming. Our framework builds on advantages of both data-driven and manually curated construction of molecular interaction maps, regulatory

Boolean models, and metabolic network rather than automatic reconstructions and their associated issues. It is able to combine reliability on the interactions depicted in large-scale static and dynamic networks, along with dealing with a lack of omics data in less addressed biological fields such as RASFs and breast CAFs.

In greater detail, we started by developing state-of-the-art molecular interaction maps for RA and generic CAFs, improving on previously published work, namely the RA-map **[200]** and the CAF-map from the ASCN resource **[204]** as a means to accurately map mechanistic representation of implicated pathways underlying disease pathogenesis. The RA-map V2 and CAF-map V2 are standardized graphical representations, fully committed to implement community-driven FAIR principles **[226]** for findability, accessibility, interoperability and reproducibility. Indeed, both molecular interaction maps were made freely accessible *via* the web browser platform MINERVA **[234]**. Their content is compliant with SBGN PD standards **[189], [227]** for representation, SBML **[229]** for format, MIRIAM for annotations **[233]**, PMIDs and stable identifiers for references and CALM for biocuration **[231]**. All entities are annotated using HGNC symbols **[205]** for signaling and gene regulation components and BiGG IDs **[232]** for metabolic components. The use of standard identifiers for entities present within our molecular interaction maps ensured their compatibility with other tools along with facilitating data integration. Lastly, extensive annotations and easy access to content allow for transparent and facilitated reuse of resources. In addition, the manual construction of the RA-map V2 and CAF-map V2, allows one to have greater confidence in the depicted information rather than automatic network reconstructions, provide detailed curated mechanistic information, and further address a lack of omics data needed for automatic network inference. It is the case for RASFs and breast CAFs, mainly because of sample availability reasons due to the invasiveness of procedures needed to acquire

fibroblasts samples, the heterogeneity of the disease that may limit sample collection, and the research focus where the priority is not placed on fibroblasts. Indeed, in RA, omics-based research has primarily focused on different cell types (*e.g.* macrophages **[382], [383]** or chondrocytes **[384], [385]**). Similarly in cancer, involvement of the TME in pathogenic processes is a field of study based on more recent omics data generation **[58]**, **[61]**. As a result, RASFs and breast CAFs lack public omics data to use. The RA-map V2 and CAF-map V2 represent the first attempt to visualize and simplify complex information to obtain clear insights on detailed metabolic and regulatory interconnections in RA and generic CAFs. They are state-of-the static knowledge bases allowing to summarize current knowledge about molecular biological pathways and entities significant in the associated disease pathogenesis. They further allow visualization of experimental data, possibly highlighting aspects of the affected biological process and identifying differences between various conditions. Their topological analysis also enabled us to study the distribution of the network and identify structural hubs (*e.g.* HIF1, NFKB, TP53 for RA and TGFB, SMAD, HIF1A for generic CAFs) with potentially strong regulatory power.

The static study of the RA-map V2 and CAF-map V2 limiting us in the study of the dynamics of RASFs and breast CAFs, we further automatically inferred executable large-scale Boolean models from these molecular interaction maps. Building large-scale dynamic models can be a daunting and time-consuming task requiring not only the construction of the regulatory network but also the definition of interaction rules. With the CaSQ tool **[243]**, we took advantage of the similarities shared between molecular interaction maps and dynamic logical models. The latter represent great resources to decipher complex biological processes in a qualitative way underlying dynamic properties. They are very adapted to the study of cellular signaling and gene regulation processes carrying signal flow. Both regulatory models were

further contextualized to reproduce cell- and disease-specific RASFs and breast CAFs conditions. It was achieved by combining both data-driven and manual curation approaches to ensure high cellular specificity and confidence in the depicted interactions and initial conditions. The RASF- and breast CAF models are compliant with systems biology standards of SBML-*qual* **[244]** for the format, are fully annotated, and are publicly available in two repositories of biological models, namely Cell Collective **[245]** and BioModels **[246], [247]**. Qualitative biological coherence of the regulatory models behavior was assessed against experimental evidence extracted from the scientific literature at three distinct levels (*i.e.* generic regulatory and metabolic pathways along with global cellular behavior), mainly reproducing experimental observations. One advantage of such models lies in their ability to help identify unknown regulatory cross-talks and direct or indirect effects of specific components or pathways on each other. Overall, generating and parameterizing a logical model from manual network construction along with data analysis and biocuration allows to avoid issues associated with automatic and non-curated methodologies (*e.g.* improper reconstruction of reactions or incorrect compartmentalization leading to incorrect representation). In the field of RA, it is the second attempt to grasp the dynamic of RASFs pathogenic activity but the first attempt to include the key role of metabolism. In the cancer field, our executable Boolean model represents the first attempt to assess CAFs dynamic pathogenic activity, let alone in a cancer-specific manner or by including metabolic processes. Such regulatory models can be analyzed as they are, taking advantage of their construction linked to cellular phenotypes to identify the most important hubs or pathways in each dynamic cellular behavior and answer specific biological questions in a qualitative manner. This study can be envisaged in a modular way to study each cellular phenotype separately, or in a global way to confirm existing knowledge or identify new crosstalks.

The qualitative study of the impact of gene regulatory and cell signaling systems upon metabolic subprocesses not being sufficient to address stoichiometry of biochemical fluxes, we coupled both regulatory models with MitoCore generic reconstruction of central human metabolism **[250]**. The choice of the metabolic model was based on two factors: the reliability of the depicted reactions, manually curated for MitoCore, rather than automatic metabolic reconstruction, and because of our metabolic sub-section of interest, central carbon metabolism rather than whole metabolism. However, in principle the framework is adaptable to any type of constraint-based metabolic model. The proposed framework only extracts additional metabolic constraints to apply on the metabolic network from metabolic components with a proven "inactive" asymptotic behavior under cell- and disease-specific regulatory conditions. It allows the pipeline to automatically handle models with hundreds of components. A main strength of this approach lies in the reliability of both regulatory and metabolic manually curated models rather than data-driven networks. Our approach is inspired by the central doctrine of immunometabolism, namely the tight interconnections between immune regulatory processes and metabolic machinery and the necessity to integrate the dynamic study of these various biological layers to unravel RASFs and CAFs metabolic reprogramming. It further improves on previous attempts to couple Boolean models with metabolism, such as FlexFlux **[222]**. In FlexFlux the discrete qualitative states of the Boolean regulatory network are translated into several user-defined continuous intervals, while in this framework only metabolic reaction fluxes whose regulatory components have maximal trap-spaces values equal to 0 are constrained. This choice is motivated by the difficulty of manually defining initial values and qualitative states to continuous intervals equivalence for every component of large regulatory models. In addition, this framework adopts the asynchronous update as less deterministic than synchronous and the identification of trap-spaces, using value propagation, to provide more comprehensive analysis of the regulatory

model and find states closer to the biological reality. This approach can facilitate the analysis of models with a higher number of inputs. Finally, the need for user-defined transcription factors to target gene relationships, as in the PROM method **[221]** or r-deFBA **[223]**, a daunting task in very large scale regulatory models such as ours, is not required in our framework. This facilitates integrated dynamic analysis of large biological systems such as RASFs and breast CAFs immunometabolic crosstalks and impact in the associated pathogenesis.

After proving the adaptability of our hybrid modeling framework to both RASFs and breast CAFs regulatory contexts, we further packaged it as a python tool named MetaLo for a broader range of applications. This open-source package can be used by a wide variety of users with multidisciplinary backgrounds through the command line or the graphical interface. Moreover, this package is interoperable with other systems biology tools due to the standard format of the molecular interaction maps and both regulatory and metabolic networks. Starting from a standardized molecular interaction map and a constraint-based metabolic reconstruction, MetaLo automatically applies all steps of our hybrid coupling framework (*i.e.* inference of the regulatory Boolean model, initialisation of the latter according to user-defined initial conditions, computation of regulatory trap-spaces as asymptotic regulatory behavior, identification of long-term inactive metabolic components, translation into additional metabolic constraints, optimal metabolic distribution analysis). Overall, MetaLo is intended to help leverage immunometabolic crosstalks in other complex diseases to advance knowledge by elucidating regulatory impacts upon metabolic processes.

Application of our innovative hybrid coupling framework represents the first computational attempt to study immuno-metabolic crosstalks in RASFs. Simulation of the hybrid RASF model revealed a highly glycolytic

metabolism, along with a decreased oxidative metabolism for ATP production and confirmed a hypoxic environment around RASFs. Comparison with the control FBA results clearly demonstrate a metabolic reprogramming of RASFs. These results are consistent with recent experimental studies highlighting a glycolytic switch in RASFs **[165], [173]**. RASFs metabolic alterations are generally attributed only to their stressful microenvironment but may also be considered from the perspective of metabolite exchange between RASFs and other cells of the RA joint. Indeed, FBA results demonstrated several additional altered metabolic pathways in RASFs, including fatty acids, amino acids, and reductive carboxylation. The latter observations have not yet been experimentally studied in RASFs but are similar to the ones made in cells going through a reverse Warburg effect to turn into "metabolic slaves", generating energy-rich fuels and nutrients to feed neighboring cells and help sustain their aggressive activity **[27]**. Thus, our hybrid model is valuable for providing suggestions which can be further experimentally validated, contributing to a better-informed experimental design. Similarly, RASFs reside close to bio-energetically demanding cells (*e.g.* immune cells, endothelial cells, chondrocytes), experience a glycolytic switch and, according to these simulations, secrete high levels of energy-rich fuels and nutrients. Said nutrients are known to be involved in disease-associated behaviors **[386]** and some experimental evidence suggests intracellular metabolic exchanges between RASFs and neighboring cells **[171]**. Thus, based on the latter experimental observations and our *in-silico* simulations, we propose the innovative hypothese according to which a reverse Warburg effect occurs between RASFs and other RA joint cells to influence the inflammatory and destructive processes associated with the pathogenesis of RA. In greater detail, RASFs would undergo a metabolic switch and reprogram their metabolism to (i) adapt and survive within their new hypoxic environment, (ii) maintain their aggressive phenotypes (*e.g.* extensive proliferation and tissue invasion, reduced contact inhibition,

resistance to apoptosis, driver of angiogenesis), and (iii) provide crucial metabolic intermediates to neighboring cells of the rheumatic joint to help sustain their pathogenic activity. Indeed, a shift in glycolysis is a hallmark of inflammatory cells in RA (*e.g.* macrophages, monocytes, B cells, T cells, dendritic cells) **[387]** and RASFs metabolic reprogramming could support such cells anabolic processes by meeting their high energy demand. For instance, by secreting high-levels of energy-rich nutrients (*e.g.* fatty acids, amino acids, lactate), RASFs may benefit immune cells by providing a critical energy source and metabolic intermediates to support their functions of cytokine production and immune response regulation and overall their activation and survival within the inflamed joint. It has been shown that B cells upregulate amino acid transporters and increase the utilization of specific amino acids, such as glutamine and serine **[388]**, probably for nucleotide synthesis and antibody production. The high presence of the latter amino acids in the RA joint could be due to the metabolic reprogramming of RASFs. Macrophages also require energy to perform their functions, including phagocytosis, cytokine production, and antigen presentation **[382]**. Their metabolic state is further recognized to influence their cytokine production profiles **[389]**. Thus, nutrient availability in the RA joint may directly impact the production of pro-inflammatory cytokines by macrophages. RASFs may modulate the cytokine profile of macrophages, potentially influencing the immune response and inflammation in the rheumatic joint. Additionally, adequate nutrient availability can affect cytokine production of T cells **[390]**. Secretion of such nutrients by RASFs may contribute to the modulation of T cell cytokine profiles and their immune-regulatory functions. Finally, endothelial cells forming the lining of blood vessels or osteoclasts in the synovium are critical for angiogenesis and bone resorption activities. The high secretion of energy-rich nutrients by RASFs may promote these cells function by providing them essential nutrients. However, their metabolic needs have not yet been studied.

Simulations of individual and combined knock-outs and knock-ins of the RASF-specific regulatory initial conditions revealed HIF1 as the critical regulator of RASFs metabolic reprogramming. HIF1 is a master transcriptional factor involved in cellular and developmental response to hypoxia. Already identified in RA as a key effector of inflammation, angiogenesis, and cartilage destruction **[323], [391]**, HIF1 appears to be further involved in RASFs metabolic alterations. Its precise mode of action cannot be fully deduced from our *in-silico* simulations, but HIF1 may promote a glycolytic energy production switch by upregulating the expression of glucose transporters (*i.e.* GLUT1 and GLUT3), and/or transcription of enzymes responsible for intracellular glucose breakdown through glycolysis (*e.g.* hexokinase, phosphofructokinase-1, aldolase). In parallel, HIF1 might decrease ATP production through mitochondrial oxidative pathways by transactivating genes responsible for O_2 demand and mitochondrial activity such as pyruvate dehydrogenase kinase 1 or max interactor 1. Considered together, these various properties enable HIF1 to enhance glycolysis rates as a crucial step of metabolic response to hypoxia **[392]**, particularly in the rheumatic joint.

Similarly, simulations of our hybrid breast CAF-specific network constitute, to our knowledge, the first hybrid modeling attempt to address breast CAFs regulatory impact upon their metabolism. Our findings depicted a hypoxic and acidic TME along with a highly glycolytic metabolism and almost null oxidative fluxes for energy production in breast CAFs. Increased production and secretion of energy-rich fuels (*e.g.* pyruvate, lactate, amino acids, fatty acids) along with decreased secretion of oxidative by-products (*e.g.* CO_2, H_2O) were reported, fully reproducing the experimentally observed reverse Warburg effect in CAFs **[393]**. Fibroblasts would undergo metabolic reprogramming and turn into “metabolic servants”, generating high levels of energy-rich fuels through pentose phosphate pathway or amino acids

synthesis. These nutrients would feed cancer cells in macromolecular building blocks and sustain their aggressive phenotype. Such metabolic alterations are suspected to be driven directly by signals from cancer cells, illustrating an extensive crosstalk within the TME.

Systematic individual knock-outs and knock-ins of breast CAF-specific initial conditions simulations identified HIF1 as the regulatory activating stimuli of breast CAFs metabolic reprogramming. HIF1 is known as a master transcriptional factor involved in homeostasis and cellular response to hypoxia. The latter is a major hallmark of solid tumors as they quickly outgrow their blood supply to support their continuous growth and proliferation leaving parts of the tumor with almost null concentration of oxygen. Angiogenesis, metastasis, and drug resistance benefit from this hypoxic state **[394]**. To sustain such aggressive behaviors in this challenging environment, cancer cells need additional fueling. As a result, this chronic hypoxic and acidic environment, generated by cancer cells to maintain their tumorigenic phenotype, was recently suspected to induce breast CAFs reverse Warburg effect and promote BC progression **[394]**. Our findings fully support this hypothesis and further identify HIF1 as a main molecular regulator. In response to cancer cells hypoxic paracrine signals, breast CAFs would activate transcription of glycolytic genes along with glucose transporters, suppress oxygen consumption, by-pass oxidative pathways, and induce a reverse Warburg effect. Thus, we hypothesize that targeting the metabolic reprogramming of fibroblasts through HIF1 pro-glycolytic and anti-oxidative transcriptional activity within a therapeutic strategy including the TME could benefit the treatment of BC.

Metabolic reprogramming of fibroblasts appears to be a crucial element in the pathogenesis of two complex diseases as different as BC and RA. Due to the similarity of the framework applied to contextualize the generic MitoCore

network in both diseases, a comparison of altered metabolic pathways can be performed (**Table S2** and **Table S3**). Out of the seven metabolic enzymes with an asymptotic regulatory behavior equal to 0 and leading to constrain associated metabolic reactions in the MitoCore model in both biological contexts, five are shared (*i.e.* CI_MitoCore, CIII_MitoCore and CIV_MitoCore in OXPHOS, ICDHxm and PDHm for TCA). Additionally, six similar metabolites with asymptotic regulatory behavior equal to 0 lead to constrain additional metabolic reactions in MitoCore in both RASFs and breast CAFs regulatory models (*i.e.* accoa_m, akg_m, cit_m, fum_m, icit_m, mal_L_m for TCA). In order to identify whether such common constraints are sufficient to observe metabolic alterations similar to those of RASFs and breast CAFs, an additional FBA was undertaken on MitoCore. Objective function was set as maximal ATP production and metabolic constraints were extracted from enzymes and metabolites with an asymptotic regulatory behavior equal to 0 in both regulatory models. Results (**Table S4**) depict a reprogrammed metabolism with high glycolytic flux for energy production, along with low oxidative fluxes. High secretion of lactate and energy-rich nutrients (*e.g.* amino acids and fatty acids) is shown. The proportion of total energy production in the form of ATP from glycolysis is calculated at 85.05%. These results, although slightly different at the flux value level, reproduce quite faithfully the metabolic alterations observed in RASFs and breast CAFs. This already leads us to suspect a similar process of metabolic reprogramming in RASFs and breast CAFs. In addition, a thorough analysis of the altered metabolic pathways was undertaken. Overall, metabolic pathways directly related to energy production are altered in the same manner (*i.e.* increased glycolysis, decreased OXPHOS and TCA). Oxidative by-products are accordingly altered in both breast CAFs and RASFs (e.g. increased lactate and secretion, decreased CO_2 and H_2O secretion). The fibroblasts environment, respectively BC TME and RA joint, appears to be similarly modified (*e.g.* decreased O_2 uptake and increased H^+ secretion).

Metabolic pathways not directly involved in ATP production are additionally affected. For instance, disease-specific regulatory conditions similarly reprogram amino acids and fatty acids pathways in RA and BC-associated fibroblasts probably due to their importance in the biosynthesis of macromolecules for cells of aggressive phenotype. Indeed, secretion of building blocks is additionally increased in both situations. Certain pathways are similarly altered but raise the question of their interest under different environmental conditions. For instance, reductive carboxylation is similarly increased in breast CAFs and RASFs. Acting as a novel glutamine pathway, it supports the growth of cells depicting mitochondrial deficiencies. Warburg originally hypothesized that cancer-like cells presented a mitochondrial defect **[395]** but later work refuted it **[25]**. Such studies have not yet been conducted in both types of fibroblasts. Further experimental investigations are needed to decipher their mitochondrial status and identify a potential benefit from reductive carboxylation reactions. Altogether, mitochondrial and cytosolic transporters and shuttle pathways are affected, not necessarily in the same way, but all due to the reprogramming of upstream metabolic pathways producing their metabolite of interest. Finally, butanoate metabolism is not affected similarly in breast CAFs and RASFs. However, it is typically involved in processes associated with intestinal fermentation, its alterations do not seem to be significant in a cancerous or autoimmune context.

Beyond the many shared altered metabolic pathways, the key molecular regulator was also identified as HIF1 in both RASFs and breast CAFs reverse Warburg effect. Already recognized in RA as a driver of inflammation, angiogenesis, and cartilage destruction **[323]**, targeting HIF1 has not yet been proposed within a therapeutic strategy aiming at the resolution of metabolic reprogramming in fibroblasts. In BC, therapeutic opportunities targeting HIF1 appeared until very recently to be limited to its metastatic or driver of tumor-proliferation activities. Growing interest in metabolic targeting to

address pro-tumor characteristics resulted in a few insights such as Honokiol as an inhibitor of HIF1-mediated glycolysis to halt BC cells growth **[396]**. However, its interest in breast CAFs has not yet been investigated. Finally, studies in other types of human fibroblasts have recognized a key role for HIF1 (*e.g.* in anti-aging and regeneration in dermal fibroblasts **[397]**, attenuating fibrosis and delaying vascular remodeling in systemic sclerosis-associated fibroblasts **[398])** but its targeting in the resolution of fibroblasts metabolic reprogramming has not yet been studied.

According to our findings and given the shared metabolic alterations, probable benefits for surrounding cells of the pathogenic microenvironment, and regulatory molecular driver, we assume the existence of a common mechanism directing the phenotypic transformation of fibroblasts through a HIF1-driven metabolic reprogramming in BC and RA. In both situations, regulation of reverse Warburg effect, already recognized for breast CAFs and suggested here for RASFs, enables them to (i) adapt and survive within a new hypoxic and acidic environment, (ii) maintain their aggressive phenotype, and (iii) actively participate in the amplification of the associated diseases debilitating symptoms by establishing metabolic crosstalks with neighboring cells of the rheumatic joint or the breast TME.

6 PERSPECTIVES

Our modeling framework, further packaged in the open-source MetaLo Python package captures the complexity of signaling and gene regulation processes upon RASFs and breast CAFs metabolism. However, for the moment, it provides a one-way view of biological events. According to the central doctrine of immunometabolism, there is a bidirectional crosstalk between regulatory and metabolic processes. Thus, considering the update of the regulatory network from metabolic analysis outputs may provide an even more comprehensive understanding of events associated with both reverse Warburg effect in RASFs and breast CAFs and cover an additional layer of integrated dynamic study.

Identification of regulatory molecular drivers for RASFs and breast CAFs metabolic reprogramming relies heavily on the setting of regulatory initial conditions. It is worth mentioning that finding meaningful initial conditions for key molecules, and especially for models inputs, constitutes a real challenge that becomes more evident when working with less-studied diseases or entities. Additionally, although we covered a variety of regulatory input combinations and while inputs are suspected to exert the most significant role upon our networks, we did not systematically assess the impact of internal components. An extensive, if not exhaustive (for computational reasons), analysis of the combinations involving internal components could shed light on the precise mechanism of action of HIF1 in both biological contexts.

From the previous point stems an additional perspective on this work. Identification of regulatory molecular drivers was not only restricted to regulatory inputs in the breast CAF hybrid model because they are suspected to exert the most significant role upon our networks but also because it is very

computationally expensive to test the effect of inputs and internal nodes systematically. Indeed, from a purely computational point of view and as demonstrated in the computation of all input combinations for the breast CAF model, the trap-space search step of our framework is a very time-consuming step. After successfully replacing the package handling this step, namely BioLQM **[250],** by Trappist **[259]** in the packaging of MetaLo, it might be worthwhile adapting this step in the framework too. This would probably allow us to obtain expanded results for RASFs combined knock-outs and knock-ins simulations and to obtain results for breast CAFs. Thus, we could broaden the range of combinations tested and maybe further include additional ones.

Finally, the various results and hypotheses proposed in this thesis being based solely on computational simulations, they obviously deserve thorough experimental validation. This work can serve as a solid basis for *in-vitro* validation suggestions, facilitating contacts with experimental partners.

7 CONCLUSION

Deciphering the interplay between regulatory immune processes and metabolism provides great insights to unravel the key metabolic reprogramming of rheumatoid arthritis synovial fibroblasts (RASFs) and breast cancer-associated fibroblasts (CAFs). In this context, hybrid computational approaches are highly relevant and contribute to the development of innovative strategies considering multiple layers of intertwined biological processes and entities. In this PhD thesis, I present the construction of the two first large-scale hybrid models for RASFs and breast CAFs covering major pathogenic signaling, gene regulation, and metabolic processes. Both hybrid models combine throroughly validated asynchronous cell- and disease-specific regulatory Boolean models, which are automatically inferred from up-to-date molecular interaction maps, with a generic reconstruction of human central metabolism. Generation of these hybrid models was carried out through our innovative modeling framework, further successfully packaged in the MetaLo Python package, and the translation of regulatory asymptotic behavior impact upon metabolic subprocesses. In this regard, we leveraged both data-driven and manual curation approaches to ensure high cellular specificity and confidence in the depicted interactions and metabolic network contextualization. MetaLo can be applied to other biological mechanisms, starting with standardized molecular interaction maps and generic metabolic networks, as long as there is a biological interface linking them. Our *in-silico* simulations reproduced the experimentally observed glycolytic switch in RASFs and reverse Warburg effect in breast CAFs. They further enabled us to suggest three innovative hypotheses according to which (i) a reverse Warburg effect occurs between RASFs and neighboring cells of the RA joint, (ii) RASFs and breast CAFs undergo a similar metabolic reprogramming, and (iii) its primary regulatory

driver is HIF1. In greater details, we suggest that, following paracrine hypoxic signals emitted in the RA joint and the breast TME, RASFs and breast CAFs, would reprogram their energy production pathways to (i) adapt and survive within their pathogenic environment, (ii) maintain their aggressive phenotype, and (iii) produce high-levels of energy-rich fuels and nutrients for surrounding cells. We propose HIF1 as a potential therapeutic target to be validated experimentally and as a promising avenue for RA and breast cancer treatment by targeting RASFs and breast CAFs reverse Warburg effect.

APPENDICES

Supplementary figure 1. Jupyter notebook describing the application of the complete framework to obtain the hybrid RASF model.

Hybrid_Modeling_Framework.ipynb 1.03 MiB

In [1]:

```
import ginsim
import biolqm
from colomoto_jupyter import tabulate
import pandas as pd
import numpy as np
import seaborn as sns
from matplotlib import pyplot as plt

try:
    import cobra
except ImportError:
    import sys
    !{sys.executable} -m pip install cobra
    import cobra

cmp = sns.diverging_palette(0, 255, as_cmap=True)
```

Out [1]: This notebook has been executed using the docker image `colomoto/colomoto-docker:2021-10-01`

1. Loading the two models of interest

- The CaSQ-generated RASF-specific boolean model;
- MitoCore constraint-based model of human metabolism.

1. 1. Load the RASF-model

In [2]:

```
RASF_model = biolqm.load("RASF-model.sbml")
```

The sanitize function is used to generate human-friendly node IDs and rescale the layout to improve the model's readability.

Note: this cell may take a few minutes to run.

In [3]:

```
RASF_model = biolqm.sanitize(RASF_model)

layout = RASF_model.getLayout()
layout.scale(0.4)

lrg = biolqm.to_ginsim(RASF_model)

ginsim.show(lrg, save="RASF-model.svg")
```

Out [3]: Saved as RASF-model.svg

1.2. Load MitoCore

In [4]:
```
import logging
cobra.io.sbml.LOGGER.setLevel(logging.ERROR)

MitoCore = cobra.io.read_sbml_model('mitocore_v1.01.xml')
```

2. Value propagation

We show that the **input conditions** (here, based on literature) strongly control the whole network.

In [5]:
```
inits = pd.read_csv("RASF-specific_input_conditions.tsv", sep="\t", index_col=0)
dic_inits = inits.to_dict()

inits
```

Out [5]:

Type to search

	C1
FASLG	1
FGF1	1
HIF1	1
IKBANFKB1RELA_complex	1
IL17A_Extracellular_space_Space	1
IL18	1
IL6_Extracellular_space_Space	1
M_atp_c_simple_molecule	1
M_glc_D_e_simple_molecule	1
MIR192_rna	0
PDGFA	1
RANKL	1
SFRP5	0
TGFB1	1
TNF_Extracellular_space_Space	1
WNT5A	1

Definition of some helper functions and color mapping rules to perform value propagation and visualize the result.

In [6]:
```
# Transforms a dictionary into a dash-like pattern used for space restrictions.
# If a model has 4 components A, B, C, D in this order,
#  {A:0, D:1} => "0--1"

def dash_pattern(model, dict_vals):
```

```
    specific_comps = dict_vals.keys()
    str_pattern = ""
    for comp in model.getComponents():
        if comp.toString() in specific_comps:
            str_pattern += str(dict_vals.get(comp.toString()))
        else :
            str_pattern += "-"
    return(str_pattern)

def restrict_model(model, **dict_vals):
    pattern = dash_pattern(model, dict_vals)
    return biolqm.restrict(model, pattern)

def fill_fixed(data, names, functions, mddman):
    all_values = [f for f in functions]
    for comp, func in zip(names, functions):
        if mddman.isleaf(func): data[comp] = func
        else: data[comp] = -1


def get_fixed_pattern(all_names, model, as_dict=False):
    # Build a container for the results
    pattern = {key: 100 for key in all_names}

    # Model manager and core components
    mddman = model.getMDDManager()
    core_components = [node.getNodeID() for node in model.getComponents()]
    extra_components = [node.getNodeID() for node in model.getExtraComponents()]

    # 1/ Non-extra values: if the model was not reduced, core components may also contain fixed values
    fill_fixed(pattern, core_components, model.getLogicalFunctions(), mddman)

    # Special value for input components
    for node in model.getComponents():
        if node.isInput():
            pattern[node.getNodeID()] = -2


    # 2/ Extra values : only available after reduction/percolation
    # Functions of each component
    fill_fixed(pattern, extra_components, model.getExtraLogicalFunctions(), mddman)

    if as_dict: return pattern
    return pd.Series(pattern, dtype=np.byte)

def get_fixed(gs_model, restricted_model, as_dict=False):
    name_components = [ n.getId() for n in gs_model.getNodeOrder() ]
    return get_fixed_pattern(name_components, restricted_model, as_dict)

def show_fixed(gs_model, styler, fixed_pattern, save=None):
    styler.setState(fixed_pattern.values.tobytes())
    return ginsim.show(gs_model, style=styler, save=save)


# Define color mapping rules
styler_fixed = ginsim.lrg_style(lrg)
styler_fixed.mapState2Color(0, 255, 255, 255)
styler_fixed.mapState2Color(1, 100, 100, 255)
styler_fixed.mapState2Color(-1, 255, 100, 100)
```

In [7]:

```
data = []

for init_name, values in dic_inits.items():
    lqm_model_restricted = restrict_model(RASF_model, **values)
    data.append( get_fixed(lrg, lqm_model_restricted) )

df = pd.concat(data, axis=1, keys=[name for name in dic_inits])
```

The result of value propagation can be visualized in the following heatmap where each line represents a component of the system and the column represent the input condition.

- A **white cell** denotes that the corresponding component is **fixed at 0** by value propagation in this input condition;
- A **blue cell** denotes that the corresponding component is **fixed at 1** by value propagation in this input condition;
- A **red cells** denote components **which are not fixed** by value propagation in this input condition.

In [8]:
```
plt.figure(figsize=(8,80))

sns.heatmap(df, center=0, cmap=cmp, cbar=False)
```

Out [8]:
```
<AxesSubplot:>
```

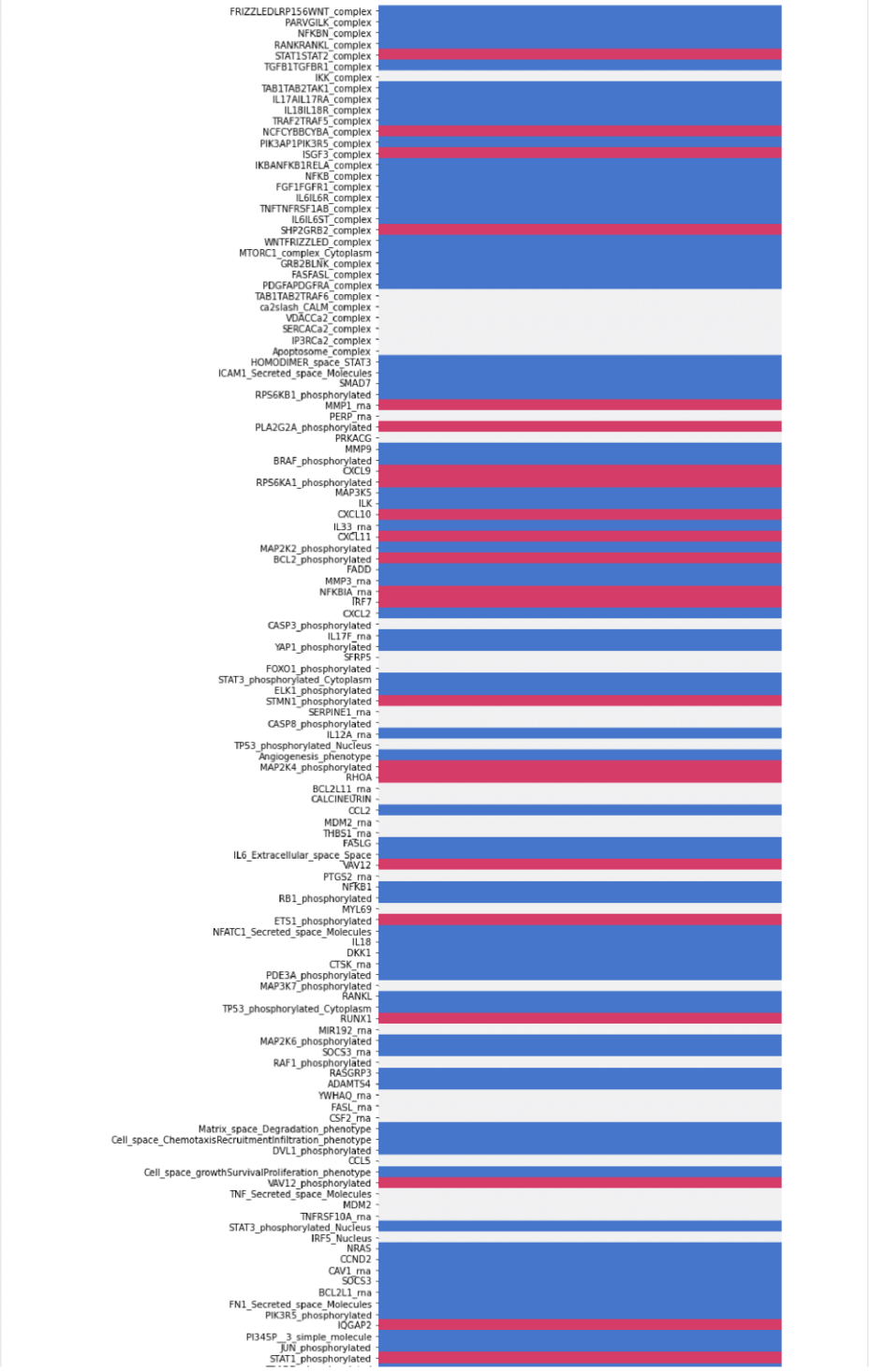
FRIZZLEDLRP156WNT_complex
PARVGILK_complex
NFKBN_complex
RANKRANKL_complex
STAT1STAT2_complex
TGFB1TGFBR1_complex
IKK_complex
TAB1TAB2TAK1_complex
IL17AIL17RA_complex
IL18IL18R_complex
TRAF2TRAF5_complex
NCFCYBBCYBA_complex
PIK3AP1PIK3R5_complex
ISGF3_complex
IKBANFKB1RELA_complex
NFKB_complex
FGF1FGFR1_complex
IL6IL6R_complex
TNFTNFRSF1AB_complex
IL6IL6ST_complex
SHP2GRB2_complex
WNTFRIZZLED_complex
MTORC1_complex_Cytoplasm
GRB2BLNK_complex
FASFASL_complex
PDGFAPDGFRA_complex
TAB1TAB2TRAF6_complex
ca2slash_CALM_complex
VDACCa2_complex
SERCACa2_complex
IP3RCa2_complex
Apoptosome_complex
HOMODIMER_space_STAT3
ICAM1_Secreted_space_Molecules
SMAD7
RPS6KB1_phosphorylated
MMP1_rna
PERP_rna
PLA2G2A_phosphorylated
PRKACG
MMP9
BRAF_phosphorylated
CXCL9
RPS6KA1_phosphorylated
MAP3K5
ILK
CXCL10
IL33_rna
CXCL11
MAP2K2_phosphorylated
BCL2_phosphorylated
FADD
MMP3_rna
NFKBIA_rna
IRF7
CXCL2
CASP3_phosphorylated
IL17F_rna
YAP1_phosphorylated
SFRP5
FOXO1_phosphorylated
STAT3_phosphorylated_Cytoplasm
ELK1_phosphorylated
STMN1_phosphorylated
SERPINE1_rna
CASP8_phosphorylated
IL12A_rna
TP53_phosphorylated_Nucleus
Angiogenesis_phenotype
MAP2K4_phosphorylated
RHOA
BCL2L11_rna
CALCINEURIN
CCL2
MDM2_rna
THBS1_rna
FASLG
IL6_Extracellular_space_Space
VAV12
PTGS2_rna
NFKB1
RB1_phosphorylated
MYL69
ETS1_phosphorylated
NFATC1_Secreted_space_Molecules
IL18
DKK1
CTSK_rna
PDE3A_phosphorylated
MAP3K7_phosphorylated
RANKL
TP53_phosphorylated_Cytoplasm
RUNX1
MIR192_rna
MAP2K6_phosphorylated
SOCS3_rna
RAF1_phosphorylated
RASGRP3
ADAMTS4
YWHAQ_rna
FASL_rna
CSF2_rna
Matrix_space_Degradation_phenotype
Cell_space_ChemotaxisRecruitmentInfiltration_phenotype
DVL1_phosphorylated
CCL5
Cell_space_growthSurvivalProliferation_phenotype
VAV12_phosphorylated
TNF_Secreted_space_Molecules
MDM2
TNFRSF10A_rna
STAT3_phosphorylated_Nucleus
IRF5_Nucleus
NRAS
CCND2
CAV1_rna
SOCS3
BCL2L1_rna
FN1_Secreted_space_Molecules
PIK3R5_phosphorylated
IQGAP2
PI345P__3_simple_molecule
JUN_phosphorylated
STAT1_phosphorylated

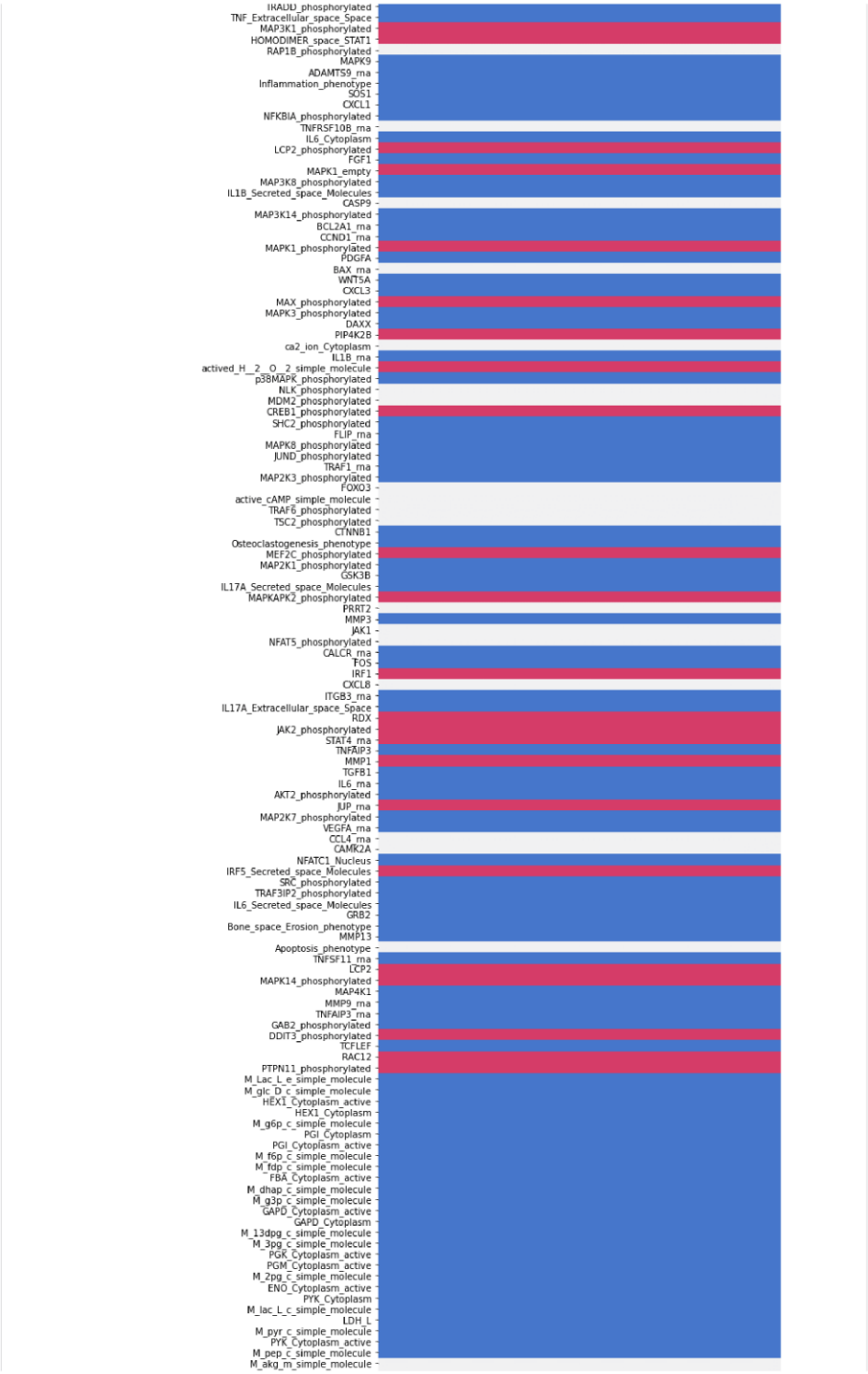
IKAUU_phosphorylated
TNF_Extracellular_space_Space
MAP3K1_phosphorylated
HOMODIMER_space_STAT1
RAP1B_phosphorylated
MAPK9
ADAMTS9_rna
Inflammation_phenotype
SOS1
CXCL1
NFKBIA_phosphorylated
TNFRSF10B_rna
IL6_Cytoplasm
LCP2_phosphorylated
FGF1
MAPK1_empty
MAP3K8_phosphorylated
IL1B_Secreted_space_Molecules
CASP9
MAP3K14_phosphorylated
BCL2A1_rna
CCND1_rna
MAPK1_phosphorylated
PDGFA
BAX_rna
WNT5A
CXCL3
MAX_phosphorylated
MAPK3_phosphorylated
DAXX
PIP4K2B
ca2_ion_Cytoplasm
IL1B_rna
actived_H__2__O__2_simple_molecule
p38MAPK_phosphorylated
NLK_phosphorylated
MDM2_phosphorylated
CREB1_phosphorylated
SHC2_phosphorylated
FLIP_rna
MAPK8_phosphorylated
JUND_phosphorylated
TRAF1_rna
MAP2K3_phosphorylated
FOXO3
active_cAMP_simple_molecule
TRAF6_phosphorylated
TSC2_phosphorylated
CTNNB1
Osteoclastogenesis_phenotype
MEF2C_phosphorylated
MAP2K1_phosphorylated
GSK3B
IL17A_Secreted_space_Molecules
MAPKAPK2_phosphorylated
PRRT2
MMP3
JAK1
NFAT5_phosphorylated
CALCR_rna
FOS
IRF1
CXCL8
ITGB3_rna
IL17A_Extracellular_space_Space
RDX
JAK2_phosphorylated
STAT4_rna
TNFAIP3
MMP1
TGFB1
IL6_rna
AKT2_phosphorylated
JUP_rna
MAP2K7_phosphorylated
VEGFA_rna
CCL4_rna
CAMK2A
NFATC1_Nucleus
IRF5_Secreted_space_Molecules
SRC_phosphorylated
TRAF3IP2_phosphorylated
IL6_Secreted_space_Molecules
GRB2
Bone_space_Erosion_phenotype
MMP13
Apoptosis_phenotype
TNFSF11_rna
LCP2
MAPK14_phosphorylated
MAP4K1
MMP9_rna
TNFAIP3_rna
GAB2_phosphorylated
DDIT3_phosphorylated
TCFLEF
RAC1.2
PTPN11_phosphorylated
M_Lac_L_e_simple_molecule
M_glc_D_c_simple_molecule
HEX1_Cytoplasm_active
HEX1_Cytoplasm
M_g6p_c_simple_molecule
PGI_Cytoplasm
PGI_Cytoplasm_active
M_f6p_c_simple_molecule
M_fdp_c_simple_molecule
FBA_Cytoplasm_active
M_dhap_c_simple_molecule
M_g3p_c_simple_molecule
GAPD_Cytoplasm_active
GAPD_Cytoplasm
M_13dpg_c_simple_molecule
M_3pg_c_simple_molecule
PGK_Cytoplasm_active
PGM_Cytoplasm_active
M_2pg_c_simple_molecule
ENO_Cytoplasm_active
PYK_Cytoplasm
M_lac_L_c_simple_molecule
LDH_L
M_pyr_c_simple_molecule
PYK_Cytoplasm_active
M_pep_c_simple_molecule
M_akg_m_simple_molecule

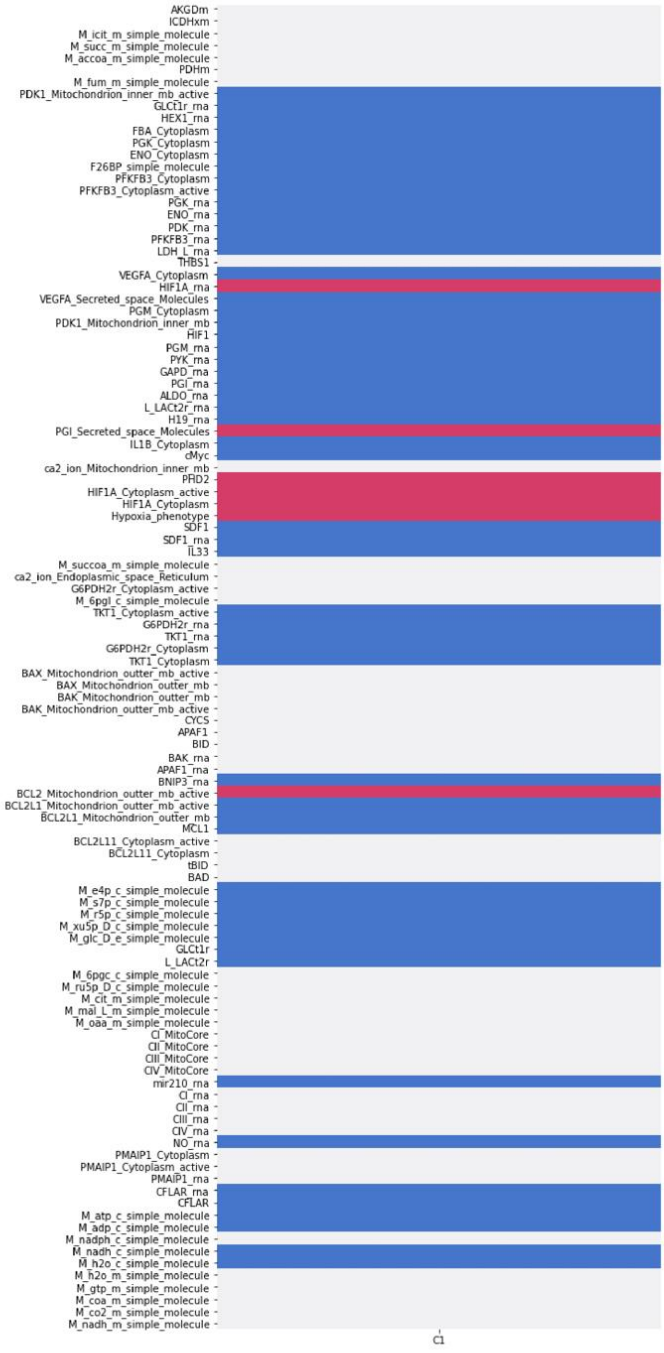

Propagated inputs for a specific input condition can also be mapped on the regulatory graph using the same color code.

In [9]:

```
fixed = data[0]

show_fixed(lrg, styler_fixed, fixed, save="RASF-model_value_propagation.svg")
```

Out [9]: Saved as RASF-model_value_propagation.svg

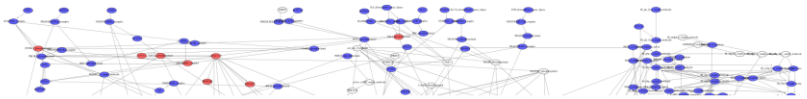

3. Identification of RASF-model's trap-spaces

3.1. Using the output of value propagation as a new set of initial conditions

The biolqm.perturbation function enables the construction of a variant of the model, where the logical function of one or several components has been modified. A textual parameter describes the modification:

```
component%0 defines a knockout of a component
component%1 defines an ectopic expression
```

To perturbate the model, the output dataframe of value propagation is transformed as a list of perturbations in the form **'component1%value component2%value ... componentN%value'**.

In [10]:
```
df = df[df.C1 >= 0]
df["modifs"]= df.index.map(str) + "%" + df["C1"].map(str)
modifications = pd.DataFrame(df["modifs"]).copy()
modifications = modifications.reset_index(drop=True)
pert = modifications["modifs"].tolist()
perturbations = " ".join(pert)
```

In [11]:
```
RASF_model_perturbated = biolqm.perturbation(RASF_model, perturbations)
```

3.2. Identification of RASF-model's regulatory trap-spaces

A trap-space, also called stable motif or called symbolic steady state, is a partially assigned state such that all possible successors of all states which belong to the motif also belong to the motif. Like stable states, these stable motifs can be identified efficiently using constraint-solving methods.

In [12]:
```
trapspaces = biolqm.trapspace(RASF_model_perturbated)
trapspaces_df = pd.DataFrame(trapspaces)

trapspaces_df.columns = (trapspaces_df.columns.str.replace("_complex", "")
                         .str.replace('_Secreted_space_Molecules','')
                         .str.replace('_phosphorylated','')
                         .str.replace("_Cytoplasm","")
                         .str.replace('_simple_molecule', '')
                         .str.replace('_active', '')
                         .str.replace('M_', '')
                         .str.replace('_rna','')
                         .str.replace('_Nucleus','')
                         .str.replace('_empty','')
                         .str.replace('_Extracellular_space_Space','')
                         .str.replace('_Secreted_space_Molecules', '')
                         .str.replace('_space','')
                         .str.replace('_Mitochondrion_outter_mb','')
                         .str.replace('_Mitochondrion_inner_mb',''))

trapspaces_df
```

Out [12]: Type to search

	FRIZZLEDLRP156WNT	PARVGILK	NFKBN	RANKRANKL	STAT1STAT2	TGFB1TGFBR1	I
0	1	1	1	1	1	1	(
1	1	1	1	1	1	1	(
2	1	1	1	1	1	1	(
3	1	1	1	1	1	1	(
4	1	1	1	1	1	1	(
5	1	1	1	1	1	1	(
6	1	1	1	1	1	1	(
7	1	1	1	1	1	1	(

4. Projection of regulatory trap-spaces on metabolic compounds

4.1. Extraction of metabolic compounds

To extract common enzymes and metabolites between MitoCore and the RASF-model we generate:

- The list of enzymes in MitoCore;
- The list of metabolites in MitoCore;
- The list of compounds (both enzymes and metabolites) in the RASF-model.

These list are used to compare both models and automatically extract common components (with their class: "metabolic enzyme" or "metabolite"). We exclude common metabolic intermediates.

In [13]:
```
RASF_model_components = trapspaces_df.columns.values

MitoCore_Enzymes = [r.id for r in MitoCore.reactions]

MitoCore_Metabolites = [m.id for m in MitoCore.metabolites]
```

4.1.1. Extracting common metabolic enzymes

In [14]:
```
common_enzymes = list((set(RASF_model_components).intersection(MitoCore_Enzymes)))
```

4.1.2. Extracting common metabolites

We limit the metabolite matching by excluding a list of predefined compounds which are considered by MitoCore as metabolites but are common metabolic intermediates.

In [15]:
```
intermediates = ["atp_c", "adp_c", "adn_c", "adp_m", "amp_c", "amp_m", "atp_m", "cdp_m", "cmp_c", "co_c", "co_
e",
                 "co2_c", "co2_e", "co2_m", "coa_c", "coa_m", "ctp_c", "fe2_c", "fe2_e", "fe2_m", "ficytC_c",
                 "ficytC_e", "ficytC_m", "gdp_c", "gdp_m", "gtp_c", "gtp_m", "h_c", "h_e", "h_m", "h2o_c", "h2o
_m",
                 "h2o2_c"," h2o2_m", "hco3_c", "hco3_e", "hco3_m", "nad_c", "nad_e", "nad_m", "nadh_c", "nadh_
e",
                 "nadh_m", "nadp_c", "nadp_m", "nadph_c", "nadph_m", "no_c", "no_e", "o2_c", "o2_e", "o2_m", "o
2s_m",
                 "pheme_c", "pheme_m", "pi_c", "pi_e", "pi_m", "q10_m", "q10h2_m"]
```

In [16]:
```
common_metabolites = list(set(RASF_model_components).intersection(MitoCore_Metabolites)-set(intermediates))
```

4.2. Projecting metabolic components' regulatory trap-spaces

4.2.1. Projecting metabolic enzymes' regulatory trap-spaces

In [17]:
```
trapspaces_metabolic_enzymes = trapspaces_df[common_enzymes]
```

4.2.2. Projecting metabolites' regulatory trap-spaces

In [18]:
```
trapspaces_metabolites = trapspaces_df[common_metabolites]
```

5. Flux Balance Analysis (FBA)

Definition of an **ATP_total** objective function representing maximum cellular ATP production through glycolysis and oxidative phosphorylation:

In [19]:
```
MitoCore.objective = ["PYK", "PGK", "CV_MitoCore"]
```

5.1. FBA n°1: Control

In [20]:
```
ATP_total_CTL = MitoCore.optimize().objective_value
```

In [21]:
```
MitoCore.summary()
```

Out [21]:

Type to search

Metabolite	Reaction	Flux	C-Number	C-Flux
acac_e	EX_acac_e	0.114	4	2.49%
ala_L_e	EX_ala_L_e	0.01	3	0.16%
arg_L_e	EX_arg_L_e	0.007	6	0.23%
asn_L_e	EX_asn_L_e	0.01	4	0.22%
asp_L_e	EX_asp_L_e	0.154	4	3.36%
bhb_e	EX_bhb_e	0.048	4	1.05%
but_e	EX_but_e	0.006	4	0.13%
cyan_e	EX_cyan_e	0.001	1	0.01%
cys_L_e	EX_cys_L_e	0.001	3	0.02%
glc_D_e	EX_glc_D_e	0.9	6	29.48%
gly_e	EX_gly_e	0.009	2	0.10%
glyc_e	EX_glyc_e	0.01	3	0.16%
h_e	EX_h_e	3.458	0	0.00%
hco3_e	EX_hco3_e	1.71	1	9.34%
hdca_e	EX_hdca_e	0.4684	16	40.92%
his_L_e	EX_his_L_e	0.01	6	0.33%
ile_L_e	EX_ile_L_e	0.004	6	0.13%
lac_L_e	EX_lac_L_e	0.575	3	9.42%

Metabolite	Reaction	Flux	C-Number	C-Flux
leu_L_e	EX_leu_L_e	0.016	6	0.52%
lys_L_e	EX_lys_L_e	0.03	6	0.98%
o2_e	EX_o2_e	19.8	0	0.00%
pro_L_e	EX_pro_L_e	0.004	5	0.11%
ser_L_e	EX_ser_L_e	0.017	3	0.28%
thr_L_e	EX_thr_L_e	0.012	4	0.26%
val_L_e	EX_val_L_e	0.011	5	0.30%
co2_e	EX_co2_e	-18.31	1	99.96%
h2o_e	EX_h2o_e	-16.7	0	0.00%
nh4_e	EX_nh4_e	-0.362	0	0.00%
tcynt_e	EX_tcynt_e	-0.001	1	0.01%
urea_e	EX_urea_e	-0.007	1	0.04%

In [22]:
```
solution = MitoCore.optimize()

ATP_glycolysis_CTL = (solution.fluxes['PYK'] + solution.fluxes['PGK'])/(solution.objective_value)

print("The proportion of global ATP production through glycolysis in control conditions is", round(ATP_glycolys
is_CTL, 4), ".")
```

Out [22]:
```
The proportion of global ATP production through glycolysis in control conditions is 0.0405 .
```

5.2. FBA n°2: RASF-specific

5.2.1. Constraining metabolic fluxes with regulatory trap-spaces

5.2.1.1. Constraining metabolic fluxes with maximum metabolic enzymes' regulatory trap-spaces equal to 0

In [23]:
```
trapspaces_metabolic_enzymes_zero = trapspaces_metabolic_enzymes.loc[:,(trapspaces_metabolic_enzymes.max(axis=
0)) == 0]
enzymes_to_zero = trapspaces_metabolic_enzymes_zero.columns.values.tolist()

enzymes_to_zero
```

Out [23]:
```
['PDHm',
 'CI_MitoCore',
 'CIV_MitoCore',
 'ICDHxm',
 'CII_MitoCore',
 'G6PDH2r',
 'CIII_MitoCore',
 'AKGDm']
```

Setting the constraints:

In [24]:
```
for i in enzymes_to_zero:
    MitoCore.reactions.get_by_id(i).lower_bound = 0
    MitoCore.reactions.get_by_id(i).upper_bound = 0
```

5.2.1.2. Constraining metabolic fluxes with maximal metabolites' regulatory trap-spaces eual to 0

In [25]:
```
trapspaces_metabolites_zero = trapspaces_metabolites.loc[:,(trapspaces_metabolites.max(axis=0)) == 0]
metabolites_to_zero = trapspaces_metabolites_zero.columns.values.tolist()

metabolites_to_zero
```

Out [25]:
```
['succoa_m',
 'fum_m',
 '6pgl_c',
 'succ_m',
 'accoa_m',
 'cit_m',
 'icit_m',
 'ru5p_D_c',
 'mal_L_m',
 '6pgc_c',
 'akg_m',
 'oaa_m']
```

In [26]:
```
producing_reactions_metabolite_to_zero  = []

for i in metabolites_to_zero:
    producing_reactions_metabolite_to_zero1 = MitoCore.metabolites.get_by_id(i).summary().producing_flux.index.
values.tolist()
    producing_reactions_metabolite_to_zero  = producing_reactions_metabolite_to_zero + producing_reactions_meta
bolite_to_zero1
```

Setting the constraints:

In [27]:
```
for i in producing_reactions_metabolite_to_zero:
    MitoCore.reactions.get_by_id(i).lower_bound = 0
    MitoCore.reactions.get_by_id(i).upper_bound = 0
```

5.2. FBA

In [28]:
```
ATP_total_RASF = MitoCore.optimize().objective_value
```

In [29]:
```
MitoCore.summary()
```

Out [29]:

Type to search

Metabolite	Reaction	Flux	C-Number	C-Flux
asn_L_e	EX_asn_L_e	0.01	4	0.65%
asp_L_e	EX_asp_L_e	0.154	4	10.01%
glc_D_e	EX_glc_D_e	0.9	6	87.72%
gly_e	EX_gly_e	0.005	2	0.16%
glyc_e	EX_glyc_e	0.01	3	0.49%
h2o_e	EX_h2o_e	0.055	0	0.00%
his_L_e	EX_his_L_e	0.01	6	0.97%
ac_e	EX_ac_e	-0.01	2	0.32%
ala_L_e	EX_ala_L_e	-0.164	3	7.99%
co2_e	EX_co2_e	-0.169	1	2.75%
h_e	EX_h_e	-1.636	0	0.00%

Metabolite	Reaction	Flux	C-Number	C-Flux
lac_L_e	EX_lac_L_e	-1.82	3	88.69%
nh4_e	EX_nh4_e	-0.04	0	0.00%
ser_L_e	EX_ser_L_e	-0.005	3	0.24%

In [30]:

```
solution = MitoCore.optimize()

ATP_glycolysis_RASF = (solution.fluxes['PYK'] + solution.fluxes['PGK'])/(solution.objective_value)

print("The proportion of global ATP production through glycolysis in RASF-specific conditions is", round(ATP_gl
ycolysis_RASF, 4), ".")
```

Out [30]:

```
The proportion of global ATP production through glycolysis in RASF-specific conditions is 0.8505 .
```

Supplementary table 1. Complete metabolic flux distribution in control conditions with maximal ATP production as objective function.

Reaction	Flux
EX_2hb_e	0,000
EX_ac_e	0,000
EX_acac_e	-0,114
EX_akg_e	0,000
EX_ala_B_e	0,000
EX_ala_L_e	-0,010
EX_arg_L_e	-0,007
EX_argsuc_e	0,000
EX_asn_L_e	-0,010
EX_asp_L_e	-0,154
EX_bhb_e	-0,048
EX_bilirub_e	0,000
EX_biomass_e	0,000
EX_but_e	-0,006
EX_chol_e	0,000
EX_cit_e	0,000
EX_citr_L_e	0,000
EX_co_e	0,000
EX_co2_e	18,307
EX_creat_e	0,000
EX_cyan_e	-0,001
EX_cys_L_e	-0,001
EX_etoh_e	0,000
EX_fe2_e	0,000
EX_for_e	0,000
EX_fum_e	0,000
EX_glc_D_e	-0,900
EX_gln_L_e	0,000
EX_glu_L_e	0,000
EX_gly_e	-0,009
EX_glyc_e	-0,010
EX_h_e	-3,458
EX_h2o_e	16,700
EX_HC00250_e	0,000
EX_hco3_e	-1,710
EX_hdca_e	-0,468
EX_his_L_e	-0,010
EX_icit_e	0,000
EX_ile_L_e	-0,004
EX_lac_L_e	-0,575
EX_leu_L_e	-0,016
EX_lys_L_e	-0,030
EX_mal_L_e	0,000
EX_mercplac_e	0,000
EX_met_L_e	0,000
EX_nad_e	0,000
EX_nadh_e	0,000
EX_nh4_e	0,362
EX_no_e	0,000
EX_o2_e	-19,800
EX_oaa_e	0,000
EX_pchol_hs_e	0,000
EX_pcreat_e	0,000
EX_pe_hs_e	0,000
EX_phe_L_e	0,000
EX_pi_e	0,000
EX_ppa_e	0,000
EX_pro_L_e	-0,004
EX_ps_hs_e	0,000
EX_ser_L_e	-0,017
EX_so3_e	0,000
EX_succ_e	0,000
EX_tcynt_e	0,001
EX_thr_L_e	-0,012
EX_trp_L_e	0,000
EX_tsul_e	0,000
EX_tyr_L_e	0,000
EX_urea_e	0,007
EX_val_L_e	-0,011
EX_fol_e	0,000
OF_ATP_MitoCore	0,000
OF_HEME_MitoCore	0,000
OF_LIPID_MitoCore	0,000
OF_PROTEIN_Mito-Core	0,000
HEX1	0,900

G6PPer	0,000	ACITLm_MitoCore	0,000
PGI	0,900	NDPK1m	-6,388
PFK	0,900	NNT_MitoCore	0,000
FBP	0,000	ADK1m	67,884
FBA	0,900	ME2	0,000
TPI	0,909	ALATA_L	0,010
GAPD	1,810	NDPK1	1,779
PGK	1,810	FUM	0,000
PGM	1,809	ADK1	0,468
ENO	1,809	ICDHy	-0,100
PYK	3,688	ACONT	-0,100
r0122	0,000	ACITL	0,000
PEPCK	1,779	ASPTA	4,174
LDH_L	-0,575	MDH	-2,396
G6PDH2r	0,000	AKGMALtm	4,285
PGL	0,000	ASPGLUmB_MitoCore	4,011
GND	0,000	ASPTAm	-4,011
RPI	0,000	G3PD1	0,010
RPE	0,000	r0205	0,000
TKT1	0,000	FACOAL160i	0,468
TALA	0,000	C160CPT1	0,468
TKT2	0,000	PPA	0,468
PDHm	2,607	r2435	0,468
CSm	6,802	C160CPT2	0,468
ACONTm	6,802	PPAm	67,884
ICDHxm	6,873	ACOT2_MitoCore	0,000
ICDHyrm	0,029	ACADLC16_MitoCore	0,468
AKGDm	6,639	MECR16C_MitoCore	0,000
SUCOAS1m	-6,488	MTPC16_MitoCore	0,468
SUCOASm	0,000	ACADLC14_MitoCore	0,468
FUMm	6,850	MECR14C_MitoCore	0,000
MDHm	9,246	MTPC14_MitoCore	0,468
CI_MitoCore	29,371	r1447	0,468
CII_MitoCore	6,850	r0638	0,000
CIII_MitoCore	39,541	r0660	-0,468
CIV_MitoCore	19,771	r0722	0,468
CV_MitoCore	130,120	r0724	-0,468
PEPCKm	0,200	r1451	0,468
PCm	1,667	r0735	0,000
ME2m	0,000	r0728	-0,468
ME1m	0,000	r0726	0,468
r0081	0,000	r0634	-0,468

r1448	0,468	r0696	0,000
r0633	0,000	r0697	0,000
r0731	0,468	r0773	0,000
r0730	0,468	FA160ACPH	0,000
r0732	0,468	FACOAL40im	0,006
r1450	0,468	BDHm	0,048
r0791	0,000	OCOAT1m	0,178
r0734	0,468	HMGCOASim	0,000
r0733	0,468	HMGLm	0,016
r0287	0,468	LEUTAm	0,016
r1446	0,474	OIVD1m	0,016
ECOAH1m	-0,504	r0655	0,016
HACD1m	-0,504	MCCCrm	0,016
ACACT1rm	-0,682	MGCHrm	0,016
ACCOAC	0,000	ILETAm	0,004
MCOATA	0,000	OIVD3m	0,004
ACOATA	0,000	r0603	0,004
r0678	0,000	ECOAH9m	0,004
r0691	0,000	HACD9m	0,004
r0681	0,000	ACACT10m	0,004
r0682	0,000	VALTAm	0,011
r0760	0,000	OIVD2m	0,011
r0761	0,000	r0560	0,011
r0762	0,000	ECOAH12m	0,011
r0763	0,000	3HBCOAHLm	0,011
r0764	0,000	HIBDm	0,011
r0694	0,000	ACCOALm	67,879
r0695	0,000	MMSAD1m	0,011
r0765	0,000	PPCOACm	0,027
r0766	0,000	MMEm	-0,027
r0692	0,000	MMMm	0,027
r0693	0,000	MMCDm	0,000
r0767	0,000	RE2649M	67,879
r0768	0,000	THRD_L	0,012
r0769	0,000	r1155	0,012
r0770	0,000	r1154	0,012
r0712	0,000	2HBO	0,000
r0713	0,000	METAT	0,000
r0701	0,000	METAT2_MitoCore	0,000
r0702	0,000	AHC	0,000
r0771	0,000	ADNK1	0,000
r0772	0,000	CYSTS	0,000

CYSTGL	0,000
CYSO	0,000
3SALATAi	0,000
3SPYRSP	0,000
CYSTA	0,001
CYSTAm	0,000
MCPST	0,001
MCPSTm_MitoCore	0,000
r0595m_MitoCore	0,000
r0595B_MitoCore	0,000
MCLOR	0,000
r0193	0,000
TRPO2	0,000
FKYNH	0,000
KYN3OX	0,000
HKYNH	0,000
3HAO	0,000
PCLAD	0,000
r0645	0,000
AMCOXO	0,000
AMCOXO2_MitoCore	0,000
2OXOADPTmB_MitoCore	0,000
2OXOADPTmC_MitoCore	0,000
2OXOADOXm	0,030
r0541	0,030
SACCD3m	0,030
r0525	0,030
AASAD3m	0,000
R03103_MitoCore	0,030
r0450	0,030
LYSOXc_MitoCore	0,000
PPD2CSPc_MitoCore	0,000
1PPDCRc_MitoCore	0,000
1PPDCRc_NADPH_MitoCore	0,000
LPCOXc_MitoCore	0,000
RE1254C	0,000
r0594	0,000
2AMADPTmB_MitoCore	0,000
2AMADPTmC_MitoCore	0,000
PROD2mB_MitoCore	0,004
G5SADrm	-0,004
r0074	0,011
GLU5Km	0,000
G5SDym	0,000
P5CRm	0,000
P5CRxm	0,000
ORNTArm	0,007
ORNDC	0,000
PTRCOX1	0,000
r0464c_MitoCore	0,000
ABUTD	0,000
ARGDCm	0,000
AGMTm	0,000
PTRCAT1m_MitoCore	0,000
APRTO2m_MitoCore	0,000
NABTNOm	0,000
4aabutn_MitoCore	0,000
GLUDC	0,184
4ABUTtm	0,184
ABTArm	0,184
r0178	0,184
GLUDxm	0,293
GLUDym	0,000
GLUDxi	0,000
GLUDy	0,000
GLNS	0,000
GLUNm	0,000
GLUN_MitoCore	0,000
PGCD	0,001
PSERT	0,001
PSP_L	0,001
GHMT2r	0,045
FOLR2	0,000
DHFR	0,000
MTHFD	0,045
MTHFC	0,055
FTCD	0,010
FTHFL	0,000
FTHFDH	0,055
r0060	0,000
GHMT2rm	-0,027

GCCam	0,027
GCCbim	0,027
GCCcm	0,027
r0514	0,000
r0226	0,000
MTHFDm	0,000
MTHFD2m	0,000
MTHFCm	0,000
FTHFLm	0,000
FTHFDHm_MitoCore	0,000
GLYATm	0,000
AOBUTDsm	0,000
AACTOORm_MitoCore	0,000
LGTHLm_MitoCore	0,000
GLYOXm	0,000
LDH_Dm_MitoCore	0,000
CBPSam	0,000
OCBTm	0,000
NOS1	0,000
NOS2	0,000
r0129	0,000
AMPTASECG	0,000
GLUCYS	0,000
GTHS	0,000
r0399	0,000
DHPR	0,000
TYRTA	0,000
TYRTB_MitoCore	0,000
34HPPOR	0,000
HGNTOR	0,000
MACACI	0,000
FUMAC	0,000
ASNS1	0,000
r0127	0,010
HISD	0,010
URCN	0,010
IZPN	0,010
GluForTx	0,010
APAT2rm	0,000
MMSAD3m	0,000
MMSAD3m2_MitoCore	0,000
ASP1DC	0,000
CKc	0,000
CK	0,000
ACOAHi	0,000
ALCD2yf	0,000
ALCD2if	0,000
ACALDtm	0,000
ALDD2xm	0,000
ALDD2x	0,000
ACSm	0,000
ACS	0,000
ADSL1	0,000
ADSS	0,000
AMPD1	0,000
ARGN	0,007
ARGSL	0,000
ARGSS	0,000
ARGNm	0,000
ALASm	0,000
5AOPtm	0,000
PPBNGS	0,000
HMBS	0,000
UPP3S	0,000
UPPDC1	0,000
CPPPGO	0,000
PPPGOmB_MitoCore	0,000
FCLTm	0,000
PHEMEtm	0,000
HOXG	0,000
BILIRED	0,000
BILIRED2_MitoCore	0,000
PCHOLPm_hs	0,000
GLYK	0,010
GLYC3Ptm	0,000
GPAMm_hsB_Mito-Core	0,000
AGPAT1B_MitoCore	0,000
CDSm	0,000
PGPPTm	0,000
PGPP_hsm_MitoCore	0,000
CLS_hsm_MitoCore	0,000
CLPN_MitoCore	0,000
CYTK1m	0,000

NDPK3m	0,000
SPODMm	0,029
GTHP	0,000
GTHPm	0,029
GTHO	0,000
GTHOm	0,029
CITtamB	0,000
r0913	0,000
CITtbm	-0,100
r0917	0,000
r0917b_MitoCore	0,000
PIt2mB_MitoCore	-2,761
ATPtmB_MitoCore	-0,972
HtmB_MitoCore	0,000
MALtm	-1,889
MALSO3tm	0,000
MALTSULtm	0,000
MALSO4tm	0,000
SUCCt2m	0,000
r0830	0,000
r0830B_MitoCore	0,000
r0829	0,000
SUCCt3m_MitoCore	0,000
COAtmB_MitoCore	0,000
COAtmC_MitoCore	0,000
GLUt2mB_MitoCore	0,000
ORNt4mB_MitoCore	0,000
r2398B_MitoCore	0,000
r2402B_MitoCore	0,000
LYStmB_MitoCore	0,030
ORNt3mB_MitoCore	-0,007
ARGtmB_MitoCore	0,000
r1427	0,000
PYRt2m	4,274
ACACt2mB_MitoCore	0,114
FE2tm	0,000
ASNtm	0,000
r1437	0,000
GLNtm	0,000
PROtm	0,004
r1078	0,000
r1436	0,000
r1455	0,000
TRPtm_MitoCore	0,000
GLYtm	0,054
ILEt5m	0,004
LEUt5m	0,016
VALt5m	0,011
r1434	0,000
r1435	-0,027
r1440	0,000
BALAtmr	0,000
UREAtm	0,000
FUMtmB_MitoCore	0,000
BHBtmB_MitoCore	0,048
PPAtmB_MitoCore	0,000
BUTt2mB_MitoCore	0,006
FORt2mB_MitoCore	0,000
r0962B_MitoCore	0,000
CHLtmB_MitoCore	0,000
CO2tm	-16,389
H2Otm	-15,462
O2tm	19,800
GLYCtm	0,000
CYANtm	0,000
TCYNTtmB_MitoCore	0,000
CREATtmdiffir	0,000
PCREATtmdiffirB_MitoCore	0,000
r0941	1,710
r0838B_MitoCore	-0,320
Biomasst_MitoCore	0,000
PCFLOPm	0,000
PSFLIPm	0,000
PEFLIPm	0,000
Biomass_MitoCore	0,000
O2t	19,800
CO2t	-18,307
HCO3t_MitoCore	1,710
GLCt1r	0,900
HDCAtr	0,468
HDCAtm_MitoCore	0,000
L_LACt2r	0,575
BHBt	0,048

ACACt2	0,114	CHOLtu	0,000
ETOHt	0,000	r1088	0,000
BUTt2r	0,006	ICITt_MitoCore	0,000
GLYCt	-0,010	UREAt	-0,007
r0942	0,000	r1512	0,000
r0942b_MitoCore	0,000	ARGSUCt_MitoCore	0,000
HIStiDF	0,010	MAL_Lte	0,000
ILEtec	0,004	OAAt_MitoCore	0,000
LEUtec	0,016	AKGt_MitoCore	0,000
LYStiDF	0,030	MERCPLACt_MitoCore	0,000
METtec	0,000	r0899	0,000
PHEtec	0,000	FE2t	0,000
r2534	0,012	H2Ot	-16,699
TRPt	0,000	Hct_MitoCore	6,124
VALtec	0,011	Hmt_MitoCore	-3,794
ARGtiDF	0,007	SO3t_MitoCore	0,000
ASPte	-0,154	TSULt_MitoCore	0,000
CYStec	0,001	r0940	0,000
GLUt_MitoCore	0,000	CYANt	0,001
r2525	0,000	TCYNTt	0,001
GLYt2r	0,009	r1423	0,000
PROt2r	0,004	FORt_MitoCore	0,000
r2526	0,017	FOLt_MitoCore	0,000
TYRt	0,000	NADHt_MitoCore	0,000
r2532	0,010	NADt_MitoCore	0,000
ALAt2r	0,010	NADHtm_MitoCore	0,000
FUMt_MitoCore	0,000	NADtm_MitoCore	0,000
SUMt_MitoCore	0,000	COt	0,000
r0817	0,000	NOt	0,000
NH4t3r	0,362	PCHOLHSTDe	0,000
ACt2r	0,000	PSt3	0,000
PPAt	0,000	PEt	0,000
2HBt2	0,000		

Supplementary table 2. Complete metabolic flux distribution in RASF-specific conditions with maximal ATP production as objective function.

Reaction	Flux
EX_2hb_e	0,000
EX_ac_e	0,010
EX_acac_e	0,000
EX_akg_e	0,000
EX_ala_B_e	0,000
EX_ala_L_e	0,164
EX_arg_L_e	0,000
EX_argsuc_e	0,000
EX_asn_L_e	-0,010
EX_asp_L_e	-0,154
EX_bhb_e	0,000
EX_bilirub_e	0,000
EX_biomass_e	0,000
EX_but_e	0,000
EX_chol_e	0,000
EX_cit_e	0,000
EX_citr_L_e	0,000
EX_co_e	0,000
EX_co2_e	0,224
EX_creat_e	0,000
EX_cyan_e	0,000
EX_cys_L_e	0,000
EX_etoh_e	0,000
EX_fe2_e	0,000
EX_for_e	0,000
EX_fum_e	0,000
EX_glc_D_e	-0,900
EX_gln_L_e	0,000
EX_glu_L_e	0,000
EX_gly_e	-0,005
EX_glyc_e	-0,010
EX_h_e	1,581
EX_h2o_e	0,000
EX_HC00250_e	0,000
EX_hco3_e	-0,055
EX_hdca_e	0,000
EX_his_L_e	-0,010
EX_icit_e	0,000
EX_ile_L_e	0,000
EX_lac_L_e	1,820
EX_leu_L_e	0,000
EX_lys_L_e	0,000
EX_mal_L_e	0,000
EX_mercplac_e	0,000
EX_met_L_e	0,000
EX_nad_e	0,000
EX_nadh_e	0,000
EX_nh4_e	0,040
EX_no_e	0,000
EX_o2_e	0,000
EX_oaa_e	0,000
EX_pchol_hs_e	0,000
EX_pcreat_e	0,000
EX_pe_hs_e	0,000
EX_phe_L_e	0,000
EX_pi_e	0,000
EX_ppa_e	0,000
EX_pro_L_e	0,000
EX_ps_hs_e	0,000
EX_ser_L_e	0,005
EX_so3_e	0,000
EX_succ_e	0,000
EX_tcynt_e	0,000
EX_thr_L_e	0,000
EX_trp_L_e	0,000
EX_tsul_e	0,000
EX_tyr_L_e	0,000
EX_urea_e	0,000
EX_val_L_e	0,000
EX_fol_e	0,000
OF_ATP_MitoCore	0,000
OF_HEME_MitoCore	0,000
OF_LIPID_MitoCore	0,000
OF_PROTEIN_Mito-Core	0,000
HEX1	0,900
G6PPer	0,000

PGI	0,900	NDPK1m	0,000
PFK	0,900	NNT_MitoCore	0,000
FBP	0,000	ADK1m	1,206
FBA	0,900	ME2	0,000
TPI	0,910	ALATA_L	-0,164
GAPD	1,810	NDPK1	0,174
PGK	1,810	FUM	0,000
PGM	1,810	ADK1	0,000
ENO	1,810	ICDHy	-0,010
PYK	1,984	ACONT	-0,010
r0122	0,000	ACITL	0,010
PEPCK	0,174	ASPTA	0,164
LDH_L	1,820	MDH	0,000
G6PDH2r	0,000	AKGMALtm	0,000
PGL	0,000	ASPGLUmB_MitoCore	0,000
GND	0,000	ASPTAm	0,000
RPI	0,000	G3PD1	0,010
RPE	0,000	r0205	0,000
TKT1	0,000	FACOAL160i	0,000
TALA	0,000	C160CPT1	0,000
TKT2	0,000	PPA	0,000
PDHm	0,000	r2435	0,000
CSm	0,000	C160CPT2	0,000
ACONTm	0,000	PPAm	1,206
ICDHxm	0,000	ACOT2_MitoCore	0,000
ICDHyrm	0,000	ACADLC16_MitoCore	0,000
AKGDm	0,000	MECR16C_MitoCore	0,000
SUCOAS1m	0,000	MTPC16_MitoCore	0,000
SUCOASm	0,000	ACADLC14_MitoCore	0,000
FUMm	0,000	MECR14C_MitoCore	0,000
MDHm	0,000	MTPC14_MitoCore	0,000
CI_MitoCore	0,000	r1447	0,000
CII_MitoCore	0,000	r0638	0,000
CIII_MitoCore	0,000	r0660	0,000
CIV_MitoCore	0,000	r0722	0,000
CV_MitoCore	0,667	r0724	0,000
PEPCKm	0,000	r1451	0,000
PCm	0,000	r0735	0,000
ME2m	0,000	r0728	0,000
ME1m	0,000	r0726	0,000
r0081	0,000	r0634	0,000
ACITLm_MitoCore	0,000	r1448	0,000

r0633	0,000	r0697	0,000
r0731	0,000	r0773	0,000
r0730	0,000	FA160ACPH	0,000
r0732	0,000	FACOAL40im	0,000
r1450	0,000	BDHm	0,000
r0791	0,000	OCOAT1m	0,000
r0734	0,000	HMGCOASim	0,000
r0733	0,000	HMGLm	0,000
r0287	0,000	LEUTAm	0,000
r1446	0,000	OIVD1m	0,000
ECOAH1m	0,000	r0655	0,000
HACD1m	0,000	MCCCrm	0,000
ACACT1rm	0,000	MGCHrm	0,000
ACCOAC	0,000	ILETAm	0,000
MCOATA	0,000	OIVD3m	0,000
ACOATA	0,000	r0603	0,000
r0678	0,000	ECOAH9m	0,000
r0691	0,000	HACD9m	0,000
r0681	0,000	ACACT10m	0,000
r0682	0,000	VALTAm	0,000
r0760	0,000	OIVD2m	0,000
r0761	0,000	r0560	0,000
r0762	0,000	ECOAH12m	0,000
r0763	0,000	3HBCOAHLm	0,000
r0764	0,000	HIBDm	0,000
r0694	0,000	ACCOALm	1,206
r0695	0,000	MMSAD1m	0,000
r0765	0,000	PPCOACm	0,055
r0766	0,000	MMEm	0,000
r0692	0,000	MMMm	0,000
r0693	0,000	MMCDm	0,055
r0767	0,000	RE2649M	1,206
r0768	0,000	THRD_L	0,000
r0769	0,000	r1155	0,000
r0770	0,000	r1154	0,000
r0712	0,000	2HBO	0,000
r0713	0,000	METAT	0,000
r0701	0,000	METAT2_MitoCore	0,000
r0702	0,000	AHC	0,000
r0771	0,000	ADNK1	0,000
r0772	0,000	CYSTS	0,000
r0696	0,000	CYSTGL	0,000

CYSO	0,000
3SALATAi	0,000
3SPYRSP	0,000
CYSTA	0,000
CYSTAm	0,000
MCPST	0,000
MCPSTm_MitoCore	0,000
r0595m_MitoCore	0,000
r0595B_MitoCore	0,000
MCLOR	0,000
r0193	0,000
TRPO2	0,000
FKYNH	0,000
KYN3OX	0,000
HKYNH	0,000
3HAO	0,000
PCLAD	0,000
r0645	0,000
AMCOXO	0,000
AMCOXO2_MitoCore	0,000
2OXOADPTmB_Mito-Core	0,000
2OXOADPTmC_Mito-Core	0,000
2OXOADOXm	0,000
r0541	0,000
SACCD3m	0,000
r0525	0,000
AASAD3m	0,000
R03103_MitoCore	0,000
r0450	0,000
LYSOXc_MitoCore	0,000
PPD2CSPc_MitoCore	0,000
1PPDCRc_MitoCore	0,000
1PPDCRc_NADPH_Mi-toCore	0,000
LPCOXc_MitoCore	0,000
RE1254C	0,000
r0594	0,000
2AMADPTmB_Mito-Core	0,000
2AMADPTmC_Mito-Core	0,000
PROD2mB_MitoCore	0,000
G5SADrm	0,000
r0074	0,000
GLU5Km	0,000
G5SDym	0,000
P5CRm	0,000
P5CRxm	0,000
ORNTArm	0,000
ORNDC	0,000
PTRCOX1	0,000
r0464c_MitoCore	0,000
ABUTD	0,000
ARGDCm	0,000
AGMTm	0,000
PTRCAT1m_MitoCore	0,000
APRTO2m_MitoCore	0,000
NABTNOm	0,000
4aabutn_MitoCore	0,000
GLUDC	0,000
4ABUTtm	0,000
ABTArm	0,000
r0178	0,000
GLUDxm	0,000
GLUDym	0,000
GLUDxi	0,000
GLUDy	0,010
GLNS	0,000
GLUNm	0,000
GLUN_MitoCore	0,000
PGCD	0,000
PSERT	0,000
PSP_L	0,000
GHMT2r	-0,005
FOLR2	0,000
DHFR	0,000
MTHFD	-0,005
MTHFC	0,005
FTCD	0,010
FTHFL	0,000
FTHFDH	0,005
r0060	0,000
GHMT2rm	0,000
GCCam	0,000

GCCbim	0,000
GCCcm	0,000
r0514	0,000
r0226	0,000
MTHFDm	0,000
MTHFD2m	0,000
MTHFCm	0,000
FTHFLm	0,000
FTHFDHm_MitoCore	0,000
GLYATm	0,000
AOBUTDsm	0,000
AACTOORm_MitoCore	0,000
LGTHLm_MitoCore	0,000
GLYOXm	0,000
LDH_Dm_MitoCore	0,000
CBPSam	0,000
OCBTm	0,000
NOS1	0,000
NOS2	0,000
r0129	0,000
AMPTASECG	0,000
GLUCYS	0,000
GTHS	0,000
r0399	0,000
DHPR	0,000
TYRTA	0,000
TYRTB_MitoCore	0,000
34HPPOR	0,000
HGNTOR	0,000
MACACI	0,000
FUMAC	0,000
ASNS1	0,000
r0127	0,010
HISD	0,010
URCN	0,010
IZPN	0,010
GluForTx	0,010
APAT2rm	0,000
MMSAD3m	0,000
MMSAD3m2_MitoCore	0,000
ASP1DC	0,000
CKc	0,000
CK	0,000
ACOAHi	0,010
ALCD2yf	0,000
ALCD2if	0,000
ACALDtm	0,000
ALDD2xm	0,000
ALDD2x	0,000
ACSm	0,000
ACS	0,000
ADSL1	0,000
ADSS	0,000
AMPD1	0,000
ARGN	0,000
ARGSL	0,000
ARGSS	0,000
ARGNm	0,000
ALASm	0,000
5AOPtm	0,000
PPBNGS	0,000
HMBS	0,000
UPP3S	0,000
UPPDC1	0,000
CPPPGO	0,000
PPPGOmB_MitoCore	0,000
FCLTm	0,000
PHEMEtm	0,000
HOXG	0,000
BILIRED	0,000
BILIRED2_MitoCore	0,000
PCHOLPm_hs	0,000
GLYK	0,010
GLYC3Ptm	0,000
GPAMm_hsB_Mito-Core	0,000
AGPAT1B_MitoCore	0,000
CDSm	0,000
PGPPTm	0,000
PGPP_hsm_MitoCore	0,000
CLS_hsm_MitoCore	0,000
CLPN_MitoCore	0,000
CYTK1m	0,000
NDPK3m	0,000

SPODMm	0,000
GTHP	0,000
GTHPm	0,000
GTHO	0,000
GTHOm	0,000
CITtamB	0,000
r0913	0,000
CITtbm	0,000
r0917	0,000
r0917b_MitoCore	0,000
PIt2mB_MitoCore	-1,800
ATPtmB_MitoCore	-1,800
HtmB_MitoCore	0,000
MALtm	0,000
MALSO3tm	0,000
MALTSULtm	0,000
MALSO4tm	0,000
SUCCt2m	0,000
r0830	0,000
r0830B_MitoCore	0,000
r0829	0,000
SUCCt3m_MitoCore	0,000
COAtmB_MitoCore	0,000
COAtmC_MitoCore	0,000
GLUt2mB_MitoCore	0,000
ORNt4mB_MitoCore	0,000
r2398B_MitoCore	0,000
r2402B_MitoCore	0,000
LYStmB_MitoCore	0,000
ORNt3mB_MitoCore	0,000
ARGtmB_MitoCore	0,000
r1427	0,000
PYRt2m	0,000
ACACt2mB_MitoCore	0,000
FE2tm	0,000
ASNtm	0,000
r1437	0,000
GLNtm	0,000
PROtm	0,000
r1078	0,000
r1436	0,000
r1455	0,000
TRPtm_MitoCore	0,000
GLYtm	0,000
ILEt5m	0,000
LEUt5m	0,000
VALt5m	0,000
r1434	0,000
r1435	0,000
r1440	0,000
BALAtmr	0,000
UREAtm	0,000
FUMtmB_MitoCore	0,000
BHBtmB_MitoCore	0,000
PPAtmB_MitoCore	0,000
BUTt2mB_MitoCore	0,000
FORt2mB_MitoCore	0,000
r0962B_MitoCore	0,000
CHLtmB_MitoCore	0,000
CO2tm	-0,055
H2Otm	1,745
O2tm	0,000
GLYCtm	0,000
CYANtm	0,000
TCYNTtmB_MitoCore	0,000
CREATtmdiffir	0,000
PCREATtmdiffirB_MitoCore	0,000
r0941	0,055
r0838B_MitoCore	0,000
Biomasst_MitoCore	0,000
PCFLOPm	0,000
PSFLIPm	0,000
PEFLIPm	0,000
Biomass_MitoCore	0,000
O2t	0,000
CO2t	-0,224
HCO3t_MitoCore	0,055
GLCt1r	0,900
HDCAtr	0,000
HDCAtm_MitoCore	0,000
L_LACt2r	-1,820
BHBt	0,000
ACACt2	0,000

ETOHt	0,000	CHOLtu	0,000
BUTt2r	0,000	r1088	0,000
GLYCt	-0,010	ICITt_MitoCore	0,000
r0942	0,000	UREAt	0,000
r0942b_MitoCore	0,000	r1512	0,000
HIStiDF	0,010	ARGSUCt_MitoCore	0,000
ILEtec	0,000	MAL_Lte	0,000
LEUtec	0,000	OAAt_MitoCore	0,000
LYStiDF	0,000	AKGt_MitoCore	0,000
METtec	0,000	MERCPLACt_MitoCore	0,000
PHEtec	0,000	r0899	0,000
r2534	0,000	FE2t	0,000
TRPt	0,000	H2Ot	0,000
VALtec	0,000	Hct_MitoCore	0,313
ARGtiDF	0,000	Hmt_MitoCore	0,055
ASPte	-0,154	SO3t_MitoCore	0,000
CYStec	0,000	TSULt_MitoCore	0,000
GLUt_MitoCore	0,000	r0940	0,000
r2525	0,000	CYANt	0,000
GLYt2r	0,005	TCYNTt	0,000
PROt2r	0,000	r1423	0,000
r2526	-0,005	FORt_MitoCore	0,000
TYRt	0,000	FOLt_MitoCore	0,000
r2532	0,010	NADHt_MitoCore	0,000
ALAt2r	-0,164	NADt_MitoCore	0,000
FUMt_MitoCore	0,000	NADHtm_MitoCore	0,000
SUMt_MitoCore	0,000	NADtm_MitoCore	0,000
r0817	0,000	COt	0,000
NH4t3r	0,040	NOt	0,000
ACt2r	-0,010	PCHOLHSTDe	0,000
PPAt	0,000	PSt3	0,000
2HBt2	0,000	PEt	0,000

Supplementary table 3. Complete metabolic flux distribution in breast CAF-specific conditions with maximal ATP production as objective function.

Reaction	Flux
EX_2hb_e	0,010
EX_ac_e	0,010
EX_acac_e	0,000
EX_akg_e	0,000
EX_ala_B_e	0,000
EX_ala_L_e	-0,010
EX_arg_L_e	0,000
EX_argsuc_e	0,000
EX_asn_L_e	-0,010
EX_asp_L_e	-0,154
EX_bhb_e	0,000
EX_bilirub_e	0,000
EX_biomass_e	0,000
EX_but_e	0,000
EX_chol_e	0,000
EX_cit_e	0,000
EX_citr_L_e	0,000
EX_co_e	0,000
EX_co2_e	0,410
EX_creat_e	0,000
EX_cyan_e	0,000
EX_cys_L_e	-0,001
EX_etoh_e	0,000
EX_fe2_e	0,000
EX_for_e	0,000
EX_fum_e	0,000
EX_glc_D_e	-0,900
EX_gln_L_e	0,000
EX_glu_L_e	0,000
EX_gly_e	0,000
EX_glyc_e	-0,010
EX_h_e	1,402
EX_h2o_e	0,000
EX_HC00250_e	0,000
EX_hco3_e	-0,236
EX_hdca_e	0,000
EX_his_L_e	-0,010
EX_icit_e	0,000
EX_ile_L_e	0,000
EX_lac_L_e	1,995
EX_leu_L_e	0,000
EX_lys_L_e	0,000
EX_mal_L_e	0,000
EX_mercplac_e	0,000
EX_met_L_e	0,000
EX_nad_e	0,000
EX_nadh_e	0,000
EX_nh4_e	0,225
EX_no_e	0,000
EX_o2_e	-0,001
EX_oaa_e	0,000
EX_pchol_hs_e	0,000
EX_pcreat_e	0,000
EX_pe_hs_e	0,000
EX_phe_L_e	0,000
EX_pi_e	0,000
EX_ppa_e	0,000
EX_pro_L_e	0,000
EX_ps_hs_e	0,000
EX_ser_L_e	0,000
EX_so3_e	0,001
EX_succ_e	0,000
EX_tcynt_e	0,000
EX_thr_L_e	-0,010
EX_trp_L_e	0,000
EX_tsul_e	0,000
EX_tyr_L_e	0,000
EX_urea_e	0,000
EX_val_L_e	0,000
EX_fol_e	0,000
OF_ATP_MitoCore	0,000
OF_HEME_MitoCore	0,000
OF_LIPID_MitoCore	0,000
OF_PROTEIN_MitoCore	0,000
HEX1	0,900
G6PPer	0,000

PGI	0,900	NDPK1m	0,000
PFK	0,900	NNT_MitoCore	0,000
FBP	0,000	ADK1m	1,115
FBA	0,900	ME2	0,000
TPI	0,910	ALATA_L	0,010
GAPD	1,810	NDPK1	0,174
PGK	1,810	FUM	0,000
PGM	1,810	ADK1	0,000
ENO	1,810	ICDHy	-0,010
PYK	1,984	ACONT	-0,010
r0122	0,000	ACITL	0,010
PEPCK	0,174	ASPTA	0,164
LDH_L	1,995	MDH	0,000
G6PDH2r	0,000	AKGMALtm	0,000
PGL	0,000	ASPGLUmB_MitoCore	0,000
GND	0,000	ASPTAm	0,000
RPI	0,000	G3PD1	0,010
RPE	0,000	r0205	0,000
TKT1	0,000	FACOAL160i	0,000
TALA	0,000	C160CPT1	0,000
TKT2	0,000	PPA	0,000
PDHm	0,000	r2435	0,000
CSm	0,000	C160CPT2	0,000
ACONTm	0,000	PPAm	1,115
ICDHxm	0,000	ACOT2_MitoCore	0,000
ICDHyrm	0,000	ACADLC16_MitoCore	0,000
AKGDm	0,000	MECR16C_MitoCore	0,000
SUCOAS1m	0,000	MTPC16_MitoCore	0,000
SUCOASm	0,000	ACADLC14_MitoCore	0,000
FUMm	0,000	MECR14C_MitoCore	0,000
MDHm	0,000	MTPC14_MitoCore	0,000
CI_MitoCore	0,000	r1447	0,000
CII_MitoCore	0,000	r0638	0,000
CIII_MitoCore	0,000	r0660	0,000
CIV_MitoCore	0,000	r0722	0,000
CV_MitoCore	0,667	r0724	0,000
PEPCKm	0,000	r1451	0,000
PCm	0,000	r0735	0,000
ME2m	0,000	r0728	0,000
ME1m	0,000	r0726	0,000
r0081	0,000	r0634	0,000
ACITLm_MitoCore	0,000	r1448	0,000

r0633	0,000	r0697	0,000
r0731	0,000	r0773	0,000
r0730	0,000	FA160ACPH	0,000
r0732	0,000	FACOAL40im	0,000
r1450	0,000	BDHm	0,000
r0791	0,000	OCOAT1m	0,000
r0734	0,000	HMGCOASim	0,000
r0733	0,000	HMGLm	0,000
r0287	0,000	LEUTAm	0,000
r1446	0,000	OIVD1m	0,000
ECOAH1m	0,000	r0655	0,000
HACD1m	0,000	MCCCrm	0,000
ACACT1rm	0,000	MGCHrm	0,000
ACCOAC	0,000	ILETAm	0,000
MCOATA	0,000	OIVD3m	0,000
ACOATA	0,000	r0603	0,000
r0678	0,000	ECOAH9m	0,000
r0691	0,000	HACD9m	0,000
r0681	0,000	ACACT10m	0,000
r0682	0,000	VALTAm	0,000
r0760	0,000	OIVD2m	0,000
r0761	0,000	r0560	0,000
r0762	0,000	ECOAH12m	0,000
r0763	0,000	3HBCOAHLm	0,000
r0764	0,000	HIBDm	0,000
r0694	0,000	ACCOALm	1,115
r0695	0,000	MMSAD1m	0,000
r0765	0,000	PPCOACm	0,236
r0766	0,000	MMEm	0,000
r0692	0,000	MMMm	0,000
r0693	0,000	MMCDm	0,236
r0767	0,000	RE2649M	1,115
r0768	0,000	THRD_L	0,010
r0769	0,000	r1155	0,000
r0770	0,000	r1154	0,000
r0712	0,000	2HBO	-0,010
r0713	0,000	METAT	0,000
r0701	0,000	METAT2_MitoCore	0,000
r0702	0,000	AHC	0,000
r0771	0,000	ADNK1	0,000
r0772	0,000	CYSTS	0,000
r0696	0,000	CYSTGL	0,000

CYSO	0,001
3SALATAi	0,001
3SPYRSP	0,001
CYSTA	0,000
CYSTAm	0,000
MCPST	0,000
MCPSTm_MitoCore	0,000
r0595m_MitoCore	0,000
r0595B_MitoCore	0,000
MCLOR	0,000
r0193	0,000
TRPO2	0,000
FKYNH	0,000
KYN3OX	0,000
HKYNH	0,000
3HAO	0,000
PCLAD	0,000
r0645	0,000
AMCOXO	0,000
AMCOXO2_MitoCore	0,000
2OXOADPTmB_MitoCore	0,000
2OXOADPTmC_MitoCore	0,000
2OXOADOXm	0,000
r0541	0,000
SACCD3m	0,000
r0525	0,000
AASAD3m	0,000
R03103_MitoCore	0,000
r0450	0,000
LYSOXc_MitoCore	0,000
PPD2CSPc_MitoCore	0,000
1PPDCRc_MitoCore	0,000
1PPDCRc_NADPH_Mito-Core	0,000
LPCOXc_MitoCore	0,000
RE1254C	0,000
r0594	0,000
2AMADPTmB_MitoCore	0,000
2AMADPTmC_MitoCore	0,000
PROD2mB_MitoCore	0,000
G5SADrm	0,000
r0074	0,000
GLU5Km	0,000
G5SDym	0,000
P5CRm	0,000
P5CRxm	0,000
ORNTArm	0,000
ORNDC	0,000
PTRCOX1	0,000
r0464c_MitoCore	0,000
ABUTD	0,000
ARGDCm	0,000
AGMTm	0,000
PTRCAT1m_MitoCore	0,000
APRTO2m_MitoCore	0,000
NABTNOm	0,000
4aabutn_MitoCore	0,000
GLUDC	0,000
4ABUTtm	0,000
ABTArm	0,000
r0178	0,000
GLUDxm	0,000
GLUDym	0,000
GLUDxi	0,185
GLUDy	0,000
GLNS	0,000
GLUNm	0,000
GLUN_MitoCore	0,000
PGCD	0,000
PSERT	0,000
PSP_L	0,000
GHMT2r	0,000
FOLR2	0,000
DHFR	0,000
MTHFD	0,000
MTHFC	0,010
FTCD	0,010
FTHFL	0,000
FTHFDH	0,010
r0060	0,000
GHMT2rm	0,000
GCCam	0,000
GCCbim	0,000
GCCcm	0,000

r0514	0,000	ALCD2yf	0,000
r0226	0,000	ALCD2if	0,000
MTHFDm	0,000	ACALDtm	0,000
MTHFD2m	0,000	ALDD2xm	0,000
MTHFCm	0,000	ALDD2x	0,000
FTHFLm	0,000	ACSm	0,000
FTHFDHm_MitoCore	0,000	ACS	0,000
GLYATm	0,000	ADSL1	0,000
AOBUTDsm	0,000	ADSS	0,000
AACTOORm_MitoCore	0,000	AMPD1	0,000
LGTHLm_MitoCore	0,000	ARGN	0,000
GLYOXm	0,000	ARGSL	0,000
LDH_Dm_MitoCore	0,000	ARGSS	0,000
CBPSam	0,000	ARGNm	0,000
OCBTm	0,000	ALASm	0,000
NOS1	0,000	5AOPtm	0,000
NOS2	0,000	PPBNGS	0,000
r0129	0,000	HMBS	0,000
AMPTASECG	0,000	UPP3S	0,000
GLUCYS	0,000	UPPDC1	0,000
GTHS	0,000	CPPPGO	0,000
r0399	0,000	PPPGOmB_MitoCore	0,000
DHPR	0,000	FCLTm	0,000
TYRTA	0,000	PHEMEtm	0,000
TYRTB_MitoCore	0,000	HOXG	0,000
34HPPOR	0,000	BILIRED	0,000
HGNTOR	0,000	BILIRED2_MitoCore	0,000
MACACI	0,000	PCHOLPm_hs	0,000
FUMAC	0,000	GLYK	0,010
ASNS1	0,000	GLYC3Ptm	0,000
r0127	0,010	GPAMm_hsB_MitoCore	0,000
HISD	0,010	AGPAT1B_MitoCore	0,000
URCN	0,010	CDSm	0,000
IZPN	0,010	PGPPTm	0,000
GluForTx	0,010	PGPP_hsm_MitoCore	0,000
APAT2rm	0,000	CLS_hsm_MitoCore	0,000
MMSAD3m	0,000	CLPN_MitoCore	0,000
MMSAD3m2_MitoCore	0,000	CYTK1m	0,000
ASP1DC	0,000	NDPK3m	0,000
CKc	0,000	SPODMm	0,000
CK	0,000	GTHP	0,000
ACOAHi	0,010	GTHPm	0,000

GTHO	0,000
GTHOm	0,000
CITtamB	0,000
r0913	0,000
CITtbm	0,000
r0917	0,000
r0917b_MitoCore	0,000
PIt2mB_MitoCore	-1,800
ATPtmB_MitoCore	-1,800
HtmB_MitoCore	0,000
MALtm	0,000
MALSO3tm	0,000
MALTSULtm	0,000
MALSO4tm	0,000
SUCCt2m	0,000
r0830	0,000
r0830B_MitoCore	0,000
r0829	0,000
SUCCt3m_MitoCore	0,000
COAtmB_MitoCore	0,000
COAtmC_MitoCore	0,000
GLUt2mB_MitoCore	0,000
ORNt4mB_MitoCore	0,000
r2398B_MitoCore	0,000
r2402B_MitoCore	0,000
LYStmB_MitoCore	0,000
ORNt3mB_MitoCore	0,000
ARGtmB_MitoCore	0,000
r1427	0,000
PYRt2m	0,000
ACACt2mB_MitoCore	0,000
FE2tm	0,000
ASNtm	0,000
r1437	0,000
GLNtm	0,000
PROtm	0,000
r1078	0,000
r1436	0,000
r1455	0,000
TRPtm_MitoCore	0,000
GLYtm	0,000
ILEt5m	0,000
LEUt5m	0,000
VALt5m	0,000
r1434	0,000
r1435	0,000
r1440	0,000
BALAtmr	0,000
UREAtm	0,000
FUMtmB_MitoCore	0,000
BHBtmB_MitoCore	0,000
PPAtmB_MitoCore	0,000
BUTt2mB_MitoCore	0,000
FORt2mB_MitoCore	0,000
r0962B_MitoCore	0,000
CHLtmB_MitoCore	0,000
CO2tm	-0,236
H2Otm	1,564
O2tm	0,000
GLYCtm	0,000
CYANtm	0,000
TCYNTtmB_MitoCore	0,000
CREATtmdiffir	0,000
PCREATtmdiffirB_Mito-Core	0,000
r0941	0,236
r0838B_MitoCore	0,000
Biomasst_MitoCore	0,000
PCFLOPm	0,000
PSFLIPm	0,000
PEFLIPm	0,000
Biomass_MitoCore	0,000
O2t	0,001
CO2t	-0,410
HCO3t_MitoCore	0,236
GLCt1r	0,900
HDCAtr	0,000
HDCAtm_MitoCore	0,000
L_LACt2r	-1,995
BHBt	0,000
ACACt2	0,000
ETOHt	0,000
BUTt2r	0,000
GLYCt	-0,010

r0942	0,000
r0942b_MitoCore	0,000
HIStiDF	0,010
ILEtec	0,000
LEUtec	0,000
LYStiDF	0,000
METtec	0,000
PHEtec	0,000
r2534	0,010
TRPt	0,000
VALtec	0,000
ARGtiDF	0,000
ASPte	-0,154
CYStec	0,001
GLUt_MitoCore	0,000
r2525	0,000
GLYt2r	0,000
PROt2r	0,000
r2526	0,000
TYRt	0,000
r2532	0,010
ALAt2r	0,010
FUMt_MitoCore	0,000
SUMt_MitoCore	0,000
r0817	0,000
NH4t3r	0,225
ACt2r	-0,010
PPAt	0,000
2HBt2	-0,010
CHOLtu	0,000
r1088	0,000
ICITt_MitoCore	0,000
UREAt	0,000
r1512	0,000
ARGSUCt_MitoCore	0,000
MAL_Lte	0,000
OAAt_MitoCore	0,000
AKGt_MitoCore	0,000
MERCPLACt_MitoCore	0,000
r0899	0,000
FE2t	0,000
H2Ot	0,000
Hct_MitoCore	0,142
Hmt_MitoCore	0,236
SO3t_MitoCore	-0,001
TSULt_MitoCore	0,000
r0940	0,000
CYANt	0,000
TCYNTt	0,000
r1423	0,000
FORt_MitoCore	0,000
FOLt_MitoCore	0,000
NADHt_MitoCore	0,000
NADt_MitoCore	0,000
NADHtm_MitoCore	0,000
NADtm_MitoCore	0,000
COt	0,000
NOt	0,000
PCHOLHSTDe	0,000
PSt3	0,000
PEt	0,000

Supplementary table 4. Main uptake and secretion reactions according to the objective function of maximum ATP production when only common metabolites and enzymes with asymptotic regulatory behavior equal to 0 in both RASFs and breast CAFs Boolean models are constrained.

Uptake

Metabolite	Reaction	Flux	C-number	C-flux
arg_L_e	EX_arg_L_e	0.007	6	0.66%
asn_L_e	EX_asn_L_e	0.01	4	0.63%
asp_L_e	EX_asp_L_e	0.154	4	9.64%
glc_D_e	EX_glc_D_e	0.9	6	84.52%
gly_e	EX_gly_e	0.009	2	0.28%
glyc_e	EX_glyc_e	0.01	3	0.47%
hco3_e	EX_hco3_e	0.084	1	1.31%
his_L_e	EX_his_L_e	0.01	6	0.94%
o2_e	EX_o2_e	0.096	0	0.00%
ser_L_e	EX_ser_L_e	0.017	3	0.80%
thr_L_e	EX_thr_L_e	0.012	4	0.75%

Secretion

Metabolite	Reaction	Flux	C-number	C-flux
ala_L_e	EX_ala_L_e	-0.092	3	4.32%
co2_e	EX_co2_e	-0.344	1	5.38%
h2o_e	EX_h2o_e	-0.018	0	0.00%
h_e	EX_h_e	-1.545	0	0.00%
lac_L_e	EX_lac_L_e	-1.882	3	88.37%
nh4_e	EX_nh4_e	-0.164	0	0.00%
succ_e	EX_succ_e	-0.029	4	1.82%
urea_e	EX_urea_e	-0.007	1	0.11%

BIBLIOGRAPHY

[1] D. Mathis and S. E. Shoelson, 'Immunometabolism: an emerging frontier', *Nat. Rev. Immunol.*, vol. 11, no. 2, Art. no. 2, Feb. 2011, doi: 10.1038/nri2922.

[2] S. Chandrashekara, 'The treatment strategies of autoimmune disease may need a different approach from conventional protocol: A review', *Indian J. Pharmacol.*, vol. 44, no. 6, pp. 665–671, 2012, doi: 10.4103/0253-7613.103235.

[3] 'Metabolic Syndrome - Treatment | NHLBI, NIH', May 27, 2022. https://www.nhlbi.nih.gov/health/metabolic-syndrome/treatment (accessed Jun. 29, 2023).

[4] Y. S. Lee and J. Olefsky, 'Chronic tissue inflammation and metabolic disease', *Genes Dev.*, vol. 35, no. 5–6, pp. 307–328, Jan. 2021, doi: 10.1101/gad.346312.120.

[5] L. Makowski, M. Chaib, and J. C. Rathmell, 'Immunometabolism: From basic mechanisms to translation', *Immunol. Rev.*, vol. 295, no. 1, pp. 5–14, 2020, doi: 10.1111/imr.12858.

[6] S. Daemen and J. D. Schilling, 'The Interplay Between Tissue Niche and Macrophage Cellular Metabolism in Obesity', *Front. Immunol.*, vol. 10, p. 3133, 2019, doi: 10.3389/fimmu.2019.03133.

[7] D. G. Ryan and L. A. J. O'Neill, 'Krebs Cycle Reborn in Macrophage Immunometabolism', *Annu. Rev. Immunol.*, vol. 38, pp. 289–313, Apr. 2020, doi: 10.1146/annurev-immunol-081619-104850.

[8] E. M. Pålsson-McDermott and L. A. J. O'Neill, 'Targeting immunometabolism as an anti-inflammatory strategy', *Cell Res.*, vol. 30, no. 4, Art. no. 4, Apr. 2020, doi: 10.1038/s41422-020-0291-z.

[9] H. Huang, L. Long, P. Zhou, N. M. Chapman, and H. Chi, 'mTOR signaling at the crossroads of environmental signals and T-cell fate decisions', *Immunol. Rev.*, vol. 295, no. 1, pp. 15–38, May 2020, doi: 10.1111/imr.12845.

[10] J. Jellusova, 'The role of metabolic checkpoint regulators in B cell survival and transformation', *Immunol. Rev.*, vol. 295, no. 1, pp. 39–53, May 2020, doi: 10.1111/imr.12855.

[11] N. van Teijlingen Bakker and E. J. Pearce, 'Cell-intrinsic metabolic regulation of mononuclear phagocyte activation: Findings from the tip of the iceberg', *Immunol. Rev.*, vol. 295, no. 1, pp. 54–67, May 2020, doi: 10.1111/imr.12848.

[12] E. E. West, N. Kunz, and C. Kemper, 'Complement and human T cell metabolism: Location, location, location', *Immunol. Rev.*, vol. 295, no. 1, pp. 68–81, May 2020, doi: 10.1111/imr.12852.

[13] A. Bahadoran, L. Bezavada, and H. S. Smallwood, 'Fueling influenza and the immune response: Implications for metabolic reprogramming during influenza infection and immunometabolism', *Immunol. Rev.*, vol. 295, no. 1, pp. 140–166, May 2020, doi: 10.1111/imr.12851.

[14] W. J. Turbitt, C. Buchta Rosean, K. S. Weber, and L. A. Norian, 'Obesity and CD8 T cell metabolism: Implications for anti-tumor immunity and cancer immunotherapy outcomes', *Immunol. Rev.*, vol. 295, no. 1, pp. 203–219, May 2020, doi: 10.1111/imr.12849.

[15] H. L. Caslin, M. Bhanot, W. R. Bolus, and A. H. Hasty, 'Adipose tissue macrophages: Unique polarization and bioenergetics in obesity', *Immunol. Rev.*, vol. 295, no. 1, pp. 101–113, May 2020, doi: 10.1111/imr.12853.

[16] C. Li, R. G. Spallanzani, and D. Mathis, 'Visceral adipose tissue Tregs and the cells that nurture them', *Immunol. Rev.*, vol. 295, no. 1, pp. 114–125, May 2020, doi: 10.1111/imr.12850.

[17] H. Wang, C.-H. Lu, and P.-C. Ho, 'Metabolic adaptation orchestrates tissue context-dependent behavior in regulatory T cells', *Immunol. Rev.*, vol. 295, no. 1, pp. 126–139, May

2020, doi: 10.1111/imr.12844.
[18] ‘Microbiome, bile acids, and obesity: How microbially modified metabolites shape anti-tumor immunity - Sipe - 2020 - Immunological Reviews - Wiley Online Library’, vol. 295, no. 1, pp. 220–239, doi: 10.1111/imr.12856.
[19] P. J. Siska, K. Singer, K. Evert, K. Renner, and M. Kreutz, ‘The immunological Warburg effect: Can a metabolic-tumor-stroma score (MeTS) guide cancer immunotherapy?’, *Immunol. Rev.*, vol. 295, no. 1, pp. 187–202, May 2020, doi: 10.1111/imr.12846.
[20] X. Teng, J. Brown, S.-C. Choi, W. Li, and L. Morel, ‘Metabolic determinants of lupus pathogenesis’, *Immunol. Rev.*, vol. 295, no. 1, pp. 167–186, May 2020, doi: 10.1111/imr.12847.
[21] P. J. McGuire, ‘Chemical individuality in T cells: A Garrodian view of immunometabolism’, *Immunol. Rev.*, vol. 295, no. 1, pp. 82–100, May 2020, doi: 10.1111/imr.12854.
[22] Y. Gong, J. Yang, Y. Wang, L. Xue, and J. Wang, ‘Metabolic factors contribute to T-cell inhibition in the ovarian cancer ascites’, *Int. J. Cancer*, vol. 147, no. 7, pp. 1768–1777, 2020, doi: 10.1002/ijc.32990.
[23] O. Warburg, F. Wind, and E. Negelein, ‘THE METABOLISM OF TUMORS IN THE BODY’, *J. Gen. Physiol.*, vol. 8, no. 6, pp. 519–530, Mar. 1927, doi: 10.1085/jgp.8.6.519.
[24] D. Hanahan and R. A. Weinberg, ‘Hallmarks of cancer: the next generation’, *Cell*, vol. 144, no. 5, pp. 646–674, Mar. 2011, doi: 10.1016/j.cell.2011.02.013.
[25] S. Weinhouse, ‘The Warburg hypothesis fifty years later’, *Z. Für Krebsforsch. Klin. Onkol.*, vol. 87, no. 2, pp. 115–126, Jan. 1976, doi: 10.1007/BF00284370.
[26] R. J. DeBerardinis and N. S. Chandel, ‘We need to talk about the Warburg effect’, *Nat. Metab.*, vol. 2, no. 2, Art. no. 2, Feb. 2020, doi: 10.1038/s42255-020-0172-2.
[27] S. Pavlides *et al.*, ‘The reverse Warburg effect: aerobic glycolysis in cancer associated fibroblasts and the tumor stroma’, *Cell Cycle Georget. Tex*, vol. 8, no. 23, pp. 3984–4001, Dec. 2009, doi: 10.4161/cc.8.23.10238.
[28] C. Hu, Y. Xuan, X. Zhang, Y. Liu, S. Yang, and K. Yang, ‘Immune cell metabolism and metabolic reprogramming’, *Mol. Biol. Rep.*, vol. 49, no. 10, pp. 9783–9795, Oct. 2022, doi: 10.1007/s11033-022-07474-2.
[29] M. G. Vander Heiden, L. C. Cantley, and C. B. Thompson, ‘Understanding the Warburg Effect: The Metabolic Requirements of Cell Proliferation’, *Science*, vol. 324, no. 5930, pp. 1029–1033, May 2009, doi: 10.1126/science.1160809.
[30] M. V. Liberti and J. W. Locasale, ‘The Warburg Effect: How Does it Benefit Cancer Cells?’, *Trends Biochem. Sci.*, vol. 41, no. 3, pp. 211–218, Mar. 2016, doi: 10.1016/j.tibs.2015.12.001.
[31] J. W. Locasale and L. C. Cantley, ‘Altered metabolism in cancer’, *BMC Biol.*, vol. 8, p. 88, Jun. 2010, doi: 10.1186/1741-7007-8-88.
[32] F. M. Marelli-Berg, H. Fu, and C. Mauro, ‘Molecular mechanisms of metabolic reprogramming in proliferating cells: implications for T-cell-mediated immunity’, *Immunology*, vol. 136, no. 4, pp. 363–369, 2012, doi: 10.1111/j.1365-2567.2012.03583.x.
[33] R. J. DeBerardinis, J. J. Lum, G. Hatzivassiliou, and C. B. Thompson, ‘The biology of cancer: metabolic reprogramming fuels cell growth and proliferation’, *Cell Metab.*, vol. 7, no. 1, pp. 11–20, Jan. 2008, doi: 10.1016/j.cmet.2007.10.002.
[34] Y. Li, Z. Sha, and H. Peng, ‘Metabolic Reprogramming in Kidney Diseases: Evidence and Therapeutic Opportunities’, *Int. J. Nephrol.*, vol. 2021, p. 5497346, Oct. 2021, doi: 10.1155/2021/5497346.
[35] C. N. S. Allen, S. P. Arjona, M. Santerre, and B. E. Sawaya, ‘Hallmarks of Metabolic Reprogramming and Their Role in Viral Pathogenesis’, *Viruses*, vol. 14, no. 3, p. 602, Mar. 2022, doi: 10.3390/v14030602.
[36] M. Rudiansyah *et al.*, ‘Coronavirus disease 2019 (COVID-19) update: From

metabolic reprogramming to immunometabolism', *J. Med. Virol.*, vol. 94, no. 10, pp. 4611–4627, Oct. 2022, doi: 10.1002/jmv.27929.
[37] 'Cancer [World Health Organization]'. https://www.who.int/news-room/fact-sheets/detail/cancer (accessed Jun. 29, 2023).
[38] H. Sung *et al.*, 'Global Cancer Statistics 2020: GLOBOCAN Estimates of Incidence and Mortality Worldwide for 36 Cancers in 185 Countries', *CA. Cancer J. Clin.*, vol. 71, no. 3, pp. 209–249, 2021, doi: 10.3322/caac.21660.
[39] R. L. Siegel, K. D. Miller, N. S. Wagel, and A. Jemal, 'Cancer statistics, 2023', *Cancer J. Clin.*, vol. 73, no. 1, pp. 17–48, Jan. 2023, doi: 10.3322/caac.21763.
[40] 'Pathogenesis of cancer'. https://www.slideshare.net/jaineeljd007/pathogenesis-of-cancer (accessed Jun. 30, 2023).
[41] D. Hanahan and R. A. Weinberg, 'The Hallmarks of Cancer', *Cell*, vol. 100, no. 1, pp. 57–70, Jan. 2000, doi: 10.1016/S0092-8674(00)81683-9.
[42] R. Baghban *et al.*, 'Tumor microenvironment complexity and therapeutic implications at a glance', *Cell Commun. Signal.*, vol. 18, no. 1, p. 59, Apr. 2020, doi: 10.1186/s12964-020-0530-4.
[43] 'Genes and Cancer', *Cancer.Net*, Mar. 26, 2012. https://www.cancer.net/navigating-cancer-care/cancer-basics/genetics/genes-and-cancer (accessed Jun. 30, 2023).
[44] 'The Genetics of Cancer [NCI]', Apr. 22, 2015. https://www.cancer.gov/about-cancer/causes-prevention/genetics (accessed Jun. 30, 2023).
[45] 'Environmental Mutagens and Gene Expression | Learn Science at Scitable'. http://www.nature.com/scitable/topicpage/environmental-mutagens-cell-signalling-and-dna-repair-1090 (accessed Jun. 30, 2023).
[46] 'World Cancer Day [World Health Organization]'. https://www.who.int/europe/news/item/03-02-2021-world-cancer-day-know-the-facts-tobacco-and-alcohol-both-cause-cancer (accessed Jun. 30, 2023).
[47] P. Boffetta, M. Hashibe, C. La Vecchia, W. Zatonski, and J. Rehm, 'The burden of cancer attributable to alcohol drinking', *Int. J. Cancer*, vol. 119, no. 4, pp. 884–887, Aug. 2006, doi: 10.1002/ijc.21903.
[48] C. Maltoni, F. Minardi, and J. F. Holland, 'Physical Carcinogens', in *Holland-Frei Cancer Medicine. 5th edition*, BC Decker, 2000. Accessed: Jun. 30, 2023. [Online]. Available: https://www.ncbi.nlm.nih.gov/books/NBK20770/
[49] M. Nasterlack, 'Pesticides and childhood cancer: An update', *Int. J. Hyg. Environ. Health*, vol. 210, no. 5, pp. 645–657, Oct. 2007, doi: 10.1016/j.ijheh.2007.03.001.
[50] J. B. Liao, 'Viruses and human cancer', *Yale J. Biol. Med.*, vol. 79, no. 3–4, pp. 115–122, Dec. 2006.
[51] P. Anand *et al.*, 'Cancer is a preventable disease that requires major lifestyle changes', *Pharm. Res.*, vol. 25, no. 9, pp. 2097–2116, Sep. 2008, doi: 10.1007/s11095-008-9661-9.
[52] L. H. Kushi *et al.*, 'American Cancer Society Guidelines on Nutrition and Physical Activity for cancer prevention: reducing the risk of cancer with healthy food choices and physical activity', *CA. Cancer J. Clin.*, vol. 56, no. 5, pp. 254–281; quiz 313–314, 2006, doi: 10.3322/canjclin.56.5.254.
[53] L. Zhong *et al.*, 'Small molecules in targeted cancer therapy: advances, challenges, and future perspectives', *Signal Transduct. Target. Ther.*, vol. 6, no. 1, Art. no. 1, May 2021, doi: 10.1038/s41392-021-00572-w.
[54] D. Zahavi and L. Weiner, 'Monoclonal Antibodies in Cancer Therapy', *Antibodies*, vol. 9, no. 3, p. 34, Jul. 2020, doi: 10.3390/antib9030034.
[55] G. Housman *et al.*, 'Drug Resistance in Cancer: An Overview', *Cancers*, vol. 6, no. 3, pp. 1769–1792, Sep. 2014, doi: 10.3390/cancers6031769.
[56] 'Why Do Cancer Treatments Stop Working? [NCI]', Dec. 21, 2016. https://www.cancer.gov/about-cancer/treatment/research/drug-combo-resistance (accessed

Jun. 30, 2023).
[57] O. De Wever and M. Mareel, 'Role of tissue stroma in cancer cell invasion', *J. Pathol.*, vol. 200, no. 4, pp. 429–447, 2003, doi: 10.1002/path.1398.
[58] N. A. Giraldo *et al.*, 'The clinical role of the TME in solid cancer', *Br. J. Cancer*, vol. 120, no. 1, Art. no. 1, Jan. 2019, doi: 10.1038/s41416-018-0327-z.
[59] C. M. Neophytou, M. Panagi, T. Stylianopoulos, and P. Papageorgis, 'The Role of Tumor Microenvironment in Cancer Metastasis: Molecular Mechanisms and Therapeutic Opportunities', *Cancers*, vol. 13, no. 9, Art. no. 9, Jan. 2021, doi: 10.3390/cancers13092053.
[60] S. Guo and C.-X. Deng, 'Effect of Stromal Cells in Tumor Microenvironment on Metastasis Initiation', *Int. J. Biol. Sci.*, vol. 14, no. 14, pp. 2083–2093, Nov. 2018, doi: 10.7150/ijbs.25720.
[61] N. M. Anderson and M. C. Simon, 'Tumor Microenvironment', *Curr. Biol. CB*, vol. 30, no. 16, pp. R921–R925, Aug. 2020, doi: 10.1016/j.cub.2020.06.081.
[62] Q. Ping *et al.*, 'Cancer-associated fibroblasts: overview, progress, challenges, and directions', *Cancer Gene Ther.*, vol. 28, no. 9, Art. no. 9, Sep. 2021, doi: 10.1038/s41417-021-00318-4.
[63] P. J. Asif, C. Longobardi, M. Hahne, and J. P. Medema, 'The Role of Cancer-Associated Fibroblasts in Cancer Invasion and Metastasis', *Cancers*, vol. 13, no. 18, p. 4720, Sep. 2021, doi: 10.3390/cancers13184720.
[64] R. S. Joshi, S. S. Kanugula, S. Sudhir, M. P. Pereira, S. Jain, and M. K. Aghi, 'The Role of Cancer-Associated Fibroblasts in Tumor Progression', *Cancers*, vol. 13, no. 6, Art. no. 6, Jan. 2021, doi: 10.3390/cancers13061399.
[65] T. Simon and B. Salhia, 'Cancer-Associated Fibroblast Subpopulations With Diverse and Dynamic Roles in the Tumor Microenvironment', *Mol. Cancer Res. MCR*, vol. 20, no. 2, pp. 183–192, Feb. 2022, doi: 10.1158/1541-7786.MCR-21-0282.
[66] F.-T. Wang, W. Sun, J.-T. Zhang, and Y.-Z. Fan, 'Cancer-associated fibroblast regulation of tumor neo-angiogenesis as a therapeutic target in cancer', *Oncol. Lett.*, vol. 17, no. 3, pp. 3055–3065, Mar. 2019, doi: 10.3892/ol.2019.9973.
[67] A. Costa *et al.*, 'Fibroblast Heterogeneity and Immunosuppressive Environment in Human Breast Cancer', *Cancer Cell*, vol. 33, no. 3, pp. 463-479.e10, Mar. 2018, doi: 10.1016/j.ccell.2018.01.011.
[68] S. Madar, I. Goldstein, and V. Rotter, ''Cancer associated fibroblasts'--more than meets the eye', *Trends Mol. Med.*, vol. 19, no. 8, pp. 447–453, Aug. 2013, doi: 10.1016/j.molmed.2013.05.004.
[69] A. Arina *et al.*, 'Tumor-associated fibroblasts predominantly come from local and not circulating precursors', *Proc. Natl. Acad. Sci.*, vol. 113, no. 27, pp. 7551–7556, Jul. 2016, doi: 10.1073/pnas.1600363113.
[70] O. W. Petersen *et al.*, 'Epithelial to Mesenchymal Transition in Human Breast Cancer Can Provide a Nonmalignant Stroma', *Am. J. Pathol.*, vol. 162, no. 2, pp. 391–402, Feb. 2003, doi: 10.1016/S0002-9440(10)63834-5.
[71] E. M. Zeisberg, S. Potenta, L. Xie, M. Zeisberg, and R. Kalluri, 'Discovery of Endothelial to Mesenchymal Transition as a Source for Carcinoma-Associated Fibroblasts', *Cancer Res.*, vol. 67, no. 21, pp. 10123–10128, Nov. 2007, doi: 10.1158/0008-5472.CAN-07-3127.
[72] B. G. Cuiffo and A. E. Karnoub, 'Mesenchymal stem cells in tumor development', *Cell Adhes. Migr.*, vol. 6, no. 3, pp. 220–230, May 2012, doi: 10.4161/cam.20875.
[73] N. C. Direkze *et al.*, 'Bone Marrow Contribution to Tumor-Associated Myofibroblasts and Fibroblasts', *Cancer Res.*, vol. 64, no. 23, pp. 8492–8495, Dec. 2004, doi: 10.1158/0008-5472.CAN-04-1708.
[74] M. Quante *et al.*, 'Bone Marrow-Derived Myofibroblasts Contribute to the Mesenchymal Stem Cell Niche and Promote Tumor Growth', *Cancer Cell*, vol. 19, no. 2, pp. 257–272, Feb. 2011, doi: 10.1016/j.ccr.2011.01.020.
[75] R. Kanzaki and K. Pietras, 'Heterogeneity of cancer-associated fibroblasts:

Opportunities for precision medicine', *Cancer Sci.*, vol. 111, no. 8, pp. 2708–2717, Aug. 2020, doi: 10.1111/cas.14537.
[76] Y. Chen, K. M. McAndrews, and R. Kalluri, 'Clinical and therapeutic relevance of cancer-associated fibroblasts', *Nat. Rev. Clin. Oncol.*, vol. 18, no. 12, pp. 792–804, Dec. 2021, doi: 10.1038/s41571-021-00546-5.
[77] C. Bonneau *et al.*, 'A subset of activated fibroblasts is associated with distant relapse in early luminal breast cancer', *Breast Cancer Res.*, vol. 22, no. 1, p. 76, Jul. 2020, doi: 10.1186/s13058-020-01311-9.
[78] L. Yu, X. Chen, X. Sun, L. Wang, and S. Chen, 'The Glycolytic Switch in Tumors: How Many Players Are Involved?', *J. Cancer*, vol. 8, no. 17, pp. 3430–3440, Sep. 2017, doi: 10.7150/jca.21125.
[79] L. M. Becker *et al.*, 'Epigenetic Reprogramming of Cancer-Associated Fibroblasts Deregulates Glucose Metabolism and Facilitates Progression of Breast Cancer', *Cell Rep.*, vol. 31, no. 9, p. 107701, Jun. 2020, doi: 10.1016/j.celrep.2020.107701.
[80] T. Fiaschi *et al.*, 'Reciprocal Metabolic Reprogramming through Lactate Shuttle Coordinately Influences Tumor-Stroma Interplay', *Cancer Res.*, vol. 72, no. 19, pp. 5130–5140, Sep. 2012, doi: 10.1158/0008-5472.CAN-12-1949.
[81] D. Zhang *et al.*, 'Metabolic Reprogramming of Cancer-Associated Fibroblasts by IDH3α Downregulation', *Cell Rep.*, vol. 10, no. 8, pp. 1335–1348, Mar. 2015, doi: 10.1016/j.celrep.2015.02.006.
[82] P. Porporato, R. Dadhich, S. Dhup, T. Copetti, and P. Sonveaux, 'Anticancer Targets in the Glycolytic Metabolism of Tumors: A Comprehensive Review', *Front. Pharmacol.*, vol. 2, 2011, Accessed: Jul. 03, 2023. [Online]. Available: https://www.frontiersin.org/articles/10.3389/fphar.2011.00049
[83] T. Bertero *et al.*, 'Tumor-stroma mechanics coordinate amino acid availability to sustain tumor growth and malignancy', *Cell Metab.*, vol. 29, no. 1, pp. 124-140.e10, Jan. 2019, doi: 10.1016/j.cmet.2018.09.012.
[84] R. D. Leone *et al.*, 'Glutamine blockade induces divergent metabolic programs to overcome tumor immune evasion', *Science*, vol. 366, no. 6468, pp. 1013–1021, Nov. 2019, doi: 10.1126/science.aav2588.
[85] Y. Zhang *et al.*, 'Suppression of Tumor Energy Supply by Liposomal Nanoparticle-Mediated Inhibition of Aerobic Glycolysis', *ACS Appl. Mater. Interfaces*, vol. 10, no. 3, pp. 2347–2353, Jan. 2018, doi: 10.1021/acsami.7b16685.
[86] L. M. Phan, S.-C. J. Yeung, and M.-H. Lee, 'Cancer metabolic reprogramming: importance, main features, and potentials for precise targeted anti-cancer therapies', *Cancer Biol. Med.*, vol. 11, no. 1, pp. 1–19, Mar. 2014, doi: 10.7497/j.issn.2095-3941.2014.01.001.
[87] B. Dwarakanath and V. Jain, 'Targeting glucose metabolism with 2-deoxy-D-glucose for improving cancer therapy', *Future Oncol. Lond. Engl.*, vol. 5, no. 5, pp. 581–585, Jun. 2009, doi: 10.2217/fon.09.44.
[88] G. S. Price, R. L. Page, J. E. Riviere, J. M. Cline, and D. E. Thrall, 'Pharmacokinetics and toxicity of oral and intravenous lonidamine in dogs', *Cancer Chemother. Pharmacol.*, vol. 38, no. 2, pp. 129–135, 1996, doi: 10.1007/s002800050460.
[89] Y. Liu *et al.*, 'A Small-Molecule Inhibitor of Glucose Transporter 1 Downregulates Glycolysis, Induces Cell-Cycle Arrest, and Inhibits Cancer Cell Growth In Vitro and In Vivo', *Mol. Cancer Ther.*, vol. 11, no. 8, pp. 1672–1682, Aug. 2012, doi: 10.1158/1535-7163.MCT-12-0131.
[90] T. E. Wood *et al.*, 'A novel inhibitor of glucose uptake sensitizes cells to FAS-induced cell death', *Mol. Cancer Ther.*, vol. 7, no. 11, pp. 3546–3555, Nov. 2008, doi: 10.1158/1535-7163.MCT-08-0569.
[91] K.-H. Wu *et al.*, 'The apple polyphenol phloretin inhibits breast cancer cell migration and proliferation via inhibition of signals by type 2 glucose transporter', *J. Food Drug Anal.*, vol. 26, no. 1, pp. 221–231, Jan. 2018, doi: 10.1016/j.jfda.2017.03.009.
[92] Y. Li *et al.*, 'Succinate/NLRP3 Inflammasome Induces Synovial Fibroblast

Activation: Therapeutical Effects of Clematichinenoside AR on Arthritis', *Front. Immunol.*, vol. 7, 2016, Accessed: Jul. 03, 2023. [Online]. Available: https://www.frontiersin.org/articles/10.3389/fimmu.2016.00532
[93] C.-H. Wu *et al.*, 'In vitro and in vivo study of phloretin-induced apoptosis in human liver cancer cells involving inhibition of type II glucose transporter', *Int. J. Cancer*, vol. 124, no. 9, pp. 2210–2219, May 2009, doi: 10.1002/ijc.24189.
[94] W. W. Wheaton *et al.*, 'Metformin inhibits mitochondrial complex I of cancer cells to reduce tumorigenesis', *eLife*, vol. 3, p. e02242, May 2014, doi: 10.7554/eLife.02242.
[95] X. Liu, I. L. Romero, L. M. Litchfield, E. Lengyel, and J. W. Locasale, 'Metformin Targets Central Carbon Metabolism and Reveals Mitochondrial Requirements in Human Cancers', *Cell Metab.*, vol. 24, no. 5, pp. 728–739, Nov. 2016, doi: 10.1016/j.cmet.2016.09.005.
[96] S. Gurrapu *et al.*, 'Monocarboxylate Transporter 1 Inhibitors as Potential Anticancer Agents', *ACS Med. Chem. Lett.*, vol. 6, no. 5, pp. 558–561, May 2015, doi: 10.1021/acsmedchemlett.5b00049.
[97] U. E. Martinez-Outschoorn *et al.*, 'Oxidative stress in cancer associated fibroblasts drives tumor-stroma co-evolution', *Cell Cycle*, vol. 9, no. 16, pp. 3276–3296, Aug. 2010, doi: 10.4161/cc.9.16.12553.
[98] S. Crawford, 'Anti-inflammatory/antioxidant use in long-term maintenance cancer therapy: a new therapeutic approach to disease progression and recurrence', *Ther. Adv. Med. Oncol.*, vol. 6, no. 2, pp. 52–68, Mar. 2014, doi: 10.1177/1758834014521111.
[99] Y. Fu *et al.*, 'The reverse Warburg effect is likely to be an Achilles' heel of cancer that can be exploited for cancer therapy', *Oncotarget*, vol. 8, no. 34, pp. 57813–57825, Aug. 2017, doi: 10.18632/oncotarget.18175.
[100] A. Le *et al.*, 'Inhibition of lactate dehydrogenase A induces oxidative stress and inhibits tumor progression', *Proc. Natl. Acad. Sci.*, vol. 107, no. 5, pp. 2037–2042, Feb. 2010, doi: 10.1073/pnas.0914433107.
[101] L. Wilde *et al.*, 'Metabolic coupling and the Reverse Warburg Effect in cancer: Implications for novel biomarker and anticancer agent development', *Semin. Oncol.*, vol. 44, no. 3, pp. 198–203, Jun. 2017, doi: 10.1053/j.seminoncol.2017.10.004.
[102] D. Monti *et al.*, 'Pilot study demonstrating metabolic and anti-proliferative effects of in vivo anti-oxidant supplementation with N-Acetylcysteine in Breast Cancer', *Semin. Oncol.*, vol. 44, no. 3, pp. 226–232, Jun. 2017, doi: 10.1053/j.seminoncol.2017.10.001.
[103] Z. Zhao, F. Han, S. Yang, J. Wu, and W. Zhan, 'Oxamate-mediated inhibition of lactate dehydrogenase induces protective autophagy in gastric cancer cells: Involvement of the Akt–mTOR signaling pathway', *Cancer Lett.*, vol. 358, no. 1, pp. 17–26, Mar. 2015, doi: 10.1016/j.canlet.2014.11.046.
[104] C. B. Colen *et al.*, 'Metabolic targeting of lactate efflux by malignant glioma inhibits invasiveness and induces necrosis: an in vivo study', *Neoplasia N. Y. N*, vol. 13, no. 7, pp. 620–632, Jul. 2011, doi: 10.1593/neo.11134.
[105] S. P. Mathupala, C. B. Colen, P. Parajuli, and A. E. Sloan, 'Lactate and malignant tumors: A therapeutic target at the end stage of glycolysis', *J. Bioenerg. Biomembr.*, vol. 39, no. 1, pp. 73–77, Feb. 2007, doi: 10.1007/s10863-006-9062-x.
[106] P. Cirri and P. Chiarugi, 'Cancer-associated-fibroblasts and tumour cells: a diabolic liaison driving cancer progression', *Cancer Metastasis Rev.*, vol. 31, no. 1, pp. 195–208, Jun. 2012, doi: 10.1007/s10555-011-9340-x.
[107] A. Kohlmann *et al.*, 'Fragment Growing and Linking Lead to Novel Nanomolar Lactate Dehydrogenase Inhibitors', *J. Med. Chem.*, vol. 56, no. 3, pp. 1023–1040, Feb. 2013, doi: 10.1021/jm3014844.
[108] J. Papaconstantinou and S. P. Colowick, 'The Role of Glycolysis in the Growth of Tumor Cells: II. THE EFFECT OF OXAMIC ACID ON THE GROWTH OF HELA CELLS IN TISSUE CULTURE', *J. Biol. Chem.*, vol. 236, no. 2, pp. 285–288, Feb. 1961, doi: 10.1016/S0021-9258(18)64353-4.

[109] J. Billiard *et al.*, 'Quinoline 3-sulfonamides inhibit lactate dehydrogenase A and reverse aerobic glycolysis in cancer cells', *Cancer Metab.*, vol. 1, no. 1, p. 19, Sep. 2013, doi: 10.1186/2049-3002-1-19.
[110] R. Rani and V. Kumar, 'Recent Update on Human Lactate Dehydrogenase Enzyme 5 (hLDH5) Inhibitors: A Promising Approach for Cancer Chemotherapy', *J. Med. Chem.*, vol. 59, no. 2, pp. 487–496, Jan. 2016, doi: 10.1021/acs.jmedchem.5b00168.
[111] M. D. Shelley *et al.*, 'Stereo-specific cytotoxic effects of gossypol enantiomers and gossypolone in tumour cell lines', *Cancer Lett.*, vol. 135, no. 2, pp. 171–180, Jan. 1999, doi: 10.1016/S0304-3835(98)00302-4.
[112] M. R. Flack *et al.*, 'Oral gossypol in the treatment of metastatic adrenal cancer', *J. Clin. Endocrinol. Metab.*, vol. 76, no. 4, pp. 1019–1024, Apr. 1993, doi: 10.1210/jcem.76.4.8473376.
[113] C. Van Poznak *et al.*, 'Oral gossypol in the treatment of patients with refractory metastatic breast cancer: a phase I/II clinical trial', *Breast Cancer Res. Treat.*, vol. 66, no. 3, pp. 239–248, Apr. 2001, doi: 10.1023/a:1010686204736.
[114] C. Granchi, I. Paterni, R. Rani, and F. Minutolo, 'Small-molecule inhibitors of human LDH5', *Future Med. Chem.*, vol. 5, no. 16, pp. 1967–1991, Oct. 2013, doi: 10.4155/fmc.13.151.
[115] M. Manerba *et al.*, 'Galloflavin (CAS 568-80-9): a novel inhibitor of lactate dehydrogenase', *ChemMedChem*, vol. 7, no. 2, pp. 311–317, Feb. 2012, doi: 10.1002/cmdc.201100471.
[116] F. Farabegoli, M. Vettraino, M. Manerba, L. Fiume, M. Roberti, and G. Di Stefano, 'Galloflavin, a new lactate dehydrogenase inhibitor, induces the death of human breast cancer cells with different glycolytic attitude by affecting distinct signaling pathways', *Eur. J. Pharm. Sci.*, vol. 47, no. 4, pp. 729–738, Nov. 2012, doi: 10.1016/j.ejps.2012.08.012.
[117] C. Granchi *et al.*, 'Discovery of N-Hydroxyindole-Based Inhibitors of Human Lactate Dehydrogenase Isoform A (LDH-A) as Starvation Agents against Cancer Cells', *J. Med. Chem.*, vol. 54, no. 6, pp. 1599–1612, Mar. 2011, doi: 10.1021/jm101007q.
[118] L. Fiume, M. Manerba, M. Vettraino, and G. Di Stefano, 'Inhibition of lactate dehydrogenase activity as an approach to cancer therapy', *Future Med. Chem.*, vol. 6, no. 4, pp. 429–445, Mar. 2014, doi: 10.4155/fmc.13.206.
[119] M. Maftouh *et al.*, 'Synergistic interaction of novel lactate dehydrogenase inhibitors with gemcitabine against pancreatic cancer cells in hypoxia', *Br. J. Cancer*, vol. 110, no. 1, Art. no. 1, Jan. 2014, doi: 10.1038/bjc.2013.681.
[120] C. C. Schneider *et al.*, 'Metabolic alteration – Overcoming therapy resistance in gastric cancer via PGK-1 inhibition in a combined therapy with standard chemotherapeutics', *Int. J. Surg.*, vol. 22, pp. 92–98, Oct. 2015, doi: 10.1016/j.ijsu.2015.08.020.
[121] J. Chen, J. Xie, Z. Jiang, B. Wang, Y. Wang, and X. Hu, 'Shikonin and its analogs inhibit cancer cell glycolysis by targeting tumor pyruvate kinase-M2', *Oncogene*, vol. 30, no. 42, Art. no. 42, Oct. 2011, doi: 10.1038/onc.2011.137.
[122] M. S. Goldberg and P. A. Sharp, 'Pyruvate kinase M2-specific siRNA induces apoptosis and tumor regression', *J. Exp. Med.*, vol. 209, no. 2, pp. 217–224, Jan. 2012, doi: 10.1084/jem.20111487.
[123] B. Clem *et al.*, 'Small-molecule inhibition of 6-phosphofructo-2-kinase activity suppresses glycolytic flux and tumor growth', *Mol. Cancer Ther.*, vol. 7, no. 1, pp. 110–120, Jan. 2008, doi: 10.1158/1535-7163.MCT-07-0482.
[124] S. Cardaci, E. Desideri, and M. R. Ciriolo, 'Targeting aerobic glycolysis: 3-bromopyruvate as a promising anticancer drug', *J. Bioenerg. Biomembr.*, vol. 44, no. 1, pp. 17–29, Feb. 2012, doi: 10.1007/s10863-012-9422-7.
[125] S. Ganapathy-Kanniappan and J.-F. H. Geschwind, 'Tumor glycolysis as a target for cancer therapy: progress and prospects', *Mol. Cancer*, vol. 12, p. 152, Dec. 2013, doi: 10.1186/1476-4598-12-152.
[126] K. Almutairi, J. Nossent, D. Preen, H. Keen, and C. Inderjeeth, 'The global

prevalence of rheumatoid arthritis: a meta-analysis based on a systematic review', *Rheumatol. Int.*, vol. 41, no. 5, pp. 863–877, May 2021, doi: 10.1007/s00296-020-04731-0.
[127] K. H. Costenbader, S.-C. Chang, F. Laden, R. Puett, and E. W. Karlson, 'Geographic Variation in Rheumatoid Arthritis Incidence among Women in the United States', *Arch. Intern. Med.*, vol. 168, no. 15, pp. 1664–1670, Aug. 2008, doi: 10.1001/archinte.168.15.1664.
[128] Y. Alamanos and A. A. Drosos, 'Epidemiology of adult rheumatoid arthritis', *Autoimmun. Rev.*, vol. 4, no. 3, pp. 130–136, Mar. 2005, doi: 10.1016/j.autrev.2004.09.002.
[129] L. Pina Vegas, J. Drouin, R. Dray-Spira, and A. Weill, 'Prevalence, mortality, and treatment of patients with rheumatoid arthritis: A cohort study of the French National Health Data System, 2010–2019', *Joint Bone Spine*, vol. 90, no. 1, p. 105460, Jan. 2023, doi: 10.1016/j.jbspin.2022.105460.
[130] 'Brief Report: Rheumatoid Arthritis as the Underlying Cause of Death in Thirty-One Countries, 1987–2011: Trend Analysis of World Health Organization Mortality Database', doi: 10.1002/art.40091.
[131] J. S. Smolen *et al.*, 'Rheumatoid arthritis', *Nat. Rev. Dis. Primer*, vol. 4, no. 1, Art. no. 1, Feb. 2018, doi: 10.1038/nrdp.2018.1.
[132] J. Morović-Vergles, '[Pathophysiology of rheumatoid arthritis]', *Reumatizam*, vol. 50, no. 2, pp. 15–17, 2003.
[133] M. S. Akram *et al.*, 'Challenges for biosimilars: focus on rheumatoid arthritis', *Crit. Rev. Biotechnol.*, vol. 41, no. 1, pp. 121–153, Jan. 2021, doi: 10.1080/07388551.2020.1830746.
[134] J. S. Smolen, D. Aletaha, M. Koeller, M. H. Weisman, and P. Emery, 'New therapies for treatment of rheumatoid arthritis', *Lancet Lond. Engl.*, vol. 370, no. 9602, pp. 1861–1874, Dec. 2007, doi: 10.1016/S0140-6736(07)60784-3.
[135] J. L. Newton, S. M. J. Harney, B. P. Wordsworth, and M. A. Brown, 'A review of the MHC genetics of rheumatoid arthritis', *Genes Immun.*, vol. 5, no. 3, pp. 151–157, May 2004, doi: 10.1038/sj.gene.6364045.
[136] I. B. McInnes and G. Schett, 'The pathogenesis of rheumatoid arthritis', *N. Engl. J. Med.*, vol. 365, no. 23, pp. 2205–2219, Dec. 2011, doi: 10.1056/NEJMra1004965.
[137] N. Bottini and G. S. Firestein, 'Epigenetics in rheumatoid arthritis: a primer for rheumatologists', *Curr. Rheumatol. Rep.*, vol. 15, no. 11, p. 372, Nov. 2013, doi: 10.1007/s11926-013-0372-9.
[138] K. P. Liao, L. Alfredsson, and E. W. Karlson, 'Environmental influences on risk for rheumatoid arthritis', *Curr. Opin. Rheumatol.*, vol. 21, no. 3, pp. 279–283, May 2009, doi: 10.1097/BOR.0b013e32832a2e16.
[139] L. Klareskog, P. K. Gregersen, and T. W. J. Huizinga, 'Prevention of autoimmune rheumatic disease: state of the art and future perspectives', *Ann. Rheum. Dis.*, vol. 69, no. 12, pp. 2062–2066, Dec. 2010, doi: 10.1136/ard.2010.142109.
[140] A. Alsaber *et al.*, 'Influence of Ambient Air Pollution on Rheumatoid Arthritis Disease Activity Score Index', *Int. J. Environ. Res. Public. Health*, vol. 17, no. 2, Art. no. 2, Jan. 2020, doi: 10.3390/ijerph17020416.
[141] S.-C. Bae and Y. H. Lee, 'Causal association between body mass index and risk of rheumatoid arthritis: A Mendelian randomization study', *Eur. J. Clin. Invest.*, vol. 49, no. 4, p. e13076, 2019, doi: 10.1111/eci.13076.
[142] J. S. Lawrence, 'Heberden Oration, 1969. Rheumatoid arthritis--nature or nurture?', *Ann. Rheum. Dis.*, vol. 29, no. 4, pp. 357–379, Jul. 1970, doi: 10.1136/ard.29.4.357.
[143] 'Rheumatoid Arthritis and Pregnancy: Effects of Pregnancy on Rheumatoid Arthritis, Preconception Counseling, Peripartum Concerns', Oct. 2022, Accessed: Jul. 03, 2023. [Online]. Available: https://emedicine.medscape.com/article/335186-overview
[144] D. Alpízar-Rodríguez, N. Pluchino, G. Canny, C. Gabay, and A. Finckh, 'The role of female hormonal factors in the development of rheumatoid arthritis', *Rheumatology*, vol. 56, no. 8, pp. 1254–1263, Aug. 2017, doi: 10.1093/rheumatology/kew318.
[145] S. Li, Y. Yu, Y. Yue, Z. Zhang, and K. Su, 'Microbial Infection and Rheumatoid

Arthritis', *J. Clin. Cell. Immunol.*, vol. 4, no. 6, p. 174, Dec. 2013, doi: 10.4172/2155-9899.1000174.
[146] V. Yılmaz, E. Umay, İ. Gündoğdu, Z. Ö. Karaahmet, and A. E. Öztürk, 'Rheumatoid Arthritis: Are psychological factors effective in disease flare?', *Eur. J. Rheumatol.*, vol. 4, no. 2, pp. 127–132, Jun. 2017, doi: 10.5152/eurjrheum.2017.16100.
[147] O. Benjamin, A. Goyal, and S. L. Lappin, 'Disease-Modifying Antirheumatic Drugs (DMARD)', in *StatPearls*, Treasure Island (FL): StatPearls Publishing, 2023. Accessed: Jul. 03, 2023. [Online]. Available: http://www.ncbi.nlm.nih.gov/books/NBK507863/
[148] J. R. Vane and R. M. Botting, 'The mechanism of action of aspirin', *Thromb. Res.*, vol. 110, no. 5–6, pp. 255–258, Jun. 2003, doi: 10.1016/s0049-3848(03)00379-7.
[149] E. M. Dennison and C. Cooper, 'Corticosteroids in rheumatoid arthritis', *BMJ*, vol. 316, no. 7134, pp. 789–790, Mar. 1998.
[150] J. Swierkot *et al.*, 'Rheumatoid arthritis in a patient with common variable immunodeficiency: difficulty in diagnosis and therapy', *Clin. Rheumatol.*, vol. 25, no. 1, pp. 92–94, Feb. 2006, doi: 10.1007/s10067-005-1141-6.
[151] M. Bécède *et al.*, 'Risk profiling for a refractory course of rheumatoid arthritis', *Semin. Arthritis Rheum.*, vol. 49, no. 2, pp. 211–217, Oct. 2019, doi: 10.1016/j.semarthrit.2019.02.004.
[152] E. H. Choy, A. F. Kavanaugh, and S. A. Jones, 'The problem of choice: current biologic agents and future prospects in RA', *Nat. Rev. Rheumatol.*, vol. 9, no. 3, pp. 154–163, Mar. 2013, doi: 10.1038/nrrheum.2013.8.
[153] U. Müller-Ladner, C. Ospelt, S. Gay, O. Distler, and T. Pap, 'Cells of the synovium in rheumatoid arthritis. Synovial fibroblasts', *Arthritis Res. Ther.*, vol. 9, no. 6, p. 223, Dec. 2007, doi: 10.1186/ar2337.
[154] N. Bottini and G. S. Firestein, 'Duality of fibroblast-like synoviocytes in RA: passive responders and imprinted aggressors', *Nat. Rev. Rheumatol.*, vol. 9, no. 1, pp. 24–33, Jan. 2013, doi: 10.1038/nrrheum.2012.190.
[155] H. G. Fassbender and M. Simmling-Annefeld, 'The potential aggressiveness of synovial tissue in rheumatoid arthritis', *J. Pathol.*, vol. 139, no. 3, pp. 399–406, 1983, doi: 10.1002/path.1711390314.
[156] C. R. L. Machado *et al.*, 'Morphofunctional analysis of fibroblast-like synoviocytes in human rheumatoid arthritis and mouse collagen-induced arthritis', *Adv. Rheumatol.*, vol. 63, no. 1, p. 1, Jan. 2023, doi: 10.1186/s42358-022-00281-0.
[157] J. D. Turner and A. Filer, 'The role of the synovial fibroblast in rheumatoid arthritis pathogenesis', *Curr. Opin. Rheumatol.*, vol. 27, no. 2, pp. 175–182, Mar. 2015, doi: 10.1097/BOR.0000000000000148.
[158] M. Juarez, A. Filer, and C. D. Buckley, 'Fibroblasts as therapeutic targets in rheumatoid arthritis and cancer', *Swiss Med. Wkly.*, vol. 142, p. w13529, 2012, doi: 10.4414/smw.2012.13529.
[159] S. Hirohata *et al.*, 'Induction of fibroblast-like cells from CD34(+) progenitor cells of the bone marrow in rheumatoid arthritis', *J. Leukoc. Biol.*, vol. 70, no. 3, pp. 413–421, Sep. 2001.
[160] J. Ohata *et al.*, 'Fibroblast-like synoviocytes of mesenchymal origin express functional B cell-activating factor of the TNF family in response to proinflammatory cytokines', *J. Immunol. Baltim. Md 1950*, vol. 174, no. 2, pp. 864–870, Jan. 2005, doi: 10.4049/jimmunol.174.2.864.
[161] Z. Wu *et al.*, 'Fibroblast-like synoviocytes in rheumatoid arthritis: Surface markers and phenotypes', *Int. Immunopharmacol.*, vol. 93, p. 107392, Apr. 2021, doi: 10.1016/j.intimp.2021.107392.
[162] D. N. Dorst *et al.*, 'Targeting of fibroblast activation protein in rheumatoid arthritis patients: imaging and ex vivo photodynamic therapy', *Rheumatol. Oxf. Engl.*, vol. 61, no. 7, pp. 2999–3009, Aug. 2021, doi: 10.1093/rheumatology/keab664.
[163] S. E. Gabriel and C. S. Crowson, 'Risk factors for cardiovascular disease in

rheumatoid arthritis', *Curr. Opin. Rheumatol.*, vol. 24, no. 2, pp. 171–176, Mar. 2012, doi: 10.1097/BOR.0b013e32834ff2fd.
[164] E. Gremese and G. Ferraccioli, 'The metabolic syndrome: the crossroads between rheumatoid arthritis and cardiovascular risk', *Autoimmun. Rev.*, vol. 10, no. 10, pp. 582–589, Aug. 2011, doi: 10.1016/j.autrev.2011.04.018.
[165] P. G. de Oliveira, M. Farinon, E. Sanchez-Lopez, S. Miyamoto, and M. Guma, 'Fibroblast-Like Synoviocytes Glucose Metabolism as a Therapeutic Target in Rheumatoid Arthritis', *Front. Immunol.*, vol. 10, p. 1743, Aug. 2019, doi: 10.3389/fimmu.2019.01743.
[166] S. A. Clayton, L. MacDonald, M. Kurowska-Stolarska, and A. R. Clark, 'Mitochondria as Key Players in the Pathogenesis and Treatment of Rheumatoid Arthritis', *Front. Immunol.*, vol. 12, 2021, Accessed: Jul. 03, 2023. [Online]. Available: https://www.frontiersin.org/articles/10.3389/fimmu.2021.673916
[167] S. P. Young *et al.*, 'The impact of inflammation on metabolomic profiles in patients with arthritis', *Arthritis Rheum.*, vol. 65, no. 8, pp. 2015–2023, Aug. 2013, doi: 10.1002/art.38021.
[168] C. Ma, J. Wang, F. Hong, and S. Yang, 'Mitochondrial Dysfunction in Rheumatoid Arthritis', *Biomolecules*, vol. 12, no. 9, p. 1216, Sep. 2022, doi: 10.3390/biom12091216.
[169] S. Takahashi *et al.*, 'Glutaminase 1 plays a key role in the cell growth of fibroblast-like synoviocytes in rheumatoid arthritis', *Arthritis Res. Ther.*, vol. 19, no. 1, p. 76, Apr. 2017, doi: 10.1186/s13075-017-1283-3.
[170] M. Guma *et al.*, 'Choline kinase inhibition in rheumatoid arthritis', *Ann. Rheum. Dis.*, vol. 74, no. 7, pp. 1399–1407, Jul. 2015, doi: 10.1136/annrheumdis-2014-205696.
[171] A. Ramírez de Molina *et al.*, 'Choline kinase as a link connecting phospholipid metabolism and cell cycle regulation: Implications in cancer therapy', *Int. J. Biochem. Cell Biol.*, vol. 40, no. 9, pp. 1753–1763, Jan. 2008, doi: 10.1016/j.biocel.2008.01.013.
[172] K. Glunde, Z. M. Bhujwalla, and S. M. Ronen, 'Choline metabolism in malignant transformation', *Nat. Rev. Cancer*, vol. 11, no. 12, pp. 835–848, Nov. 2011, doi: 10.1038/nrc3162.
[173] U. Fearon, M. M. Hanlon, S. M. Wade, and J. M. Fletcher, 'Altered metabolic pathways regulate synovial inflammation in rheumatoid arthritis', *Clin. Exp. Immunol.*, vol. 197, no. 2, pp. 170–180, Aug. 2019, doi: 10.1111/cei.13228.
[174] G. Abboud, S.-C. Choi, N. Kanda, L. Zeumer-Spataro, D. C. Roopenian, and L. Morel, 'Inhibition of Glycolysis Reduces Disease Severity in an Autoimmune Model of Rheumatoid Arthritis', *Front. Immunol.*, vol. 9, p. 1973, 2018, doi: 10.3389/fimmu.2018.01973.
[175] G. Song *et al.*, 'Inhibition of hexokinases holds potential as treatment strategy for rheumatoid arthritis', *Arthritis Res. Ther.*, vol. 21, no. 1, p. 87, Apr. 2019, doi: 10.1186/s13075-019-1865-3.
[176] Y. Zhao, X. Yan, X. Li, Y. Zheng, S. Li, and X. Chang, 'PGK1, a glucose metabolism enzyme, may play an important role in rheumatoid arthritis', *Inflamm. Res.*, vol. 65, no. 10, pp. 815–825, Oct. 2016, doi: 10.1007/s00011-016-0965-7.
[177] R. Garcia-Carbonell *et al.*, 'Critical Role of Glucose Metabolism in Rheumatoid Arthritis Fibroblast-like Synoviocytes', *Arthritis Rheumatol.*, vol. 68, no. 7, pp. 1614–1626, 2016, doi: 10.1002/art.39608.
[178] M. F. Bustamante *et al.*, 'Hexokinase 2 as a novel selective metabolic target for rheumatoid arthritis', *Ann. Rheum. Dis.*, vol. 77, no. 11, pp. 1636–1643, Nov. 2018, doi: 10.1136/annrheumdis-2018-213103.
[179] T. Okano *et al.*, '3-bromopyruvate ameliorate autoimmune arthritis by modulating Th17/Treg cell differentiation and suppressing dendritic cell activation', *Sci. Rep.*, vol. 7, no. 1, Art. no. 1, Feb. 2017, doi: 10.1038/srep42412.
[180] T. McGarry *et al.*, 'JAK/STAT Blockade Alters Synovial Bioenergetics, Mitochondrial Function, and Proinflammatory Mediators in Rheumatoid Arthritis', *Arthritis Rheumatol.*, vol. 70, no. 12, pp. 1959–1970, 2018, doi: 10.1002/art.40569.

[181] M. Biniecka *et al.*, 'Dysregulated bioenergetics: a key regulator of joint inflammation', *Ann. Rheum. Dis.*, vol. 75, no. 12, pp. 2192–2200, Dec. 2016, doi: 10.1136/annrheumdis-2015-208476.
[182] H.-J. Son *et al.*, 'Metformin attenuates experimental autoimmune arthritis through reciprocal regulation of Th17/Treg balance and osteoclastogenesis', *Mediators Inflamm.*, vol. 2014, p. 973986, 2014, doi: 10.1155/2014/973986.
[183] W. Fujii *et al.*, 'Monocarboxylate transporter 4, associated with the acidification of synovial fluid, is a novel therapeutic target for inflammatory arthritis', *Arthritis Rheumatol. Hoboken NJ*, vol. 67, no. 11, pp. 2888–2896, Nov. 2015, doi: 10.1002/art.39270.
[184] Y. Zou *et al.*, 'Inhibition of 6-phosphofructo-2-kinase suppresses fibroblast-like synoviocytes-mediated synovial inflammation and joint destruction in rheumatoid arthritis', *Br. J. Pharmacol.*, vol. 174, no. 9, pp. 893–908, May 2017, doi: 10.1111/bph.13762.
[185] S. Trefely *et al.*, 'Kinome Screen Identifies PFKFB3 and Glucose Metabolism as Important Regulators of the Insulin/Insulin-like Growth Factor (IGF)-1 Signaling Pathway', *J. Biol. Chem.*, vol. 290, no. 43, pp. 25834–25846, Oct. 2015, doi: 10.1074/jbc.M115.658815.
[186] Y. Li *et al.*, 'Succinate induces synovial angiogenesis in rheumatoid arthritis through metabolic remodeling and HIF-1α/VEGF axis', *Free Radic. Biol. Med.*, vol. 126, pp. 1–14, Oct. 2018, doi: 10.1016/j.freeradbiomed.2018.07.009.
[187] K. W. Kohn, 'Molecular Interaction Map of the Mammalian Cell Cycle Control and DNA Repair Systems', *Mol. Biol. Cell*, vol. 10, no. 8, pp. 2703–2734, Aug. 1999, doi: 10.1091/mbc.10.8.2703.
[188] K. Shahzad and J. J. Loor, 'Application of Top-Down and Bottom-up Systems Approaches in Ruminant Physiology and Metabolism', *Curr. Genomics*, vol. 13, no. 5, pp. 379–394, Aug. 2012, doi: 10.2174/138920212801619269.
[189] N. L. Novère *et al.*, 'The Systems Biology Graphical Notation', *Nat. Biotechnol.*, vol. 27, no. 8, Art. no. 8, Aug. 2009, doi: 10.1038/nbt.1558.
[190] K. W. Kohn and Y. Pommier, 'Molecular interaction map of the p53 and Mdm2 logic elements, which control the Off–On switch of p53 in response to DNA damage', *Biochem. Biophys. Res. Commun.*, vol. 331, no. 3, pp. 816–827, Jun. 2005, doi: 10.1016/j.bbrc.2005.03.186.
[191] E. Caron *et al.*, 'A comprehensive map of the mTOR signaling network', *Mol. Syst. Biol.*, vol. 6, no. 1, p. 453, Jan. 2010, doi: 10.1038/msb.2010.108.
[192] S. Tripathi *et al.*, 'The gastrin and cholecystokinin receptors mediated signaling network: a scaffold for data analysis and new hypotheses on regulatory mechanisms', *BMC Syst. Biol.*, vol. 9, no. 1, p. 40, Jul. 2015, doi: 10.1186/s12918-015-0181-z.
[193] L. Grieco, L. Calzone, I. Bernard-Pierrot, F. Radvanyi, B. Kahn-Perlès, and D. Thieffry, 'Integrative Modelling of the Influence of MAPK Network on Cancer Cell Fate Decision', *PLOS Comput. Biol.*, vol. 9, no. 10, p. e1003286, Oct. 2013, doi: 10.1371/journal.pcbi.1003286.
[194] M. Ostaszewski *et al.*, 'COVID19 Disease Map, a computational knowledge repository of virus–host interaction mechanisms', *Mol. Syst. Biol.*, vol. 17, no. 10, p. e10387, Oct. 2021, doi: 10.15252/msb.202110387.
[195] 'AsthmaMap: An interactive knowledge repository for mechanisms of asthma', *J. Allergy Clin. Immunol.*, vol. 147, no. 3, pp. 853–856, Mar. 2021, doi: 10.1016/j.jaci.2020.11.032.
[196] C. Pereira *et al.*, 'CyFi-MAP: an interactive pathway-based resource for cystic fibrosis', *Sci. Rep.*, vol. 11, no. 1, Art. no. 1, Nov. 2021, doi: 10.1038/s41598-021-01618-3.
[197] K. A. Fujita *et al.*, 'Integrating Pathways of Parkinson's Disease in a Molecular Interaction Map', *Mol. Neurobiol.*, vol. 49, no. 1, pp. 88–102, Feb. 2014, doi: 10.1007/s12035-013-8489-4.
[198] G. Wu, L. Zhu, J. E. Dent, and C. Nardini, 'A comprehensive molecular interaction map for rheumatoid arthritis', *PloS One*, vol. 5, no. 4, p. e10137, Apr. 2010, doi:

10.1371/journal.pone.0010137.
[199] H. Ogata, S. Goto, K. Sato, W. Fujibuchi, H. Bono, and M. Kanehisa, 'KEGG: Kyoto Encyclopedia of Genes and Genomes', *Nucleic Acids Res.*, vol. 27, no. 1, pp. 29–34, Jan. 1999, doi: 10.1093/nar/27.1.29.
[200] V. Singh *et al.*, 'RA-map: building a state-of-the-art interactive knowledge base for rheumatoid arthritis', *Database J. Biol. Databases Curation*, vol. 2020, p. baaa017, Apr. 2020, doi: 10.1093/database/baaa017.
[201] A. Krämer, J. Green, J. Pollard, and S. Tugendreich, 'Causal analysis approaches in Ingenuity Pathway Analysis', *Bioinforma. Oxf. Engl.*, vol. 30, no. 4, pp. 523–530, Feb. 2014, doi: 10.1093/bioinformatics/btt703.
[202] N. J. Krogan, S. Lippman, D. A. Agard, A. Ashworth, and T. Ideker, 'The cancer cell map initiative: defining the hallmark networks of cancer', *Mol. Cell*, vol. 58, no. 4, pp. 690–698, May 2015, doi: 10.1016/j.molcel.2015.05.008.
[203] O. Rozenblatt-Rosen *et al.*, 'The Human Tumor Atlas Network: Charting Tumor Transitions across Space and Time at Single-Cell Resolution', *Cell*, vol. 181, no. 2, pp. 236–249, Apr. 2020, doi: 10.1016/j.cell.2020.03.053.
[204] I. Kuperstein *et al.*, 'Atlas of Cancer Signalling Network: a systems biology resource for integrative analysis of cancer data with Google Maps', *Oncogenesis*, vol. 4, no. 7, p. e160, Jul. 2015, doi: 10.1038/oncsis.2015.19.
[205] E. A. Bruford *et al.*, 'HUGO Gene Nomenclature Committee (HGNC) recommendations for the designation of gene fusions', *Leukemia*, vol. 35, no. 11, Art. no. 11, Nov. 2021, doi: 10.1038/s41375-021-01436-6.
[206] UniProt Consortium, 'UniProt: the Universal Protein Knowledgebase in 2023', *Nucleic Acids Res.*, vol. 51, no. D1, pp. D523–D531, Jan. 2023, doi: 10.1093/nar/gkac1052.
[207] G. Stelzer *et al.*, 'The GeneCards Suite: From Gene Data Mining to Disease Genome Sequence Analyses', *Curr. Protoc. Bioinforma.*, vol. 54, no. 1, p. 1.30.1-1.30.33, 2016, doi: 10.1002/cpbi.5.
[208] M. Safran *et al.*, 'The GeneCards Suite', in *Practical Guide to Life Science Databases*, I. Abugessaisa and T. Kasukawa, Eds., Singapore: Springer Nature, 2021, pp. 27–56. doi: 10.1007/978-981-16-5812-9_2.
[209] A. Noronha *et al.*, 'ReconMap: an interactive visualization of human metabolism', *Bioinforma. Oxf. Engl.*, vol. 33, no. 4, pp. 605–607, Feb. 2017, doi: 10.1093/bioinformatics/btw667.
[210] J. L. Robinson *et al.*, 'An atlas of human metabolism', *Sci. Signal.*, vol. 13, no. 624, p. eaaz1482, Mar. 2020, doi: 10.1126/scisignal.aaz1482.
[211] A. Saadatpour and R. Albert, 'A comparative study of qualitative and quantitative dynamic models of biological regulatory networks', *EPJ Nonlinear Biomed. Phys.*, vol. 4, no. 1, Art. no. 1, Dec. 2016, doi: 10.1140/epjnbp/s40366-016-0031-y.
[212] S. A. Kauffman, 'Metabolic stability and epigenesis in randomly constructed genetic nets', *J. Theor. Biol.*, vol. 22, no. 3, pp. 437–467, Mar. 1969, doi: 10.1016/0022-5193(69)90015-0.
[213] R. Thomas, 'Boolean formalization of genetic control circuits', *J. Theor. Biol.*, vol. 42, no. 3, pp. 563–585, Dec. 1973, doi: 10.1016/0022-5193(73)90247-6.
[214] V. Singh, A. Naldi, S. Soliman, and A. Niarakis, 'A large-scale Boolean model of the Rheumatoid Arthritis Fibroblast-Like Synoviocytes predicts drug synergies in the arthritic joint'. bioRxiv, p. 2023.01.16.524300, Jan. 19, 2023. doi: 10.1101/2023.01.16.524300.
[215] A. Montagud *et al.*, 'Patient-specific Boolean models of signalling networks guide personalised treatments', *eLife*, vol. 11, p. e72626, Feb. 2022, doi: 10.7554/eLife.72626.
[216] G. Selvaggio *et al.*, 'Hybrid Epithelial–Mesenchymal Phenotypes Are Controlled by Microenvironmental Factors', *Cancer Res.*, vol. 80, no. 11, pp. 2407–2420, Jun. 2020, doi: 10.1158/0008-5472.CAN-19-3147.
[217] J. D. Orth, I. Thiele, and B. Ø. Palsson, 'What is flux balance analysis?', *Nat.*

Biotechnol., vol. 28, no. 3, Art. no. 3, Mar. 2010, doi: 10.1038/nbt.1614.
[218] O. Folger, L. Jerby, C. Frezza, E. Gottlieb, E. Ruppin, and T. Shlomi, 'Predicting selective drug targets in cancer through metabolic networks', *Mol. Syst. Biol.*, vol. 7, p. 501, Jun. 2011, doi: 10.1038/msb.2011.35.
[219] T. Shlomi, T. Benyamini, E. Gottlieb, R. Sharan, and E. Ruppin, 'Genome-Scale Metabolic Modeling Elucidates the Role of Proliferative Adaptation in Causing the Warburg Effect', *PLoS Comput. Biol.*, vol. 7, no. 3, p. e1002018, Mar. 2011, doi: 10.1371/journal.pcbi.1002018.
[220] I. Larsson, M. Uhlén, C. Zhang, and A. Mardinoglu, 'Genome-Scale Metabolic Modeling of Glioblastoma Reveals Promising Targets for Drug Development', *Front. Genet.*, vol. 11, 2020, Accessed: Jul. 03, 2023. [Online]. Available: https://www.frontiersin.org/articles/10.3389/fgene.2020.00381
[221] S. Chandrasekaran and N. D. Price, 'Probabilistic integrative modeling of genome-scale metabolic and regulatory networks in Escherichia coli and Mycobacterium tuberculosis', *Proc. Natl. Acad. Sci. U. S. A.*, vol. 107, no. 41, pp. 17845–17850, Oct. 2010, doi: 10.1073/pnas.1005139107.
[222] L. Marmiesse, R. Peyraud, and L. Cottret, 'FlexFlux: combining metabolic flux and regulatory network analyses', *BMC Syst. Biol.*, vol. 9, p. 93, Dec. 2015, doi: 10.1186/s12918-015-0238-z.
[223] L. Liu and A. Bockmayr, 'Regulatory dynamic enzyme-cost flux balance analysis: A unifying framework for constraint-based modeling', *J. Theor. Biol.*, vol. 501, p. 110317, Sep. 2020, doi: 10.1016/j.jtbi.2020.110317.
[224] A. Mazein *et al.*, 'Systems medicine disease maps: community-driven comprehensive representation of disease mechanisms', *NPJ Syst. Biol. Appl.*, vol. 4, p. 21, 2018, doi: 10.1038/s41540-018-0059-y.
[225] M. Ostaszewski *et al.*, 'Community-driven roadmap for integrated disease maps', *Brief. Bioinform.*, vol. 20, no. 2, pp. 659–670, Mar. 2019, doi: 10.1093/bib/bby024.
[226] M. D. Wilkinson *et al.*, 'The FAIR Guiding Principles for scientific data management and stewardship', *Sci. Data*, vol. 3, no. 1, Art. no. 1, Mar. 2016, doi: 10.1038/sdata.2016.18.
[227] N. Le Novère, 'Quantitative and logic modelling of molecular and gene networks', *Nat. Rev. Genet.*, vol. 16, no. 3, Art. no. 3, Mar. 2015, doi: 10.1038/nrg3885.
[228] A. Funahashi, M. Morohashi, H. Kitano, and N. Tanimura, 'CellDesigner: a process diagram editor for gene-regulatory and biochemical networks', *BIOSILICO*, vol. 1, no. 5, pp. 159–162, Nov. 2003, doi: 10.1016/S1478-5382(03)02370-9.
[229] M. Hucka *et al.*, 'The Systems Biology Markup Language (SBML): Language Specification for Level 3 Version 2 Core', *J. Integr. Bioinforma.*, vol. 15, no. 1, p. 20170081, Mar. 2018, doi: 10.1515/jib-2017-0081.
[230] H. Mi and P. Thomas, 'PANTHER pathway: an ontology-based pathway database coupled with data analysis tools', *Methods Mol. Biol. Clifton NJ*, vol. 563, pp. 123–140, 2009, doi: 10.1007/978-1-60761-175-2_7.
[231] A. Niarakis *et al.*, 'Setting the basis of best practices and standards for curation and annotation of logical models in biology-highlights of the [BC]2 2019 CoLoMoTo/SysMod Workshop', *Brief. Bioinform.*, vol. 22, no. 2, pp. 1848–1859, Mar. 2021, doi: 10.1093/bib/bbaa046.
[232] Z. A. King *et al.*, 'BiGG Models: A platform for integrating, standardizing and sharing genome-scale models', *Nucleic Acids Res.*, vol. 44, no. Database issue, pp. D515–D522, Jan. 2016, doi: 10.1093/nar/gkv1049.
[233] N. Le Novère *et al.*, 'Minimum information requested in the annotation of biochemical models (MIRIAM)', *Nat. Biotechnol.*, vol. 23, no. 12, pp. 1509–1515, Dec. 2005, doi: 10.1038/nbt1156.
[234] P. Gawron *et al.*, 'MINERVA—a platform for visualization and curation of molecular interaction networks', *NPJ Syst. Biol. Appl.*, vol. 2, p. 16020, Sep. 2016, doi:

10.1038/npjsba.2016.20.
[235] D. S. Wishart *et al.*, 'DrugBank: a comprehensive resource for in silico drug discovery and exploration', *Nucleic Acids Res.*, vol. 34, no. Database issue, pp. D668-672, Jan. 2006, doi: 10.1093/nar/gkj067.
[236] D. Mendez *et al.*, 'ChEMBL: towards direct deposition of bioassay data', *Nucleic Acids Res.*, vol. 47, no. D1, pp. D930–D940, Jan. 2019, doi: 10.1093/nar/gky1075.
[237] P. Shannon *et al.*, 'Cytoscape: a software environment for integrated models of biomolecular interaction networks', *Genome Res.*, vol. 13, no. 11, pp. 2498–2504, Nov. 2003, doi: 10.1101/gr.1239303.
[238] F. Mizoguchi *et al.*, 'Functionally distinct disease-associated fibroblast subsets in rheumatoid arthritis', *Nat. Commun.*, vol. 9, no. 1, p. 789, Feb. 2018, doi: 10.1038/s41467-018-02892-y.
[239] R. Navab *et al.*, 'Prognostic gene-expression signature of carcinoma-associated fibroblasts in non-small cell lung cancer', *Proc. Natl. Acad. Sci. U. S. A.*, vol. 108, no. 17, pp. 7160–7165, Apr. 2011, doi: 10.1073/pnas.1014506108.
[240] E. W. Sayers *et al.*, 'Database resources of the National Center for Biotechnology Information', *Nucleic Acids Res.*, vol. 50, no. D1, pp. D20–D26, Dec. 2021, doi: 10.1093/nar/gkab1112.
[241] M. A. Freeberg *et al.*, 'The European Genome-phenome Archive in 2021', *Nucleic Acids Res.*, vol. 50, no. D1, pp. D980–D987, Jan. 2022, doi: 10.1093/nar/gkab1059.
[242] M. E. Ritchie *et al.*, 'limma powers differential expression analyses for RNA-sequencing and microarray studies', *Nucleic Acids Res.*, vol. 43, no. 7, p. e47, Apr. 2015, doi: 10.1093/nar/gkv007.
[243] S. S. Aghamiri, V. Singh, A. Naldi, T. Helikar, S. Soliman, and A. Niarakis, 'Automated inference of Boolean models from molecular interaction maps using CaSQ', *Bioinformatics*, vol. 36, no. 16, pp. 4473–4482, May 2020, doi: 10.1093/bioinformatics/btaa484.
[244] C. Chaouiya *et al.*, 'SBML qualitative models: a model representation format and infrastructure to foster interactions between qualitative modelling formalisms and tools', *BMC Syst. Biol.*, vol. 7, no. 1, p. 135, Dec. 2013, doi: 10.1186/1752-0509-7-135.
[245] T. Helikar *et al.*, 'The Cell Collective: Toward an open and collaborative approach to systems biology', *BMC Syst. Biol.*, vol. 6, no. 1, p. 96, Aug. 2012, doi: 10.1186/1752-0509-6-96.
[246] M. Glont *et al.*, 'BioModels: expanding horizons to include more modelling approaches and formats', *Nucleic Acids Res.*, vol. 46, no. D1, pp. D1248–D1253, Jan. 2018, doi: 10.1093/nar/gkx1023.
[247] R. S. Malik-Sheriff *et al.*, 'BioModels—15 years of sharing computational models in life science', *Nucleic Acids Res.*, vol. 48, no. D1, pp. D407–D415, Jan. 2020, doi: 10.1093/nar/gkz1055.
[248] J. G. T. Zañudo and R. Albert, 'An effective network reduction approach to find the dynamical repertoire of discrete dynamic networks', *Chaos Woodbury N*, vol. 23, no. 2, p. 025111, Jun. 2013, doi: 10.1063/1.4809777.
[249] H. Klarner, A. Bockmayr, and H. Siebert, 'Computing Symbolic Steady States of Boolean Networks', in *Cellular Automata*, J. Wąs, G. Ch. Sirakoulis, and S. Bandini, Eds., in Lecture Notes in Computer Science. Cham: Springer International Publishing, 2014, pp. 561–570. doi: 10.1007/978-3-319-11520-7_59.
[250] A. Naldi, 'BioLQM: A Java Toolkit for the Manipulation and Conversion of Logical Qualitative Models of Biological Networks', *Front. Physiol.*, vol. 9, p. 1605, 2018, doi: 10.3389/fphys.2018.01605.
[251] P. D. Thomas, D. Ebert, A. Muruganujan, T. Mushayahama, L.-P. Albou, and H. Mi, 'PANTHER: Making genome-scale phylogenetics accessible to all', *Protein Sci.*, vol. 31, no. 1, pp. 8–22, 2022, doi: 10.1002/pro.4218.
[252] A. C. Smith, F. Eyassu, J.-P. Mazat, and A. J. Robinson, 'MitoCore: a curated

constraint-based model for simulating human central metabolism', *BMC Syst. Biol.*, vol. 11, no. 1, p. 114, Nov. 2017, doi: 10.1186/s12918-017-0500-7.
[253] A. Saadatpour, Ré. Albert, and T. C. Reluga, 'A REDUCTION METHOD FOR BOOLEAN NETWORK MODELS PROVEN TO CONSERVE ATTRACTORS', *SIAM J. Appl. Dyn. Syst.*, vol. 12, no. 4, pp. 1997–2011, 2013, doi: 10.1137/13090537X.
[254] C. Hernandez, M. Thomas-Chollier, A. Naldi, and D. Thieffry, 'Computational Verification of Large Logical Models-Application to the Prediction of T Cell Response to Checkpoint Inhibitors', *Front. Physiol.*, vol. 11, p. 558606, 2020, doi: 10.3389/fphys.2020.558606.
[255] A. Naldi *et al.*, 'The CoLoMoTo Interactive Notebook: Accessible and Reproducible Computational Analyses for Qualitative Biological Networks', *Front. Physiol.*, vol. 9, p. 680, 2018, doi: 10.3389/fphys.2018.00680.
[256] A. Ebrahim, J. A. Lerman, B. O. Palsson, and D. R. Hyduke, 'COBRApy: COnstraints-Based Reconstruction and Analysis for Python', *BMC Syst. Biol.*, vol. 7, p. 74, Aug. 2013, doi: 10.1186/1752-0509-7-74.
[257] J. Hunt, 'The wxPython GUI Library', in *Advanced Guide to Python 3 Programming*, J. Hunt, Ed., in Undergraduate Topics in Computer Science. Cham: Springer International Publishing, 2019, pp. 73–86. doi: 10.1007/978-3-030-25943-3_8.
[258] L. Nelson, E. F. Churchill, L. Denoue, J. Helfman, and P. Murphy, 'Gooey interfaces: an approach for rapidly repurposing digital content', in *CHI '04 Extended Abstracts on Human Factors in Computing Systems*, in CHI EA '04. New York, NY, USA: Association for Computing Machinery, Apr. 2004, pp. 1293–1296. doi: 10.1145/985921.986047.
[259] V.-G. Trinh, B. Benhamou, K. Hiraishi, and S. Soliman, 'Minimal Trap Spaces of Logical Models are Maximal Siphons of Their Petri Net Encoding', in *Computational Methods in Systems Biology*, I. Petre and A. Păun, Eds., in Lecture Notes in Computer Science. Cham: Springer International Publishing, 2022, pp. 158–176. doi: 10.1007/978-3-031-15034-0_8.
[260] A. Marrelli *et al.*, 'Angiogenesis in rheumatoid arthritis: a disease specific process or a common response to chronic inflammation?', *Autoimmun. Rev.*, vol. 10, no. 10, pp. 595–598, Aug. 2011, doi: 10.1016/j.autrev.2011.04.020.
[261] A. Baier, I. Meineckel, S. Gay, and T. Pap, 'Apoptosis in rheumatoid arthritis', *Curr. Opin. Rheumatol.*, vol. 15, no. 3, pp. 274–279, May 2003, doi: 10.1097/00002281-200305000-00015.
[262] P. K. Panagopoulos and G. I. Lambrou, 'Bone erosions in rheumatoid arthritis: recent developments in pathogenesis and therapeutic implications', *J. Musculoskelet. Neuronal Interact.*, vol. 18, no. 3, pp. 304–319, Sep. 2018.
[263] S. Zhou, H. Lu, and M. Xiong, 'Identifying Immune Cell Infiltration and Effective Diagnostic Biomarkers in Rheumatoid Arthritis by Bioinformatics Analysis', *Front. Immunol.*, vol. 12, p. 726747, 2021, doi: 10.3389/fimmu.2021.726747.
[264] D. Aletaha and J. S. Smolen, 'Diagnosis and Management of Rheumatoid Arthritis: A Review', *JAMA*, vol. 320, no. 13, pp. 1360–1372, Oct. 2018, doi: 10.1001/jama.2018.13103.
[265] C. M. Quiñonez-Flores, S. A. González-Chávez, and C. Pacheco-Tena, 'Hypoxia and its implications in rheumatoid arthritis', *J. Biomed. Sci.*, vol. 23, no. 1, p. 62, Aug. 2016, doi: 10.1186/s12929-016-0281-0.
[266] S. E. Sweeney and G. S. Firestein, 'Rheumatoid arthritis: regulation of synovial inflammation', *Int. J. Biochem. Cell Biol.*, vol. 36, no. 3, pp. 372–378, Mar. 2004, doi: 10.1016/s1357-2725(03)00259-0.
[267] S. M. Krane, W. Conca, M. L. Stephenson, E. P. Amento, and M. B. Goldring, 'Mechanisms of matrix degradation in rheumatoid arthritis', *Ann. N. Y. Acad. Sci.*, vol. 580, pp. 340–354, 1990, doi: 10.1111/j.1749-6632.1990.tb17943.x.
[268] U. Steffen, G. Schett, and A. Bozec, 'How Autoantibodies Regulate Osteoclast

Induced Bone Loss in Rheumatoid Arthritis', *Front. Immunol.*, vol. 10, p. 1483, 2019, doi: 10.3389/fimmu.2019.01483.
[269] C. M. Weyand and J. J. Goronzy, 'Immunometabolism in early and late stages of rheumatoid arthritis', *Nat. Rev. Rheumatol.*, vol. 13, no. 5, pp. 291–301, May 2017, doi: 10.1038/nrrheum.2017.49.
[270] V. Pucino *et al.*, 'Metabolic Checkpoints in Rheumatoid Arthritis', *Front. Physiol.*, vol. 11, p. 347, 2020, doi: 10.3389/fphys.2020.00347.
[271] J.-W. Kim and C. V. Dang, 'Multifaceted roles of glycolytic enzymes', *Trends Biochem. Sci.*, vol. 30, no. 3, pp. 142–150, Mar. 2005, doi: 10.1016/j.tibs.2005.01.005.
[272] O. Yi *et al.*, 'Lactate metabolism in rheumatoid arthritis: Pathogenic mechanisms and therapeutic intervention with natural compounds', *Phytomedicine Int. J. Phytother. Phytopharm.*, vol. 100, p. 154048, Jun. 2022, doi: 10.1016/j.phymed.2022.154048.
[273] M. Zong *et al.*, 'Glucose-6-phosphate isomerase promotes the proliferation and inhibits the apoptosis in fibroblast-like synoviocytes in rheumatoid arthritis', *Arthritis Res. Ther.*, vol. 17, no. 1, p. 100, Apr. 2015, doi: 10.1186/s13075-015-0619-0.
[274] X. Chang and C. Wei, 'Glycolysis and rheumatoid arthritis', *Int. J. Rheum. Dis.*, vol. 14, no. 3, pp. 217–222, Aug. 2011, doi: 10.1111/j.1756-185X.2011.01598.x.
[275] Q. Fang, C. Zhou, and K. S. Nandakumar, 'Molecular and Cellular Pathways Contributing to Joint Damage in Rheumatoid Arthritis', *Mediators Inflamm.*, vol. 2020, p. 3830212, 2020, doi: 10.1155/2020/3830212.
[276] T. Kmiołek and A. Paradowska-Gorycka, 'miRNAs as Biomarkers and Possible Therapeutic Strategies in Rheumatoid Arthritis', *Cells*, vol. 11, no. 3, p. 452, Jan. 2022, doi: 10.3390/cells11030452.
[277] S. S. Makarov, 'NF-kappaB in rheumatoid arthritis: a pivotal regulator of inflammation, hyperplasia, and tissue destruction', *Arthritis Res.*, vol. 3, no. 4, pp. 200–206, 2001, doi: 10.1186/ar300.
[278] M. Taghadosi, M. Adib, A. Jamshidi, M. Mahmoudi, and E. Farhadi, 'The p53 status in rheumatoid arthritis with focus on fibroblast-like synoviocytes', *Immunol. Res.*, vol. 69, no. 3, pp. 225–238, Jun. 2021, doi: 10.1007/s12026-021-09202-7.
[279] F.-Y. Yu *et al.*, 'MiR-92a inhibits fibroblast-like synoviocyte proliferation and migration in rheumatoid arthritis by targeting AKT2', *J. Biosci.*, vol. 43, no. 5, pp. 911–919, Dec. 2018.
[280] R. Kalluri and M. Zeisberg, 'Fibroblasts in cancer', *Nat. Rev. Cancer*, vol. 6, no. 5, pp. 392–401, May 2006, doi: 10.1038/nrc1877.
[281] L. Monteran and N. Erez, 'The Dark Side of Fibroblasts: Cancer-Associated Fibroblasts as Mediators of Immunosuppression in the Tumor Microenvironment', *Front. Immunol.*, vol. 10, p. 1835, Aug. 2019, doi: 10.3389/fimmu.2019.01835.
[282] P. Lu, V. M. Weaver, and Z. Werb, 'The extracellular matrix: a dynamic niche in cancer progression', *J. Cell Biol.*, vol. 196, no. 4, pp. 395–406, Feb. 2012, doi: 10.1083/jcb.201102147.
[283] C. Han, T. Liu, and R. Yin, 'Biomarkers for cancer-associated fibroblasts', *Biomark. Res.*, vol. 8, no. 1, p. 64, Nov. 2020, doi: 10.1186/s40364-020-00245-w.
[284] X. Chen and E. Song, 'Turning foes to friends: targeting cancer-associated fibroblasts', *Nat. Rev. Drug Discov.*, vol. 18, no. 2, pp. 99–115, Feb. 2019, doi: 10.1038/s41573-018-0004-1.
[285] B. C. Özdemir *et al.*, 'Depletion of carcinoma-associated fibroblasts and fibrosis induces immunosuppression and accelerates pancreas cancer with reduced survival', *Cancer Cell*, vol. 25, no. 6, pp. 719–734, Jun. 2014, doi: 10.1016/j.ccr.2014.04.005.
[286] T. Liu, L. Zhou, D. Li, T. Andl, and Y. Zhang, 'Cancer-Associated Fibroblasts Build and Secure the Tumor Microenvironment', *Front. Cell Dev. Biol.*, vol. 7, 2019, Accessed: Jul. 06, 2023. [Online]. Available: https://www.frontiersin.org/articles/10.3389/fcell.2019.00060
[287] B. Erdogan and D. J. Webb, 'Cancer-associated fibroblasts modulate growth factor

signaling and extracellular matrix remodeling to regulate tumor metastasis', *Biochem. Soc. Trans.*, vol. 45, no. 1, pp. 229–236, Feb. 2017, doi: 10.1042/BST20160387.
[288] I. Kim, S. Choi, S. Yoo, M. Lee, and I.-S. Kim, 'Cancer-Associated Fibroblasts in the Hypoxic Tumor Microenvironment', *Cancers*, vol. 14, no. 14, p. 3321, Jul. 2022, doi: 10.3390/cancers14143321.
[289] J. Thiery, 'Modulation of the antitumor immune response by cancer-associated fibroblasts: mechanisms and targeting strategies to hamper their immunosuppressive functions', *Explor. Target. Anti-Tumor Ther.*, vol. 3, no. 5, pp. 598–629, 2022, doi: 10.37349/etat.2022.00103.
[290] I. Belhabib, S. Zaghdoudi, C. Lac, C. Bousquet, and C. Jean, 'Extracellular Matrices and Cancer-Associated Fibroblasts: Targets for Cancer Diagnosis and Therapy?', *Cancers*, vol. 13, no. 14, p. 3466, Jul. 2021, doi: 10.3390/cancers13143466.
[291] X. Guo *et al.*, 'Cancer-Associated Fibroblasts Promote Migration and Invasion of Non-Small Cell Lung Cancer Cells via miR-101-3p Mediated VEGFA Secretion and AKT/eNOS Pathway', *Front. Cell Dev. Biol.*, vol. 9, p. 764151, Dec. 2021, doi: 10.3389/fcell.2021.764151.
[292] R.-P. Czekay, D.-J. Cheon, R. Samarakoon, S. M. Kutz, and P. J. Higgins, 'Cancer-Associated Fibroblasts: Mechanisms of Tumor Progression and Novel Therapeutic Targets', *Cancers*, vol. 14, no. 5, p. 1231, Feb. 2022, doi: 10.3390/cancers14051231.
[293] Y. Attieh *et al.*, 'Cancer-associated fibroblasts lead tumor invasion through integrin-β3–dependent fibronectin assembly', *J. Cell Biol.*, vol. 216, no. 11, pp. 3509–3520, Nov. 2017, doi: 10.1083/jcb.201702033.
[294] X.-J. Shen *et al.*, 'Caveolin-1 is a Modulator of Fibroblast Activation and a Potential Biomarker for Gastric Cancer', *Int. J. Biol. Sci.*, vol. 11, no. 4, pp. 370–379, Feb. 2015, doi: 10.7150/ijbs.10666.
[295] E. Sahai *et al.*, 'A framework for advancing our understanding of cancer-associated fibroblasts', *Nat. Rev. Cancer*, vol. 20, no. 3, Art. no. 3, Mar. 2020, doi: 10.1038/s41568-019-0238-1.
[296] N. Erez, M. Truitt, P. Olson, and D. Hanahan, 'Cancer-Associated Fibroblasts Are Activated in Incipient Neoplasia to Orchestrate Tumor-Promoting Inflammation in an NF-κB-Dependent Manner', *Cancer Cell*, vol. 17, no. 2, pp. 135–147, Feb. 2010, doi: 10.1016/j.ccr.2009.12.041.
[297] E. Brouwer *et al.*, 'Hypoxia inducible factor-1-alpha (HIF-1alpha) is related to both angiogenesis and inflammation in rheumatoid arthritis', *Clin. Exp. Rheumatol.*, vol. 27, no. 6, pp. 945–951, 2009.
[298] P. A. Guerne, B. L. Zuraw, J. H. Vaughan, D. A. Carson, and M. Lotz, 'Synovium as a source of interleukin 6 in vitro. Contribution to local and systemic manifestations of arthritis', *J. Clin. Invest.*, vol. 83, no. 2, pp. 585–592, Feb. 1989, doi: 10.1172/JCI113921.
[299] J. A. Gracie *et al.*, 'A proinflammatory role for IL-18 in rheumatoid arthritis', *J. Clin. Invest.*, vol. 104, no. 10, pp. 1393–1401, Nov. 1999, doi: 10.1172/JCI7317.
[300] V. Byrd, X. M. Zhao, W. L. McKeehan, G. G. Miller, and J. W. Thomas, 'Expression and functional expansion of fibroblast growth factor receptor T cells in rheumatoid synovium and peripheral blood of patients with rheumatoid arthritis', *Arthritis Rheum.*, vol. 39, no. 6, pp. 914–922, Jun. 1996, doi: 10.1002/art.1780390607.
[301] S. Rosengren, M. Corr, and D. L. Boyle, 'Platelet-derived growth factor and transforming growth factor beta synergistically potentiate inflammatory mediator synthesis by fibroblast-like synoviocytes', *Arthritis Res. Ther.*, vol. 12, no. 2, p. R65, 2010, doi: 10.1186/ar2981.
[302] H. Cheon, S.-J. Yu, D. H. Yoo, I. J. Chae, G. G. Song, and J. Sohn, 'Increased expression of pro-inflammatory cytokines and metalloproteinase-1 by TGF-beta1 in synovial fibroblasts from rheumatoid arthritis and normal individuals', *Clin. Exp. Immunol.*, vol. 127, no. 3, pp. 547–552, Mar. 2002, doi: 10.1046/j.1365-2249.2002.01785.x.
[303] M. Sen, M. Chamorro, J. Reifert, M. Corr, and D. A. Carson, 'Blockade of Wnt-

5A/frizzled 5 signaling inhibits rheumatoid synoviocyte activation', *Arthritis Rheum.*, vol. 44, no. 4, pp. 772–781, Apr. 2001, doi: 10.1002/1529-0131(200104)44:4<772::AID-ANR133>3.0.CO;2-L.
[304] Y.-J. Kwon, S.-W. Lee, Y.-B. Park, S.-K. Lee, and M.-C. Park, 'Secreted frizzled-related protein 5 suppresses inflammatory response in rheumatoid arthritis fibroblast-like synoviocytes through down-regulation of c-Jun N-terminal kinase', *Rheumatol. Oxf. Engl.*, vol. 53, no. 9, pp. 1704–1711, Sep. 2014, doi: 10.1093/rheumatology/keu167.
[305] H. Takayanagi *et al.*, 'Involvement of receptor activator of nuclear factor κB ligand/osteoclast differentiation factor in osteoclastogenesis from synoviocytes in rheumatoid arthritis', *Arthritis Rheum.*, vol. 43, no. 2, pp. 259–269, 2000, doi: 10.1002/1529-0131(200002)43:2<259::AID-ANR4>3.0.CO;2-W.
[306] S. Kotake *et al.*, 'IL-17 in synovial fluids from patients with rheumatoid arthritis is a potent stimulator of osteoclastogenesis', *J. Clin. Invest.*, vol. 103, no. 9, pp. 1345–1352, May 1999, doi: 10.1172/JCI5703.
[307] K. Fukuda, Y. Miura, T. Maeda, S. Hayashi, T. Matsumoto, and R. Kuroda, 'Expression profiling of genes in rheumatoid fibroblast-like synoviocytes regulated by Fas ligand via cDNA microarray analysis', *Exp. Ther. Med.*, vol. 22, no. 3, p. 1000, Sep. 2021, doi: 10.3892/etm.2021.10432.
[308] L. Nejatbakhsh Samimi, E. Farhadi, M. N. Tahmasebi, A. Jamshidi, A. Sharafat Vaziri, and M. Mahmoudi, 'NF-κB signaling in rheumatoid arthritis with focus on fibroblast-like synoviocytes', *Autoimmun. Highlights*, vol. 11, no. 1, p. 11, Aug. 2020, doi: 10.1186/s13317-020-00135-z.
[309] A. Lee *et al.*, 'Tumor necrosis factor α induces sustained signaling and a prolonged and unremitting inflammatory response in rheumatoid arthritis synovial fibroblasts', *Arthritis Rheum.*, vol. 65, no. 4, pp. 928–938, Apr. 2013, doi: 10.1002/art.37853.
[310] S. Li, Z. Jin, and X. Lu, 'MicroRNA-192 suppresses cell proliferation and induces apoptosis in human rheumatoid arthritis fibroblast-like synoviocytes by downregulating caveolin 1', *Mol. Cell. Biochem.*, vol. 432, no. 1–2, pp. 123–130, Aug. 2017, doi: 10.1007/s11010-017-3003-3.
[311] M. M. Cerinic *et al.*, 'Synoviocytes from osteoarthritis and rheumatoid arthritis produce plasminogen activators and plasminogen activator inhibitor-1 and display u-PA receptors on their surface', *Life Sci.*, vol. 63, no. 6, pp. 441–453, 1998, doi: 10.1016/s0024-3205(98)00293-8.
[312] M. A. Akhavani, L. Madden, I. Buysschaert, B. Sivakumar, N. Kang, and E. M. Paleolog, 'Hypoxia upregulates angiogenesis and synovial cell migration in rheumatoid arthritis', *Arthritis Res. Ther.*, vol. 11, no. 3, p. R64, 2009, doi: 10.1186/ar2689.
[313] Y. Lu *et al.*, 'Glucose-6-Phosphate Isomerase (G6PI) Mediates Hypoxia-Induced Angiogenesis in Rheumatoid Arthritis', *Sci. Rep.*, vol. 7, no. 1, Art. no. 1, Jan. 2017, doi: 10.1038/srep40274.
[314] J. D. Cañete *et al.*, 'Antiangiogenic effects of anti-tumor necrosis factor alpha therapy with infliximab in psoriatic arthritis', *Arthritis Rheum.*, vol. 50, no. 5, pp. 1636–1641, May 2004, doi: 10.1002/art.20181.
[315] G. Azizi, R. Boghozian, and A. Mirshafiey, 'The potential role of angiogenic factors in rheumatoid arthritis', *Int. J. Rheum. Dis.*, vol. 17, no. 4, pp. 369–383, May 2014, doi: 10.1111/1756-185X.12280.
[316] H. G. Zhang *et al.*, 'Gene therapy that inhibits nuclear translocation of nuclear factor kappaB results in tumor necrosis factor alpha-induced apoptosis of human synovial fibroblasts', *Arthritis Rheum.*, vol. 43, no. 5, pp. 1094–1105, May 2000, doi: 10.1002/1529-0131(200005)43:5<1094::AID-ANR20>3.0.CO;2-V.
[317] T. Pap, U. Müller-Ladner, R. E. Gay, and S. Gay, 'Fibroblast biology: Role of synovial fibroblasts in the pathogenesis of rheumatoid arthritis', *Arthritis Res.*, vol. 2, no. 5, pp. 361–367, 2000, doi: 10.1186/ar113.
[318] L. Danks *et al.*, 'RANKL expressed on synovial fibroblasts is primarily responsible

for bone erosions during joint inflammation', *Ann. Rheum. Dis.*, vol. 75, no. 6, pp. 1187–1195, Jun. 2016, doi: 10.1136/annrheumdis-2014-207137.
[319] M. A. Shelef, D. A. Bennin, D. F. Mosher, and A. Huttenlocher, 'Citrullination of fibronectin modulates synovial fibroblast behavior', *Arthritis Res. Ther.*, vol. 14, no. 6, p. R240, 2012, doi: 10.1186/ar4083.
[320] Y. Matsuo *et al.*, 'Local fibroblast proliferation but not influx is responsible for synovial hyperplasia in a murine model of rheumatoid arthritis', *Biochem. Biophys. Res. Commun.*, vol. 470, no. 3, pp. 504–509, Feb. 2016, doi: 10.1016/j.bbrc.2016.01.121.
[321] F. Hu *et al.*, 'Hypoxia-inducible factor-1α perpetuates synovial fibroblast interactions with T cells and B cells in rheumatoid arthritis', *Eur. J. Immunol.*, vol. 46, no. 3, pp. 742–751, Mar. 2016, doi: 10.1002/eji.201545784.
[322] B. Muz, H. Larsen, L. Madden, S. Kiriakidis, and E. M. Paleolog, 'Prolyl hydroxylase domain enzyme 2 is the major player in regulating hypoxic responses in rheumatoid arthritis', *Arthritis Rheum.*, vol. 64, no. 9, pp. 2856–2867, Sep. 2012, doi: 10.1002/art.34479.
[323] S. Hua and T. H. Dias, 'Hypoxia-Inducible Factor (HIF) as a Target for Novel Therapies in Rheumatoid Arthritis', *Front. Pharmacol.*, vol. 7, p. 184, Jun. 2016, doi: 10.3389/fphar.2016.00184.
[324] H. Matsuno *et al.*, 'The role of TNF-alpha in the pathogenesis of inflammation and joint destruction in rheumatoid arthritis (RA): a study using a human RA/SCID mouse chimera', *Rheumatol. Oxf. Engl.*, vol. 41, no. 3, pp. 329–337, Mar. 2002, doi: 10.1093/rheumatology/41.3.329.
[325] S. Nakae, S. Saijo, R. Horai, K. Sudo, S. Mori, and Y. Iwakura, 'IL-17 production from activated T cells is required for the spontaneous development of destructive arthritis in mice deficient in IL-1 receptor antagonist', *Proc. Natl. Acad. Sci. U. S. A.*, vol. 100, no. 10, pp. 5986–5990, May 2003, doi: 10.1073/pnas.1035999100.
[326] A. Valin *et al.*, 'IL6/sIL6R regulates TNFα-inflammatory response in synovial fibroblasts through modulation of transcriptional and post-transcriptional mechanisms', *BMC Mol. Cell Biol.*, vol. 21, p. 74, Oct. 2020, doi: 10.1186/s12860-020-00317-7.
[327] J.-Y. Wu *et al.*, 'Chrysoeriol suppresses hyperproliferation of rheumatoid arthritis fibroblast-like synoviocytes and inhibits JAK2/STAT3 signaling', *BMC Complement. Med. Ther.*, vol. 22, p. 73, Mar. 2022, doi: 10.1186/s12906-022-03553-w.
[328] S.-Y. Hwang *et al.*, 'IL-17 induces production of IL-6 and IL-8 in rheumatoid arthritis synovial fibroblasts via NF-κB- and PI3-kinase/Akt-dependent pathways', *Arthritis Res. Ther.*, vol. 6, no. 2, pp. R120–R128, 2004, doi: 10.1186/ar1038.
[329] J. K. Ahn *et al.*, 'Role of hypoxia-inducible factor-1alpha in hypoxia-induced expressions of IL-8, MMP-1 and MMP-3 in rheumatoid fibroblast-like synoviocytes', *Rheumatol. Oxf. Engl.*, vol. 47, no. 6, pp. 834–839, Jun. 2008, doi: 10.1093/rheumatology/ken086.
[330] S. A. Agere, N. Akhtar, J. M. Watson, and S. Ahmed, 'RANTES/CCL5 Induces Collagen Degradation by Activating MMP-1 and MMP-13 Expression in Human Rheumatoid Arthritis Synovial Fibroblasts', *Front. Immunol.*, vol. 8, p. 1341, 2017, doi: 10.3389/fimmu.2017.01341.
[331] M. Xue *et al.*, 'Endogenous MMP-9 and not MMP-2 promotes rheumatoid synovial fibroblast survival, inflammation and cartilage degradation', *Rheumatol. Oxf. Engl.*, vol. 53, no. 12, pp. 2270–2279, Dec. 2014, doi: 10.1093/rheumatology/keu254.
[332] B. Bartok and G. S. Firestein, 'Fibroblast-like synoviocytes: key effector cells in rheumatoid arthritis', *Immunol. Rev.*, vol. 233, no. 1, pp. 233–255, Jan. 2010, doi: 10.1111/j.0105-2896.2009.00859.x.
[333] L. Magyari *et al.*, 'Interleukins and interleukin receptors in rheumatoid arthritis: Research, diagnostics and clinical implications', *World J. Orthop.*, vol. 5, no. 4, pp. 516–536, Sep. 2014, doi: 10.5312/wjo.v5.i4.516.
[334] P. S. Burrage, K. S. Mix, and C. E. Brinckerhoff, 'Matrix metalloproteinases: role

in arthritis', *Front. Biosci. J. Virtual Libr.*, vol. 11, pp. 529–543, Jan. 2006, doi: 10.2741/1817.
[335] S. M. Jung, K. W. Kim, C.-W. Yang, S.-H. Park, and J. H. Ju, 'Cytokine-mediated bone destruction in rheumatoid arthritis', *J. Immunol. Res.*, vol. 2014, p. 263625, 2014, doi: 10.1155/2014/263625.
[336] M. Harada *et al.*, 'Vascular endothelial growth factor in patients with rheumatoid arthritis', *Scand. J. Rheumatol.*, vol. 27, no. 5, pp. 377–380, 1998, doi: 10.1080/03009749850154429.
[337] E. Berra, E. Benizri, A. Ginouvès, V. Volmat, D. Roux, and J. Pouysségur, 'HIF prolyl-hydroxylase 2 is the key oxygen sensor setting low steady-state levels of HIF-1α in normoxia', *EMBO J.*, vol. 22, no. 16, pp. 4082–4090, Aug. 2003, doi: 10.1093/emboj/cdg392.
[338] D. Trisciuoglio, A. Iervolino, G. Zupi, and D. Del Bufalo, 'Involvement of PI3K and MAPK signaling in bcl-2-induced vascular endothelial growth factor expression in melanoma cells', *Mol. Biol. Cell*, vol. 16, no. 9, pp. 4153–4162, Sep. 2005, doi: 10.1091/mbc.e04-12-1087.
[339] C.-M. Zhang, J. Zhao, and H.-Y. Deng, 'MiR-155 promotes proliferation of human breast cancer MCF-7 cells through targeting tumor protein 53-induced nuclear protein 1', *J. Biomed. Sci.*, vol. 20, no. 1, p. 79, Oct. 2013, doi: 10.1186/1423-0127-20-79.
[340] 'Cancers | Free Full-Text | Cancer-Associated Fibroblasts in Breast Cancer Treatment Response and Metastasis'. https://www.mdpi.com/2072-6694/13/13/3146 (accessed Jul. 06, 2023).
[341] C. Guido *et al.*, 'Metabolic reprogramming of cancer-associated fibroblasts by TGF-β drives tumor growth', *Cell Cycle*, vol. 11, no. 16, pp. 3019–3035, Aug. 2012, doi: 10.4161/cc.21384.
[342] M. F. Santolla *et al.*, 'miR-221 stimulates breast cancer cells and cancer-associated fibroblasts (CAFs) through selective interference with the A20/c-Rel/CTGF signaling', *J. Exp. Clin. Cancer Res. CR*, vol. 37, no. 1, p. 94, May 2018, doi: 10.1186/s13046-018-0767-6.
[343] A. Bronisz *et al.*, 'Reprogramming of the tumour microenvironment by stromal PTEN-regulated miR-320', *Nat. Cell Biol.*, vol. 14, no. 2, pp. 159–167, Dec. 2011, doi: 10.1038/ncb2396.
[344] S. Wen *et al.*, 'Cancer-associated fibroblast (CAF)-derived IL32 promotes breast cancer cell invasion and metastasis via integrin β3-p38 MAPK signalling', *Cancer Lett.*, vol. 442, pp. 320–332, Feb. 2019, doi: 10.1016/j.canlet.2018.10.015.
[345] L. Xiang, Z. Song, and G. Rong, 'Taxotere-induced WNT16 Expression in Carcinoma-Associated Fibroblasts Might Associate with Progression and Chemoresistance of Breast Cancer', *Ann. Clin. Lab. Sci.*, vol. 50, no. 2, pp. 205–212, Mar. 2020.
[346] P. De Marco *et al.*, 'GPER signalling in both cancer-associated fibroblasts and breast cancer cells mediates a feedforward IL1β/IL1R1 response', *Sci. Rep.*, vol. 6, p. 24354, Apr. 2016, doi: 10.1038/srep24354.
[347] S. Jansson *et al.*, 'The PDGF pathway in breast cancer is linked to tumour aggressiveness, triple-negative subtype and early recurrence', *Breast Cancer Res. Treat.*, vol. 169, no. 2, pp. 231–241, Jun. 2018, doi: 10.1007/s10549-018-4664-7.
[348] F. Pelon *et al.*, 'Cancer-associated fibroblast heterogeneity in axillary lymph nodes drives metastases in breast cancer through complementary mechanisms', *Nat. Commun.*, vol. 11, no. 1, p. 404, Jan. 2020, doi: 10.1038/s41467-019-14134-w.
[349] J. Suh, D.-H. Kim, Y.-H. Lee, J.-H. Jang, and Y.-J. Surh, 'Fibroblast growth factor-2, derived from cancer-associated fibroblasts, stimulates growth and progression of human breast cancer cells via FGFR1 signaling', *Mol. Carcinog.*, vol. 59, no. 9, pp. 1028–1040, Sep. 2020, doi: 10.1002/mc.23233.
[350] N. Erez, S. Glanz, Y. Raz, C. Avivi, and I. Barshack, 'Cancer associated fibroblasts express pro-inflammatory factors in human breast and ovarian tumors', *Biochem. Biophys.*

Res. Commun., vol. 437, no. 3, pp. 397–402, Aug. 2013, doi: 10.1016/j.bbrc.2013.06.089.
[351] P. Chen, Q. Mo, B. Wang, D. Weng, P. Wu, and G. Chen, 'Breast cancer associated fibroblasts promote MCF-7 invasion in vitro by secretion of HGF', *J. Huazhong Univ. Sci. Technol. Med. Sci. Hua Zhong Ke Ji Xue Xue Bao Yi Xue Ying Wen Ban Huazhong Keji Daxue Xuebao Yixue Yingdewen Ban*, vol. 32, no. 1, pp. 92–96, Feb. 2012, doi: 10.1007/s11596-012-0016-8.
[352] W. Chen *et al.*, 'Crosstalk between TGF-β signaling and miRNAs in breast cancer metastasis', *Tumor Biol.*, vol. 37, no. 8, pp. 10011–10019, Aug. 2016, doi: 10.1007/s13277-016-5060-8.
[353] A. M. Araujo *et al.*, 'Stromal oncostatin M cytokine promotes breast cancer progression by reprogramming the tumor microenvironment', *J. Clin. Invest.*, vol. 132, no. 7, p. e148667, Apr. 2022, doi: 10.1172/JCI148667.
[354] G. Murphy *et al.*, 'Mechanisms for pro matrix metalloproteinase activation', *APMIS Acta Pathol. Microbiol. Immunol. Scand.*, vol. 107, no. 1, pp. 38–44, Jan. 1999, doi: 10.1111/j.1699-0463.1999.tb01524.x.
[355] M. Jo, R. D. Lester, V. Montel, B. Eastman, S. Takimoto, and S. L. Gonias, 'Reversibility of epithelial-mesenchymal transition (EMT) induced in breast cancer cells by activation of urokinase receptor-dependent cell signaling', *J. Biol. Chem.*, vol. 284, no. 34, pp. 22825–22833, Aug. 2009, doi: 10.1074/jbc.M109.023960.
[356] W. Zhang *et al.*, 'CXCL5/CXCR2 axis in tumor microenvironment as potential diagnostic biomarker and therapeutic target', *Cancer Commun. Lond. Engl.*, vol. 40, no. 2–3, pp. 69–80, Mar. 2020, doi: 10.1002/cac2.12010.
[357] R. M. Balliet *et al.*, 'Mitochondrial oxidative stress in cancer-associated fibroblasts drives lactate production, promoting breast cancer tumor growth: understanding the aging and cancer connection', *Cell Cycle Georget. Tex*, vol. 10, no. 23, pp. 4065–4073, Dec. 2011, doi: 10.4161/cc.10.23.18254.
[358] L. W. S. Finley and M. C. Haigis, 'Metabolic regulation by SIRT3: implications for tumorigenesis', *Trends Mol. Med.*, vol. 18, no. 9, pp. 516–523, Sep. 2012, doi: 10.1016/j.molmed.2012.05.004.
[359] M. C. Haigis, C.-X. Deng, L. W. S. Finley, H.-S. Kim, and D. Gius, 'SIRT3 is a mitochondrial tumor suppressor: a scientific tale that connects aberrant cellular ROS, the Warburg effect, and carcinogenesis', *Cancer Res.*, vol. 72, no. 10, pp. 2468–2472, May 2012, doi: 10.1158/0008-5472.CAN-11-3633.
[360] A. Orimo *et al.*, 'Stromal fibroblasts present in invasive human breast carcinomas promote tumor growth and angiogenesis through elevated SDF-1/CXCL12 secretion', *Cell*, vol. 121, no. 3, pp. 335–348, May 2005, doi: 10.1016/j.cell.2005.02.034.
[361] J. Winkler, A. Abisoye-Ogunniyan, K. J. Metcalf, and Z. Werb, 'Concepts of extracellular matrix remodelling in tumour progression and metastasis', *Nat. Commun.*, vol. 11, no. 1, p. 5120, Oct. 2020, doi: 10.1038/s41467-020-18794-x.
[362] Y.-E. Du *et al.*, 'MiR-205/YAP1 in Activated Fibroblasts of Breast Tumor Promotes VEGF-independent Angiogenesis through STAT3 Signaling', *Theranostics*, vol. 7, no. 16, pp. 3972–3988, 2017, doi: 10.7150/thno.18990.
[363] M. J. Del Rey *et al.*, 'Hif-1α Knockdown Reduces Glycolytic Metabolism and Induces Cell Death of Human Synovial Fibroblasts Under Normoxic Conditions', *Sci. Rep.*, vol. 7, no. 1, p. 3644, Jun. 2017, doi: 10.1038/s41598-017-03921-4.
[364] K. Sun *et al.*, 'Oxidized ATM-mediated glycolysis enhancement in breast cancer-associated fibroblasts contributes to tumor invasion through lactate as metabolic coupling', *EBioMedicine*, vol. 41, pp. 370–383, Mar. 2019, doi: 10.1016/j.ebiom.2019.02.025.
[365] K. M. Perrott, C. D. Wiley, P.-Y. Desprez, and J. Campisi, 'Apigenin suppresses the senescence-associated secretory phenotype and paracrine effects on breast cancer cells', *GeroScience*, vol. 39, no. 2, pp. 161–173, Apr. 2017, doi: 10.1007/s11357-017-9970-1.
[366] A. J. Trimboli *et al.*, 'Pten in stromal fibroblasts suppresses mammary epithelial tumours', *Nature*, vol. 461, no. 7267, pp. 1084–1091, Oct. 2009, doi: 10.1038/nature08486.

[367] Q. Zhang, L. Lei, and D. Jing, 'Knockdown of SERPINE1 reverses resistance of triple-negative breast cancer to paclitaxel via suppression of VEGFA', *Oncol. Rep.*, vol. 44, no. 5, pp. 1875–1884, Nov. 2020, doi: 10.3892/or.2020.7770.
[368] J. H. Kim *et al.*, 'Calsequestrin 2 overexpression in breast cancer increases tumorigenesis and metastasis by modulating the tumor microenvironment', *Mol. Oncol.*, vol. 16, no. 2, pp. 466–484, Jan. 2022, doi: 10.1002/1878-0261.13136.
[369] C. F. Singer *et al.*, 'MMP-2 and MMP-9 Expression in Breast Cancer-Derived Human Fibroblasts is Differentially Regulated by Stromal-Epithelial Interactions', *Breast Cancer Res. Treat.*, vol. 72, no. 1, pp. 69–77, Mar. 2002, doi: 10.1023/A:1014918512569.
[370] P. Fernández-Nogueira, G. Fuster, Á. Gutierrez-Uzquiza, P. Gascón, N. Carbó, and P. Bragado, 'Cancer-Associated Fibroblasts in Breast Cancer Treatment Response and Metastasis', *Cancers*, vol. 13, no. 13, Art. no. 13, Jan. 2021, doi: 10.3390/cancers13133146.
[371] Z. Fasoulakis, G. Kolios, V. Papamanolis, and E. N. Kontomanolis, 'Interleukins Associated with Breast Cancer', *Cureus*, vol. 10, no. 11, p. e3549, Nov. 2018, doi: 10.7759/cureus.3549.
[372] B. Chiavarina *et al.*, 'HIF1-alpha functions as a tumor promoter in cancer associated fibroblasts, and as a tumor suppressor in breast cancer cells: Autophagy drives compartment-specific oncogenesis', *Cell Cycle Georget. Tex*, vol. 9, no. 17, pp. 3534–3551, Sep. 2010, doi: 10.4161/cc.9.17.12908.
[373] D. Fukumura *et al.*, 'Tumor induction of VEGF promoter activity in stromal cells', *Cell*, vol. 94, no. 6, pp. 715–725, Sep. 1998, doi: 10.1016/s0092-8674(00)81731-6.
[374] Y. Ruan, H. Ogana, E. Gang, H. N. Kim, and Y.-M. Kim, 'Wnt Signaling in the Tumor Microenvironment', *Adv. Exp. Med. Biol.*, vol. 1270, pp. 107–121, 2021, doi: 10.1007/978-3-030-47189-7_7.
[375] L. J. Hofland, B. van der Burg, C. H. J. van Eijck, D. M. Sprij, P. M. van Koetsveld, and S. W. J. Lamberts, 'Role of tumor-derived fibroblasts in the growth of primary cultures of human breast-cancer cells: Effects of epidermal growth factor and the somatostatin analogue octreotide', *Int. J. Cancer*, vol. 60, no. 1, pp. 93–99, 1995, doi: 10.1002/ijc.2910600114.
[376] N. Willumsen *et al.*, 'Fibrotic activity quantified in serum by measurements of type III collagen pro-peptides can be used for prognosis across different solid tumor types', *Cell. Mol. Life Sci.*, vol. 79, no. 4, p. 204, Mar. 2022, doi: 10.1007/s00018-022-04226-0.
[377] D. Katoh, Y. Kozuka, A. Noro, T. Ogawa, K. Imanaka-Yoshida, and T. Yoshida, 'Tenascin-C Induces Phenotypic Changes in Fibroblasts to Myofibroblasts with High Contractility through the Integrin αvβ1/Transforming Growth Factor β/SMAD Signaling Axis in Human Breast Cancer', *Am. J. Pathol.*, vol. 190, no. 10, pp. 2123–2135, Oct. 2020, doi: 10.1016/j.ajpath.2020.06.008.
[378] J. Yang *et al.*, 'Glycolysis reprogramming in cancer-associated fibroblasts promotes the growth of oral cancer through the lncRNA H19/miR-675-5p/PFKFB3 signaling pathway', *Int. J. Oral Sci.*, vol. 13, no. 1, p. 12, Mar. 2021, doi: 10.1038/s41368-021-00115-7.
[379] Z. Li, C. Sun, and Z. Qin, 'Metabolic reprogramming of cancer-associated fibroblasts and its effect on cancer cell reprogramming', *Theranostics*, vol. 11, no. 17, pp. 8322–8336, Jul. 2021, doi: 10.7150/thno.62378.
[380] E. J. Pearce and E. L. Pearce, 'Driving immunity: all roads lead to metabolism', *Nat. Rev. Immunol.*, vol. 18, no. 2, Art. no. 2, Feb. 2018, doi: 10.1038/nri.2017.139.
[381] A.-L. Barabási and Z. N. Oltvai, 'Network biology: understanding the cell's functional organization', *Nat. Rev. Genet.*, vol. 5, no. 2, pp. 101–113, Feb. 2004, doi: 10.1038/nrg1272.
[382] R. W. Kinne, R. Bräuer, B. Stuhlmüller, E. Palombo-Kinne, and G.-R. Burmester, 'Macrophages in rheumatoid arthritis', *Arthritis Res.*, vol. 2, no. 3, pp. 189–202, 2000, doi: 10.1186/ar86.
[383] X. Yang, Y. Chang, and W. Wei, 'Emerging role of targeting macrophages in

rheumatoid arthritis: Focus on polarization, metabolism and apoptosis', *Cell Prolif.*, vol. 53, no. 7, p. e12854, Jun. 2020, doi: 10.1111/cpr.12854.
[384] M. Otero and M. B. Goldring, 'Cells of the synovium in rheumatoid arthritis. Chondrocytes', *Arthritis Res. Ther.*, vol. 9, no. 5, p. 220, Oct. 2007, doi: 10.1186/ar2292.
[385] C.-C. Tseng *et al.*, 'Dual Role of Chondrocytes in Rheumatoid Arthritis: The Chicken and the Egg', *Int. J. Mol. Sci.*, vol. 21, no. 3, p. 1071, Feb. 2020, doi: 10.3390/ijms21031071.
[386] G.-X. Ruan and A. Kazlauskas, 'Lactate engages receptor tyrosine kinases Axl, Tie2, and vascular endothelial growth factor receptor 2 to activate phosphoinositide 3-kinase/Akt and promote angiogenesis', *J. Biol. Chem.*, vol. 288, no. 29, pp. 21161–21172, Jul. 2013, doi: 10.1074/jbc.M113.474619.
[387] U. Fearon, M. M. Hanlon, A. Floudas, and D. J. Veale, 'Cellular metabolic adaptations in rheumatoid arthritis and their therapeutic implications', *Nat. Rev. Rheumatol.*, vol. 18, no. 7, pp. 398–414, Jul. 2022, doi: 10.1038/s41584-022-00771-x.
[388] L. Xu *et al.*, 'Metabolomics in rheumatoid arthritis: Advances and review', *Front. Immunol.*, vol. 13, p. 961708, Aug. 2022, doi: 10.3389/fimmu.2022.961708.
[389] O. Kolliniati, E. Ieronymaki, E. Vergadi, and C. Tsatsanis, 'Metabolic Regulation of Macrophage Activation', *J. Innate Immun.*, vol. 14, no. 1, pp. 51–68, Jul. 2021, doi: 10.1159/000516780.
[390] S. Cohen, K. Danzaki, and N. J. MacIver, 'Nutritional effects on T-cell immunometabolism', *Eur. J. Immunol.*, vol. 47, no. 2, pp. 225–235, Feb. 2017, doi: 10.1002/eji.201646423.
[391] T. Gaber, R. Dziurla, R. Tripmacher, G. R. Burmester, and F. Buttgereit, 'Hypoxia inducible factor (HIF) in rheumatology: low O2! See what HIF can do!', *Ann. Rheum. Dis.*, vol. 64, no. 7, pp. 971–980, Jul. 2005, doi: 10.1136/ard.2004.031641.
[392] N. C. Denko, 'Hypoxia, HIF1 and glucose metabolism in the solid tumour', *Nat. Rev. Cancer*, vol. 8, no. 9, pp. 705–713, Sep. 2008, doi: 10.1038/nrc2468.
[393] L. Liang *et al.*, '"Reverse Warburg effect" of cancer-associated fibroblasts (Review)', *Int. J. Oncol.*, vol. 60, no. 6, p. 67, Jun. 2022, doi: 10.3892/ijo.2022.5357.
[394] B. Muz, P. de la Puente, F. Azab, and A. K. Azab, 'The role of hypoxia in cancer progression, angiogenesis, metastasis, and resistance to therapy', *Hypoxia*, vol. 3, pp. 83–92, Dec. 2015, doi: 10.2147/HP.S93413.
[395] O. Warburg, 'On the Origin of Cancer Cells', *Science*, vol. 123, no. 3191, pp. 309–314, Feb. 1956, doi: 10.1126/science.123.3191.309.
[396] X. Yi, M. Qi, M. Huang, S. Zhou, and J. Xiong, 'Honokiol Inhibits HIF-1α-Mediated Glycolysis to Halt Breast Cancer Growth', *Front. Pharmacol.*, vol. 13, 2022, Accessed: Jul. 08, 2023. [Online]. Available: https://www.frontiersin.org/articles/10.3389/fphar.2022.796763
[397] A. Pagani *et al.*, 'Deferiprone Stimulates Aged Dermal Fibroblasts via HIF-1α Modulation', *Aesthet. Surg. J.*, vol. 41, no. 4, pp. 514–524, Apr. 2021, doi: 10.1093/asj/sjaa142.
[398] A. Xiong and Y. Liu, 'Targeting Hypoxia Inducible Factors-1α As a Novel Therapy in Fibrosis', *Front. Pharmacol.*, vol. 8, 2017, Accessed: Jul. 08, 2023. [Online]. Available: https://www.frontiersin.org/articles/10.3389/fphar.2017.00326

SCIENTIFIC COMMUNICATIONS

PUBLICATIONS

Aghakhani, S; Zerrouk, N; Niarakis, A. Metabolic reprogramming of fibroblasts as therapeutic target in rheumatoid arthritis and cancer: deciphering key mechanisms using computational systems biology approaches. *Cancers* **2021**, 13, 35. https://doi.org/10.3390/cancers13010035.

Zerrouk, N*; **Aghakhani, S***; Singh, V; Augé, F; Niarakis, A. A mechanistic cellular atlas of the rheumatic joint. *Frontiers in Systems Biology* **2022**, 2:925791. https://10.3389/fsysb.2022.925791.

Aghakhani, S; E Silva Saffar, Sacha; Soliman, S; Niarakis, A. Metabolic reprogramming in rheumatoid arthritis synovial fibroblasts: a hybrid modeling approach. *PLoS Computational Biology* **2022**, 18(12): e1010408. https://doi.org/10.1371/journal.pcbi.1010408.

Aghakhani, S; E Silva Saffar, Sacha; Soliman, S; Niarakis, A. Hybrid computational modeling highlights reverse Warburg effect in breast cancer-associated fibroblasts. *Computational and Structural Biotechnology Journal.* **2023**. https://doi.org/10.1016/j.csbj.2023.08.015.

Aghakhani, S; Niarakis, A; Soliman, S. MetaLo: Metabolic analysis of Logical models extracted from molecular interaction maps. *Under preparation*.

POSTERS

Aghakhani, S; Soliman, S; Niarakis, A. Fibroblasts as therapeutic targets: computational modeling of metabolic reprogramming in rheumatoid arthritis

synovial fibroblasts and cancer-associated fibroblasts. *Computational Systems Biology of Cancer* **2020**, online.

Aghakhani, S; Soliman, S; Niarakis, A. Computational modeling of the metabolic reprogramming in rheumatoid arthritis synovial fibroblasts and cancer-associated fibroblasts. *5th Disease Map Community Meeting* **2020**, online. https://doi.org/10.5281/zenodo.4267832

Aghakhani, S; Soliman, S; Niarakis, A. Computational modeling of the metabolic reprogramming in rheumatoid arthritis synovial fibroblasts. *6th Disease Map Community Meeting* **2021**, online.

Aghakhani, S; Soliman, S; Niarakis, A. Metabolic reprogramming in rheumatoid arthritis synovial fibroblasts: a hybrid modeling approach. *European Conference on Computational Biology* **2022**, Sitges (Spain).

Zerrouk, N*; **Aghakhani, S***; Singh, V; Augé, F; Niarakis, A. A multicellular atlas of the rheumatic joint. *European Conference on Computational Biology* **2022**, Sitges (Spain).

Aghakhani, S; E Silva Saffar, S; Soliman, S; Niarakis, A. A large-scale hybrid model to study metabolic reprogramming in cancer-associated fibroblasts. *ONCOLille Days* **2022**, Lille (France).

ORAL COMMUNICATION

Aghakhani, S; Niarakis, A; Soliman, S. Metabolic analysis of logical models infered from molecular interaction maps. *Building Immune Digital Twins*, **2023**, Orsay (France).